SPOLEČNOST-
ARMÁDA-
TECHNOLOGIE-
ŽIVOTNÍ
PROSTŘEDÍ

2015

Sborník 13. odborného semináře

Materiály a technologie ve výrobě speciální techniky

seminář pořádaný pod záštitou firem

NITECH výroba a.s.
nitridační technologie, plazmová nitridace

Zwick / Roell

OLYMPUS

20. května 2015
UO Brno, ulice Šumavská 4, budova č. 8
Brno

Organizují

BVV Veletrhy Brno

Veletrhy Brno, a. s.

TnUAD v Trenčíne
Fakulta špeciálnej techniky

Univerzita obrany
Katedra strojírenství

ISBN: 978-80-7231-999-2

Již tradiční, XIII. Odborný seminář ”Materiály a technologie ve výrobě speciální techniky”, se koná jako součást účasti AČR na veletrhu IDET 2015 ve dnech 19. - 21. května 2015 v Brně, v České republice.

XIII. odborný seminář svým zaměřením na problematiku materiálů a technologií výroby speciální techniky, vytváří prostor pro výměnu zkušeností z oblasti výzkumu, vývoje a výroby speciální techniky včetně zabezpečení její jakosti. V těchto oblastech se řeší celá řada nových problémů a výměna zkušeností je jedním z prostředků jak přispět k rozvoji technické úrovně a kvality materiálního vybavení AČR a interoperabilitě s ostatními armádami NATO.

Všechny dodané příspěvky v anglickém, českém a slovenském jazyce jsou publikovány ve sborníku konference na CD. Anglicky psané příspěvky vybrané organizačním výborem budou publikovány v časopise MANUFACTURING TECHNOLOGY, v databázi SCOPUS.

Obsah:

Revize standardu ke kvalitě ISO 9001:2015 a návazně AQAP/ČOS
Martin Dvořák…… 5
Material analysis of projectile hard core
Ján Bezecný, Ján Štrba, Andrej Dubec……... 9
Analysis of surface integrity in hardened steel Vanadis (1.2379)
Viliam Cibulka, Mária Šurláková´…… 15
Riadenie výkonnosti a kvality procesov výroby pomocou vybraných technických ukazovateľov údržby
Viliam Cibulka…… 21
Surface treatment technologies for wear resistance increasing of 42CrMo4 steel
Van Thanh Doan, David Kusmic, Miroslav Pospichal……... 25
The Assessment of Selected Mechanical Properties of Steel after Application of Plasma Nitriding
David Dobrocký, David Kusmič…… 31
The Al alloy materials and their quality
Josef Formánek, Ludmila Kučerová……... 38
Influence of admixtures on mechanical features of artillery barrels
Ondrej Híreš, Peter Lipták, Danka Rakúsová……. 42
Material Analysis of Nickel Superalloy for Military Technology
Petr Jonšta, Irena Vlčková, Zdeněk Jonšta……. 45
Damage tolerance of high-speed machined integral panels made from 2024-T351 aluminium alloy
Josef Klement, Petr Augustin…….. 52
Influence of Projectile Base Modifications
Adolf Jílek, Jan Kusák…… 60
Material analysis of damaged breech locking element of machine gun
David Kusmic, Zbynek Studeny, Emil Svoboda…… 66
Variability of application, special equipment operation using renewable sources of energy
Peter Lipták, Ivan Kopecký, Danka Rakúsová……... 72
Application of modern technologies and materials in improving an ballistic protection
Peter Lipták, Ivan Kopecký…… 79
Reliability of Special Technique Materials
Peter Lipták, Jiří Stodola……. 86
Compressive creep testing of MoSi2-SiC nanocomposites
Natália Luptáková, Beáta Ballógová, Petr Dymáček…….. 89
Statistical monitoring of decrease of surface eccentricity and hole of barrel tubes from high strength steels under the production conditions
Jozef Majerík, Jozef Šandora, Jaroslav Jambor…….. 93

The Effect of Plasma Nitriding Parameters on the Thickness of Nitrided Layers
Ondrej Pilch, Frantisek Snahnican, Vojtech Hruby, Zbynek Studeny…… 100
Characteristics of plasma nitrided layers
Zdenek Pokorny, Zbyněk Studeny, Miroslav Pospichal, Zdenek Joska, Vojtech Hruby…….. 105
Influence of initial carbon concentration on nitride layers
Miroslav Pospíchal, Renata Dvořáková, Zbyněk Studený, Zdeněk Pokorný……. 112
Experimental Detection of the Characteristics Magnetorheological Dampers Applied into Military Vehicles Operated in Multinational Missions
Vladimír Sedlák, Mariana Kuffová……. 118
Deposition of aluminium oxide (Al2O3) coatings on aluminium substrate using anodizing processes
Frantisek Snahnican…… 124
Material Analysis of 120 mm Mortar Projectile Stabilizer
Zbyněk Studeny, Zdenek Pokorny, David Kusmič, Emil Svoboda…… 132
Problematika střel typu frangible
Václav Svachouček, Ivo Adam……... 139
Application of duplex layer on piston rings
Milan Vnouček, Antonín Kříž, Karel Radl……. 152

Revize standardu ke kvalitě ISO 9001:2015 a návazně AQAP/ČOS

Základním normativním dokumentem pro vytvoření, údržbu, posuzování a certifikaci systému managementu jakosti (SMJ) dodavatelů je v současné době platná norma EN ISO 9001:2008 v ČR vydaná jako ČSN EN ISO 9001:2009. Tato norma stanovuje požadavky na SMJ, vychází z předešlých verzí ISO 9001 od roku 1987. Za dobu využívání prošla několika revizemi, naposledy v roce 2008. Každá revize s sebou přináší nové změny jak z pohledu výstavby a údržby SMJ tak i směrem k procesu jeho posuzování a certifikace. V době platnosti normy se sleduje její praktický přínos a hledá se cesta ke zlepšování. Poslední připravovaná revize vychází ze shromážděných zkušeností a poznatků z praktického naplňování v rámci celosvětového průzkumu uživatelů a požadavků a připomínek jednotlivých zemí. Důležitým dokumentem je koncepce technické komise ISO/TC 176 (Management kvality a prokazování kvality) a další dokumenty. Jedná se o tzv. velkou revizi a norma doznává zásadních změn.

Pracovní skupina ISO/TC176/SC2/WG24 vypracovala harmonogram revize ISO 9001, a byly zahájeny práce, které jsou v současné době před dokončením. Počátkem roku 2016 se předpokládá vydání národní verze ČSN.

Hlavní změny vycházejí z následujících důvodů:

- Větší důraz na řízení rizik
- Celosvětové změny podnikatelského prostředí (zvyšující se význam služeb, komplexnější dodavatelský řetězec, globalizace, dosažitelnost informací atd.)
- Sjednocení struktury, textu a terminologie norem řešících integrované systémy managementu
- Snížení důrazu na dokumentaci

Přínosem pro organizace bude aplikace přílohy SL, která byla vytvořena jako povinná a univerzální kostra pro normy řešících i jiné systémy managementu. Dojde tím ke zjednodušení dokumentace dodavatelů, pokud aplikují více norem (např. kvalitu a enviroment). Naopak jako zatím ne zcela optimální se jeví snížení důrazu na dokumentované záznamy. Zatím je ale předčasné připravovanou normu hodnotit. Souhlas s návrhem normy vyslovilo 64 členských zemí ISO/ITC 176, to představuje 89% členských zemí.

Přechodné období pro certifikaci odsouhlasily IAF (International Accredation Forum a ISO CASCO (Committee on Conformity Assessment) jako 3 leté od data vydání ISO 9001:2015. Jinými slovy platnost certifikace podle ISO 9001:2008 zanikne po 3 letech od data vydání nové normy. Stejný model bude použit i u národní verze ČSN.

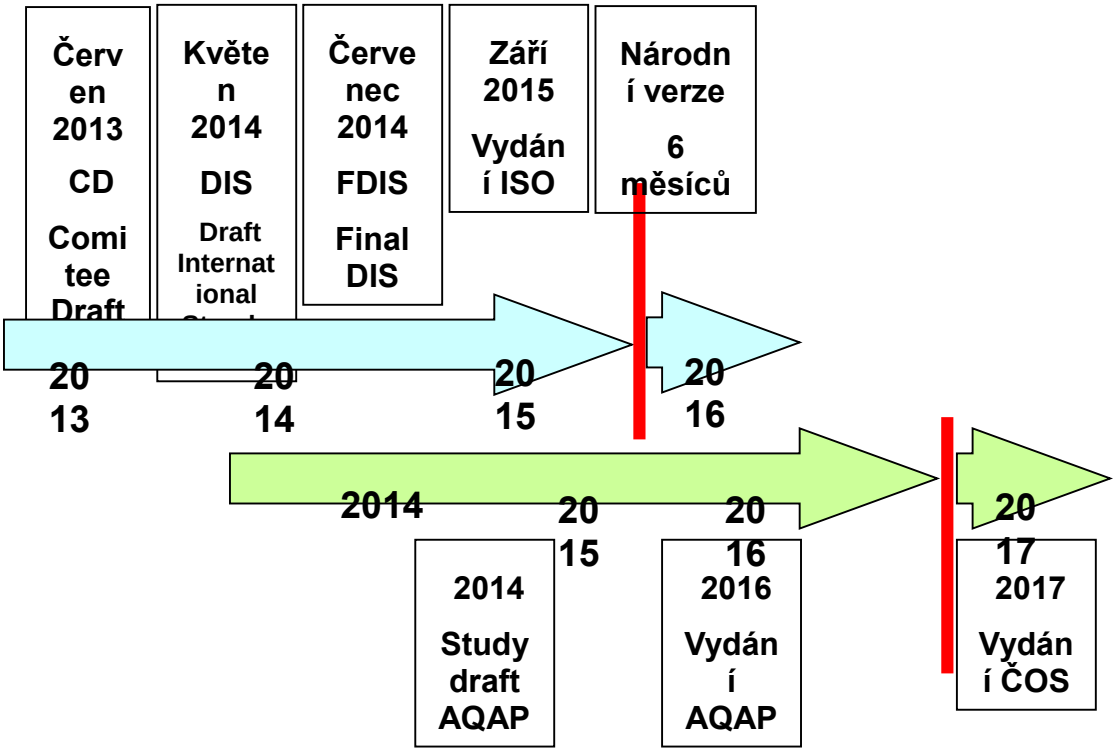

Výše uvedená nová norma bude opět základem pro revizi publikace AQAP (Allied Quality Assurance Publication), kterou budou státy NATO smluvně využívat při státním ověřování jakosti. Tuto oblast řeší v rámci NATO pracovní skupina WG2 výboru pro řízení životního cyklu AC/327 NATO. Členství a obhajobu národních zájmů ve WG2 zabezpečuje Úřad pro obrannou standardizaci, katalogizaci a státní ověřování jakosti. Práce na revizi AQAP byly zahájeny počátkem roku 2014. Výsledkem bylo vypracování tzv. „study draftu“, který vycházel z návrhu ISO/DIS 9001 na přelomu roku 2014 a 2015. Podle harmonogramu WG2 by měla být nová publikace AQAP schválena v rámci NATO na počátku roku 2016.

Oproti současným publikacím bude mít nová publikace AQAP odlišnou strukturu. Struktura požadavků publikace již nebude sledovat strukturu normy ISO 9001. Základním požadavkem je ustavit, zdokumentovat, implementovat, posuzovat a zdokonalovat efektivní systém managementu kvality v souladu s normou ISO 9001. V další části bude uveden soubor specifických požadavků přímo souvisejících s vytvořením podpory pro státní ověřování jakosti. Standardní požadavky zůstávají, tj. rozplánování výroby, zkoušení a testování výrobku vedoucí ke splnění požadavků smlouvy. Důraz bude kladen na management rizik. Přístup dodavatele při realizaci smlouvy by měl být obecně založený na rizicích. Řízení rizik bude souviset nejen s vlastní výrobou, ale bude i základem pro stanovení přiměřeného rozsahu kontrolní činnosti v rámci státního ověřování jakosti.

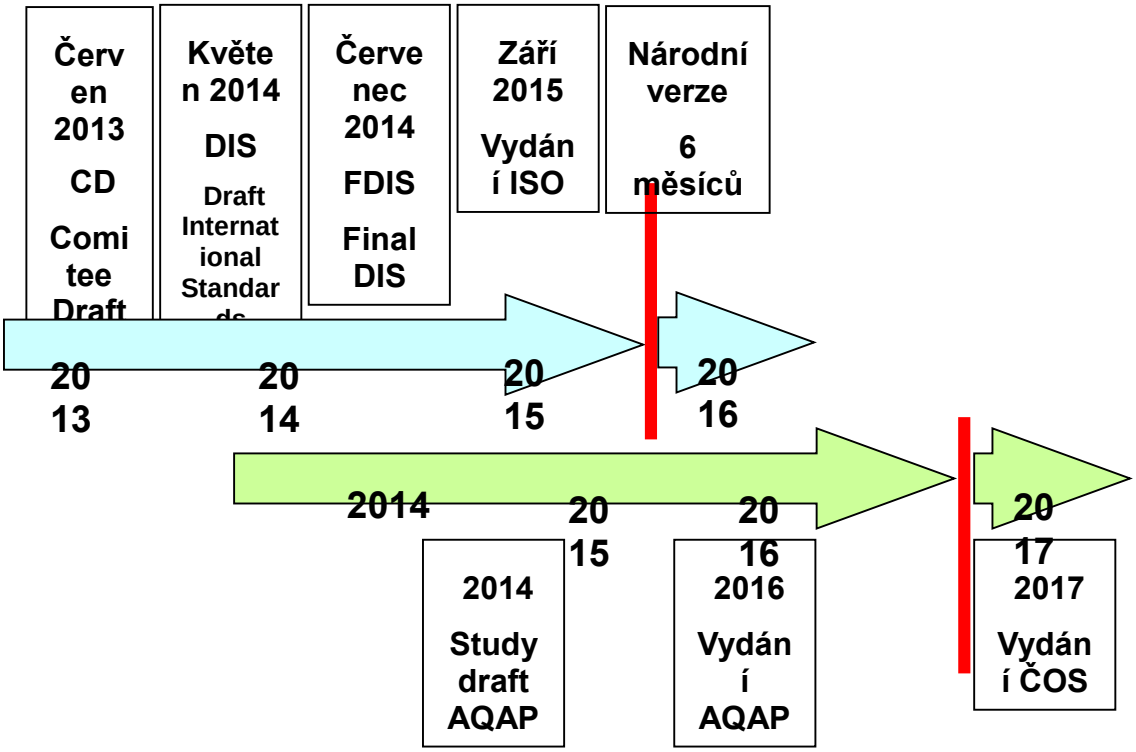

Podstatné pro uživatele rovněž bude, že nová publikace AQAP nahradí současné publikace AQAP 2110, AQAP 2120 a AQAP 2130. Vznikne tak jediná publikace obsahující požadavky NATO na ověřování kvality při návrhu, vývoji a výrobě. Publikace bude vůči dodavatelům uplatňována bez ohledu na rozsah státního ověřování jakosti, předmět smlouvy, nebo plánovaný rozsah činnosti dodavatele vedoucí k naplnění smlouvy.

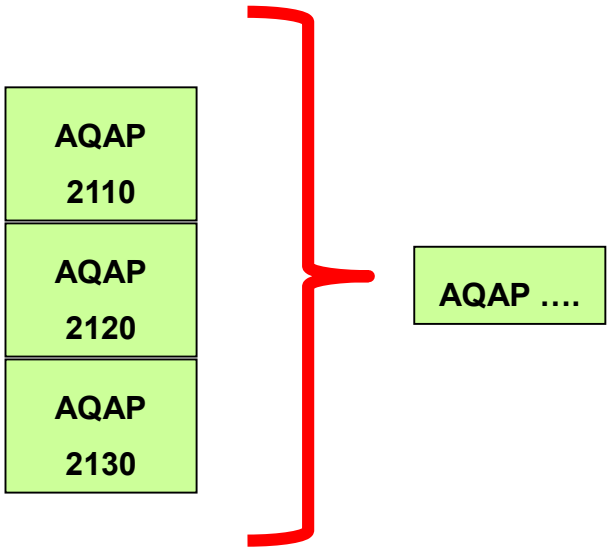

Je nutné poznamenat, že přístup NATO k certifikaci dle publikace AQAP zůstává neměnný. Publikace nebude sloužit ke komerční certifikaci systémů managementu kvality. Audity podle této publikace prováděné ve státech NATO příslušnými národními úřady ověřování jakosti mají charakter zákaznického auditu.

Standardy AQAP jsou v ČR implementovány formou Českých obranných standardů (ČOS). Nový AQAP nebude výjimkou a bude také zpracován v národní verzi a vydán jako ČOS. Termín vydání ČOS se předpokládá v roce 2017. Tento standard bude uplatňován ve smlouvách na dodávky

pro obranu a bezpečnost státu, které podléhají státnímu ověřování jakosti a dále pro provádění auditů systémů managementu kvality dodavatelů. Úřad bude nadále realizovat tyto audity a vydávat Osvědčení o shodě systému managementu kvality dodavatele s tímto AQAP/ČOS. Přechodné období bude rovněž jako u civilní ISO 9001:2015 3 leté. Úřad zajistí v součinnosti AOBP včasné poskytování informací k novému standardu a souvisejícím procesům pro podniky obranného a bezpečnostního průmysl včetně organizace školení podle požadavků průmyslu.

Ing. Martin Dvořák,Ph.D.

Ředitel Úř OSK SOJ

Material analysis of projectile hard core

Ján Bezecný[1], Ján Štrba[2], Andrej Dubec[1]
[1]University of Alexander Dubček in Trenčín. Faculty of Industrial Technologies. Department of Materials Engineering. I. Krasku 491/30. 020 01 Púchov. Slovakia. E-mail: jan.bezecny@fpt.tnuni.sk, andrej.dubec@fpt.tnuni.sk
[2]Faculty of Special Technology, Alexander Dubček University of Trenčín, Pri parku 19, 911 06 Trenčín, Slovak republic, E-mail:jan.strba@tnuni.sk

Ammunition projectiles disposal armored facilities used hard core as the main effect. The hard core has a smaller diameter than the calibre of gun. The core of the projectile is made of tungsten carbide, titanium, molybdenum or depleted uranium with a hardness of 80 to 120 measures by the Rockwell hardness test. The core must be not only hard but also tough and have a high bending strength. Knowledge of the hard core chemical composition, which the attacker uses, is important in relation to provide ballistic protection, minimization of radioactive risk and optimization of conditions for disposing of old ammunition. The basic tool for detection of the necessary data is material analysis. This analysis provides information about the weight, chemical composition and material microstructure of the hard core.

Keywords: Ammunition, Hard core, Material analysis, Chemical composition, Material microstructure

1 History

After the First World War, which was first introduced, tanks underwent rapid development and growing strength of their weapons and armor. In response thus formed anti-tank weapons, which should be able to reliably destroy armored vehicles, and these weapons were needed to develop appropriate ammunition. In the interwar period therefore began to emerge different types of armour-piercing ammunition, the trend continued during WW2. The easiest piercing charged normal piercing bullet, marked in English AP (Armour Piercing). Most often made of steel, and its ability to break armor depend on the kinetic energy evolving from the muzzle velocity - this means that penetration missiles and decreased with increasing distance. In ordinary steel, but it would be at high risk of fragmentation of the projectile on impact with the armor, it was therefore used in the production of steel with high carbon steel which gave higher hardness and prevented fragmentation projectile in contact with the armor. The destructive effect was observed in AP charge the same as for conventional projectile - causing internal damage to the masses and efect called spalling when pieces of armor vehicles, rivets and other parts armor, divorced when passing missiles were thrown through the interior and causing damage to equipment and injury tank or death of crew members.

AP projectile could break the normal steel armor, but had trouble against cemented armor, which increased the likelihood of fragmentation. Cemented armor created by applying a layer of carbon steel followed by quenching to give an armored plate, which had hardened top layer. On impact, this armor is often AP bullet shattered or deformed, was therefore developed an improved ammunition type APC (Armor Piercing Capped) that possessed the tip of mild steel. The cover "main" cutting edge projectile on impact with deformed and swallowed part of the impact force to protect itself from shattering shot or distortions. AP ammo type and APC was effective against armor, but its shape, designed to be the best penetration ability (ie. short spike) in flight he was too much air resistance, thus reducing the effective range. This problem was solved by adding the ballistic tip, or a prolonged spike of mild steel, which was mounted on top of the shot itself and to significantly improve its aerodynamic properties. Upon impact, thanks to the soft material ballistic tip easily deformed, and thus had little adverse effect on the ability of penetrating projectile itself. The combination of ballistic tip with AP ammo in English called APBC (Armour Piercing, Ballistic Cap), whereas the APC ammunition, the resulting charge called a APCBC (Armour Piercing Capped, Ballistic Cap).

APCBC projectile had a good ballistic properties and good penetration, but still relied on the damage through its own weight and tear armor, and if the spalling occurred, or if the bullet did not hit an important part of the tank, the damage was not serious enough to disable the vehicle combat. Efforts to increase the destructive effect protipancéřového ammunition therefore led to the addition of explosive ingredients. Inside the cavity of the shot was made, into which was placed a small charge of explosive squib provided delayed. It had explosives detonate after penetrating bullet armor, and subsequent detonation shot shattered into deadly shrapnel that flew in all directions, destroying the tank equipment and caused serious injury or death of the crew of the affected vehicles. The explosive charge was added to both the type of ammunition APCBC which was carrying explosive, or could be combined with AP or APBC ammunition - in the first case arose charge type APHE (Armour Piercing High Explosive). In the second case it was the type of ammunition APHEBC (Armour Piercing High Explosive, Ballistic Cap.

During the Second World War on the battlefield appeared increasingly better protected tanks and other armored vehicles, and it was therefore necessary to construct weapons capable of breaking through getting stronger armor. As already mentioned, dependent on the ammunition piercing kinetic energy supplied through the muzzle velocity, the simplest solution would appear to increase the amount of propellant mixture, thereby increasing the muzzle velocity. Such a solution would however be very impractical and expensive, as more propellant mixture would inevitably increase as the charge itself, and he would then have to be constructed new barrel and the new conclusion, able to accommodate larger charge. The idea to increase the muzzle velocity by reducing the caliber of the bullet itself and lightening but triumphed, and gave rise to the type of APCR ammunition (Armour Piercing Composite Rigid). This type of ammunition projectile was made of very hard material (e.g. tungsten carbide), and was placed in a light aluminum alloy container. These missiles were significantly increased muzzle velocity because lighter bullet was driven in the same amount of propellant mixture as conventional ammunition, and were able to break considerably stronger armor. Their disadvantage but the absence of explosive ingredients, which, combined with lower weight meant less damage caused inside the target. Less weight also mean a faster decrease in speed and thus the loss of kinetic energy, which meant less effective range and lower penetration capability over long distances. APCR projectile moreover have a higher probability of a reflection from the armor plating, particularly in the case of the inclined armor. Usually there it was available only a very small amount (max. several pieces on the board) of the scarcity of materials for their production, and its cost [1, 2].

At the request of the expert's examination was made object – hard core, see in **Fig. 1**, which has all the characteristic elements of its use in ammunition characterized as Armour Piercing Composite Rigid (APCR) or Armour piercing discarding sabot (APDS), see in **Fig. 2**.

Fig. 1 *General view of the penetrator (hard core), reduced 2,4x*

2 Construction of projectile

The body of projectile consists of hard core and sabot. The hard core hasn't some explosives and fuses. The hard core has a smaller diameter than the calibre of gun. The core of the projectile is made of tungsten carbide, titanium, molybdenum or depleted uranium with a hardness of 80 to 120 measures by the Rockwell hardness test. The core must be not only hard but also tough and have a high bending strength. The sabot is released from the core when striking armour or already during the flight trajectory by the centrifugal forces or air resistance. The sabot can have various shapes [3, 4]. The sabot is released from the core when striking armour or already during the flight trajectory by the centrifugal forces or air resistance. The sabot can have various shapes [5].

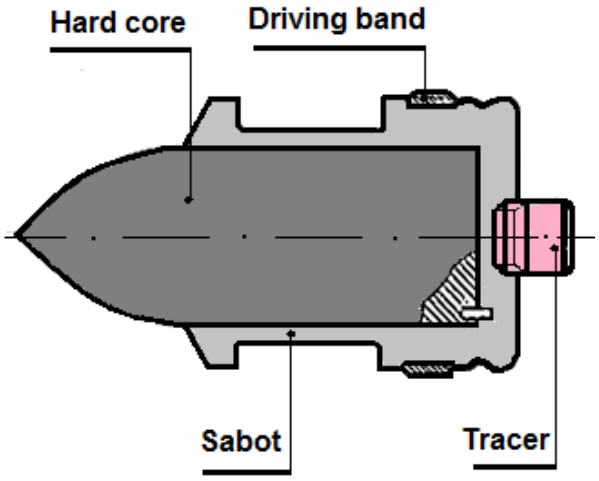

Fig. 2 *Construction of projectile APDS [6]*

3 Material analysis of penetrator

Material analysis was performed in the range: density measurements, X-ray phase analysis, microscopic evaluation of microstructure and microfractographic evaluation of fracture surfaces. This analysis was applied in order to determine the basic characteristics of the penetrator material and the assignment of its scheduled use. The analyzed penetrator had a length of about 168 mm and a diameter of 19 mm.

Density measurement

Density measurement was performed by a traditional way, that is, the measurement of weight and volume. From the measured values was calculated density of the penetrator material 14,9 g/cm^3.

X-ray analysis

X-ray diffraction method was used for detection of the phase composition of the penetrator [7]. Measurements were carried out in laboratories MtF STU Trnava by Philips diffractometer. From the results that are listed in **Fig. 3** follows, that the penetrator contains two basic components namely WC and Co. Commonly used name of this type of material is sintered carbide. The presence of other elements such as uranium was not found.

Metallographic analysis

A cross-section was prepared from the analyzed item, using a diamond abrasive disk of the Srtuers abrasive cutting machine. This cross-section was hot-molded into bakelite using LECO PR-20 machine. Metallographic section was executed in two stages due to high hardness of the material. Plane grinding (PG) was executed using a surface grinding machine with a diamond abrasive disk. Fine cutting and polishing was performed using a metallographic abrasive cutting machine Struers Abramin. To evaluate the microstructure the optical metallographic microscopes Neophot-32 were used. These enabled observation in both light and dark field as well as the use of the polarized light [7, 8]. The microstructure is documented in **Figs. 4,5** and **6**. There were no large pores detected in the microstructure (the number and size of pores can be evaluated as small) as commonly are when powder metallurgy technology is used. The microstructure was two-component and based on the previous findings of the X-ray analyzes it was possible to deduce that it consisted of the elements of Wolfram Carbide built in Co bonding.

Laboratória štruktúrnych analýz
Katedra materiálového inžinierstva, MtF STU

Report on Search/Match

Catalogue Description: D:\Program Files\WinZDS\MATEC Dubnica
Path: D:\Program Files\WinZDS\MATEC Dubnica
File Name: spek.ZDS
Type: ZDS Date: 3 IV 2015, 16:53
Sample Description: spek

Step [°]	Angle range [°]	Time [s]	Wavelength [A]	Voltage [kV]	Current [mA]	Slits
0.050	29.975 - 139.975	2.0	Co 1.788965	.	.	

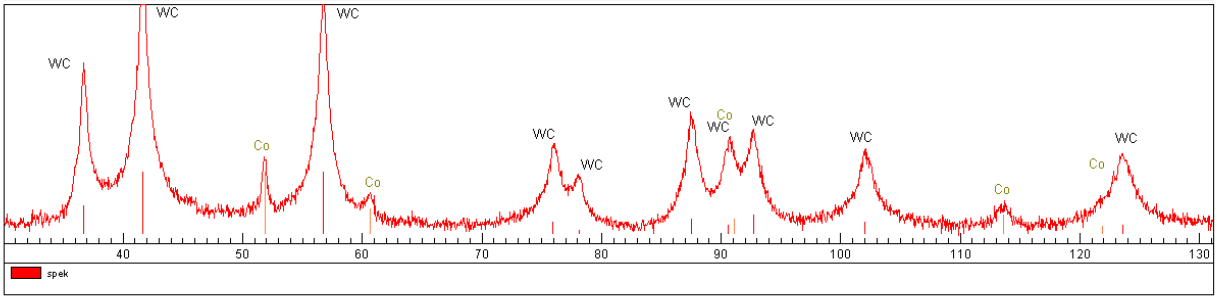

------ S a m p l e ------ 2Θ [°]	I/Io	d [A]	25-1047 Unnamed mineral WC	15-806 Cobalt Co
36.715	61	2.840	2.840 / 45	
41.645	100	2.516	2.518 / 100	
51.815	25	2.047		2.047 / 100
56.745	86	1.8823	1.884 / 100	
60.635	9	1.7720		1.772 / 40
75.925	28	1.4541	1.4540 / 20	
78.125	16	1.4194	1.4200 / 6	
87.485	18	1.2937	1.2940 / 25	
90.355	16	1.2611		
90.725	21	1.2571	1.2590 / 14	1.2532 / 25
92.705	32	1.2362	1.2360 / 30	
102.015	10	1.1509	1.1510 / 20	
113.785	10	1.0678		1.0688 / 30
121.546	2	1.0250		1.0233 / 12

Fig. 3 *The results of X-ray analysis*

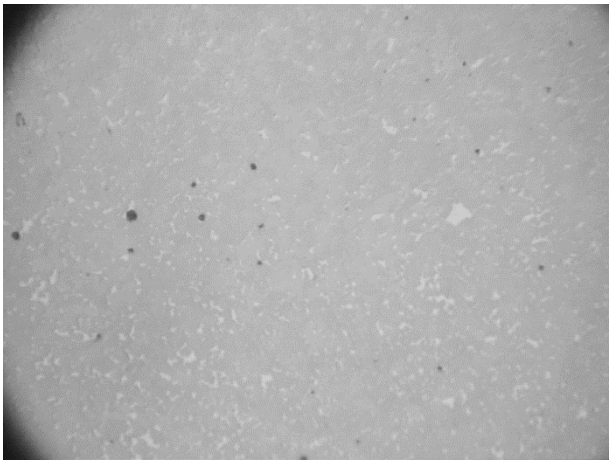

Fig. 4 *Character of microstructure without etching in light field, zoomed 100x*

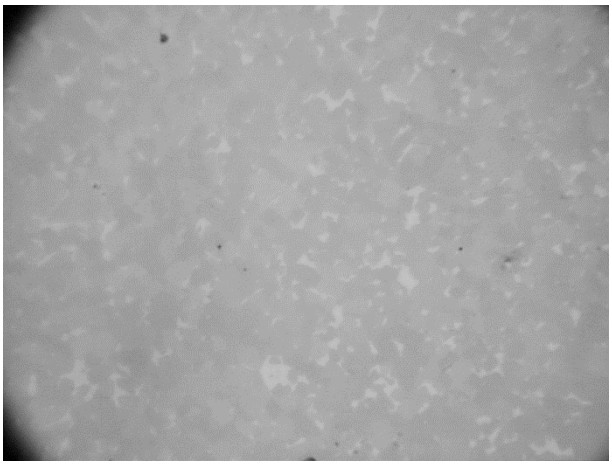

Fig. 5 *Character of microstructure without etching in dark field, zoomed 100x*

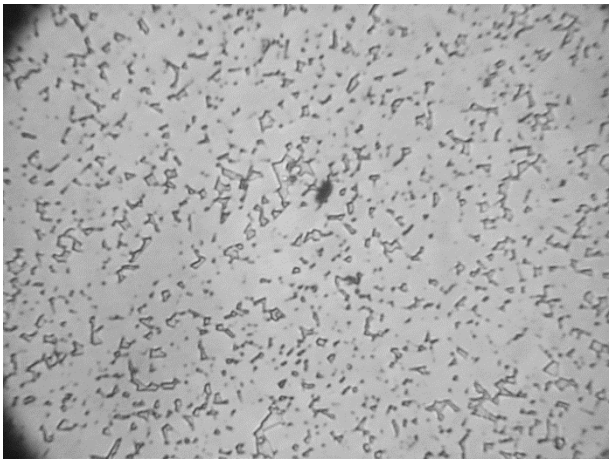

Fig. 6 *Microstructure after etching in light field, zoomed 100x*

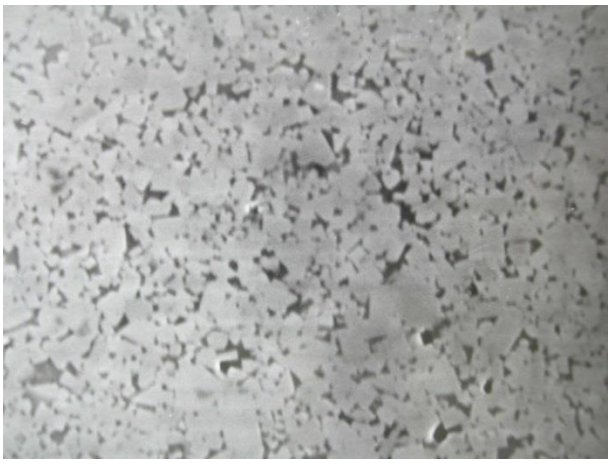

Fig. 7 *The microstructure obtained by SEM, zoomed 500x*

Microfractographic analysis

The observation with a line electron microscope SEM TESLA BS 301 was performed as part of the micrographic analysis. The mode of secondary ejected and re-dissipated electrons was used during the observation. To determine the micromechanisms of deformation were laboratory prepared fracture surface by breaking of notched specimens with impact load. The micromorphology of the rupture surfaces, observed in the mode of secondary ejected electrons [7, 8], is shown in **Fig. 8**. The mechanism of decohesion of fragile and hard phases of WC and Co bonding agent was prevailing in the samples. Ductile failure was observed only in small degree. The maximum grain size of WC is about 5 μm. To achieve a perfect differentiation of the

individual phases at the metallographic section, the mode of re-dissipated electrons was used. Character of microstructure is documented in **Fig. 7**. Co phase is dark gray colored, is relatively uniformly distributed.

Fig. 9 *Micromorphology of fracture surfaces, zoomed. 3500x*

4 Conclusion

From the performed analysis it can be concluded that the penetrator is made of WC-Co alloy with the density of 14.9 g/cm³. The density does not exceed normal values for given type of product and similar materials produced with the use of powder metallurgy. This type of penetrator with diameter of 19 mm is most often used as part of ammunition caliber 27 or 30 mm. It's a high probability core of projectile type Armour Piercing Discarding Sabot (APDS) [6], which probably comes from an unknown institutional research tasks. It is used in the sixties of the last century and it was not produced in the former Czechoslovakia. The front part of the penetrator is rounded which implies that its usage is to direct shooting at short distances up to 100 meters. This penetrator is used for the BVP transporter in direct shooting at objects such as armored vehicles, concrete covers, etc. Nowadays is used thin slim ammunition with sagittate stabilization. Penetrators are produced from high-strength ammunition steel.

References:

[1] GREXA, J., BEER, S., KOMENDA, J. (1984). *Ammunition I,* (in Czech), VA Brno

[2] GALETA, A., LIPTÁK, P., BUKOVINSKÝ, I. (2005). *Ammunition and explosives, part I.,* (in Slovak), Alexander Dubček University in Trenčín, Trenčín

[3] ŠTRBA, J., PIVKO, Š. (2013). *Ammunition and explosives, part III.,* (in Slovak), Alexander Dubček University in Trenčín, Trenčín

[4] BEER, S., KOMENDA, J., JEDLIČKA, L. (2004). *Ammunition,* (in Czech), UO Brno.

[5] KUSÁK, J. and collective (2008). *Basic design of ammunition I.,* (in Czech) UP Pardubice

[6] ŠTRBA, J., GABRIŠ, M. (2013). *Former Warsaw Pact Ammunition Handbook, VOL1, Land Forces Ammunition - Explosives, Projectiles and Grenades,* (in English), EOD Trenčín

[7] PTÁČEK, L., et al. (2003). *Material science I,* (in Czech), pp. 315 – 404, academic publisher CERM, Brno, ISBN 80-7204-283-1

[8] JANDOŠ, F., ŘÍMAN, R., GEMPERLE, A., (1985). *Utilization of modern laboratory methods in metallography,* (in Czech), pp. 21-202, SNTL Publisher, Prague

Analysis of surface integrity in hardened steel Vanadis (1.2379)

Viliam Cibulka[1], Mária Šurláková[1]
[1]Faculty of Special Technology, Alexander Dubcek University of Trencin. Pri Parku 19, 911 05 Trenčín. Slovakia. E-mail: viliam.cibulka@tnuni.sk, maria.surlakova@tnuni.sk

In this paper, the influences of cutting speed, depth of cut, feed, workpiece hardness (51, 55, 58, 62 and 65±1 HRC, and nose radius on surface integrity in finish dry hard turning of the hardened tool steel AISI D2 by utilizing the polycrystalline cubic boron nitride PCBN inserts were experimentally investigated. The surface roughness values are in the range of 0.34-0-86 µm between 150 and 301–m/min cutting speeds and totally attains a surface finish of grinding. The "residual cutting" materials, material plastic deformation, and even cohesion in the machined surface and cold welding effect do occur and hence influence on the surface integrity. In this paper the authors conducted detailed analysis directly from number sources about surface integrity.

Keywords: Hardened tool steel, surface integrity, surface morphology, cutting parameters

1 Introduction

According to literature [1, 2] the finish dry hard turning (FDHT) is defined as the single-point turning process of materials harder than 50 HRC under the condition of small feed and fine depth of cut by utilizing appropriate cutting tools without or minimizing the use of cutting fluid in order to reach good surface quality, dimensional and form tolerances, and surface integrity close to those obtained grinding. It has gained more attention owing to its substantial advantages, such as reducing the time of finish machining, declining the cost of manufacturing, and eliminating the hazard of cutting fluid by using dry machining compared to grinding [3-5]. Therefore, FDHT has become an alternative machining process for grinding processes of hardened steels due to improvements in the performance of hard-tool materials [6, 7]. Numerous investigations have been carried out to study the surface integrity in turning operations. Thiele et al. [8] have investigated the effects of tool cutting edge geometry and workpiece hardness (41, 47, and 57 HRC) on the surface roughness in finish hard turning of AISI 52100 steel. The results showed that the cutting edge geometry has significant influence on the surface roughness, and that large edge hones lead to higher surface roughness values than small edge hone. Then, Rech et al. [9] have found that hard turning process has capacities to produce a low surface roughness (Ra<0.20 µm) during a long cutting time and also to induce compressive residual stresses when turning of case-hardened 27MnCr5 at low feed rate and low cutting speed. Besides, the effects of cutting edge geometry, workpiece hardness, feed rate and cutting speed on surface roughness in finish hard turning of AISI H13 steel were experimentally investigated by Ozel et al. [10]. In this study, the results showed that the effects of workpiece hardness, cutting edge geometry, feed rate, and cutting speed on surface roughness are statistically significant. In addition, Umbrello and Jawahir [11] have predicted the white layer formation during machining of hardened AISI 52100 steel with three different hardness levels of 56, 62, and 66 HRC by utilizing a finite element mode. Okada et al. [12] have investigated cutting performance of CBN tools and PVD-coated carbide tools in end-milling of hardened steel. In this study, the influence of workpiece hardness on surface roughness was summarized. Aouici, et al. [13] have experimentally investigated the influences of cutting speed, feed, depth of cut, and workpiece hardness on the surface roughness in turning hardened steel AISI H11. However, workpiece materials has only been hardened to the low hardness with 40, 45, and 50 HRC. Later, Rech and Moisan [14] have studied the influence of workpiece hardness and cutting speed on the cip formation and forces in hard turning of hardened steel AISI H13, whereas, surface integrity was not investigated in this paper. Besides, Chen et al. [15] have investigated the surface micro-topography in hard turning of GCr15 bearing steel by using the polycrystalline cubic boron nitride (PCBN) tools. The results showed that feed rate has greater influence on surface roughness than cutting speed. It is well known that the hardened tool steel AISI D2 is a kind of a difficult-to-cut material. However, it is revealed from the literatures reviewed above that, up to present, there are still few studies about focusing on the influence of cutting speed, depth of cut, feed, workpiece hardness, and nose radius on surface integrity in FDHT of the hardened tool steel AISI D2 at different hardness levels in the range from 51 to 65±1 HRC. Here, a study aims to experimentally investigate the effect of these variables on surface integrity and their changing mechanisms.

2 Experimental procedures

In this study, the bar of tool steel AISI D2 (Cr12MoV) was used. The chemical composition is presented in Table 1. The bars of 48 mm diameter and 300 mm length were used. In order to effectively utilize the FDHT process in the manufacturing industries, the hardened tool steel at different hardness levels were considered for this study with a polycrystalline cubic boron nitride (PCBN) insert. The results showed that the toll steel AISI D2 could get fine-needle martensite, high diffusion, and uniform distribution fine-grain carbide if using the quenching temperatures of 1000-1040˚C [16]. According to the methods of heat treatment in the literature [17], the specimens were inserted into an electrical resistance furnace at 1000-1040˚C, then quenched in oil, and finally tempered at various low temperatures (100,

220, 350, 520, and 550˚C). The hardness values of the differently treated specimens were estimated by Rockwell hardness tester. At least three readings have been taken to estimate the average value of hardness of every specimen. The obtained hardened specimens were in five hardness levels of 51, 55, 58, 62, and 65±1 HRC.

C	Cr	Mo	Mn	Si	P	S	V
1,55	11,25	0,45	0,35	0,35	0,025	0,025	0,20

Table. 1 *Statistical evaluation of results values from figures 3a,3b*

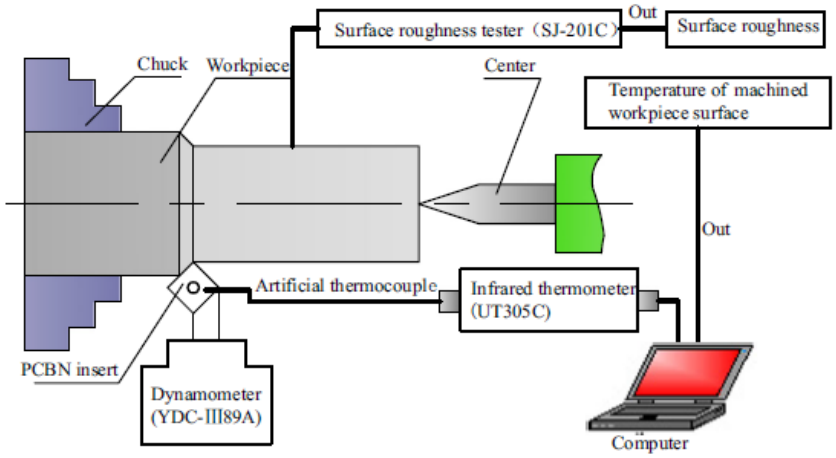

Fig. 1 *Schematic diagram of the measurement system [25]*

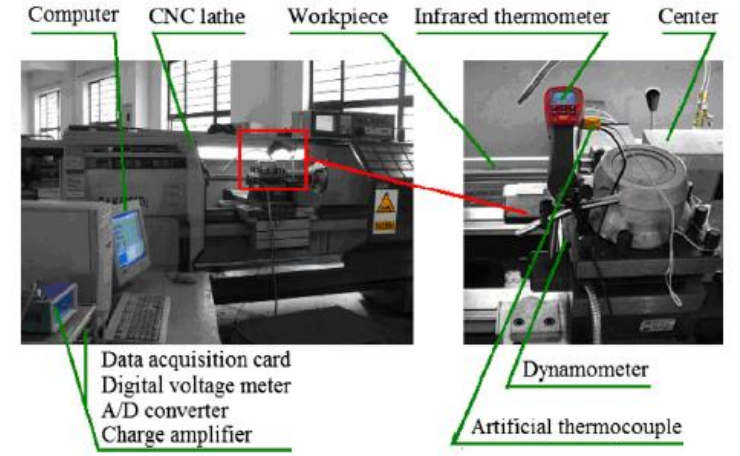

(a) CNC lathe (b) Artificial thermocouple, infrared thermometer, and dynamometer

(c) Surface roughness tester

Fig. 2 *Experimental setup [25]*

The inserts were clamped in a piezoelectric three-component turning dynamometer (type: YDC-III89) tool holder. Except for the nose radius, all the composite PCBN inserts used for the experiments has the same tool geometry parameters. The measurement system of the experimental investigation was made up of the CNC lathe, dynamometer (type: YDC:III89), infrared thermometer with accessory artificial thermo-couple

(type:UT305C), scanning electron microscopy (SEM, type: JSM-6700F), and 3D profilometer (type: Newview5022, America).

As presented in Fig. 2, FDHT test were conducted by using a CNC lathe (Fig. 3a) varying from 0 to 2200 rpm and a maximum power of 9.5 kW at a room temperature of about 22˚C and relative humidity of about 40%. A portable surface roughness tester made in Japanese (type: SJ-201C, Fig. 3c) was used to measure surface roughness (Ra). Surface roughness was measured seven times in different places along the feed direction after each turning operation.

Temperatures of machined workpiece surface were measured by means of an infrared thermometer, and then data was saved in a computer. Temperatures of the cutting tools were measured by using an artificial thermocouple plugged into a small hole of 1.2 mm diameter where it is 2.5 mm distant from the tip of the cutting tool. And temperature of tool was presented on the display of the infrared thermometer when the FDHT was over. Schematic diagram and testing ground of the temperature measurement are described in Fig. 4.

After mounting, grinding, polishing, and etching (etchant used: 4% nitric acid alcohol solution for 40s), microstructural examination of the machined surface were carried out by using a SEM. The polishing has been carried out by using a semiautomatic grinding and polishing machine from Buehler shown in Fig. 4. The processes are as follows:

- **Grinding: using UltraPrep (9 μm) metal-bonded disc at the normal load of 20 N and 120 r/min (roating direction is the same) for 5 min.**
- **Polishing: using surface of preparation with the TriDent polishing cloth (3 μm) of and the MetaDi polishing liquid at the normal load of 25 N and 120 r/min (rotating direction is the same) is for 10 min. Figure 5a, b is the finished specimens.**

The machined surface morphology examination was carried out by using SEM. The metallographic samples were extracted from the machined surfaces and the analyzed by using a 3D profilemeter. Elemental mapping of the machined surfaces was conducted in a SEM equipped with energy dispersive X-ray spectroscopy (EDS) detector. Fig. 6 presents the SEM micrographs of the metallurgical structure of the hardened tool steel AISI D2 a different hardness levels of 51±1, 55±1, 62±1, 58±1, and 65±1 HRC, respectively.

Fig. 3 *Testing ground of the temperaturemeasurement [25]*

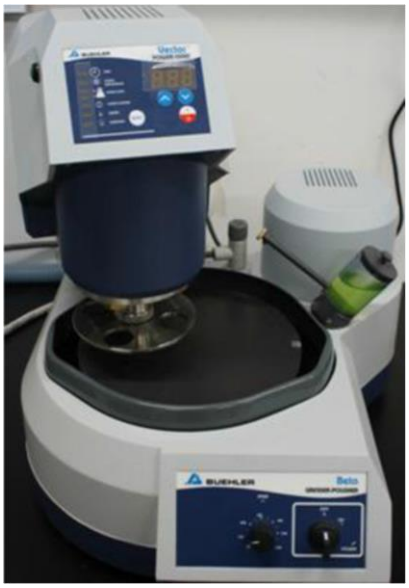

Fig. 4 *Semi-automatic grinding and polishing machine [25]*

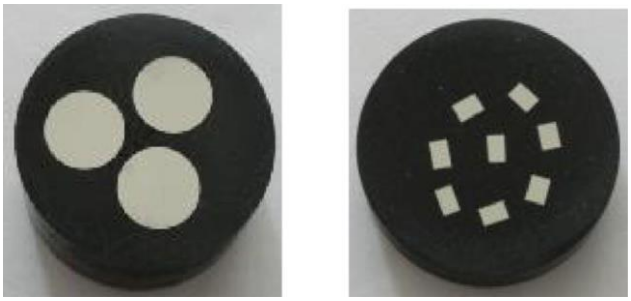

Fig. 5 Finished specimens [25]

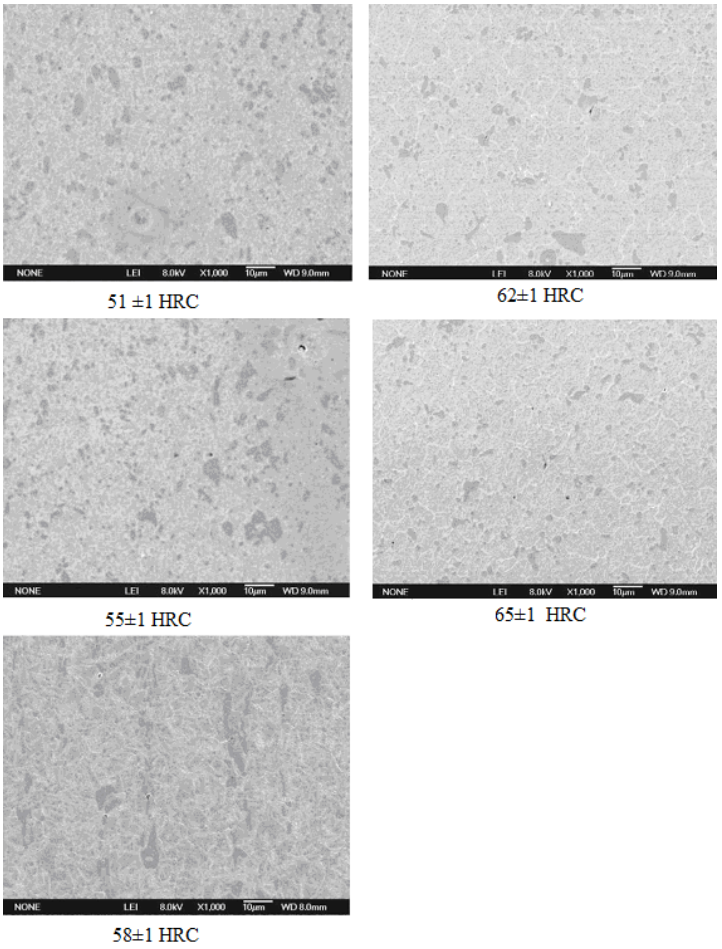

Fig. 6 *SEM micrograph of the microstructureof hardened tool steel [25]*

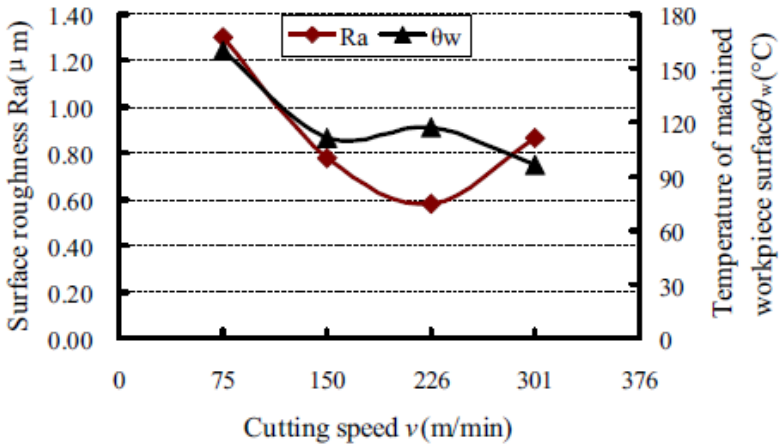

Fig. 7 *The effect of cutting speed on the surface roughness [25]*

Figure 7 shows that the cutting speed has a more important influence on the surface roughness in FDHT of hardened steel AISI D2, especially at lower cutting speeds of 75-226 m/min. it can be seen from Fig.8 that the surface roughness firstly decreases and then increases with increments of the cutting speed. As a shown clearly in this figure, the surface roughness attains the highest peak of 1,29 μm at a cutting speed of 75 m/min.

3 Conclusions

In this paper, experimentations by utilizing FDHT of the hardened tool steel AISI D2 at different hardness levels were conducted with the PCBN tool inserts. The influences of the cutting speed, feed, depth of cut, workpiece hardness, and nose radius on surface roughness in a FDHT process have been analyzed by mean of utilizing various experimental ways and analysis methods. From the previous results, the following conclusions can be drawn:

- **the ploughing, serious squeeze, and elastic deformation effect have more significant effect on the surface roughness than those black fusion welding materials and side flows effect, and the surface roughness are in the range of 0,34-0,86 μm as the cutting speed ranges between 150 and 301 m/min and totally can attain a surface finish of grinding,**
- **the surface roughness is not very sensitive to the depth of cut in the range from 0,10 to 0,25 mm. the "residual cutting" materials, more serious material plastic deformation, and even cohesion in the machined surface and cold welding effect do occur and have influence on the surface integrity.**
- **The tiny grooves and severe plastic flow occur in the machined surface, and extensive material flows at lower feeds have important influence on the surface integrity. The subsurface damages produced by the turning process also do occur and become severer at the larger feeds. It is the friction on the tool flank face that induces the localized stretch, plastic deformation, and even dilacerations of subsurface material.**
- **The cutting difficulty of the hardened workpiece with hardness greater than 50 HRC can be divided into the following different grades: 50<*H*≤55 HRC, easy cutting, 55<*H*<62 HRC, moderate cutting, and *H*≥62 HRC, difficult cutting. The thermal softening, serious material side flows at the feed marks, squeezing effect between the tool flank face, and the machined surface contains several additional crystalline particles resulted from heat melting and condensation.**
- **Values of the surface roughness attain a lowest value of 0,34 μm at a nose radius of 0,8 mm in the range from 0,4 to 1,6 mm nose radius. The heat effect is greater than the geometry effect as the nose radius attains a certain value.**

Acknowledgement

The paper was developed in range of solution of ITMS 261102300099 project „Trenčin University called by Alexander Dubček in Trenčín is willing to offer high-class and modern education".

References

[1] Meyer R, Köhler J, Denkena B (2012) Influence of the tool comer radius on the tool wear and process forces during hard turning. Int J Adv Manuf Technol 58(9-12):933-940

[2] Yong H, Liang SY (2004) Modelling of CBN tool flank wear progression in finish hard turning. ASME J Manuf Sci Eng 126:98-106

[3] Klocke F, Brinksmeier E, Weinent K (2005) Capability profile of hard cutting and grinding processes. Ann CIRP 54(2):552-580

[4] Tang L, Huang J, Xie L (2011) Finite element modeling and simulation in dry hard orthogonal cutting AISI D2 tool steel with CBN cutting tool. Int J Adv Manuf Technol 53(9/12):1167-1181

[5] Tang L, Gao C, Huang J, Lin X, Zhang J (2013) Experimental investigation of the three-component forces in finish dry hard turning of hardened tool steel at different hardness levels. Int J Adv Manuf Technol 70(9-12):1721-1729

[6] Meye R, Köhler J, Denkena B (2011) Influence of the tool comer radius on the tool wear and process forces during hard turning. INt J Adv Manuf Technol 58(2012):933-940

[7] Gaitonde VN, Karnik SR, Figueira L, Figueira L, Paulo Davim J (2011) Performance comparison of conventional and wiper ceramic inserts in hard turning through artificial neural network modeling. INt J Adv Manuf Technol 52:101-114

[8] Thiele JD, Melkote SN (1999) Effect of cutting edge geometry and workpiece hardness on surface generation in the finish hard turning of AISI 52100 steel. J Mater Process Technol 94:216-226

[9] Rech J, Moisan A (2003) Surface integrity in finish hard turning of case-hardened steels. Int J Mach Tool Manuf 43:543-550

[10] Ozel T, Hsu TK, Zeren E (2005) Effects of cutting edge geometry, workpiece hardness, feed rate and cutting speed on surface roughness and forces in finish turning of hardened AISI H13 steel. Int J Adv Manuf Technol 25:262-926

[11] Umbrello D, Jawahir I (2009) Numerical modeling of the influence of process parameters and work-piece hardness on white layer formation in AISI 52100 steel. INt J Adv Manuf Technol 44:955-968

[12] Okada M, Hosokawa A, Taraka R, Ueda T (2011) Cutting performace of PVD-coated carbide and CBN tools in harmilling. Int J Mach Tool Manuf 51:127-132

[13] Rech J, Moisan A (2013) Surface integrity in finish hard turning of case-hardened steels. Int J Adv Manuf Technol 43:543-550

[14] Aouici H, Yallese MA, Chaoui C, Mabrouki T, Rigal JF (2012) Analysis of surface roughness and cutting force components in hard turning with CBN tool: Prediction model and cutting conditions optimization. Measurement 45:344-353

[15] Chen T, Li SY, Han BX, Liu GJ (2014) Study on cutting force and surface micro-topography of hard turning of GCr15 steel. Int J Adv Manuf Technol 9-12:1639-1645

[16] Zhou AQ, Deng FY (2001) Experimental study on the heat treatment process for Cr12MoV steel. Die Mould Ind 000:55-57

[17] Wang LJ, Miao B, Meng XX (2005) Analysis on the hardness and maetallographic structure of Cr12MoV Steel under different heat treatment. Die Mould INd 000:2-56

[18] Dogra M, Sharma VS, Sachdeva A, Suri NM, Dureja JS (2010) Tool wear, chip formation and workpiece surface issues in CBN hard turning: a review. Int J Precis Eng Manuf 11(2):341-358

[19] Liu Z, Zhou J, Wan Y (2006) Tool materials for high speed machining and their fabrication technologies. Mater Mech Eng 30(5):1-4

[20] Pang JZ, Wang MJ, Duan CZ (2009) Surface roughness in high-speed side milling of hardened mold steel. J Dalian Univ Technol 49:216-221

[21] Xu J (2009) Study on high speed cutting hardened steel with the coated insert (CN35). South China University of Technology, Dissertation

[22] Femández-Abia AI, Barreiro J, López de Lacalle LN, Martinez S (2011) Effect of very high cutting speeds on shearing cutting forces and roughness in dry turning of austenitic stainless steels. Int J Adv Manuf Technol 57:61-69

[23] Kishawy H, Elbestawi M (1999) Effects of process parameters on material side flow during hard turning. In J Mach Tool Manuf 39:1017-1030

[24] Al-Ahmari AMA (2007) Predictive machinability models for a selected hard material in turning operations. J Mater Process Technol 190:305-311

[25] Tang L, Gao Ch, Huang J, Shen H, Lin X (2014) Experimental investigation of surface integrity in finish dry hard turning oh hardened tool steel at different hardness levels. Int J Adv Manuf Technology

Riadenie výkonnosti a kvality procesov výroby pomocou vybraných technických ukazovateľov údržby

Viliam Cibulka [1]
[1]Fakulta špeciálnej techniky, Trenčianska univerzita Alexandra Dubčeka v Trenčíne, Pri parku 19, 91106 Trenčín, Slovensko, E-mail: viliam.cibulka@tnuni.sk

V príspevku sú uvedené poznatky autora získané so zavadzania vybraných technických ukazovateľov výkonnosti údržby a prínosy z neho vyplývajúce pre príslušný výrobný podnik. Celý postup zavádzania technických ukazovateľov v podniku je zdokumentovaný, počínajúc analýzou súčasného stavu riadenia výkonnosti procesov výroby v podniku, výberu kritických procesov (úseku) výroby, návrh vybraných technických ukazovateľov, návrh opatrení na zvýšenie výkonnosti a kvality procesov výroby a tiež ich udržateľnosti.

Kľúčové slová: výroba, výkonnosť procesov, kvalita procesov, technické ukazovatele údržby, udržateľnosť

1 Úvod

Na Slovensku je v súvislosti s riadením výkonnosti a kvality procesov výroby platná európska norma STN EN 15341 - Údržba kľúčové ukazovatele výkonnosti už od roku 2007. Jej zavedenie a praktická aplikácia v podnikoch sa javí zatiaľ málo uspokojivá. Jej aplikovanie v praxi predpokladá využívanie vybranej skupiny ukazovateľov zo súboru ukazovateľov (ekonomických, technických a organizačných), ktoré umožňujú vytvoriť podmienky na efektívne riadenie výkonnosti a kvality procesov výroby v podniku. Postup ich aplikovania v praxi je taký, že na základe analýzy súčasného stavu výkonnosti a kvality procesov sa navrhujú ciele na ich zlepšenie, ktoré je spojené zároveň s výberom vhodných ukazovateľov. Na úrovni komplexných systémov, napr. výrobných liniek, sa ciele výkonnosti údržby týkajú konkrétnych parametrov výkonnosti, ktoré sa identifikujú počas analýzy. Ide obvykle o nasledovne ukazovatele napr. zlepšenie pohotovosti, zlepšenie nákladovej efektívnosti údržby, bezpečnosti a zachovanie životného prostredia, zlepšenie v nákladovo efektívnom riadení hodnoty inventára údržby; riadenie dodávateľských služieb. Ak sú predmetom zlepšovania len niektoré pracoviska na úrovni zariadení a strojov, tak je zlepšovanie zamerané na lepšie riadenie ukazovateľov, napr. spoľahlivosť, náklady, udržiavateľnosť a zabezpečenosť údržby . V rámci analýzy skúmaného objektu sa vždy zohľadňuje i vplyv externých a interných faktorov.

V rámci riadenia výkonnosti procesov podniku je potrebné venovať pozornosť i spoľahlivosti zariadení. Spoľahlivosť je všeobecná vlastnosť stroja/zariadenia spočívajúca v schopnosti plniť požadované funkcie pri zachovaní realizačných ukazovateľov v daných medziach v určitom čase podľa zadaných technických podmienok [15]. Spoľahlivosť je podľa STN EN 13306:2011 (angl. dependability) súhrn vlastností používaných na opis použiteľnosti (pohotovosti) položky a faktorov, ktoré na ňu vplývajú, tzn. funkčná spoľahlivosť, udržiavateľnosť a podporiteľnosť údržby, teda používané všeobecné opisy bez kvantitatívnych charakteristík. Spoľahlivosť sa chápe aj ako zmena kvality v čase – procesy starnutia strojov a zariadení, ich opis, možnosti pozitívneho ovplyvnenia technického stavu. Každopádne platí, že spoľahlivosť zariadenia je výrazne ovplyvňovaná vo fáze jeho prevádzkovania v podniku. Z toho dôvodu aj tejto problematike bude venovaná pozornosť na záver tohto článku, kde bude navrhnutý postup jej aplikovania v rámci procesov neustáleho zlepšovania výkonnosti a kvality procesov podniku.

2 Analýza výkonnosti technologických zariadení vo výrobe, návrh postupu a opatrení na ich zlepšenie

Predmetom analýzy a návrhu ukazovateľov výkonnosti údržby je výrobný podnik, ktorý vyrábané produkty dodáva renomovaným podnikom rámci Európy. Výrobný proces produktu je zabezpečovaný rôznymi technológiami spracovania plastov s vysokým stupňom automatizácie v nepretržitej prevádzke.

Výrobný proces produktu pozostáva z:
- predvýroby (technológie lisovania, lakovania a pokovovania),
- a montáže (kompletizácia dielcov).

Útvar údržby v podniku má stanovené nasledovné ciele:
- zaistiť prevádzkyschopnosť strojov,
- zabezpečiť prevádzkovú kvalitu a bezpečnosť strojov,
- prevenciami predchádzať poruchám na strojných zariadeniach,
- zabezpečiť zachovanie plánovaného stavu technických prostriedkov,
- vykonať opatrenia na nefunkčnom zariadení s cieľom zaistiť, aby boli splnené požiadavky pre predurčené používanie,
- optimalizovanie nákladov na plánované úlohy údržby.

Prehľad procesov údržby, ktoré tento útvar zaisťuje:

- preventívna údržba strojov a zariadení,
- vykonávanie údržby - opravy nástrojov,
- vykonávanie opráv strojov, elektrických zariadení, budov,
- diagnostická údržba,
- prediktívna údržba,
- revízie,
- analýza porúch,
- kontroly a revízie elektrických spotrebičov v priebehu ich používania.

Dlhodobo sa vo výrobe podniku vyskytovali početné poruchy technologických zariadení, hlavne v predvýrobe, ktoré spôsobovali časté výpadky technologických zariadení, ich následkom boli početné prestoje zariadení a znižovanie ich výkonnosti a kvality procesov výroby. Doposiaľ riadenie procesov údržby spočívalo hlavne v analýze už vzniknutých porúch technologických zariadení a v ich následnom odstraňovaní. V údržbe nebol aplikovaný žiadny systémový postup k riešeniu porúch a prestojov údržby. Preto sa rozhodlo uskutočniť podrobnejšiu analýzu porúch zariadení vo výrobnom úseku za dlhší časový úsek. Z dosiahnutých výsledkov vyplynili nasledovné zistenia.

Najviac poruchové boli nasledovné pracoviská vo výrobnom úseku:

- lisovanie plastov,
- pokovovanie,
- lakovanie.

Najviac poruchovým zo sledovaných pracovísk vo výrobe je pracovisko lisovania plastov, ktoré pozostáva z dvoch skupín technologických zariadení.

Za základné kľúčové ukazovatele výkonnosti údržby na základe analýzy porúch pracovísk vo výrobe podniku boli určené nasledovné:

- MTBF (Mean Time Between Failure) – stredná doba prevádzky medzi poruchami,
- MTTR (Mean Time To Repair) – stredná doba do obnovy,
- MTTF (Mean Time To Failure) – stredná doba do poruchy.

Tieto technické kľúčové ukazovatele výkonnosti procesov výroby najlepšie odpovedajú podmienkam v podniku pre stanovené cieľe riadenia výkonnosti a kvality procesov údržby a vytvárajú predpoklad na stabilizovanie ich výkonnosti a sú dobre merateľné, presné a spoľahlivé a využiteľné pri implementácii nápravných opatrení.

V ďalšej časti predmetom riadenia výkonnosti a kvality procesov bude pracovisko lisovania plastov. Preto boli vykonané sledovania procesov pracoviska počas 5 mesiacov. Výsledky sledovania procesov sú uvedené v tab. 1.

Tab. 1 Celkové vyhodnotenie porúch na pracovisku lisovania za sledované obdobie [1]

Druh poruchy	Čas trvania poruchy v minútach	Percentuálne vyjadrenie času trvania poruchy
Porucha formy	24280 min.	58 %
Porucha robota	6465 min.	15 %
Porucha stroja	11180 min.	27 %

Z tejto tabuľky vyplýva že porucha formy na pracovisku lisovania (lamanie kolíkov) predstavuje 58% celkového času prestojov (24280 min), porucha stroja spôsobila 27% prestojov (11180 min.) a porucha robota spôsobila 15% prestojov (6465 min.). Ďalšie informácie o tomto pracovisku sú namerané hodnoty ukazovateľov MTBF (Mean Time Between Failure), MTTR (Mean Time To Repair), MTTF (Mean Time To Failure), (tab. 2) za sledované obdobie. Z údajov evidovaných v tabuľke 1 vyplýva, že namerané údaje sledovaných troch ukazovateľov výkonnosti a kvality procesu majú premenlivý charakter, ktorý potvrdzuje tú skutočnosť, že proces nie je riadený a potrebné je ho stabilizovať a zaistiť stabilizovanú udržateľnosť výkonnosti procesu. Pretože namerané hodnoty údajov ukazovateľov nepotvrdzujú tendenciu zlepšovania kvality procesu odporúča sa navrhnuť nápravné opatrenia na ich zlepšenie po vykonaní analýzy dosiahnutých hodnôt vytypovaných ukazovateľov.

Následne boli navrhnuté nápravné opatrenia na zvýšenie výkonnosti a kvality procesov pracoviska lisovania. Ide o nasledovné opatrenia:

- úprava programu - komunikácie medzi lisom a robotom, ktorý odoberá jednotlivé výlisky zo vstrekovacej formy a ukladá ich na dopravníkový pás,
- zabrúsenie drážok na vyhadzovačoch, aby sa odstránilo zalomenie ihiel,
- zväčšenie rádiusu na spodnej časti kolíkov s cieľom zvýšenia odolnosti kolíka voči šmykovému treniu,
- povrchová úprava kolíkov z dôvodu zvýšenia pevnosti kolíkov pri vŕtaní dier aby sa minimalizovala pravdepodobnosť zalomenia kolíkov,
- inštalácia priemyselnej kamery na odhalenie podmienok zalomenia kolíkov.

Tab. 2 Dosiahnuté hodnoty ukazovateľov kvality údržby pracoviska lisovania pred jeho riadením [1]

Parameter / mesiac	1.mesiac	2.mesiac	3.mesiac	4.mesiac	5.mesiac
MTTR (min.)	103	106	88	137	95
MTBF (min.)	369	303	387	374	532
MTTF (min)	263	197	297	235	435

Po implementovaní nápravných opatrení možno konštatovať, že sa vytvorili podmienky na zlepšenie stavu navrhnutých technických ukazovateľov výkonnosti a kvality procesov pracoviska lisovania a k stabilizácii výkonnosti procesov tohto pracoviska (tab. 3). Konkrétne sa stav ukazovateľa stredná doba prevádzky medzi poruchami zlepšil z pôvodných 332 minút v 1. mesiaci na 474 minút v 3. mesiaci, čo predstavuje 42,77% zlepšenie stavu ukazovateľa. Tiež ukazovateľ stredná doba do poruchy sa zlepšil zo stavu 262 minút v 1. mesiaci na 379 minút v 3. mesiaci, čo predstavuje 44,65 % nárast tohto ukazovateľa. Hodnota ukazovateľa stredná doba do obnovy pracoviska, ktorou sa hodnotí priemerná dobu opráv na strojných zariadeniach mierne poklesla o 15 minút, čo predstavuje zlepšenie hodnoty tohto ukazovateľa o 27,27 %.

Tab. 3 Dosiahnuté hodnoty ukazovateľov kvality údržby pracoviska lisovania po aplikovaní návrhov opatrení [1]

Parameter / mesiac	1.mesiac	2.mesiac	3.mesiac
MTBF (min.)	332	420	474
MTTR (min.)	70	69	55
MTTF (min.)	262	351	379

Aplikovaním navrhnutých opatrení sa dosiahli ešte i ďalšie efekty v kvalite údržby pracoviska lisovania, ktoré sú charakterizované v záverečnej kapitole príspevku.

3 Záver

Celkovo možno konštatovať, že na základe vykonanej analýzy porúch technologických zariadení vybraného podniku bolo vytypované kritické pracovisko v predvýrobe (pracovisko lisovania), pre ktoré boli navrhnuté kľúčové technické ukazovatele výkonnosti údržby z hľadiska stabilizácii výkonnosti a kvality procesov pracoviska. Následnou analýzou hodnôt kľúčových technických ukazovateľov po dobu 5 mesiacov na tomto pracovisku boli identifikované hlavné príčiny porúch na pracovisku. Na ich eliminovanie bolo navrhnutých päť nápravných opatrení. Po ich zavedení bolo meraním zistené výrazné zvyšovanie výkonnosti a kvality procesov pracoviska a zníženie nákladov na opravy strojov, tiež na nákup náhradných dielov a výrazné zníženie prestojov pracoviska.

Pozitívny vplyv aplikovaných návrhov opatrení sa prejavil tiež v oblasti kvality vyrábaných produktov na tomto pracovisku, pretože sa eliminovala tvorbu nezhodných produktov z dôvodu lámania kolíkov. Ďalšie prínosy vďaka aplikovaniu navrhnutých opatrení spočívajú v zamedzení potreby nákupu novej formy, ktorej cena je niekoľko tisíc euro. Navrhnutými nápravnými opatreniami sa dosiahlo zvýšenie celkovej efektívnosti výrobných zariadení pracoviska lisovania. Potrebné je na záver tohto príspevku zdôrazniť, že toto boli vykonané len prvé kroky k zvyšovaniu výkonnosti

a kvality procesov vytypovaného pracoviska zavedením vytypovaných technických ukazovateľov a návrhov nápravných opatrení.

Pre zaistenie udržateľnosti výkonnosti a kvality procesov pracovísk vybraného podniku sa odporúča ešte rozšíriť vytypovanú skupinu troch technických ukazovateľov údržby o ďalšie dva ukazovatele, napr. ukazovatele prevádzková spoľahlivosť a podiel údržby [2]. Aplikovanie takéjto rozšírenej skupiny ukazovateľov umožňuje lepšie stabilizovať udržateľnosť výkonnosti a kvality procesov pracovísk podniku. Konkrétne aplikácie takéjto rozšírenej skupiny ukazovateľov preukázali, že pomerne v krátkom čase je možné dosiahnuť udržateľnosť výkonnosti pracovísk podniku. Pritom nejde o náročný a zložitý postup a preto je ho vhodné, ako ďalšie pokračovania v zlepšovaní kvality procesov údržby v podniku využiť i v tomto prípade aplikácie.

Samozrejme, že v rámci neustáleho zlepšovania výkonnosti a kvality procesov vybraného podniku sa odporúča ďalej v zlepšovaní pokračovať v tomto podniku aplikovaním ešte ďalších ekonomických a organizačných ukazovateľov výkonnosti a kvality procesov pracovísk podniku. Jedine takýto komplexný prístup umožní dosiahnutie trvale stabilizovanie udržateľnosti procesov údržby a ich výkonnosti.

Táto publikácia vznikla v rámci realizácie projektu "Trenčianska univerzita Alexandra Dubčeka chce ponúkať kvalitné a moderné vzdelávanie", ITMS kód 26110230099, podporovaného z Operačného programu Vzdelávanie a financovaného zo zdrojov Európskeho sociálneho fondu.

Referencie

[1] CIBULKA ,V., FABO, M., Riadenie procesov výroby pomocou technických kľúčových ukazovateľov výkonnosti údržby, TRANSFER 2013, 13. medzinárodná vedecká konferencia, Trenčín, 17. – 18. Októbra 2013, ISBN 978-80-8075-607-9, s. 1 - 6.

[2] CIBULKA, V., Impact of quality of maintenance on operational reliability and selected technical performance indicators of a technological workplace, In: Transport means 2014 : Proceedings of the 18th international conference. Kaunas : Technologija, 2014. ISSN 2351-4604. s. 438-441.

[3] CIBULKA, V., Systém manažérstva kvality v údržbe techniky, In: Vedecké práce a štúdie Fakulty špeciálnej techniky : 2013/2014. Trenčín : TnUAD, 2014. ISBN 978-80-8075-673-4. - Roč.10, s.38-49, CD ROM.

[4] CIBULKA, V., Kvalita produktov špeciálnej techniky, In: ICMT´- 2014 : International conference on military technologies and special technologies 2014. Trenčín : TnUAD, 2014. ISBN 978-80-8075-639-0. s. 52-57, CD ROM.

[5] GRENČÍK, J. et al., Manažérstvo údržby, Synergia teórie a praxe, Vydala Slovenská spolčnosť údržby, BEKI design, s. r. o. Košice, 2013, ISBN 978-80-89522-03-3, 630 s.

[6] HELEBRANT, F., Technická diagnostika a spolehlivost, Ostrava, VŠB-TU Ostrava, Fakulta strojní, 2008, ISBN 978-80-248-1690-6.130.s..

[7] CHOVANEC, A. et al., Komplexná starostlivosť o stroje a zariadenia, Trenčín : TnUAD, 2008, 281 s., ISBN 978-80-8075-351-1.

[8] Jonker, R., Haarman, N., Value Driven Maintenance: What is the actual added value of maintenance ? Uptime, 11., http://reliabilityweb.com

[9] Parida, A., Kumar, U., Maintenance Performance Measurement - Methods, Tools and Applications,In: Maintworld 1 - 2009, Vol. I, KP – Media OY, Helsinki, ISSN 1798-7024, pp. 30 -33.

[10] Smith, R., Hawkins, B., Lean Maintenance, reduce costs, improve quality, and increase market share. Elsevier Butterworth–Heinemann, 200 Wheeler Road, Burlington, MA 01803, USA, 2004, 287 s., ISBN 0-7506-7779-1.

[11] STN EN 13306, Údržba. Terminológia údržby (Maintenance.Maintenance terminology), 2011, Slovenský ústav technickej normalizácie, Bratislava.

[12] STN EN 15 341, Údržba, Kľúčové ukazovatele výkonnosti, 2007, Slovenský ústav technickej normalizácie, Bratislava.

[13] STN EN 60300-3-11, Manažérstvo spoľahlivosti. Časť 3-11: Návod na používanie. Údržba zameraná nabezporuchovosť, Slovenský ústav technickej normalizácie, Bratislava.

[14] STN EN 61703, Matematické vyjadrenie bezporuchovosti, pohotovosti, udržiavateľnosti a zabezpečenia údržby, 2003, Slovenský ústav technickej normalizácie, Bratislava.

[15] VALENČÍK, Š., Údržba a obnova strojov, Košice: EVaOL, Strojnícka fakulta TU Košice, 2010, 417 s., ISBN 978-80-533-0514-1.

[16] VALENČÍK, Š., Metodika obnovy strojov, Košice: EVaOL, Strojnícka fakulta TU 2011, ISBN 978-80-533-0679-7, 330 s.

Surface treatment technologies for wear resistance increasing of 42CrMo4 steel

Van Thanh Doan [1], David Kusmic [2], Miroslav Pospichal[3]
[1]Faculty Of Military Technology, University of Defence in Brno, Kounicova 65, 662 10 Brno, Czech Republic. E-mail: thanhvan.doan@unob.cz
[2]Faculty Of Military Technology, University of Defence in Brno, Kounicova 65, 662 10 Brno, Czech Republic
E-mail: david.kusmic@unob.cz
[3]Faculty Of Military Technology, University of Defence in Brno, Kounicova 65, 662 10 Brno, Czech Republic
E-mail: miroslav.pospichal@unob.cz

The present study was directed to investigate the mechanical and tribological properties of 42CrMo4 (CSN 41 5142.3) steel, which was chemical–heat treated by the technologies of tenifer, manganese phosphate and plasma nitriding combining with blackening. Plasma nitriding was carried out for the samples under different condition of gas mixture under temperature of 480ºC (plasma sputtering) and 500ºC (plasma nitriding process) for 10h. Besides determining the microhardness (HV 0.05), surface hardness, and microstructure, this paper is also focused in the field of wear resistance evaluation and friction coefficient of these surface treatments. Based on "ball on flat" test, calotest, and profile observation, it was found that tenifer technology is suitable to increase the wear resistance, and manganese phosphate improved clearly not only wear resistance but also friction coefficient, which can be usable for weapon production.

Keywords: Wear resistance, Friction coefficient, Plasma nitriding, Tenifer, Manganese Phosphate

1 Introduction

Every branch of engineering is related to friction and wear, cause of their influence to surface degradations, lack of mass, energy, and failure [2], [6] . In regard to weapons, gun barrel, as the most important parts of small arms are affected by friction and wear. Tribologic degradation of material leads to reduce tactical and technical characters of weapon systems such as shot accuracy, firing range, and appearing surface failure in the barrel bore, resp. to reduce their lifetime [7][8]. The chosen steel 42CrMo4 is widely used as material for barrel, especially for small arms, ex. barrel, breech bolt, and gas piston manufacturing.
An outstanding conception to improve the tribological characteristics of materials is to combine some types of surface chemical-heated treatment. As we know [1], [3], [5] about the plasma nitriding and tenifer technology are very acceptable processes to improve hardness, wear resistance for engineering parts while manganese phosphate can enhance the friction coefficient. This paper is focused to study of increasing possibility of wear resistance of 42CrMo4 steel using the plasma nitriding, tenifer, manganese phosphate, blackening technology and duplex layer of plasma nitriding in barrel production. Tribological behavior of ISO 42CrMo4 low alloy steel treated by variety of chemical-heat treatments above was investigated under unlubricated sliding conditions or rotary motion of steel ball with presence of abrasive.

2 Experiment

Untreated samples of 42CrMo4 steel were manufactured in the form of 50x50x5 mm and marked according to Tab. ***1***.

Tab. 1 *Surface treatment and samples marking*

Number	Meaning
1	PN[1] 1 [l/h]
2	PN 2 [l/h]
3	PN 1 + blackening
4	PN 2 + blackening
5	PN 1 + manganese phosphate
6	PN 2 + manganese phosphate
7	Tenifer
8	Manganese phosphate

The elemental weight percentages of the chose material were determined by spectral analysis using the GDOES/BULK LECO SA 2000 device. Chemical composition according to ISO steel standard and result of GDOES/Bulk measurement is in agreement (see Tab. 2).

[1] Abrreviation of plasma nitriding

Tab. 2 *Chemical composition of 42CrMo4 steel (wt%)*

Element	C	Mn	Si	Cr	Ni	Mo	Cu	P	S
ISO standard	0.38-0.45	0.5-0.8	0.17-0.37	0.9-1.2	≤ 0.5	0.15 - 0.3	≤ 0.3	≤ 0.03	≤ 0.03
GDOES/Bulk	0.42	0.6	0.20	1.0	0.02	0.18	0.01	0.001	0.001

After hardening and tempering to obtain the optimal mechanical properties, the samples were cleaned and plasma nitrided (process parameters given in Tab. 3).

Tab. 3 *Plasma nitriding conditions*

Process	Temperature [°C]	Duration [h]	Pressure [Pa]	Impulse length [µs]	Interval length [µs]	Voltage [V]	Gas mixture (l/h) H_2	Gas mixture (l/h) N_2
Plasma cleaning	480	0.5	80	100	180	800	20	2
Plasma nitriding 1	500	10	280	100	140	530	24	8
Plasma nitriding 2	500	10	280	75	140	530	8	24

Plasma nitriding process No. 1 is different to plasma nitriding process No. 2 by gas composition: Nitriding 1 was processed under gas ratio of $3H_2$:$1N_2$, spite of ratio of $1H_2$:$3N_2$ used for nitriding 2. This difference of gas mixture leads to distinct microstructure and nitride layer properties.

Based on Vickers method, microhardness was measured using the LECO M 400H device under loading of 0.05 kp (0.5 N). Figure 1 specifies the progress of microhardness measurement of samples PN 1, duplex PN 1 and tenifer. Figure 2 shows progress of microhardness profile of specimens PN 2, duplex PN 2, and manganese phosphate.

Besides, the surface hardness test was carried out using the apparatus LECO LV 800.

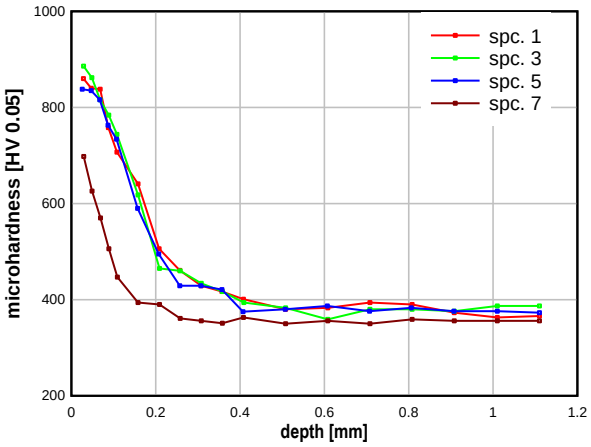

Fig. 1 *Microhardness of samples PN 1, their duplex treatment, and tenifer*

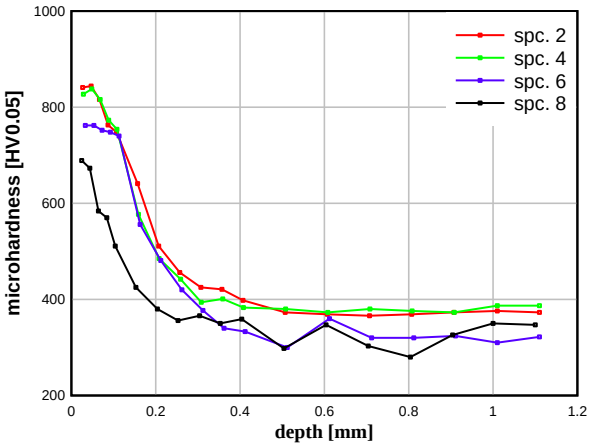

Fig. 2 *Microhardness of samples PN 2, their duplex treatment, and manganese phosphate*

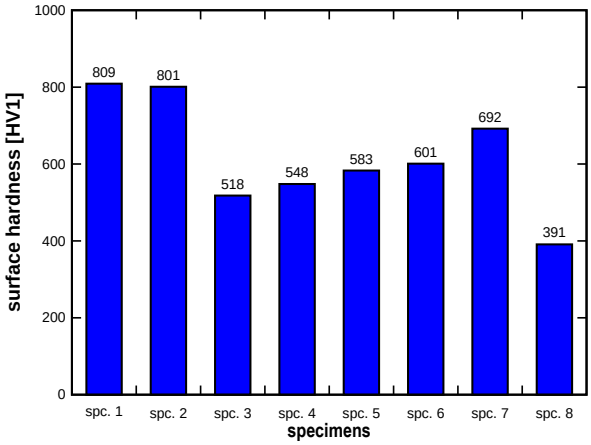

Fig. 3 *Surface hardness measurement*

The main part of experimental were related to adhesive and abrasive testing. The "*ball on flat''* tests, realized in accordance to ASTM G133-95 were carried out on the tribometer CETR UMT-3 by a steel ball of diameter 9.53 mm (3/8 inches). Parameters were set as following: applied load of 20 N, the sliding track of 20 mm, frequency of reversing motion 3 Hz, increasing load time of 10 seconds, loading duration of 180 seconds. This test allows to determine the adhesive wear and friction coefficient during sliding motion as a function of time.

Abrasive wear tests were carried out by combining calostest with profilometer. The steel ball was transferred to turn round associated presence of diamond abrasive paste of grain size 1 µm. Then at the surface appeared trace of wear. The equipment Talysurf CLI 1000 profilometer was used for evaluating depth penetration

3 Results

As seen in the Fig. 1 and Fig. 2 that duplex layers treated by plasma nitriding (samples 1, 2, 3, 4, 5, 6) have great microhardness; tenifer also has relatively high hardness too. On the contrary, manganese phosphate (spc. 8) and tenifer (spc. 7) have lower microhardness values.

The Fig. 3 also shows that manganese phosphate sample has the lowest surface hardness, and the duplex treatment decreases the surface hardness of nitrided samples. However, this affect is not equal at treatment methods and type of plasma nitriding. The duplex nitriding + blackening (samples 3, 4) decreases hardness over the duplex nitriding + manganese phosphate (samples 5, 6). Moreover, although specimen of nitriding sample 1 has higher hardness than nitriding sample 2 but after blackening and phosphate treatment, the sample of nitriding 1 reached lower hardness values than nitriding sample 2.

Degree of adhesive wear of specimens given in Fig. 4 has a same trend like surface hardness measuring (see Fig. 3). Blackening reduces adhesive wear of nitrided steel very well while manganese phosphate also reduces this wear but weaker. Nitrided specimens have the highest adhesive wear. In contrary, manganese phosphate has the lowest adhesive wear.

The other important evaluated parameter was the friction coefficient. In the most machine parts, we expect the low friction coefficient during working to reduce material degradation. The results given in Fig. 5 shows that: The manganese phosphate sample (spc. 8) exhibits a low friction coefficient and thus it allows to reduce friction coefficient of plasma nitrided samples (spc. 5, 6). These three samples were valuated friction coefficient μ just from 0.1 to 0.16 during the tests. At the contrary, blackening increases valuation μ of nitrided sample up to 0.37. Tenifer has slightly higher valuation μ than nitrided samples. On the other hand, the sample PN 2 has lower value of μ than the sample PN 1.

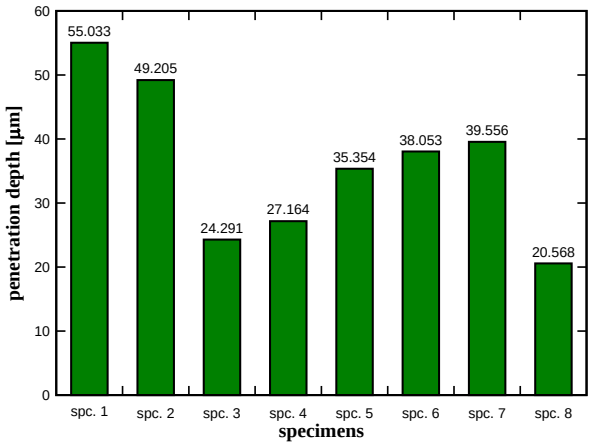

Fig. 4 *Adhesive wear*

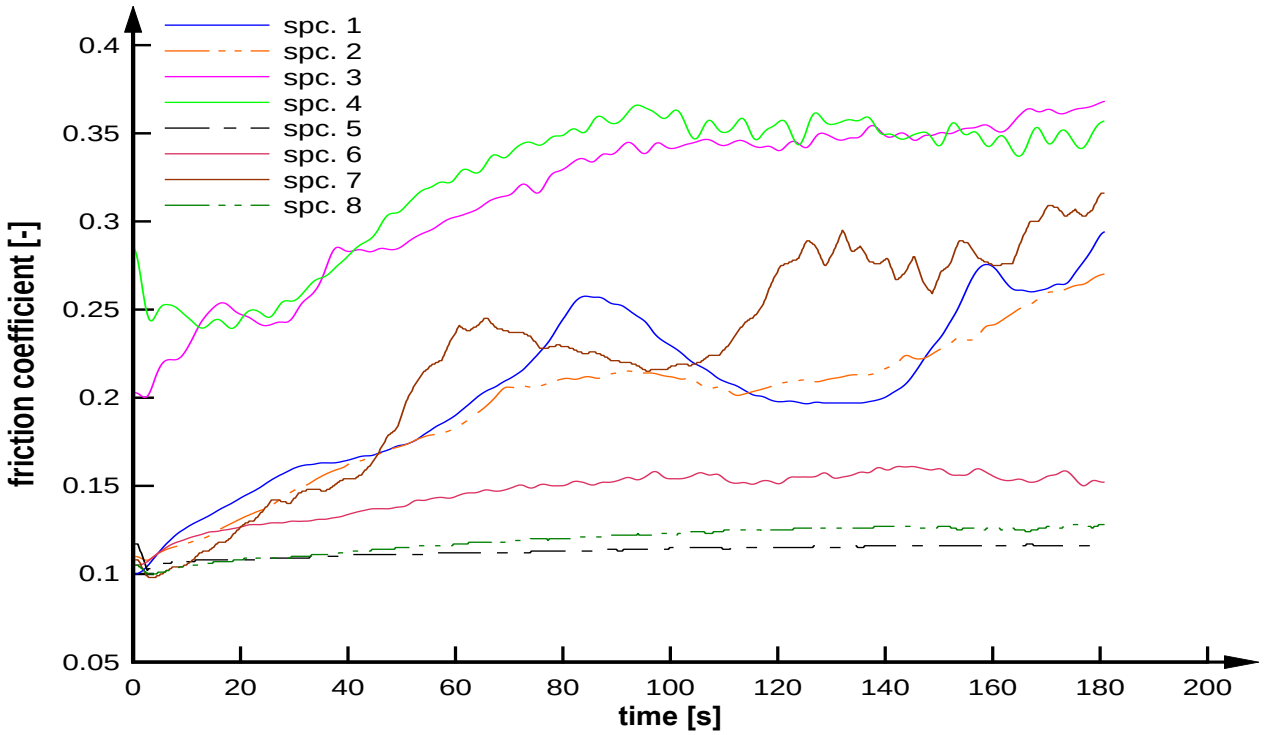

Fig. 5 *Friction coefficient*

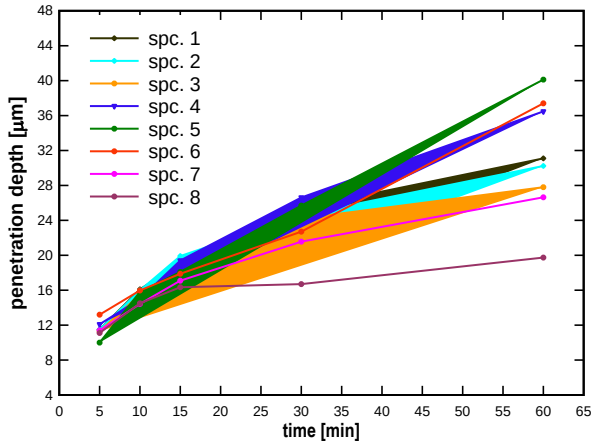

Fig. 6 *Relation of penetration depth to time*

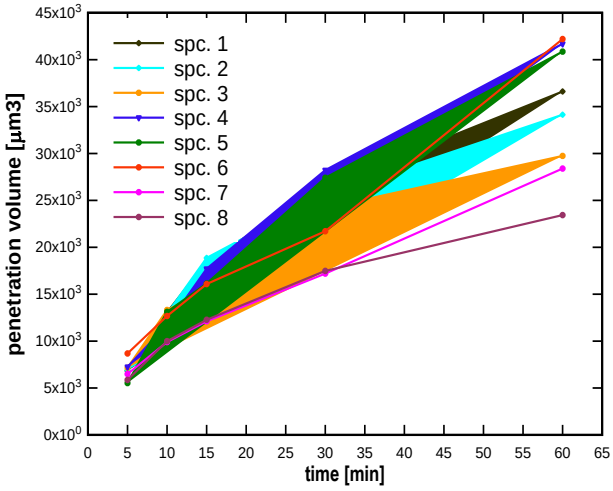

Fig. 7 *Relation of waste volume to time*

The results of abrasive tests plotted in Fig. 6 and Fig. 7 demonstrates relation between the penetration depth of steel ball or waste volume of sample surface and time. Relation of abrasive wear to test time has a form of parabola. On first phase, the wear has not a marked difference. Nevertheless, after 15 minutes testing, the difference became longer, and after 60 minutes, the difference of penetration between the samples was the greatest. Two graphs have similar tendency to each other with highest wear degradation of three samples: duplex PN 1 + manganese phosphate, duplex PN 2 + manganese phosphate and duplex PN 2 + blackening. Among them, the deepest penetration of duplex PN 1 + manganese phosphate and the highest waste volume of duplex PN 2 + manganese phosphate. These graphs also shows that the lowest wear degradation is manganese phosphate and tenifer. However, the deference between these two samples is sufficiently great.

4 Concluding

- The hardness measuring demontrates that plasma nitrided specimens and their combination with blackening and manganese phosphate (duplex treatment) have great value of microharness and surface hardness. Reversely, manganese phosphate has the lowest hardness.
- Althought plasma nitrided samples have great hardness values but they do not show a well wear resistence. This phenomenon can be explained by existence of white layer, which is created after plasma nitriding [1] [3][5]. This layer exhibits high hardness but also britlle and during calotests, by definite cycles, this layer was delaminated (damaged) and plays affects as aditional abrasive. And by this way it increases wear degradation.
- Progress of friction coefficient does not corresponds to level of adhesive wear. Duplex plasma nitriding + blackening demonstrates the highest friction coefficient but the penetration depth of the testing ball on the surface is quite small (just the manganese phosphate was better).
- Manganese phosphate and blackening supports the nitrided layer to improve not only the adhesive resistence but also the friction coefficient. Althought the effect is not the same: manganese phosphate decreases value of friction coefficient markedly while the blackening decreases significantly the adhesive wear.
- Manganese phosphate and tenifer are **the most suitable** to increase wear resistance of adhesive and abrasive type. But their application should be applied carefully because manganese phosphate can not keep this good characters in high temperature (about 300 ºC). The recommendation is to set the components treated at lower temperatures.

5 Discussion

- Calotest is primarily used to investigate the depth of thin coating and using calotest is not optimal to evalute abrasive wear because of displacement of specimens after each cycle to measuring.
- It is interesting that result of adhesive test is not coincident to hardness tendency. As seen in Fig. 3, Fig. 4 the higher is hardness, the greater is penetration depth of test steel ball, resp. the lower adhesion resistance. This result seems to be an unreality because we try to enhance surface hardness of components.
- Using technology of surface treatment, expecially plasma nitriding is an actually tendency to increase the wear resistance of weapon components, leading to decrease of friction coefficient and increasing the wear resistance Tenifer has been used in barrel production for a long time, but plasma nitriding is in the period of experience. Problem is, that the white layer is brittle and under impact and tensile loading cracking of white layer occurs and the white layer can peel off. These experiments demonstrated facility to apply the plasma nitriding technology to increase the wear resistance. However, it is nesessery to solve subsequent problems and nitriding process parameters should be carefully studied. Besides, duplex coating is a good way to create multi-layer structure to improve abrasive and adhesive wear of nitrided surface.
- It is clear that plasma nitriding of deep hole is quite different than application for plane surface. For these purpose is necessary to investigate tribological characteristics of barrel, resp. other components, it is neccesary to combine laboratory and shooting experiment.
- Except of barrel, chemical-heat treatment can be applied to other components of weapon system: sliding track, piston of gas bolt. But it should be said that lifetime of component also depends on maintenace, and working condition.

Acknowledgement

The paper was prepared with the support of the Project for the Development of the Organization and by the Specific research project 2014 of the Department of Mechanical Engineering, UoD "Promoting Research, Science and Inovation in the Field of Engineering".

References

[1] HRUBY, V. (2007). *Nová technologie úpravy hlavních součástí pistolí: navržena v rámci řešení výzkumného záměru FVT 0000404 Výzkum a vývoj moderních materiálů a technologií pro aplikace u vojenské techniky*. Univerzita obrany, Brno.

[2] SUCHANEK, J., KUKLÍK, V., ZDRAVECKÁ, E. (2007). *Abrazívní opotřebení materiálů*. České vysoké učení technické, Praha, ISBN 978-80-01-03659-4.

[3] HRUBY, V., HOLEMAR, A, (1991). *Katalog technologických listů iontové nitridace*. Brno, STROJTECH.

[4] BEČKA, J. (1997), *Tribologie*. Vyd. 1, Vydavatelství ČVUT, Praha, ISBN 8001016218.

[5] HOLEMAR, A., HRUBY, V., (1989). *Iontová nitridace v praxi*. 1. vyd. Státní nakladatelství technické literatury, Praha.

[6] HUTCHINGS, I. *New directions in tribology: plenary and invited papers from the First World Tribology Congress 8-12 September 1997* : organised by the Tribology Group of the Institution of Mechanical Engineers (IMechE). Bury St Edmunds: Published by Mechanical Engineering Publications for the Institution of Mechanical Engineers 1997, [12], 500 s. ISBN 1860580998.

[7] POPELÍNSKÝ, Lubomír. *Československé automatické zbraně a jejich tvůrci*. Vyd. 1. Praha: Naše vojsko, 1999, 198 s., [72] s. obr. příl. ISBN 8020605673.

[8] LUGS, Jaroslav. *Ruční palné zbraně: soustavný přehled ručních palných zbraní a dějin jejich výroby*. Praha: Svojtka & Co., 2003, 412 s. ISBN 8072376640.

[9] AUTAY, R., M. KCHAOU a F. DAMMAK. Friction and wear behaviour of induction hardened ISO 42CrMo4 low-alloy steel under reciprocating sliding conditions. *Proceedings of the Institution of Mechanical Engineers, Part J: Journal of Engineering Tribology*. 2014, vol. 229, issue 2, s. 115-125. DOI: 10.1177/1350650114544201.

[10] HALILA, F., C. CZARNOTA a M. NOUARI. New stochastic wear law to predict the abrasive flank wear and tool life in machining process. *Proceedings of the Institution of Mechanical Engineers, Part J: Journal of Engineering Tribology: 976-1350*. Jena: VEB Gustav Fischer, 2014, vol. 228, issue 11, s. 1243-1251. DOI: 10.1177/1350650114521405.

[11] DZIERWA, A., P. PAWLUS a W. ZELASKO. Comparison of tribological behaviors of one-process and two-process steel surfaces in ball-on-disc tests. *Proceedings of the Institution of Mechanical Engineers, Part J: Journal of Engineering Tribology: 976-1350*. Jena: VEB Gustav Fischer, 2014, vol. 228, issue 10, s. 1195-1210. DOI: 10.1177/1350650114542628.

The Assessment of Selected Mechanical Properties of Steel after Application of Plasma Nitriding

David Dobrocký[1], David Kusmič[1]
[1]Faculty of Military Technology, University of Defence in Brno. Kounicova 65, 662 10 Brno. Czech Republic. E-mail: david.dobrocky@unob.cz, david.kusmic@unob.cz

The article deals with mechanical properties of plasma nitrided steel. Experimental work was focused on evaluation of influence of plasma nitriding process to notch toughness of steel, the experimental were realised on V-notch samples of size 10x10x55 mm (according to CSN ISO 148-1 standard). Nitrided layers were applied to steel 30CrMoV9 which were subsequently evaluated by metallographic, GDOES and microhardness method. The notch toughness tests of steel were carried out using the instrumental Charpy hammer at temperatures -40 °C, +21 °C and + 70 °C. The results of experiments showed that plasma nitriding process has a direct impact on change of notch toughness parameters. The notch toughness of plasma nitrided steel was significantly decreased. The measurements thereinafter showed that values of notch toughness at low temperature (-40 °C) decreased but also at higher temperature (+70 °C). It was found a dependence of notch toughness values of plasma nitrided steel between the testing temperature and plasma nitriding process parameters.

Keywords: Plasma Nitriding, Notch Toughness, V-notch

Introduction

The experimental investigation of a failure mechanism and the values of impact energy or notched impact strength is an integral part of comprehensive research of material limit states, how states Binar et al. (2011) [1]. Many industrial applications require increased demands on components made of structural steels which therefore are further processed to achieve better properties. One of many technologies, which are used to increasing the utility of structural steels, is the plasma nitriding. Plasma nitriding is a method of surface hardening using a d. c. glow discharge to improve the elemental nitrogen to the surface of steel with subsequent diffusion into the core of material, how mention Akbari et al. (2010), Kadlec et al. (2008) and Sirin et al. (2008) [2, 3, 4]. Is generally known, that plasma nitriding increases surface hardness, wear resistance and corrosion resistance. Despite this, it is necessary to take into account the negative effect of plasma nitriding on the values of impact energy and notch toughness, which has been described in works of authors Dobrocký et al. (2014) and Dobrocký et al. (2015) [5, 6]. The submitted paper deals with the influence of selected parameters of plasma nitriding to the fracture behaviour of steel samples made of 30CrMoV9 (CSN 41 5330) steel provided with V-notches (dimensions of V-notch are in accordance with ISO 148-1 standard [7]) compared with not nitrided steel samples. Fracture behaviour of steel was evaluated by the dynamic notch toughness test using the instrumental Charpy hammer Zwick RKP 450 IWI device according to ISO 14556 standard [8] at test temperatures -40 °C, +21 °C and +70 °C. The results of notch toughness are supplemented by evaluation of surface hardness, metallographic analysis and measurement of case depth of the nitrided layer in V-notches root. In the end the fractography was performed.

Experimental procedures

The chemical composition of steel 30CrMoV9 (CSN 41 5330) was verified for selected chemical elements by GDOES/Bulk method using the LECO SA 2000 spectrometer. The measured values of elements concentrations corresponded to tolerances of the standard list values of the steel (Tab. 1).

Tab. 1 *Chemical composition of steel 30CrMoV9 (CSN 41 5330)*

Chemical composition (%wt)								
Element	C	Mn	Si	P	S	Mo	Cr	V
DIN standard	0.24 - 0.34	0.40 - 0.80	0.17 - 0.35	< 0.035	< 0.035	0.20 - 0.30	2.30 – 2.70	0.15 – 0.30
GDOES/Bulk*	0.32	0.74	0.21	0.014	0.0025	0.16	2.75	0.12

*Parameters of GDOES/Bulk analysis: U = 800 V, I = 30 mA, p(Ar) = 314 Pa.

Test samples of the size 10 x 10 x 55 mm were manufactured from the 30CrMoV9 (CSN 41 5330) steel. These samples were subsequently heat-treated through quenching and tempering. The changes of dynamic parameters of the steel after application of plasma nitriding process were investigated on the V-notch samples with a depth of notch 2 mm, which were produced on experimental samples according to the CSN ISO 148-1 standard [7]. The surfaces of specimens were grinded to the value of Ra = 0.4 μm prior to the plasma nitriding process, thereafter specimens were degreased in acetone

and dried. Thus prepared experimental samples were subsequently plasma nitrided in the PN 60/60 RÜBIG device according to the parameters marked in the Table 2. Before the actual process of plasma nitriding was the procedure of plasma cleaning performed under following conditions: T = 480 °C for 30 min, p = 80 Pa in a gas mixture $20H_2$: $2N_2$ (l/h).

Tab. 2 *Parameters of plasma nitriding process*

Parameter	Plasma cleaning	Plasma nitriding					
		I		II		III	
Temperature [°C]	480	450	450	500	500	550	550
Time/Duration [h]	0.5	10	30	8	25	6	20
Flow H_2 [l/h]	20	24	24	24	24	24	24
Flow N_2 [l/h]	2	8	8	8	8	8	8
Pressure [Pa]	80	280	280	280	280	280	280

Twenty pieces of samples were prepared for each type of plasma nitriding process. Five pieces of samples were selected for the metallographic evaluation and evaluation of case depth and fifteen pieces of samples for verification of the dynamic parameters through the notch toughness test after plasma nitriding under selected parameters of the plasma nitriding process. The group of fifteen pieces of samples, which were plasma nitrided under same condition, was divided into three subgroups of five samples. Each of subgroups were tested on the instrumented Charpy hammer at other test temperatures (-40 °C, +21 °C and +70 °C). The metallographic evaluation of the plasma nitrided steel specimens with V-notches was performed on the metallographically prepared cross-sections. The optical microscope OLYMPUS GX 51 equipped by metallographic analysis software was used for measuring of compound layer of nitrided steel samples. As a next step, the surface hardness (HV1) and the depth of the nitrided layer measuring was carried out. The depth profiles of the nitride layers in roots of V-notches were evaluated by the measuring of microhardness profiles using the automatic microhardness tester LECO M-400-H in accordance to the DIN 50190-3 standard [9]. The measurement of microhardness was carried out under loading of 50 g (HV0.05) on the two selected areas of V-notches labelled as "I" and "II" (see Figure 1). The actual evaluation of notch toughness of plasma nitrided samples with V-notches was verified using the instrumented Charpy hammer RKP 450 ZWICK IWI in accordance to the ISO 148-1 [7] and ISO 14556 standards [9]. The fractographic analysis of fracture surfaces was carried out by means of an electron scanning microscope (SEM**)** TESCAN Vega TS 5135. The morphology of fracture was documented on individual samples in the axis of fracture perpendicular to the notch, in the distance approx. 1/3 from the notch, applying the x100 and x1000 zoom.

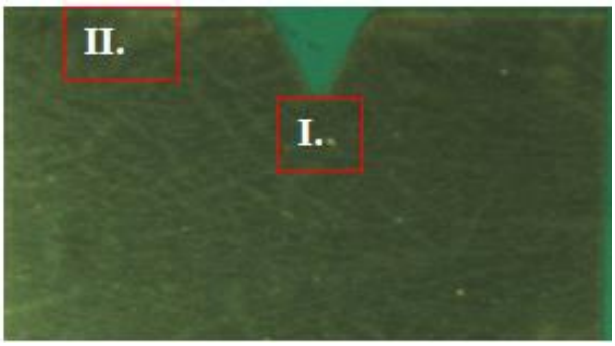

Fig. 1 *Marking the measured areas of nitrided samples*

Results and discussion

The first five plasma nitrided samples from each series was metallographic evaluated using the light microscope OLYMPUS GX 51. The evaluation was focused on the analysis of formed nitrided layers with focusing on presence of brittle compound layer in the V-notch roots and on the microstructure of steel. The assessment of formed layers was focused on the areas of V-notches marked as “I and II” as displayed in Figure 1 (there are the same areas as in the case of measurement of microhardness). The evaluation of the microstructure in areas “I and II” of V-notches showed that in any case of plasma nitriding the compound layer in V-notch root were not created. The nitrided layers were formed only by diffusion layers, as shown in Figure 2. The microstructure of nitrided samples was evaluated as tempered martensite and sorbite. The next step was nitride layer depth measurement of created nitrided layers in V-notch roots. Microhardness profile measurements were performed in roots of notches, marked as "I" and on the surface of samples marked as "II", in Figure 1 and these values were converted to the average values which were summarized for all modes of plasma nitriding in Table 3. The differences between shorter and longer nitriding duration were approximately 0.01 mm in V-notch roots, although the differences between shorter and longer nitriding duration on surfaces were twice higher. Increased case

depths in V-notch roots were achieved after shorter nitriding duration and the lowest values were obtained at nitriding temperature under 550 °C (see Table 3). The decreased values of case depth in V-notch roots are probably caused by a small diameter of V-notch root and therefore behaves as a blind cavity with limited access of plasma, as stated in the work of Pokorný et al. (2011) [10].

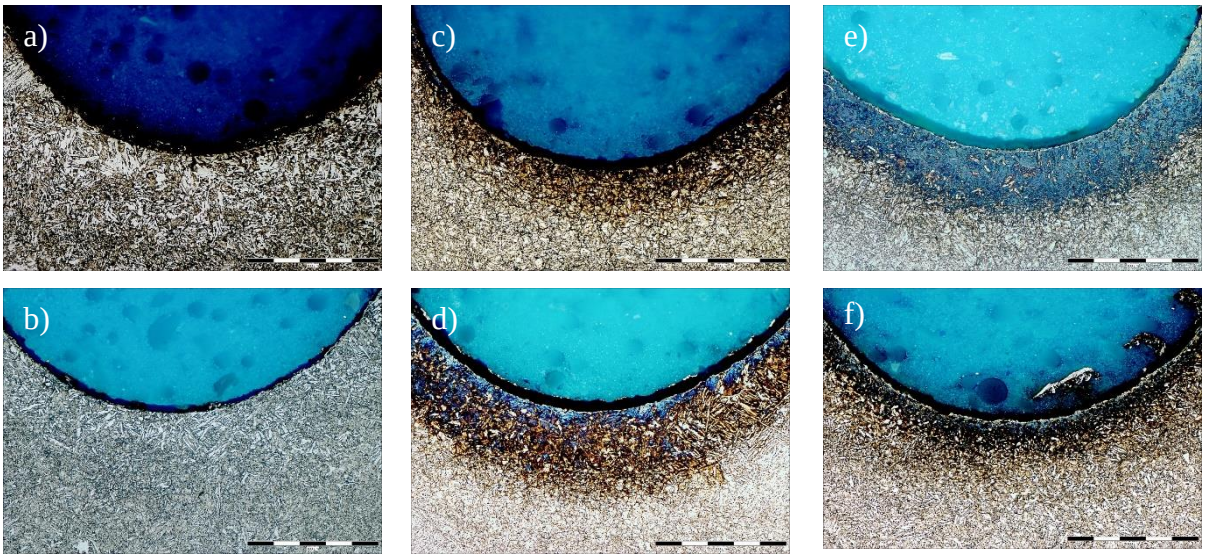

Fig. 2 *Microstructure of V-notch roots after 10 h (a) and after 30 h (b) of nitriding at 450 °C, after 8 h (c) and after 25 h (d) of nitriding at 500 °C, after 6h (e) and after 20 h (f) of nitriding at 550 °C*

It is known that the case depth of nitride layer affects a number of mechanical properties of nitrided steel such as surface hardness, fatigue limit and toughness, as stated in the work of Dobrocký et al. (2014) and (2015) [5, 6]. The values of surface hardness of the material may serve as one of the important indicators of the assumed resulting toughness. For this reason, the surface hardness was evaluated. The surface hardness of plasma nitrided steel specimens was measured using the universal hardness tester ZWICK Roell ZHU 2.5. Five measurements were carried out on each specimen and the surface hardness was set as the average value of these five values. The determined surface hardness values reached higher values, because of presence of the alloying elements in the case of used 30CrMoV6 steel. These alloying elements have high affinity for nitrogen like Al, Mo, V, Cr and W, as is stated in works of Holemář et al. (1989) and Pye (2003) [11, 12]. The monitored steel contains especially Mo, V and Cr. The results of the surface hardness of plasma nitrided samples are summarized in Table 3. The results shows that the surface hardness after plasma nitriding was increased almost three times, from the original value of 400 HV1 (quenched and tempered before plasma nitriding) up to 1167 HV1 (after plasma nitriding process at 500 °C and nitriding duration 8 hours).

Tab. 3 *The results of measurements*

Plasma nitriding parameters		**Measured case depth [mm]**		**Surface hardness [HV 1]**
Temperature [°C]	**Time [h]**	**Surface**	**V-notch**	
Ref.*	0	/	/	400.10 ± 0.40
450	10	0.15	0.07	1044.60 ± 8.46
	30	0.31	0.08	1150.53 ± 4.87
500	8	0.19	0.09	1167.73 ± 21.44
	25	0.37	0.08	1009.27 ± 0.77
550	6	0.16	0.06	985.10 ± 23.98
	20	0.31	0.05	1037.26 ± 12.11

*Reference sample (i.e. not nitrided sample)

A crucial part of the experimental work was to perform the instrumented Charpy test. The actual evaluation of notch toughness of plasma nitrided samples with V-notches was verified using the instrumented Charpy hammer RKP 450 ZWICK IWI with a maximum value of impact work 300 J and an impact velocity of 5.23 m/s, in accordance to the ISO 148-1 [7] and ISO 14556 standards [8]. The results of the absorbed energy (impact energy) and the results of achieved notch toughness values of reference samples compared with nitrided samples for all test temperatures are showed in Table

4. The values of absorbed energy and notch toughness achieved the worst results at test temperature -40 °C (the decrease was approx. of 70 % compared to the values determined at the temperature +21 °C), with increasing test temperature the values of absorbed energy and notch toughness was increased too. Though the highest values of absorbed energy and notch toughness was not achieved at test temperature +70 °C but at test temperature +21 °C (by approx. 15 %). The results also shown that longer nitriding duration at the same nitriding temperature tended to lower values of absorbed energy and notch toughness except plasma nitriding at 550 °C and test temperature -40 °C and +70 °C. It is also evident tendency of slight decrease values of absorbed energy and notch toughness with the increase of nitriding temperature in case of shorter nitriding duration. Longer nitriding duration led to higher values of absorbed energy and notch toughness only at nitriding temperature 450 °C. Higher nitriding temperatures achieved the maximum values after 20 hours at nitriding temperature 550 °C and test temperature -40 °C, after 25 hours at nitriding temperature 500 °C and test temperature +21 °C and after 20 hours at nitriding temperature 550 °C and test temperature +70 °C.

Tab. 4 *The results of absorbed energy a notch toughness at selected test temperatures*

Plasma nitriding parameters		**Test temperature [°C]**	**Absorbed energy KV [J]**	**Notch toughness KCV [J·cm^{-2}]**
Temperature [°C]	**Duration [h]**			
0 (Ref.*)	0 (Ref.*)	-40	73.29 ± 2.79	91.33 ± 3.72
450	10		25.16 ± 4.85	31.39 ± 6.05
	30		13.25 ± 0.50	16.51 ± 0.63
500	8		19.79 ± 4.85	24.63 ± 6.02
	25		15.08 ± 1.70	18.80 ± 2.12
550	6		23.83 ± 1.20	29.90 ± 1.40
	20		26.88 ± 5.26	33.66 ± 6.54
0 (Ref.*)	0 (Ref.*)	21	109.87 ± 14.13	136.87 ± 17.00
450	10		100.30 ± 2.89	125.37 ± 3.39
	30		75.09 ± 4.86	93.92 ± 6.17
500	8		95.06 ± 5.85	118.75 ± 7.41
	25		76.29 ± 0.79	95.36 ± 0.82
550	6		90.44 ± 4.24	113.19 ± 5.11
	20		70.67 ± 5.97	88.40 ± 7.54
0 (Ref.*)	0 (Ref.*)	70	94.52 ± 5.08	117.26 ± 6.31
450	10		89.38 ± 1.63	111.72 ± 2.44
	30		71.00 ± 3.63	88.38 ± 4.57
500	8		82.08 ± 4.09	102.80 ± 5.39
	25		54.55 ± 5.12	68.15 ± 6.46
550	6		72.26 ± 1.89	90.95 ± 2.62
	20		80.54 ± 2.09	100.74 ± 2.89

*Reference sample (i.e. not nitrided sample)

Thanks to measurements it was verified that all selected modes of plasma nitriding processes caused a decrease of values of absorbed energy and notch toughness compared with reference samples. This finding is consistent with previous studies of authors Dobrocký et al. (2014) and (2015), Holemář et al. (1989), Pye (2003), Lattner et al. (2014) and Madl et al. (2013) [5, 6, 11, 12, 13, 14]. The notch toughness values dependence on achieved nitrided layer depths in V-notch roots for plasma nitriding at 450 °C is displayed in Figure 3. The values of notch toughness decrease with increasing of case depth on V-notch roots. In this case of plasma nitriding process it was achieved higher value of case depth after longer nitriding duration. Figure 4 is displaying the notch toughness dependence on nitrided layer depths in V-notch roots at nitriding temperature 500 °C. In this case of plasma nitriding was achieved higher value of case depth after shorter nitriding duration. This trend was also in the case of notch toughness values how is evident in the Figure 4. The highest nitriding temperature also led to creation of higher value of case depth after shorter nitriding duration. The values of notch toughness actually with increasing nitriding duration were increased slightly except the value of notch toughness achieved at test temperature +21 °C (see Figure 5). The graphical dependences of notch toughness on case depths in V-notch roots are displayed in Figures 3 up to 5 it is evident that the highest values of notch toughness were really achieved at test temperature +21 °C. The explanation of this phenomenon has not been done in this work.

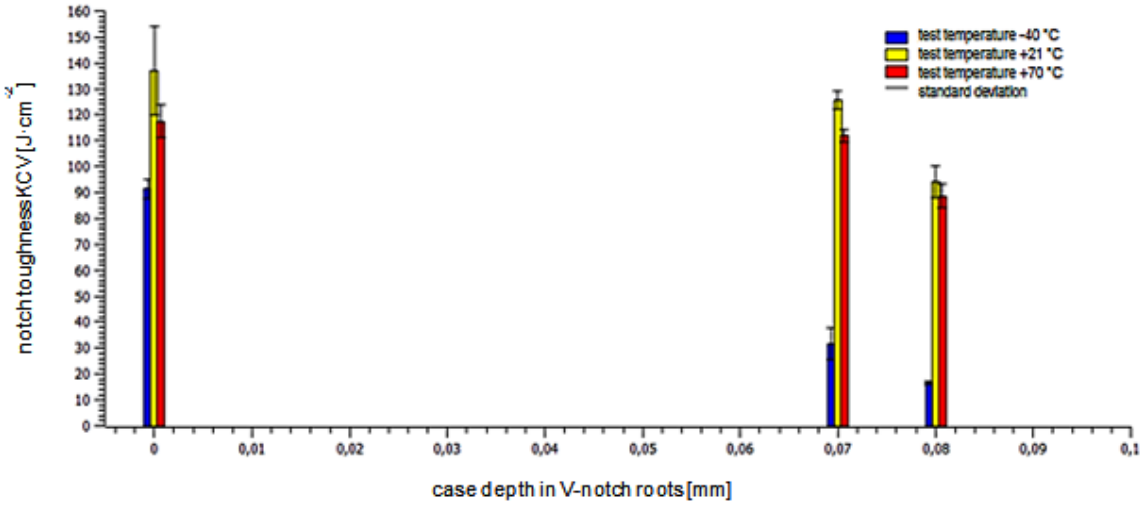

Fig. 3 *The notch toughness dependence on case depths in V-notch roots. Plasma nitriding 450 °C, 10 h and 30 h*

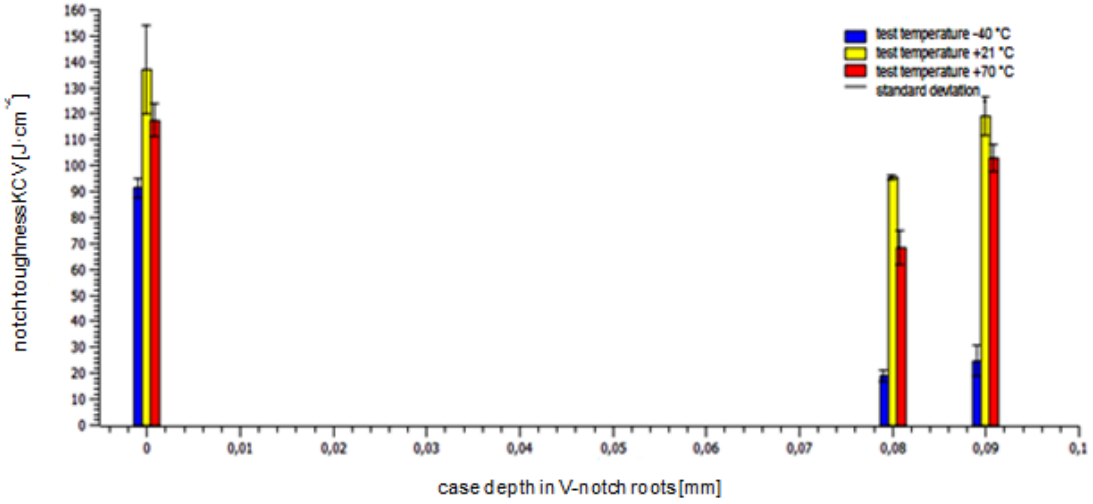

Fig. 4 *The notch toughness dependence on case depths in V-notch roots. Plasma nitriding 500 °C, 8 h and 25 h*

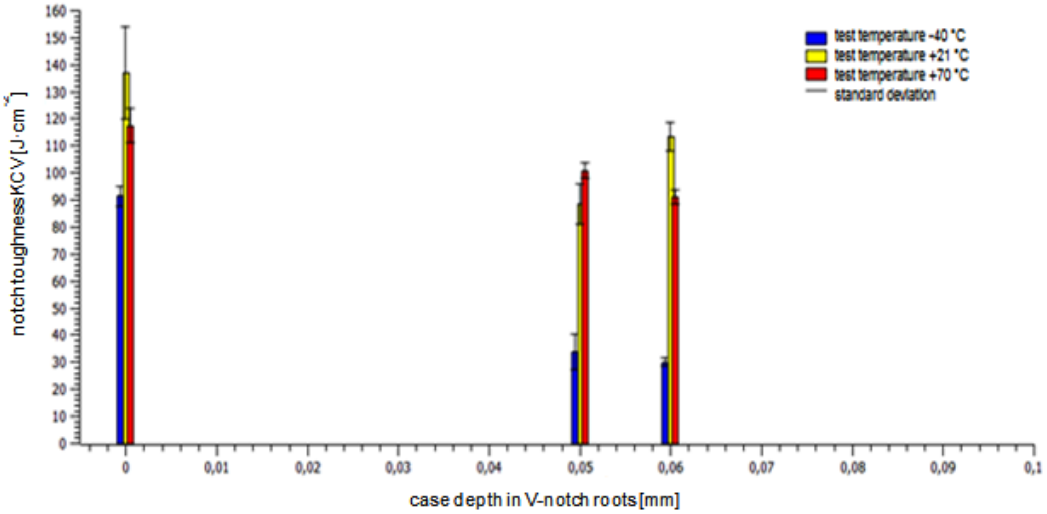

Fig. 5 *The notch toughness dependence on case depths in V-notch roots. Plasma nitriding 550 °C, 6 h and 20 h*

The final part of experimental work was a fractography analysis of fracture surfaces of broken samples. As discussed above, more significant decrease of the notch toughness values was identified at the lowest test temperature -40 °C which was approx. of 70 % compared to the value determined at the temperature +21 °C. The failure mechanism in the lowest

temperature range of test temperatures was transcrystalline quasi-cleavage (Figure 6). A different failure mechanism of 30CrMoV9 (CSN 41 5330) steel was identified. At the highest testing temperatures where the transcrystalline ductile mechanism predominate (Figure 8). It has been proved that the type of failure had an influence on the notch toughness values. The results of the fractographic analysis shows that in the zone under the notch root and in the sphere along the edges of the test samples only ductile dimple fracture mostly of shear character was identified. Micromorphology of fracture surface of the sample at a test temperature of +21 ° C has corresponded to brittle transcrystalline failure with areas transcrystalline ductile failure, i.e. it is a mixed fracture (see Figure 7).

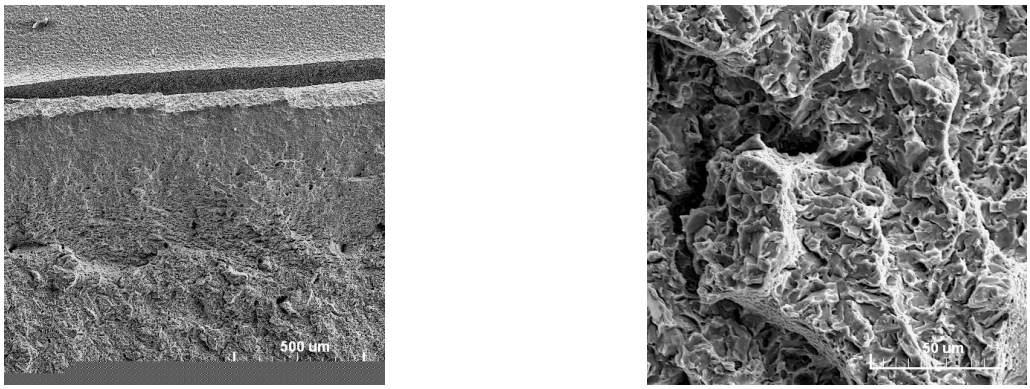

Fig. 6 *Micromorphology of fracture surface of plasma nitrided sample. Plasma nitriding 450 °C, 10 hours, test temperature -40 °C. Magnification 100x left, 1000x right*

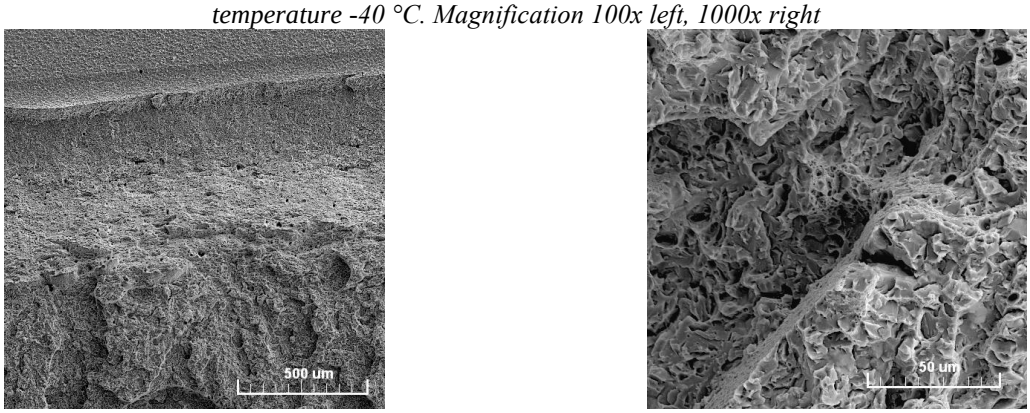

Fig. 7 *Micromorphology of fracture surface of plasma nitrided sample. Plasma nitriding 450 °C, 10 hours, test temperature +21 °C. Magnification 100x left, 1000x right*

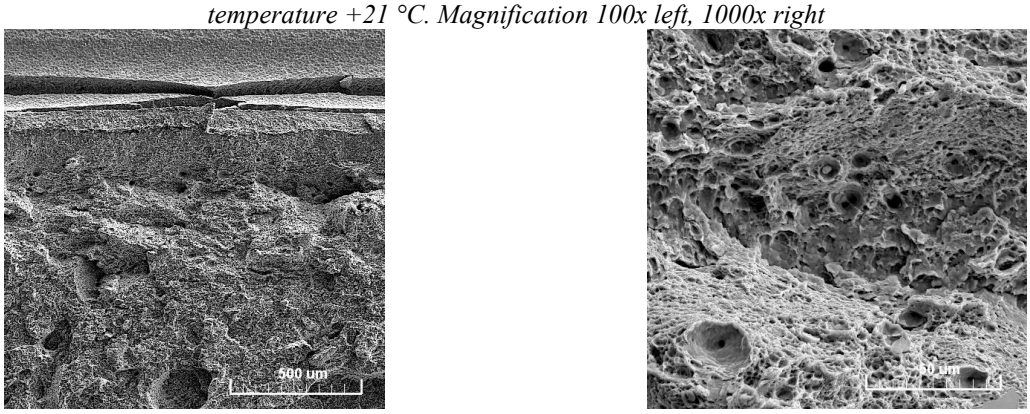

Fig. 8 *Micromorphology of fracture surface of plasma nitrided sample. Plasma nitriding 450 °C, 10 hours, test temperature +70 °C. Magnification 100x left, 1000x right*

As shown in Figures 6 up to 8 with the change of test temperature the morphology of failure surface was changed too. This phenomenon occurred in all temperature modes of plasma nitriding. From the micromorphology of fracture surfaces is visible a change of nature of fracture close the surface of V-notch. Thanks the micromorphology of fracture surfaces is the change the nature of fracture close the surface of V-notch visible. Brittle fracture characteristic for nitrided layer passes into ductile fracture towards the core of material, which is evident from Figures 7 and 8. An exception was found in the case of the fracture surface at a test temperature of -40 ° C, consisting of only brittle failure (see Figure 6).

Conclusion

The experimental work was focused on monitoring of the impact influence of plasma nitriding on to changes of selected mechanical parameters of nitrided 30CrMoV9 (CSN 41 5330) steel. It was experimentally found and confirmed the fact, that the plasma nitriding process has an effect on the reduction of the notch toughness values of 30CrMoV9 (CSN 41 5330) steel. Despite of a fact, that the case depth in V-notch roots achieved only hundredths of a millimeter, the notch toughness values were significantly reduced especially at test temperature of -40 °C. It follows from experimentally determined KCV values that the values decreased by approx. of 70 % compared to the value determined at the test temperature +21 °C. Based on the comparison of the fractographic analysis results carried out for all test temperatures and determined KCV values, the limit state occurrence can be quantified already at temperature -40 °C, because the micromorphology of failure surface determined at the test temperature -40 °C had quite brittle fractures. Generally, the plasma nitriding process increases the surface hardness, wear resistance and corrosion resistance of steel, but simultaneously decreases the notch toughness values.

Acknowledgement

The paper was prepared with the support of the Project for the Development of the Organization and by the Specific research project 2014 of the Department of Mechanical Engineering, UoD "Promoting Research, Science and Innovation in the Field of Engineering".

References

[1] BINAR, T., KADLEC, J., REJZEK, M, VLKOVSKY, M., HRUBY, V. (2011). Evaluation of the test temperature effect on failure mechanisms and notched impact strength characteristics of ultra-hard low alloy steels. In: *Strength of Materials*, Vol. 43, No. 5, pp. 537 – 542.

[2] AKBARI, A., MOHAMMADZADEH, R., TEMPLIER, C., RIVIERE, J. P. (2010): Effect of the initial microstructure on the plasma nitriding behaviour of AISI M2 hihg speed steel. In: *Surface and Coatings Technology*, vol 204, 2010, pp. 4114-4120.

[3] KADLEC, J., DVOŘÁK, M. (2008): Duplex surface treatment of stainless steel $X_{12}CrNi_{18.8}$. In: *Strength of Materials*, vol. 40, 2008, pp. 118-121.NOVY, L. (1996). Sample paper. In: *Sample Journal*, Vol. 3, No. 1, pp. 9 – 15. TTP. Switzerland.

[4] SIRIN, S. Y., SIRIN, K., KALUC, E. (2008): Effect of the ion nitriding surface hardening proces on fatigue behaviour of AISI 4340 steel. In: *Materials Characterization*, Vol. 59, 2008, pp. 351-358.

[5] DOBROCKÝ, D., DOAN, T., KUSMIČ, D., HRUBÝ, V. (2014): The Change of Notch Toughness Parameters of Steel After Plasma Nitriding. In: *ICMT´- 2014*, pp. 66-74.

[6] DOBROCKÝ, D., KUSMIČ, D. (2015): The Effect of Plasma Nitriding Process on the Change of Dynamic Parameters of Steel DIN 1654/4. In: *Manufacturing Technology*, Vol. 15, No. 1, pp. 14 – 20.

[7] ISO 148-1:2009 Metallic materials – Charpy pendulum impact test – Part 1: Test method

[8] ISO 14556:2000 Steel – Charpy V-notch pendulum impact test – Instrumented test method

[9] DIN 50190-3 – Hardness depth of heat-treated parts; determination of the effective depth of hardening after nitriding. Deutsches Institut für Normung E. V., 1979.

[10] POKORNÝ, Z., KADLEC, J., HRUBÝ, V., JOSKA, Z., TRAN, D. Q. (2011): Mechanical Properties of Steels after Plasma Nitriding Process. In: *Journal of Materials Science and Engineering*, Vol. A1, pp. 42-45.

[11] HOLEMÁŘ, A., HRUBÝ, V. (1989): Iontová nitridace v praxi. SNTL, Praha 1989, pp. 178-180.

[12] PYE, D. (2003): Practical nitriding and ferritic nitrocarburizing. 2nd edition, Ohio: ASM International Materials Park 2003, pp. 127-129.

[13] LATTNER, M., HOLESOVSKY, F. (2014): Effect of Machining the Load Capacity Notched Components. In: *Manufacturing Technology*, vol. 14, 2014, pp. 47-50.

[14] MADL, J., RAZEK, V., KOUTNY, V., KAFKA, J. (2013): Surface Integrity in Notches Machining. In: *Manufacturing Technology*, vol. 13, 2013, pp. 188-193.

The Al alloy materials and their quality

Josef Formánek[1], Ludmila Kučerová[2]
[1]Faculty of Mechanical Engineerin, Department of Machine Design, University of West Bohemia in Pilsen, Univerzitni 22, 306 14 Pilsen, Czech Republic, E-mail: formanek@kks.zcu.cz
[2]Faculty of Mechanical Engineerin, Department of Material Science and Techology, University of West Bohemia in Pilsen, Univerzitni 22, 306 14 Pilsen, Czech Republic, E-mail: skal@kmm.zcu.cz

Various materials can be used nowadays for construction of vehicles, the production machines and other technical devices, ranging from aluminum alloys and composite materials to high strength steels. For successful utilization of Al alloys, it is advantageous to use necessary calculations using FEM and computer simulation tests to verify engineering construction design. This can help to map and take advantage of the potential of the material. On the other hand, the proper observance of the manufacturing process, the chemical composition and microstructure of selected structural material can provide us with important information. Material purity, homogeneous chemical composition, the correct production process, technological processing etc., are decisive for the further use of the material for the construction elements of the technical device in the form of a fully-functioning components with the required lifetime.

Keywords: Defects, poor quality, Al alloys, fracture analysis

1 Introduction

Various materials can be used nowadays for vehicle construction, ranging from aluminium alloys and composite materials to high strength steels [1,2]. The quality of the cast, the correct production process, technological processing, etc., are crucial for the further use of the material for the construction elements of a technical device. Poor quality materials used in technical equipment can cause not only severe material damage, but they also present high safety risks for humans involved, as they can cause injury or death.

2 Prerequisite for construction

Al alloys of various compositions have long been used for components of technical equipment. In this case Al-Si alloy was used to produce part of the front fork for a downhill sports scooter (see Fig. 1)", where any technical defects not only damage certain parts, but can also be dangerous for the safety of the rider, who can be seriously injured or even killed. The front suspension is very exposed, and it requires high-quality material composition, processed in to the final form. Technical requirements with design calculations can be taken into consideration using the finite element method (FEM) and software simulations in a PC. These methods enable us to identify and fully utilize the potential of the material. However, despite the help of advanced simulation and computational software, the quality of the final product can be achieved only when the declared material is really the material specified by the manufacturer.

The front forks have a lifetime warranty, and subsequent control simulation using FEM verified that the front forks have a real long-term durability of several tens of years. The reality was however different, this part broke after about 700 km, the damage being at the front wheel mounts. Small initialization cracks were found upon closer examination (see Fig. 2). According to the basic simulation in the SW, it was verified that the carrier profile was sufficiently structurally designed to bear the load and therefore we proceeded to carry out material and fracture analysis. Metallographic sections were created and examined in detail with surprising results.

Fig. 1 *The front fork of a downhill sports scooter*

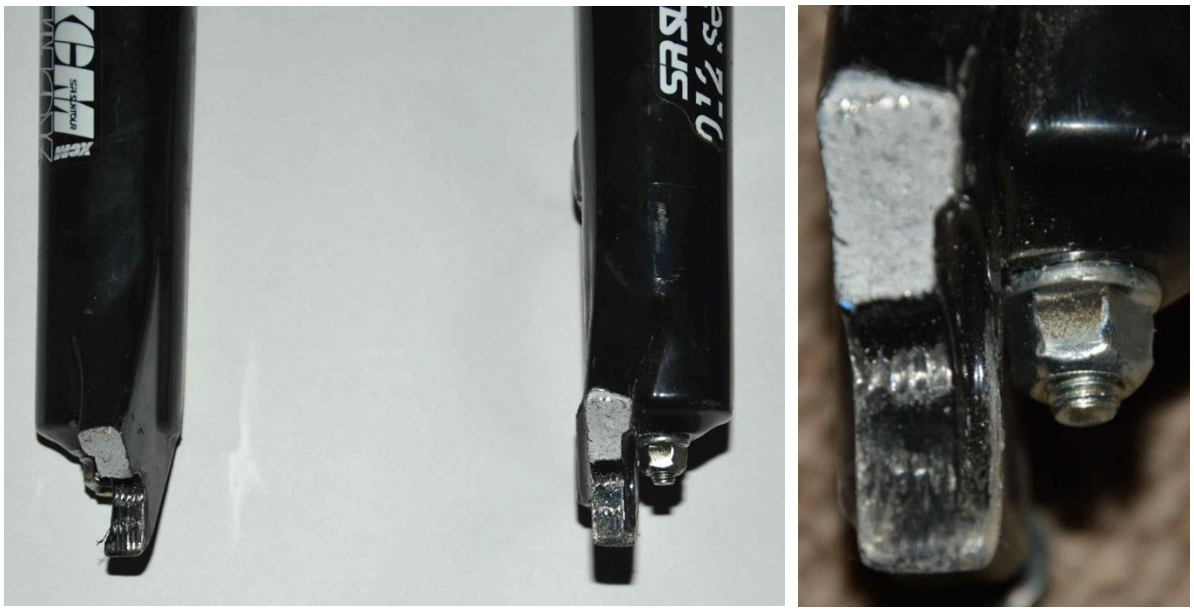

Fig. 2 *The damage to the front wheel mounts and detail of damage*

3 The material analysis

Metallographic and fractographic analysis of the fractured part was carried out using a scanning electron microscope and a light microscope with Lucia image analysis software. The material of the fork was Al-Si alloy with about 10% silicon, further alloyed by small amounts of copper, manganese and iron. Small additions of iron (around 0.2%) are beneficial for the improvement of impact resistance and endurance limit of Al-Si alloys, as was already tested with EASA alloy [3].

3.1 Microstructure analysis

A metallographic sample was prepared from an area about 1cm below the fracture surface. Many pores and shrinkages of various sizes were observed at the polished surface of the sample, proving the poor quality of the material. These defects were so large that they were also visible by the naked eye, some of them reaching sizes in the range of mm (Fig.3).

The sample was further etched using Keller reagent to reveal the microstructure. The microstructure was dendritic and rather complex, consisting of solid solution matrix with Al-Si eutectic among them (Fig.4- Fig. 6). A relatively large fraction of the microstructure, about 50%, consisted of primary aluminium α-Al dendrites distributed relatively evenly in a eutectic matrix.

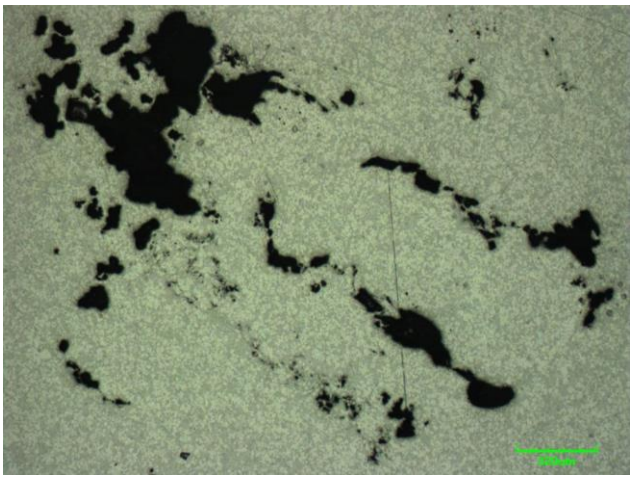

Fig. 3 *Large shrinkage in material*

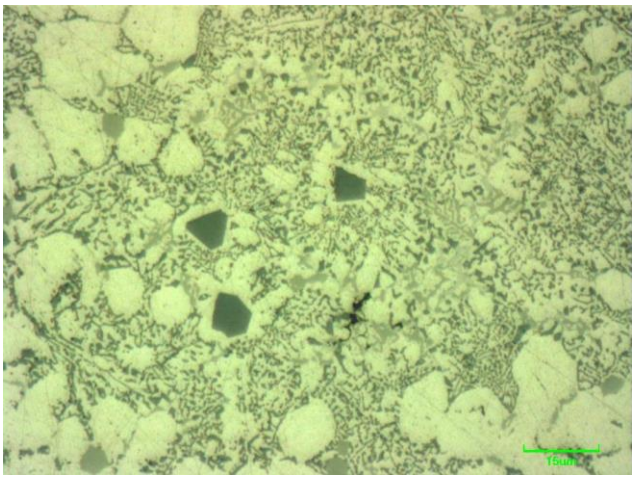

Fig. 4 *Dendritic microstructure with eutectic network and several kinds of particles*

Local chemical composition of individual structural components was established by point and linear EDX analysis. Due to the small size of some of the particles, the effect of Al-Si matrix composition influenced the obtained values and it is therefore impossible to establish the exact chemical composition of the particles.

There was a network of fine particles with higher Cu and lower Fe content along dendrite boundaries, and two kinds of larger individual particles were found inside the α-Al dendrites. Several dark sharp edged particles of primary Si were observed inside the dendritic areas and occasionally sharp edged light grey particles rich in Fe and Mn, with Fe:Mn ratio around 2:1 (Fig.5-Fig.6).

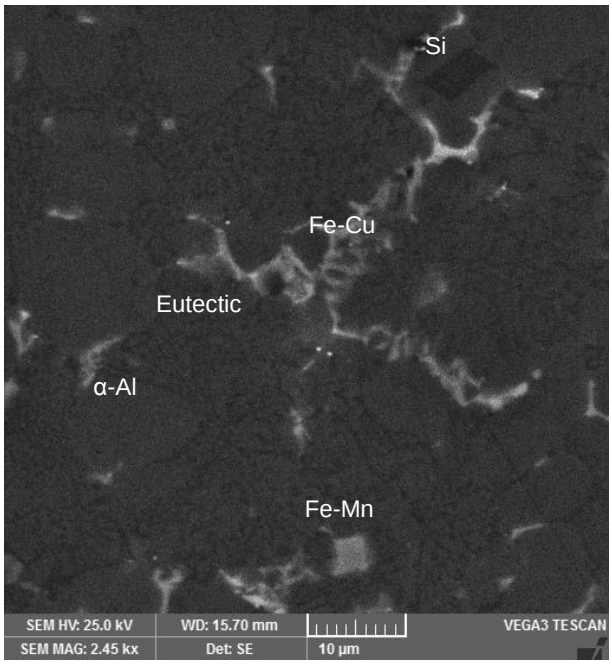

Fig. 5 *Dendritic microstructure of the fork with interdendritic eutectic network, particles at dendrite boundaries (Fe-Cu) and two kinds of larger particles inside dendritic areas (primary Si and Fe-Mn)*

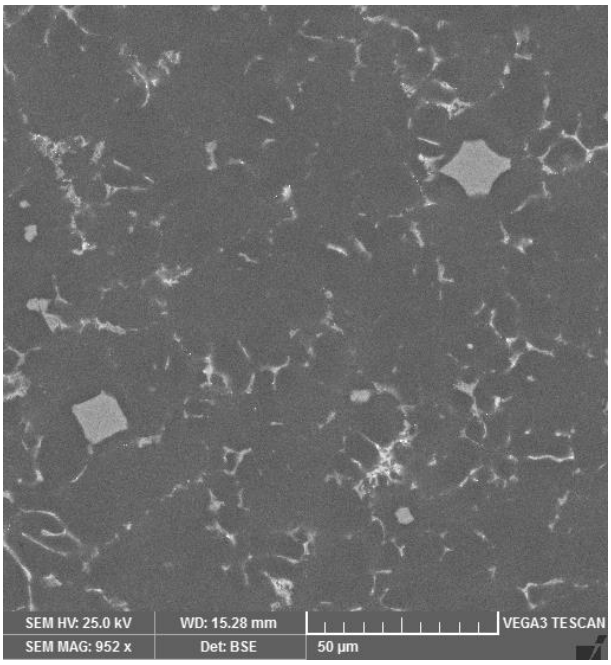

Fig. 6 *Detail of light iron-copper phase at dendrite boundaries and light iron-manganese sharp particles in BSE mode*

Fig. 7 *Fracture initiation area at the surface of the fork, larger shrinkages visible*

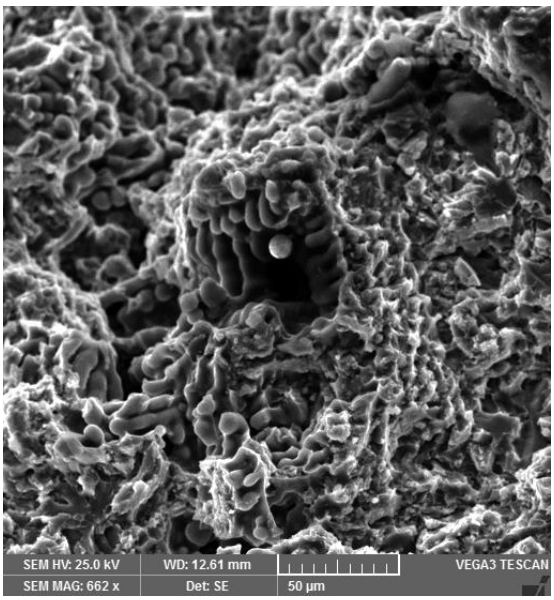

Fig. 8 *Dendrites on the fracture surface*

3.2 Fractography

Both fracture surfaces were observed using a scanning electron microscope. The initiation of the fracture was just under the surface of the thinner part of the fork (Fig.7). The characteristic appearance of shrinkage casting dendrites is clearly evident and it is in agreement with the microstructure features (Fig.8). Brittle fracture areas, sometimes with oxidised surfaces, were observed in the shrinkages. The fracture surface between the shrinkage porosity exhibited a dimple rupture character. No evidence of progressive fatigue failure was observed anywhere on the fracture surface.

It can therefore be concluded that the dimple rupture fracture surface was the result of sudden impact, overload failure. Even though Al-Si alloy was a suitable type of material for this application and the addition of iron further improved its impact resistance and endurance limit, the presence of shrinkage and porosity resulted in significant decrease of the real cross section of the part, thus contributing to the overload of the remaining volume of material.

4 Summary

A suitable Al-Si alloy was used for the front fork of a downhill sports scooter. Although the material was well chosen for this application and the part was properly designed, high shrinkage and porosity of the used material resulted in the premature overload failure of the fork. There has been a significant failure in the quality control of the output and input material in the manufacturing chain leading from the material producer to the semi-product supplier and finally to the fork producer.

It is very important for the successful industrial application of Al-Si alloys not only to ensure correct engineering costruction design with the use of FEM calculations and computer simulation tests, but also to guarantee proper oservance of the manufacturing process and the chemical composition of the chosen structural material. Only high quaity materials produced by controlled procedures and technologies can satisfy the requirement of fully-functioning components with the required lifetime, without posing a threat to human health and life and material damage.

Acknowledgement

This paper includes results created within the project MSM-SGS-2013-050. The project is subsidised by the University of West Bohemia in Pilsen.

References

[1] NOVY, L. (1996). Sample paper. In: *Sample Journal*, Vol. 3, No. 1, pp. 9 – 15. TTP. Switzerland. KUČEROVÁ, L., JIRKOVÁ, H., MAŠEK, B. The Effect of alloying on mechanical properties of advanced high strength steels, *Archives of Metallurgy and Materials*, 2014, Vol. 59, Is. 3, p.1189-1192.

[2] MAŠEK, B., et al. Improvement of Mechanical Properties of Automotive Components Using Hot Stamping With Integrated Q-P Process, *Journal of Iron and Steel Research International*, 2011, Vol. 18, p. 730-734.

[3] WANG, R., LU, W., Quality Wheels of Direct- Electrolytic Al-Si Alloy (DEASA), *SAE Technical Paper 2001-01-0820*, 2001, doi:10.4271/2001-01-0820.

[4] FORMÁNEK, J., CHVAL, Z. Comparing experimental measurement at machine and of his model with simulation in CAD. In *Experimental Stress Analysis 2008.* Ostrava: VŠB - Technical University, 2008. p. 63-66. ISBN: 978-80-248-1774-3

Influence of admixtures on mechanical features of artillery barrels

Ondrej Híreš, Peter Lipták, Danka Rakúsová

Alexander Dubcek University of Trencin, Faculty of special technology, Pri Parku 19, 91106 Trencin, Slovakia,

E-mail: ondrej.hires@tnuni.sk, peter.liptak@tnuni.sk, danka.rakusova@tnuni.sk

Abstract: The real materials contain admixtures that in a negative way affect their mechanical features. The authors of the paper have focused an attention especially on a harmful effect of sulphur, oxygen and nitrogen on the values of a yield limit, contractions and an impact value of complex alloyed steel used for production of artillery barrels.
Cemented sulphides, oxides and nitrides significantly degrade mechanical features of barrels being produced in form of spindly shafts through smith forging. The forged pieces are forged from ingots of a weight about 6 tons.
Using the electron microscopy and quantitative analysis through exposing the elements to X-ray radiation (EDX) we reviewed the possibilities of elimination of harmful admixtures, from which the worst effect was caused by sulphur bound in form of manganese sulphide MnS.
In the paper there are defined particular conclusions on mechanical features of forged pieces after hardening and tempering. There are also documented changes in a shape, amount, location and chemical composition of inclusions after having applied strong hydro etches and after having refined steel through electro slag re-melting.

Key words: Artillery Barrels, Admixtures, Mechanical Properties, Forged Pieces.

1 Characteristics of a studied steel

Complex alloyed nickel-chrome-molybdenum steel is produced in electric arc furnaces cast into 6 ton ingots and forged into a shape of sleek shafts of a length about 8 000 mm, diameter about 350 mm with a bored inside orifice about 120 mm. It is used for dynamically stressed products as tank barrels, breech plugs, hydraulic cylinders etc. For these parts a suitable strength-plasticity features ratio is requested so that these products absorb combine stress, which is generated in form of pressure, heat, collision, shear and flexion [1, 2].
Standard chemical composition and requested values of mechanical properties of 36CrNiMo4 steel used for experiments (EN 10083-1-91) are shown in table 1.

Tab. 1 *Standard chemical composition and mechanical properties of steel 36CrNiMo4 (in wt%)*

C	Ni	Cr	Mo	Si	Mn	P_{max}	S_{max}	Cu_{max}
0,35	3,00	1,00	0,25	0,30	0,40	0,025	0,025	0,30
Specified mechanical properties								
Minim. Yield point			Minim. Impact value			Minim. contraction		
873 MPa			34 $J.cm^{-2}$			25 %		

Tab. 2 *Mechanical properties of forged pieces from manufacturing production*

Forged piece Ser.	**Yield Point [MPa]**	**Contraction [%]**	**Impact value [$J.cm^{-2}$]**
4742	958	26,4	48
4743	974	30,9	52
4744	959	29,7	51
4745	964	**24,6**	54
5748	982	**21,3**	40
5749	915	30,5	48
5751	945	**22,1**	42
5752	1001	27,8	42

The mechanical properties of forged pieces were measured after their quenching and tempering, where mainly contraction often did not achieve the specified values. In table 2 there are shown mechanical features on forged pieces from manufacturing production, from which it can be seen, that three from eight analyzed semi-products did not achieve the specified parameters for contraction.
After an analysis of fracture areas of blasting corpuscles on an electron microscope JOEL JSM6610 with EDX analyser we found out, that a reason of a low contractions are sulphur and oxide admixtures. Sulphides bound to MnS are excluded in form of bars, which are slab-sided in sense of mechanical working of the forged piece (fig. 1). Oxides are bound to several elements and often they are excluded in form of lines or clumps, whereby they are mostly in polygon shape (fig.

2). We measured an amount of sulphur on forged pieces, ranging from 0,018 – 0,021 %, corresponding with a specified regulation. The highest content of sulphur was found in forged pieces with the lowest value of contraction.

3000x	100 s	250 s
Sec. electrons:	SK_α	K_α Mn

Fig. 1 *Area distribution of characteristic X-radiation Kα Mn and S in folds of baculi form shape (MnS particles)*

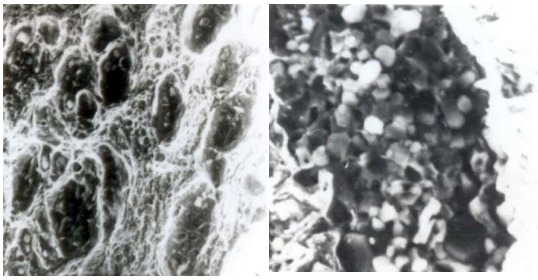

a) magnification 600x b) magnification 2000x

Fig. 2 *Polyhedral shaped clusters and rows of oxide - sulfidic folds (O, Al, Ca, Ti, Si S and Mn oxi-sulfides)*

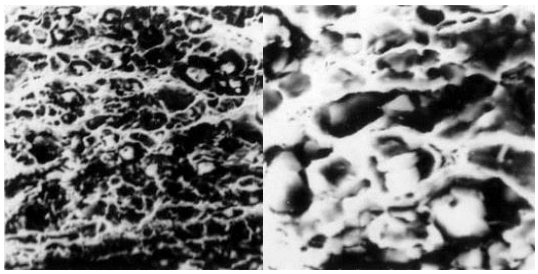

a) magnification 600x b) magnification 2000x

Fig. 3 *Angular oxide - sulfidic folds (O, Al, Ca, Ti, Si S and Mn oxi-sulfides)*

2 Reduction of sulphur and oxygen by desoxydation agents

Based on knowledge about chemical composition, shape, amount, distribution of inclusions and also their impact on modification of mechanical properties of forged pieces we focused our research on reduction of sulphur and oxygen in stage of a final desoxydation of melting [3].
Silico-calcium is used in a manufacturing technology for a final desoxydation in amount of 2, 5 kg of CaSi per a ton of steel. Gradually we increased the amount of CaSi up to 5, 8 kg per a ton of steel, whereby the best values for mechanical properties have been achieved at desoxydation with 4, 1 kg CaSi per a ton of steel. The results of mechanical properties are shown in table 3 [4].

Tab. 3 *Mechanical properties of forged products after desoxydation with 4, 1 kg CaSi per a ton of steel*

Forged piece Ser.	**Yield Point [MPa]**	**Contraction [%]**	**Impact value [J.cm^{-2}]**
4806	1117	32,3	45
4807	960	39,8	58
4808	955	40,2	63
4809	1116	31,8	41
4810	981	40,6	64
4811	962	44,0	60
4812	986	37,5	64
4813	976	44,4	67

It results from the above mentioned values that all specified mechanical properties are higher than the values stated in table 2 achieved by a valid manufacturing technology. The shape, chemical composition, distribution and amount of inclusions have significantly changed, that is proved in illustration 3. The contents of sulphur in steel decreased to a value up to 0,015 %.

3 Conclusions

By an intervention into the process of desoxydation we achieved the following benefits:

a) The mechanical values of originally produced steel have significantly increased (Table 3),
b) We achieved a change in shape, amount, distribution and chemical composition of inclusions (Fig.3).
c) The content of sulphur in steel has significantly decreased, whereby the occurrence of MnS has been eliminated.
d) Separately excluded baculiform sulphides were completely removed bound on MnS that is low-fusing and they become longer during mechanical working in mechanical working direction (Fig.1).
e) Polyedric aggregations of inclusions were removed (Fig.2).
f) We identified particles on crack surfaces that were dispersed in steel that did not have so negative influence on mechanical features.

References

1. HÍREŠ, O**.** Optimalizácia plastických vlastností NiCrMo ocele sekundárnou metalurgiou. Habilitačná práca. Brno, 2002
2. BARÉNYI, I., HÍREŠ, O**.** Mechanical Properties of Forgigs depending on the Changes in Shape and chemical Composition of Inclusions. In: METALURGIJA. - ISSN 0543-5846. - Vol49, No.4(2010), p.313-316.
3. ŠTEPÁNEK A., VYDARENÝ V. Electroslag remelting Cr-Ni-Mo alloy steels, In: Acta Metalurgica Slovaca, 3/1997, pp. 23-28
4. HÍREŠ, O**.** Mimopecná rafinácia ocelí. In: Zborník Akademická Dubnica, 1999, pp. 219
5. LIPTÁK, P., STODOLA, J. Dependability Engineering for Special Purpose Machines Equipment. Monograph. 1st Edition. A. Dubcek University of Trencin, 2011. ISBN 987-80-8075-481-5. (102 p).

Material Analysis of Nickel Superalloy for Military Technology

Petr Jonšta[1], Irena Vlčková[2], Zdeněk Jonšta[3]
[1]VÍTKOVICE HEAVY MACHINERY a.s., Ruská 2887/101, Vítkovice, 703 00 Ostrava, Czech Republic, E-mail: petr.jonsta@vitkovice.cz
[2]RMTSC, MATERIAL & METALLURGICAL RESEARCH Ltd., Ostrava, remote site VÚHŽ a.s., 739 51 Dobrá, Czech Republic, E-mail: vlckova@vuhz.cz
[3]Technical University of Ostrava, Faculty of Metallurgy and Materials Engineering, 17. listopadu 15/2172, 708 33 Ostrava-Poruba, Czech Republic, E-mail: zdenek.jonsta@vsb.cz

In the aerospace industry, the nickel-based superalloys are often used due to their ability to withstand extreme conditions. They find their use particularly as turbine blades in jet engines. An important example of this type of superalloy is INCONEL. This construction material must meet a wide range of complex requirements with regard to its properties and technological and operational characteristics that are required by the heavy duty in extreme conditions.
The INCONEL Superalloys represent multicomponent and multiphase materials with their complex alloying base and structure with distinct dendritic segregations. Their long life and reliability in operation are directly related to the microstructure, or to its stability in a long-term operational application, respectively.
The presented work deals with the evaluation of microstructural parameters at two variants of cast superalloy INCONEL 713LC, applying the light microscopy and electron microscopy, including the fractographic analysis.

Key words: Nickel superalloy, as cast condition, structural phase analysis, fractography

1. Introduction

The main stimulus for the development of material engineering in the field of heat resistant materials is the aerospace industry, in particular the construction of turbine engines. They find an important use as turbine blades for jet engines, typically in the form of nickel superalloys. A notable representation of those superalloys in this area is reflected in the fact that they currently represent more than 50 % by weight of the modern aircraft engines [1]. The extended use of superalloys in turbines is supported by the fact that the thermodynamic efficiency of a turbine increases with increasing temperature at the inlet to the turbine, which has partially become the reason for increase of the maximum operational temperature of high alloys [1-3].

This increase was made possible mainly by two factors. The first factor involves the modern processing techniques that improve the purity of alloys and thereby increase their reliability by mastering the art of a controlled crystallization and the subsequent technology of production of monocrystalline products. The second factor represents the development of alloys with higher operation temperature, mainly by the use of alloying additions, especially Re, W, Ta and Mo [3].

The turbine shaft of an aircraft engine does not consume all energy of the exhaust gases, but only a part that is necessary to drive the compressor. A reactive engine converts the remaining energy into draft force by the acceleration of the working medium (the combustion gas) inside the exhaust portion. The aircraft turbine engines changes the chemical energy of fuel into mechanical energy, with a relatively high efficiency, in the order of 30 to 45%. This extra efficiency significantly depends on the flue gas temperature at the inlet to the turbine, which can reach up to 2000 - 2200 °C, e.g. when a hydrocarbon fuel is combusted in the presence of atmospheric oxygen. Some material problems are limiting the increase of gas temperature at the turbine inlet, such as creep resistance, thermal fatigue, sulfate corrosion at high temperatures (i.e. hot corrosion), and erosion. They depend on the engine design, the cycle, and the installation position, as well as on the quality of fuel being used.

An example of the material composition in a jet aircraft engine is presented in Fig. 1.

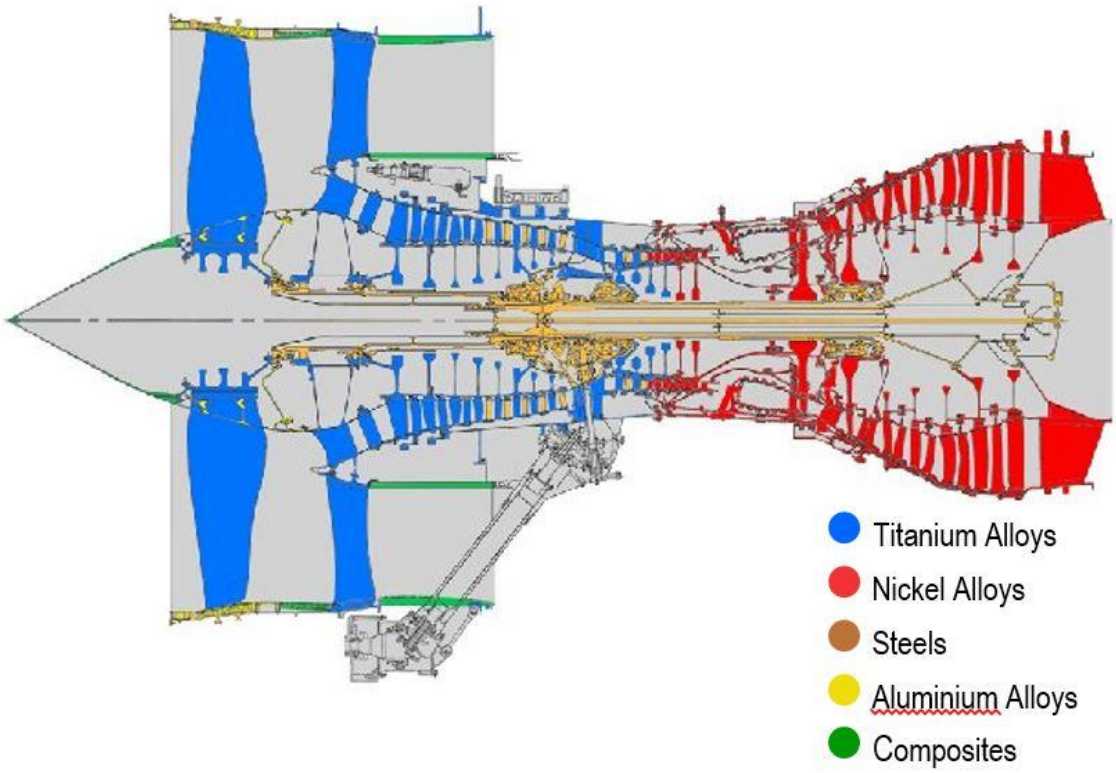

Fig. 1 *Material Composition of an Aircraft Engine [4]*

Turbine components with a highest loading are the directing and rotating blades of various geometry, which are working in different operating conditions. Significant progress has been made particularly in the improvement of geometry and cooling systems, especially at the turbine blades and the combustion chamber (a "honeycomb" structure). This helped to reduce the operating temperature of blade material by up to 350 °C against the combustion temperature [5, 6].

This progressive development allows achieving the desired service life of nickel-based superalloys, combined with a respective refractory coating for long-term applications with temperatures up to 1150 °C.

The used nickel-based superalloys tend to be considerably complex and their alloyed structures are complicated. The objective of this paper was to perform material analysis of the nickel-based superalloy INCONEL 713LC (hereinafter IN713LC), including fractographic analysis, using both the light microscopy and the scanning electron microscope method with an x-ray microanalyzer.

2. Current State Analysis

During the more than fifty-year period of development of heat resistant nickel-based superalloys hardened by γ' phase (A3B), they have undergone a number of evolution stages. This applies to the chemical composition, manufacturing technology, the set of obtained properties, and the related field of use. As a result of intensive continuous development in improving the chemical composition and technology, structural superalloys with operating temperatures of 0.9 Tt, i.e. 1000-1100 °C, were obtained, while reaching the natural boundary of their development [1]. Additional effects (increasing the corrosion resistance in gases up to 1150 °C) were achieved by using suitable refractory layers, the technology and applications that are developing at a dynamic pace.
At working temperatures above 650 °C (and up to 1150 °C) we often use those superalloys together with the refractory layers [6, 7].

With respect to the development of technology, it is possible to rank the nickel superalloys among the alloys processed by molding, the cast alloys (vacuum melting), the alloys with directed crystallization - columnar alloys, alloys with controlled crystallization - monocrystalline alloys, the alloys hardened by oxide dispersion, the alloys produced by powder metallurgy, including the alloys with superplastic properties and the new-generation alloys.

Each of these technologies has its advantages and disadvantages, and their use is ruled apparently by the technical and economic aspects. Under the new technologies used for the production of turbine blades, the most widely applied methods are the monocrystalline crystallization and the directional crystallization.
A large number of turbine blade designs continue to be produced by traditional technology of vacuum casting.

Any structural material for turbine blades must satisfy a number of strict requirements with regard to the material properties and the technological and operational characteristics, of which the most important

are the creep strength and the strength at high temperature intervals, heat resistance in the flowing hot gases having a considerable corrosive effects (sulphur compounds, vanadium compounds - i.e. hot corrosion compounds), resistance to thermal-mechanical fatigue at both high and low number of cycles, resistance to salt corrosion and sulphate corrosion, resistance to abrasive wear and erosion at high temperatures, ductility and resistance to brittle fracture at room temperature and at operating temperature, structure stability under conditions of large temperature gradients (up to about 1000 °C/cm), and the possibility of achieving the desired shape and characteristics during the technological processes [8].

As follows from the above requirements, in addition to the corresponding set of mechanical properties involving the increase in strength achieved at the expense of reduction of plasticity to the minimum allowable level, we expect at the nickel-based superalloys many other characteristics and properties, among which the corrosion resistance and technological ability have a significant impact on further directions in the development of these materials. Still more serious operational problems of the superalloys represents the high temperature corrosion caused not only by the presence of oxygen but also the presence of sulphur, sodium, vanadium, and other harmful impurities introduced with the fuel compositions and the combustion products.

Elimination of these harmful corrosive effects can be achieved by optimization of chemical composition or by applying protective diffusion coatings, as well as by an adequate preparation of the fuel and the intake air. The oldest method of achieving a heat-proof super alloy resistant to oxidation and corrosion is aluminizing, applied in practice since the sixties. Nevertheless, the positive effect of these protective layers is limited by reciprocal diffusion of aluminium alloy and the matrix components from the alloy at temperatures above 900 °C. The currently used method involves the plasma-deposited layers in a number of three or two, whereas the outer layer is based on a zirconium-stabilized oxide, and the inner layer is of MCrAlY-type, where M is represented mainly by Ni, or Co, respectively [9].

The heat-proof nickel superalloys are poly-component materials with a chemical composition that varies within a wide range. The materials are of poly-component and poly-phase type, with a microstructure in which the phases can be both stable and metastable, and these are affecting their properties significantly. During a long-term exposure to high temperatures, the undesirable TCP-phases can occur in the structure that could change its morphology and cause significant deterioration leading up to the material degradation.

3. Experimental Techniques in Materials

For the experimental study we used castings from two commercial Ni-based superalloys IN 713LC. The chemical composition of the sample indicated below as sample A is shown in Tab. I; the chemical composition of the sample designated below as sample B is shown in Tab. II.

Tab. I *Chemical Composition of the Superalloy IN 713LC (% of mass) - sample A*

C	Cr	Al	Mo	Ti	Nb	Zr	Ni
0.05	11.5	6.31	3.72	0.62	2.39	0.06	rest.

Tab. II *Chemical Composition of the Superalloy IN 713LC (% of mass) - sample B*

C	Cr	Al	Mo	Ti	Nb	Zr	Ni
0.06	12.20	6.11	4.07	0.66	2.75	0.08	rest.

As an additional information on the chemical composition of the monitored nickel superalloy IN 713LC, there is reported the mean vacancy concentration $\overline{N}_v \approx 2.30$. In relation to this figure we can declare that according to the current experience the superalloys in question probably would not be susceptible to create the undesirable σ-phase. Relevant characteristics of this parameter given by the Detert´s data (in the upward direction from $N_i - N_v = 0.66$ up to Ti parameter 6.66, resp. Al-7.6) are used in the assessment. The mean value $\overline{N}$ v is defined by formula [10]:

$$\overline{N}_v = \sum_{i=1}^{n} Mi(N_v)i,$$

where:
Nv… is the individual value of electron vacancies for the given element,
Mi….atomic fraction of the given alloying additive,
n….. is the number of considered alloying additives in the nickel-based superalloy matrix.

Given that the Ni-based superalloys (sample A and sample B) contain precipitates of Ni3-type (Ti, Al) that correspond to the phase γ' carbides or also borides, which modify the chemical composition of the base metal matrix, it would be necessary to apply a correction of the chemical composition of the base matrix (solid solution) to allow an exact evaluation of the formation conditions for the sigma-phase. Similarly, it is necessary to correct the "losses" of carbide-forming elements in carbides, or of elements bound to borides, respectively. Their concentration bound in this way must be

subtracted from the basic chemical composition of the matrix, which is then the basis for calculating the mean value $\overline{N}$ v. In any case, the content of nitrogen and oxygen did not exceed the value of 30 ppm.

Material analysis of the superalloys IN713LC in question, including fractographic analysis, was performed with use of light microscope OLYMPUS GX 51, and additionally, by the use of scanning electron microscope Quanta FEG 450 with X-ray microanalyzer TRIDENT - APEX - 4. The chemical composition was examined by fluorescence x-ray spectrometer SPECTRO XEPOS.

4. Results and discussion

A typical dendritic structure in the etched condition, sample A and sample B for a cast nickel base superalloy IN 713 LC, is shown in Fig. 2 and Fig. 3.

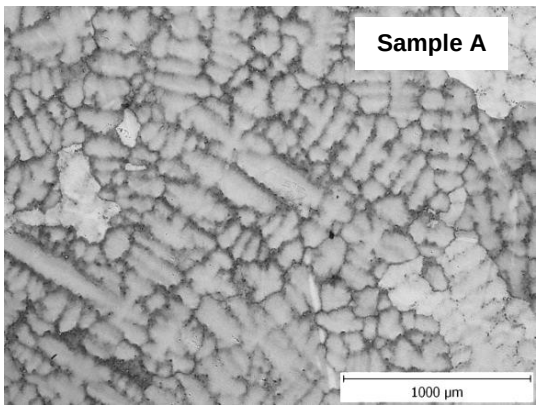

Fig. 2 *Dendritic Structure*

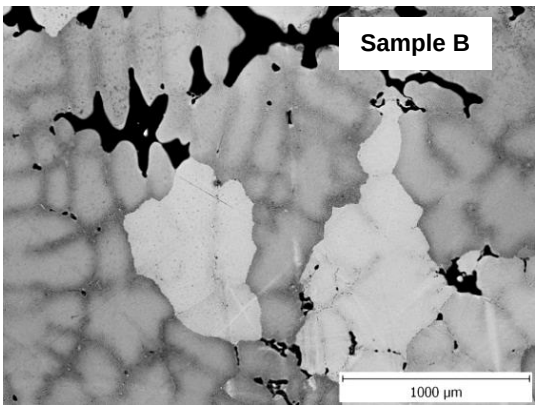

Fig. 3 *Dendritic Structure*

As apparent from Fig. 3, in sample B were detected large cracks that spread continuously over the arms of dendrites. Compared to sample A in Fig. 2, the arms are coarser. In addition, relatively large casting defects were occurring at the sample B.

To get a detailed overview of the properties achieved at the samples of superalloys IN713LC, an electron-microscopic analysis was performed. It should be noted that the presented superalloys show certain irregularities in the chemical composition, which is directly linked with the used casting process and with the evaluation of the superalloy in the state after casting. In this context the formation of large crystallites should be noted, including the strong development of segregation process.

The following phases were detected in the structure: primary MC-type carbides (Nb, Ti + Mo); phase γ'; a phase rich in Mo and Cr; a phase rich in Nb, Zr, and Si presence; and ZrS-sulfides.

Segregation processes during solidification led to a significant chemical heterogeneities in the final microstructure. In the inter-dendritic areas, very numerous eutectic formations were separated, formed mainly by coarse particles of phase γ'. Only minor fine eutectics γ' + γ were observed in the sample A (Fig. 4). Furthermore, the metal matrix involved non-homogeneously separated particles of primary carbides of MC-type, which contained varying amounts of carbide-forming elements: niobium, titanium, and molybdenum. These carbides are mainly concentrated in the inter-dendritic areas and at the grain boundaries (Fig. 5).

In the immediate vicinity of eutectics, in the sample B, relatively large phases occurred that were rich in molybdenum and chromium or nickel, zirconium, and silicon, respectively (Fig. 6). In the sample A these phases were not observed. In the sample B we also detected the presence of ZrS-sulphides in the form of thin platelets grown-in at the carbides, a phase rich in molybdenum and chromium, and phase γ´ (Fig. 7). No sulphides occurred in sample A. We did not detect either nitrides or oxidic phases in any of the analysed samples.

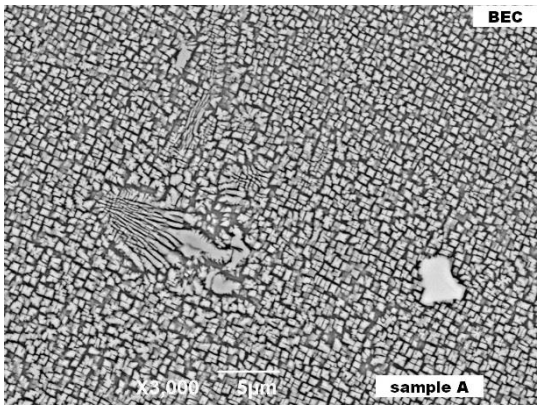

Fig. 4 *Fine eutecticum γ´+ γ*

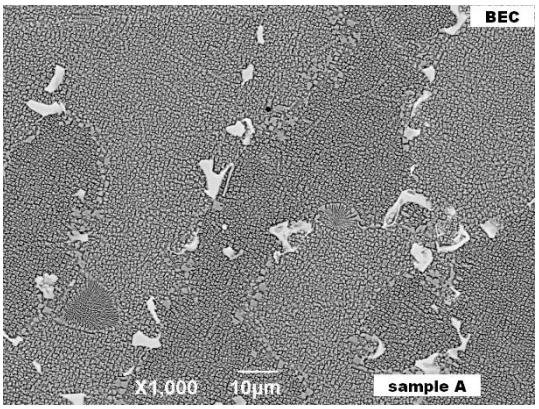

Fig. 5 *MC-carbides at the grain boundaries*

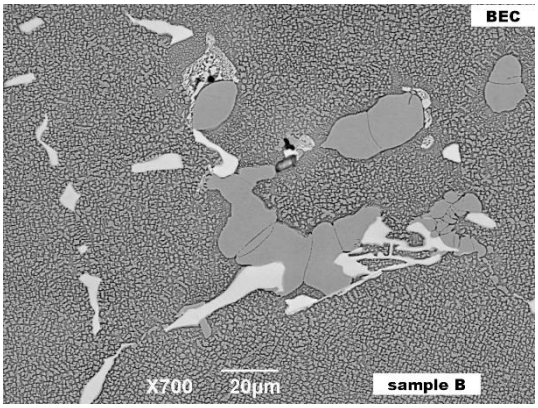

Fig. 6 *Multiphase formations around eutecticums*

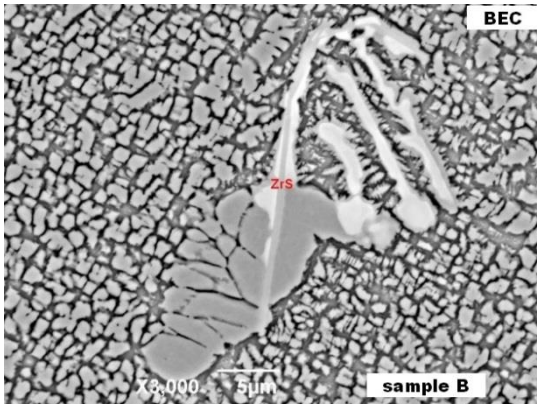

Fig. 7 *Grown-in ZrS particles*

Differences were also observed in the morphology and particles size in the hardening phase γ' of γ-matrix. Hardening particles of intermetallic phase γ', separated in the specimen A inside the dendrites, are documented in Fig. 8; the same type of separated particles inside the dendrites shows the sample B in Fig. 9.

Using electron-microscopic analysis at the sample B, a more frequent presence of cracks in the structure was confirmed. Very remarkable were the casting defects occurring in the axis of the casting - open shrinkage cavities. These defects introduce cavities, usually with coarsely crystalline surface, and are extending to a certain depth in the casting. A shrinkage cavity is result of physical process of volume reduction in a metal (shrinkage) during its solidification. The reason is therefore insufficient volume addition of melt during the solidification of casting. An example of such an open axial shrinkage, detected in the sample B, is presented in the following Fig. 10, and the inside of the shrinkage cavity is shown in Fig. 11.

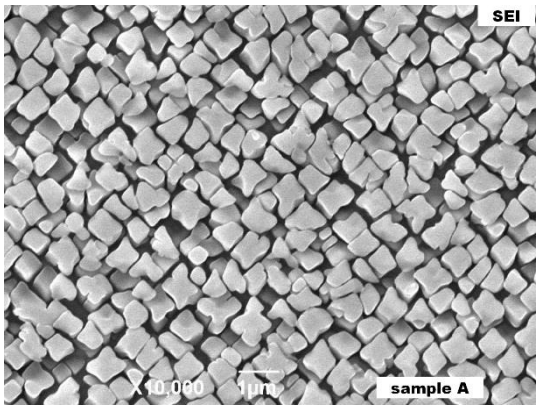

Fig. 8 *Particles γ´ inside the dendrite*

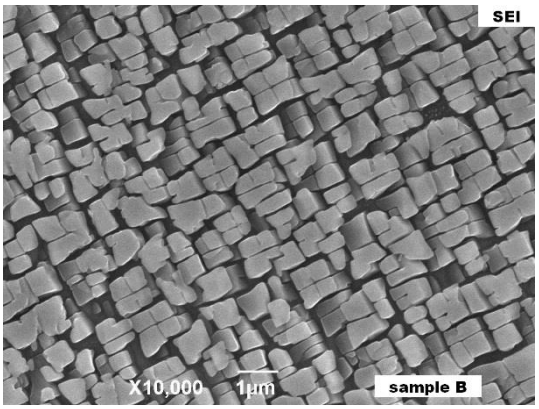

Fig. 9 *Particles γ´ inside the dendrite*

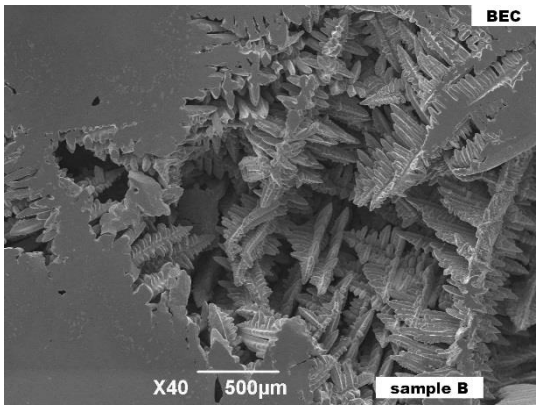

Fig. 10 *Open axial shrinkage cavity*

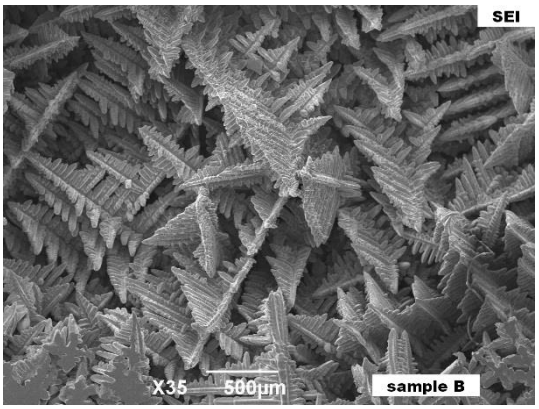

Fig. 11 *Detail of an axial shrinkage cavity*

A significant casting defect on the fracture surface in the sample B that was detected by fractographic analysis, is presented in Figures 12 and 13.

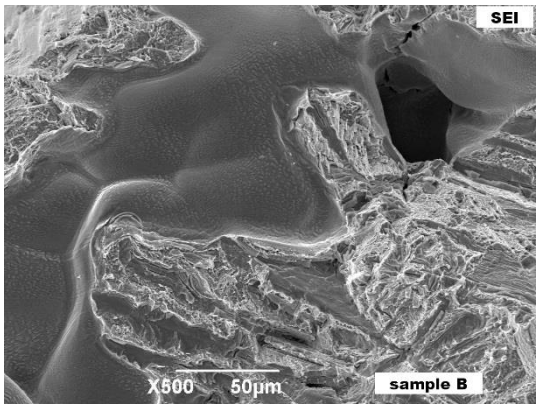

Fig. 12 *Casting defect on the fracture surface*

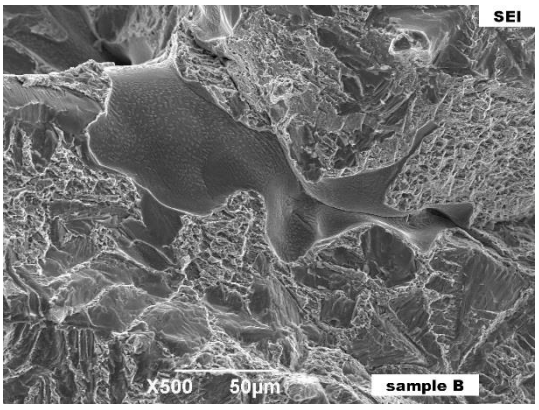

Fig. 13 *Casting defect on the fracture surface*

The presence of cracks and significant axial shrinkage cavities in the microstructure of sample B proved to be a decisive factor leading to the deterioration in the mechanical properties of the particular sample, namely not meeting the prescribed level of yield point and ductility. This was compromising the quality of the casting, which may also result in reduced reliability of the given superalloy in a real application with heavy operating conditions [11].

5. Conclusion

The contribution presents a material analysis of two heat samples (sample A and sample B) of nickel superalloy IN713LC as cast. The analysis was performed by application of light and scanning electron microscopy, including the fractographic analysis.

Both studied nickel superalloy melts have a heterogeneous structure after casting, with distinct dendritic segregations complying to the complexity of the alloying base. The precipitated phases detected structurally by phase analysis corresponded to phases commonly occurring in superalloys IN713LC after casting.

We detected particles of MC carbides, carbides, or carbon-nitrides of niobium and titanium, respectively, as well as particles of intermetallic phase type γ'- Ni_3(Ti, Al), and multiphase creations with a higher alloying content, in particular of molybdenum, chromium, or zirconium. We also identified ZrS sulphides, which; however, alike the multicomponent formations, occurred only in the sample B. The contents of oxygen and nitrogen did not exceed 30 ppm in any sample, which is consistent with the requirements for the content of these gases.

A very positive finding was that, in accordance with the mean value in lattice vacancy $\overline{N}_v$ in 3d sphere of nickel, we did not detect in any sample the undesirable TPC-phases, namely σ phase, which is involved in degradation of superalloys.

A significant difference between the sample A and sample B is expressed in the presence of cracks on the arms of the coarser dendritic structure in the sample B, and in particular, the presence of significant axial shrinkage cavities in this sample.

Owing to this fact it is possible to express the opinion that the analysis proved the cause of formation of defects in the present sample B, i.e. nonobservance of the production technology. The detected cracks

and open axial shrinkage cavities lead to reduction in the mechanical properties below the required level, and to the possibility of degradation failure of the superalloy in question.

The collected results allowed an enrichment in knowledge about the nickel-base superalloy IN713LC, in terms of ensuring its operational reliability and safety, not only in the view of its formation, morphology, and distribution of the segregated phases, but especially in terms of compliance with technological discipline during its production.

6. Acknowledgments

This work was created during the implementation of the project no. LO1203 "Regional Materials Technology Centre-sustainability program" funded by the Ministry of Education, Youth and Sports of the Czech Republic.

7. References

[1] High Temp. Alloys for Gas Turbines and Other Appl., Proc. *Int. Conf. Liege 1976, 1986, 1990, 1994, 1998.*

[2] SCHUBERT, F. Hochtemperaturwerkstoffe fur den Receiver des Solar Systems, *Studie fur die DFVLR*, 1978.

[3] SIENIAWSKI, J. Kryteria i sposoby oceny materiałów na elementy silników turbinowych, Politechnika Rzeszowska, 1995.

[4] SIMS, C., T., STOLAFF, N.,S., HAGEL, W., C. *Superalloys II*. Wiley & Sons, New York (1987), 1998.

[5] KOIZUMI, Y., KOBAYASHI, T. et al. In: *High Temp. Mat. for Power Eng.*, P.II, Liege´98.

[6] HERNAS, A., JONŠTA, Z., et. al. *Žárupevné oceli a slitiny*, ES VŠB-TU Ostrava,2009, 392 p.

[7] DONACHIE, M., J., DONACHIE, S., J. Superalloys: *a technical guide*, USA, 2002, 439 p.

[8] STRANG, A. *High Temp. Mat. for Power Eng. and Other Appl*., Liege 1998.

[9] CRANE, F., A., CHARLES, J., A. *Selection and Use of Engineering Materials*, Butterworths, London-Wellington 1986.

[10] JONŠTA, Z.,JONŠTA, P.,VODÁREK,V.,MAZANEC, K. Physical-Metallurgical Characteristics of Nickel Super Alloys of INCONEL Type. *Acta Met.Slovaca*, 13, 2007, 4.

[11] VILAMOVÁ, Š.,JANOVSKÁ, K.,KOZEL,R.,VOZŇÁKOVÁ, I., ŠVECOVÁ, E. New Trends in the Management within the Metallurgy Firms. *International Conference on Metallurgy and Materials Metal 2012.* Ostrava: Tanger, 2012, p. 1897-1903.

Damage tolerance of high-speed machined integral panels made from 2024-T351 aluminium alloy

Josef Klement[1], Petr Augustin[1]
[1]Faculty of Mechanical Engineering, Brno University of Technology. Technická 2896/2, 616 69 Brno. Czech Republic.
E-mail: klement@fme.vutbr.cz, augustin@fme.vutbr.cz

Integrally stiffened structures of commercial as well as military aircraft can be less expensive than built-up structures, yet equal in structural performance and weight. High-speed machining of integral fuselage and/or wing panels is one of possible manufacturing technologies. For structural parts loaded with cyclic tension stresses, the damage tolerant properties are most important. The article describes results of experimental investigation and computer modelling of crack growth in integrally stiffened test panels high-speed milled from 2024 alloy plate. Data necessary for modelling were achieved by testing of coupons on constant and flight-simulation cyclic loading. Residual stresses after machining were measured using strain gauge method. Integral panels were tested under constant amplitude loading with two values of amplitude and R and also under flight-simulation cyclic loading. Results of testing are compared with calculated cracks propagation curves. The comparison shows good correlation.

Keywords: Integral panels, damage tolerance, aluminium alloy 2024

Introduction

The manufacturing of aircraft is a very time consuming and expensive process. Many technologies are currently being implemented to reduce the manufacturing cost and time in order to improve quality and satisfy demand. The great success in technology has evolved in the use of monolithic manufacturing. Monolithic manufacturing consists of machining a solid billet of material into a part that would otherwise be built up from many different parts and fasteners. For example baseline fuselage panel of Boeing 777 consists of 78 individual parts and high number of fasteners. The total number of fasteners on the B 777 is about 850,000 [1]. High speed machining (HSM) or cutting (HSC) permits the economical manufacture of intricate integral components from simple and consequently low cost semi-products, e.g. plates [1-3]. According to NASA-Boeing research, cost savings up to 60% for stiffened integral panels and up to 66% for integral frames can be achieved comparing conventional machining [2]. High speed milling of aluminium alloys has got main application in aircraft manufacture. Typical milled parts include integral structural elements, e.g. wing spars, stiffened skin panels, fuselage bulkheads, frames. The machine tool spindles should have high power (20-40 kW) and rotational speed as high as 10,000 to 30,000 rpm (in some cases up to 75,000 rpm). Small end mills can be used for manufacturing complex aluminium products, where up to 90 % of the whole part may be removed as chips. Europe largest wing milling machine (at Broughton) has X axis 87 m, width 3.5 m. The machine is capable of producing three 21 m wing skins at the same time.

The article presents results of activities carried out at the Institute of Aerospace Engineering (IAE) during its participation on the 6th Framework Programme project DaToN - Innovative Fatigue and Damage Tolerance Methods for the Application of New Structural Concepts. The project was focused on the development of damage tolerance assessment tools for structures manufactured using newly developed methods. Advanced production techniques under investigation were High Speed Cutting (HSC), Laser Beam Welding and Friction Stir Welding. Structures made by these techniques are typical by their integral character. It leads to the fact that they contain less number of fatigue and corrosion critical locations. For example, about 70% of all aircraft fatigue damages are initiated on holes for rivets and bolts [4]. However comparison of the integral structures with differentially stiffened designs from the damage tolerance point of view is less optimistic and in some cases they lack the crack-arresting capability that is typical of riveted structures [5]. The project consisted of workpackages aimed to both the developing of computational models and experimental activities. Common test program was focused on collection of experimental data mainly using two-stringer panels shown in Figure 1. Analyses and verification tests performed at IAE were oriented on the panels made of 2024-T351 alloy. The panels were high speed milled from the 50 mm thick plate. The cutting speed was 1500 m/min and the feed was chosen to achieve the surface roughness Ra better than 1.6 μm. The same technology was used for manufacture CCT coupons with dimensions 375 x 100 x 2 mm from the sheet of 5 mm thickness. Residual stresses after machining were measured at the Institute of Solid Mechanics, using method of the hole located in the midpoints of the panels. Figure 2 shows the existence of compression principal stresses in surface layers as a consequence of a deformation process during cutting. The tension stresses were detected in inner skin layers.

Fig. 1 *Two-stringer panel in servo-hydraulic load frame at IAE laboratory*

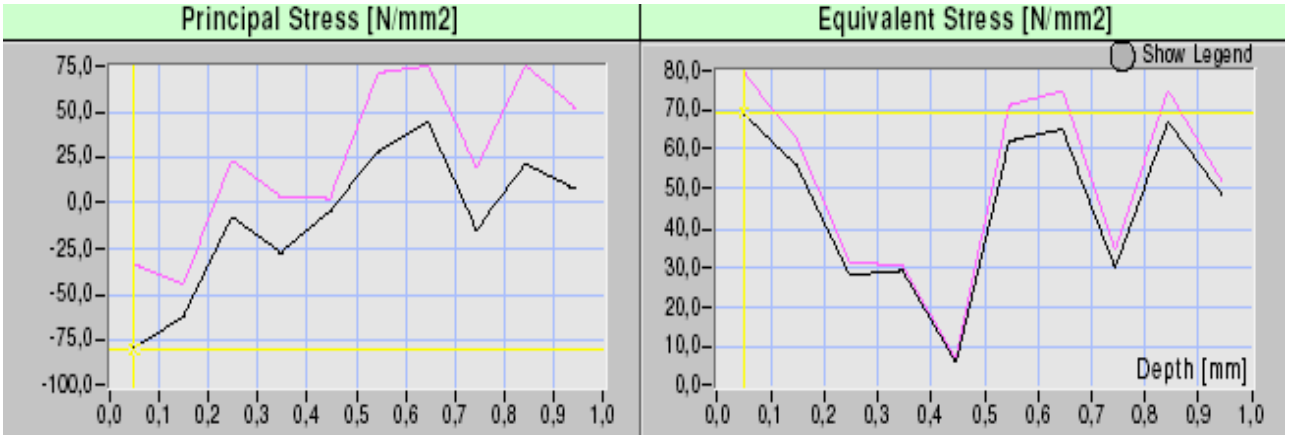

Fig.2 *Profile of the principal and equivalent residual stresses through the panel thickness after machining – integral method, EVAL RSM software, strain gauge HBM-1.5/120RY61S, hole diameter 1.8 mm*

Two-stringer panel under the constant amplitude load

Crack propagation tests of the DaToN HSC panels in the common test program were carried out under the constant amplitude loading at maximum nominal stress of 80 MPa with stress ratio of R = 0.1 and at maximum nominal stress of 110 MPa with R = 0.5 respectively [6]. Fatigue cracks in the skin were initiated on the central saw cut of 2a = 20 mm and propagated towards and through the stiffeners. Crack growth was monitored optically by travelling microscopes from both sides of the panel. Measured crack propagation curves are shown in Figures 7 and 8.

Obtained experimental data were used for verification of methodology for numerical simulations of crack propagation. Applied approach is based on stress intensity factor (SIF) functions calculated by means of finite element method software MSC Patran/Nastran. Simulation of crack propagation in a real structure requires determination of SIF for large number of crack configurations and that is why simple FE models comprising shell elements were built. It is acceptable time consuming, even when there is need of application of geometrical nonlinear solution. Stress intensity factors were calculated from strain energy release rate determined using the crack closure technique. Depending on the mesh density the crack closure technique was able to calculate the stress intensity factor values with the error of about 2%. FE model of the panel is shown in Figure 3. Since fatigue tests of panels were performed without any anti-bending device able to

restrict the displacements perpendicular to the panel plane it was necessary to involve the bending effects acting in the experiments. This is why the application of geometrical nonlinear solution was investigated. Obtained stress intensity factor functions for crack in the skin from both the linear and nonlinear FEM analyses are depicted in Figure 4.

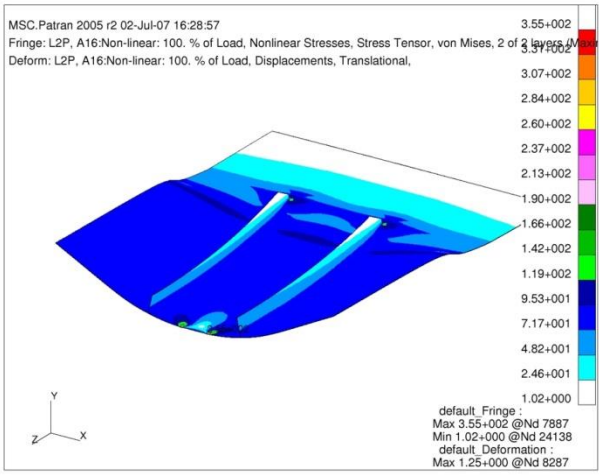

Fig. 3 *Stress contour plot for panel with central crack in the skin*

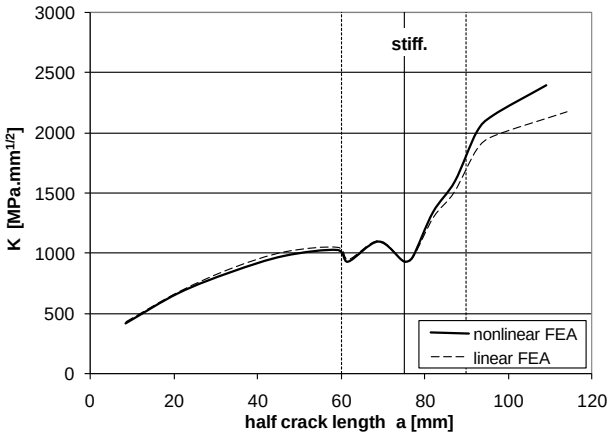

Fig. 4 *Stress intensity factor function for skin crack in two-stringer panel*

Subsequent analysis of crack propagation was performed using the software package NASGRO. Crack propagation evaluation has been based on crack growth rate data obtained from the tests of 100 mm wide and 2 mm thick CCT specimens also made of 2024-T351 alloy using HSC (see Figure 11). The data from the tests performed at stress ratios R of 0.1, 0.5 and 0.8 were subsequently expressed using three different approaches. First one is based on the NASGRO equation which is relationship between crack growth rate *da/dN* and stress intensity factor range ΔK

$$\frac{da}{dN} = C\left[\left(\frac{1-f}{1-R}\right)\Delta K\right]^n \frac{\left(1-\frac{\Delta K_{th}}{\Delta K}\right)^p}{\left(1-\frac{K_{\max}}{K_C}\right)^q}, \tag{1}$$

where ΔK_{th} is the threshold stress intensity factor range and K_C the critical stress intensity factor. The crack opening function $f = K_{op}/K_{\max}$ for plasticity-induced crack closure defined by Newman is a function of stress ratio R and plane stress/strain constraint factor α. Curve fit of crack growth rate data using NASGRO equation was applied e.g. for predictions of crack propagation under the spectrum loading using the Willenborg model since there is no alternative in NASGRO. Second approach shown in Figure 5 uses the table lookup input in NASGRO. Polynomial curve fitting was

applied to generate the points into the table. This approach was used for predictions under the constant amplitude and non-interaction spectrum loading. The last method is required for calculation of crack propagation using the Strip Yield model. In this model crack growth rate has to be expressed as a function of effective stress intensity factor range ΔK_{eff}. The effective stress intensity factor range was calculated using crack opening function f as

$$\Delta K_{eff} = \frac{1-f}{1-R}\Delta K. \tag{2}$$

Experimental data for three different stress ratios then collapsed into the single band as shown in Figure 6.

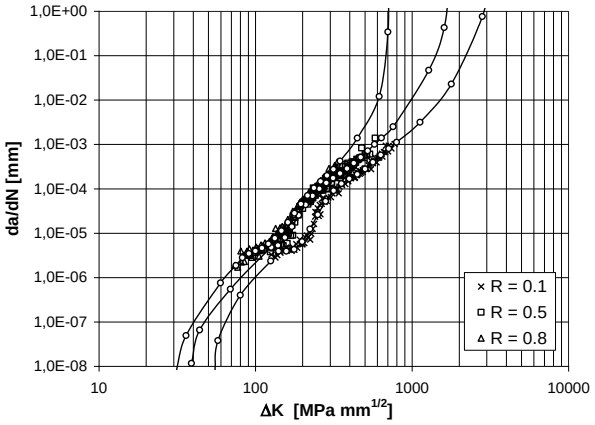

Fig. 5 *Polynomial curve fit of crack growth rate data.*

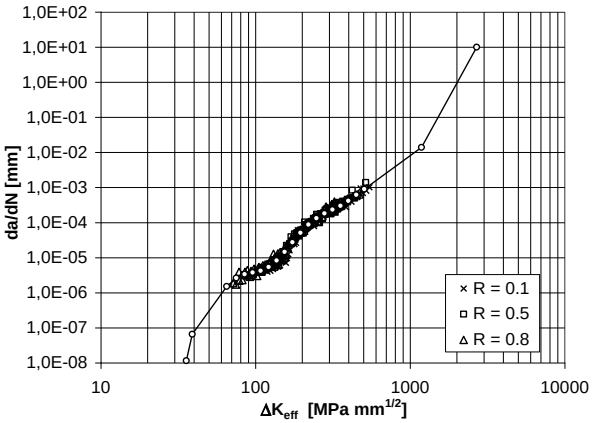

Fig. 6 *Effective stress intensity factor range against crack growth rate*

Obtained predictions of crack propagation under the constant amplitude loading in Figures 7 and 8 show good correlation with the tests on panels. It is obvious that the best results correspond to stress intensity factor functions calculated by geometrical nonlinear analysis. No significant differences in predictions based on curve fits using NASGRO equation and on the table lookup form were found.

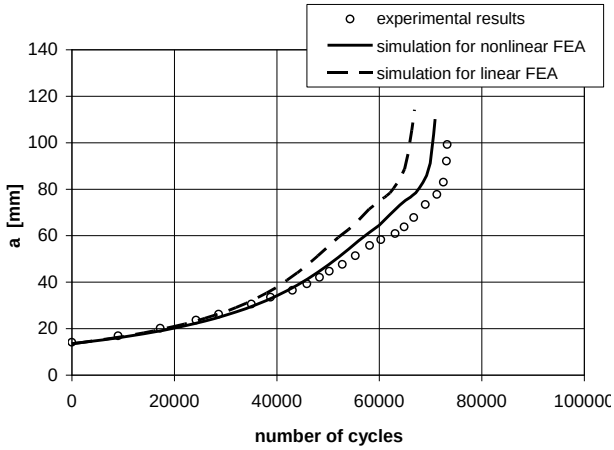

Fig. 7 *Example of prediction of crack growth in the skin of two-stringer panel using NASGRO equation versus result of the test - σ_{max} = 110 MPa, R = 0.5*

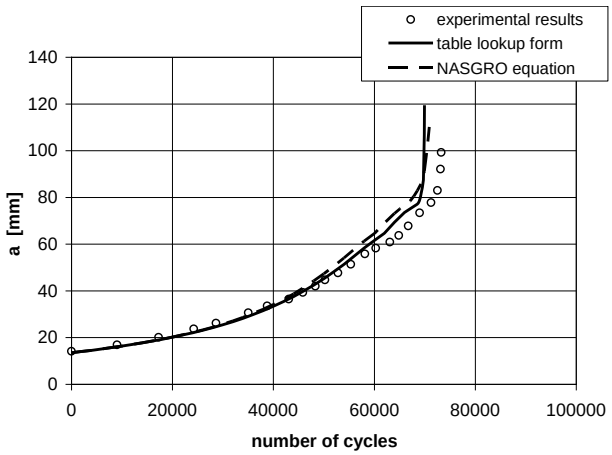

Fig. 8 *Predicted crack growth in the skin of two-stringer panel versus result of the test (nonlin. FEA) - σ_{max} = 110 MPa, R = 0.5*

Two-stringer panel under the spectrum loading

For predictions of crack growth and experimental verifications using the spectrum loading a sequence representing service loading of the transport airplane wing was prepared. Sequence is based on the load spectrum of B737-400 airplane measured by Federal Aviation Administration within the Airborne Data Monitoring Systems Research Project [7].

An important question of the development of a load sequence is the definition of the number of flights in the repetitive block defining the magnitude of highest applied load. In accordance with many sources (e.g. [8], [9]) the number of flights was established as one tenth of anticipated lifetime. The B737 design service objective of 75 000 flights than leads to the repetitive block of 7 500 flights. Another decision that has to be made is the omission of small loads. The spectrum of flight loads normalized to 7 500 flights was trimmed on the level pertaining to cumulative frequency of 315 000. Provided that the magnitude of 1g nominal flight stress is 70 MPa, the omission stress range is 12.46 MPa. This is a conservative choice in comparison with the recommendations in references [9] or [10]. Continuous flight load spectrum was than divided in ten discrete levels and subsequently distributed into different flight types with various severities. The technique of the definition of flight types in the case of gust dominated spectra of a transport aircraft applied in standardized loading sequence TWIST [8] was adopted. Consistently with the TWIST the number of flight types is the same as the number of load levels. Thus all flight types denoted by letters from A to J can differ in terms of the magnitude of the highest load level, as shown in Figure 9. The load history is created on flight by flight basis and the sequences of loads and flights (Figure 10) are randomized. All flights are closed by insertion of single compression load from the ground load spectrum. Generation of the load history is realized by the in-house computer program.

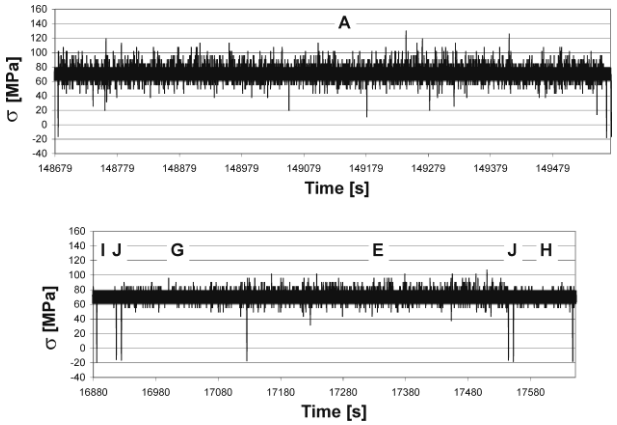

Fig. 9 *Examples of typical flights*

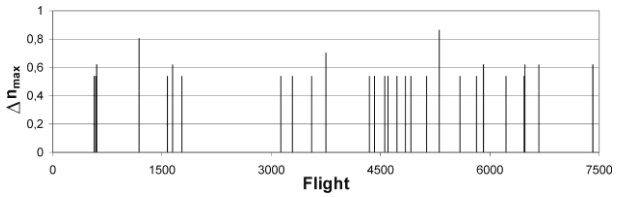

Fig. 10 *Position of the most severe flights in the sequence and magnitudes of largest load factors*

Three models in NASGRO were applied for crack growth analysis under the spectrum loading: non-interaction, Willenborg and Strip Yield model. Simple non-interaction model is fully based on crack growth rates determined from constant amplitude tests hence conservative predictions can be expected. Generalized Willenborg model deals with the crack growth retardation by implementation of the effective stress ratio

$$R_{eff} = \frac{K_{\min} - K_R}{K_{\max} - K_R} \tag{3}$$

that is used instead of the stress ratio R within the crack growth equation. Modified residual stress intensity is defined as

$$K_R = \phi \left(K_{\max}^{OL} \left(1 - \frac{\Delta a}{Z_{OL}} \right)^{\frac{1}{2}} - K_{\max} \right) \tag{4}$$

where K_{max}^{OL} is the maximum stress intensity factor for the overload cycle, Δa stands for the crack growth between the overload cycle and the current cycle and Z_{OL} is the size of the overload plastic zone. The factor Φ is defined as follows

$$\phi = \frac{1 - \frac{\Delta K_{th}}{K_{\max} - K_{\min}}}{(R_{SO} - 1)} \tag{5}$$

where R_{SO} is the shut-off value of the stress ratio K_{max}^{OL}/K_{max}. Second interaction model applied was the Strip Yield model. The Strip Yield model is based on Dugdale model modified to leave plasticity in the crack wake. It assumes that all plastic deformation is contained within a strip located along the crack line represented by finite-width rigid-perfectly plastic bar elements. They allow to calculate the crack opening stress intensity factor K_{op} from the contact stresses.

Before application on two-stringer panel, simulations of crack growth under the spectrum loading were performed for simple CCT specimen geometry. Since analytical solution of stress intensity factor function is known, it was possible to verify the crack growth analyses without the influence of imperfections of FE models. Both the analyses and verification tests (Figure 11) were performed on 100 mm wide and 2 mm thick CCT specimens. For all models the range-pair counting technique was applied. Calculated crack growth curves are shown in Figure 12. The best results were obtained with Willenborg and Strip Yield models that were able to predict the fatigue crack growth life with the error less than 9%. These two interaction models were finally applied also for simulation of crack growth in the two-stringer panel. Since the

load sequence includes compression loads, it was decided to perform the testing with the antibending guides in order to support the cracked panel in compression. It leads to the reduction of stress intensity factor values for crack in the skin and along with it to the acceleration of crack growth in the stiffener. Obtained predictions of crack propagation in the two-stringer panel under the spectrum loading in comparison with the test carried out at IAE laboratory are presented in Figure 13. In this case the crack growth lives were predicted with maximum error of about 25%.

Fig. 11 *CCT specimen with antibuckling guides used for constant amplitude and spectrum tests*

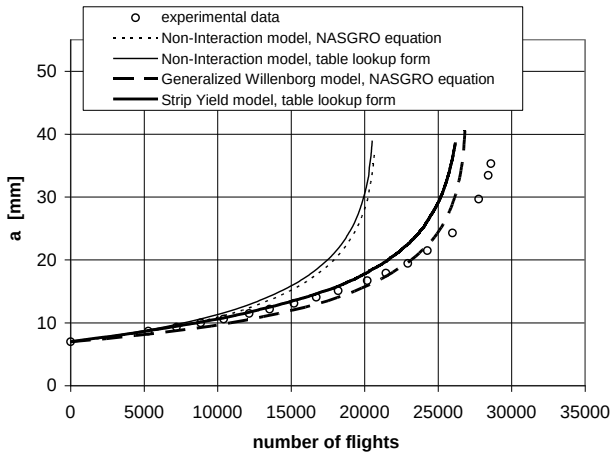

Fig. 12 *Predicted crack growth in CCT specimen under the spectrum loading versus result of the test*

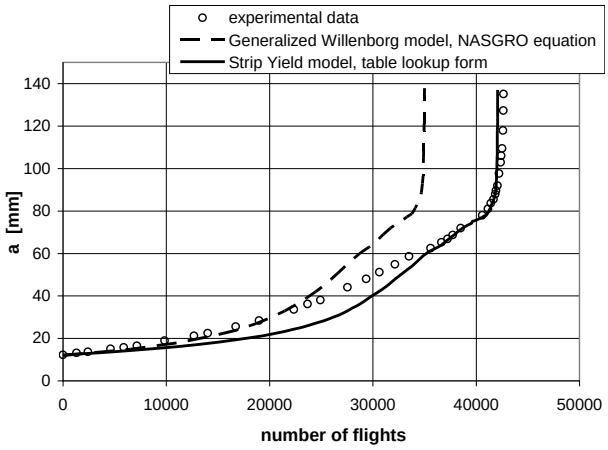

Fig. 13 *Predictions of crack growth in the skin of two-stringer HSC panel under the spectrum loading in comparison with the test*

Conclusion

Experimental investigation and computer modelling of damage tolerance properties of integrally stiffened structures were discussed in this paper. Results of simulations of crack propagation in two-stringer integrally stiffened panels manufactured using high speed cutting technique from 2024-T351 aluminium alloy were presented. Constant amplitude as well as spectrum loading was considered. Relatively wide experimental program comprising the tests on panels and CCT specimens was carried out in order to acquire the crack growth rate data and to enable verification of analyses.

References

[1] MUNROE, J., WILKINS, K., GRUBER, M.(2000). Integral Airframe Structures – Validated Feasibility Study of Integrally Stiffened Metallic Fuselage Panels for Reducing Manufacturing Costs. In: *NASA/CR-2000-209337*

[2] METSCHAN, S. (2000). Validated Feasibility Study of Integrally Stiffened Metallic Fuselage Panels for Reducing Manufacturing Costs. Cost Assessment of Manufacturing/Design Concept. In: *NASA/CR/2000-209343.*

[3] PETTIT, R.*G.*, WANG, J.J., TOH, C.(2000]. Validated Feasibility Study of Integrally Stiffened Metallic Fuselage Panels for Reducing Manufacturing Costs. In: *NASA/CR/2000/209342.*

[4] BUXBAUM, O., HUTH, H. (1987). Expansion of Cracked Fastener Holes as a Measure for Extension of Lifetime to Repair. In: *Engineering Fracture Mechanics,* Vol. 28, pp. 689/698.

[5] NESTERENKO, G.I. (2000). Comparison of Damage Tolerance of Integrally and Riveted Stiffened Structures. In: *Proceedings of the 22nd ICAS Congress* (I. Grant, (Ed.)), pp. 444.1–444.10. Optimage Ltd., Harrogate.

[6] LANCIOTTI, A., LAZZERI, L., POLESE, C. (2005). *Description of the Test Programme*. DaToN–WD–WP 3.1–1.0/DIA–UniPi, Pisa.

[7] RUSTENBERG, J., SKINN, D., TIPPS, D.O. (1998). *Statistical Loads Data for Boeing 737-400 Aircraft in Commercial Operations*. DOT/FAA/AR-98/28, FAA, Office of Aviation Research, Washington.

[8] JONGE, J.B. DE, SCHÜTZ, D., LOWAK, H., SCHIJVE, J. (1973). *A Standardized Load Sequence for Flight Simulation Tests on Transport Aircraft Wing Structures.* NLR TR 73029U, NLR, Amsterdam.

[9] LANCIOTTI, A., LAZZERI, L. (1992). Effects of Spectrum Variations on Fatigue Crack Growth. *Int. J. Fatigue,* Vol. 14, No. 5, pp. 319–324.

[10] ABELKIS, P.R. (1980). Effect of Transport Aircraft Wing Loads Spectrum Variation on Crack Growth. In: *Effect of Load Spectrum Variables on Fatigue Crack Initiation and Propagation*. ASTM STP 714 (D.F. Bryan, J.M. Potter, (Eds.)), pp. 143–169. ASTM, San Francisco.

Influence of Projectile Base Modifications

Adolf Jílek[1], Jan Kusák[2]
[1]Faculty of Military Technology, University of Defence, Kounicova 65, 622 10 Brno, Czech Republic. E-mail: adolf.jilek@unob.cz
[2]Prototypa-ZM, Ltd Company, Hudcova 78, 612 00 Brno, Czech Republic. E-mail: jan.kusak@prototypa.cz, and Institute of Energetic Materials, University Pardubice, Czech Republic

This paper is focused on the design of the outer shape of the projectile. The objective of the researchers is have a stable projectile with the lowest possible drag. Lower projectile drag means lower flight velocity decrease and also a positive ballistic effect. Projectiles with modified outer shapes, especially rear parts of the projectiles (base), are discussed in this paper. Two primary modifications are considered are specifically considered to the back part of the projectile, behind the guiding ring: adding internal channels or outer grooves. The initial hypothesis was that there would be a significant decrease in the drag coefficient due to these modifications. However, after modified projectiles were experimentally tested and aerodynamic simulations were performed in a CFD program, the hypothesis was disproven. The drag coefficient increased due to the modifications, although the inner channels and outer grooves on the back part of the projectile appeared to have a small influence on the damping of projectile swing. Detailed results of the simulations and experiments are compared and discussed below.

Keywords: Projectile, Aerodynamic, CFD, Drag

1 Introduction

In fact, development of projectile shape is as old as ballistics itself. One trend of projectile researchers is in reducing drag. Lower drag of projectile means lower flight velocity decrease during the projectile flight from launch place to the target. This projectile has a longer range or will hit a target with greater speed, i.e. with more energy. It means that the projectile has a positive ballistic impact. Reduction of the projectile drag is possible mainly by modification to its external shape.

2 Projectile Base Modifications

One of the ways to reduce the projectile drag is through changing the external shape of the projectile's base [1]. Adjusting the shape of the projectile's base went from Patent No. 304 216 [2, 3]. On the back part of the projectile's base behind the guiding ring, shape modifications were designed such that there was a reduction of bottom drag and thereby a net reduction in projectile drag.

Two main ways to modify the original projectile with a diameter of 21.04 mm (Fig. 1) were chosen. The first method, according to [1], was to create 4 internal channels (Fig. 2) in the rear part of the projectile (projectile's base) behind the guiding ring. The diameter of each of the channels is 4 mm. The axes of the internal channels are not parallel to the axis of the projectile, but are slightly offset to accommodate projectile rotation. The offset angle is given by the forward flight velocity design and the angular velocity of rotation.

The second method, according to [1], was to add 4 outer grooves to the same part of the projectile (Fig. 3) as the first method. The geometry of the grooves was based on the previous modification. Both the outer diameter of the grooves and their axes angle offsets are the same as the previous modification. In both cases, all edges are knocked and rounded as sharp edges introduce detrimental aerodynamic drag.

Fig. 1 *The original projectile, overall view*

Fig. 2 *The projectile with 4 internal channels, overall view*

Fig. 3 *The projectile with 4 outer grooves, overall view*

3 CFD Simulation

To get an idea of the influence of the modifications described in the previous section, CFD simulations were performed. For comparison, CFD simulations of the original unmodified projectile (Fig. 1) were performed in addition to the modified projectiles. The computational grid (mesh) based on the geometry from Figs. 1, 2 and 3, contains 2 to 6 million elements depending on the complexity of the geometry. One such grid, for the outer groove modification, is presented in Fig. 4.

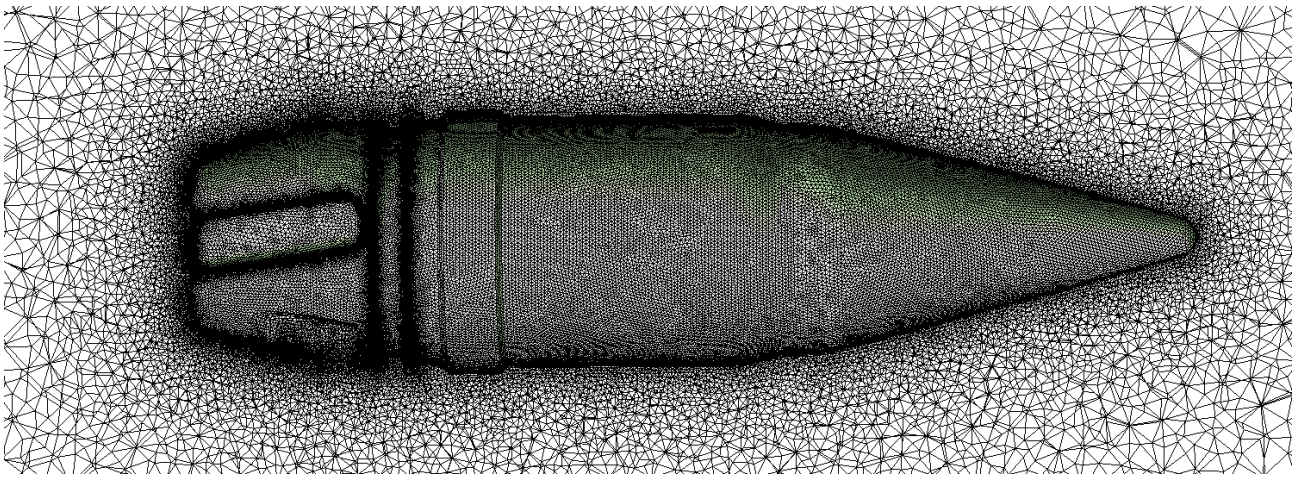

Fig. 4 *Detail of computational mesh of projectile with 4 outer grooves*

The full set of calculations were very complicated and too time intensive to perform with available computer hardware. Therefore, the calculations for this paper consist of only the axial velocity component, i.e. flight of the projectile without rotation. Computational simulation was repeated for thousands of times based on the different modifications and flight velocities. The flight velocities ranged from Mach number M = 0.6 to M = 3.

The following figures show the velocity distribution (contours of the velocity) in the flow over the original unmodified projectile (Fig. 5), the projectile with internal channels (fig. 6) and the projectile with outer grooves (Fig. 7) at the maximum Mach number of M = 3.

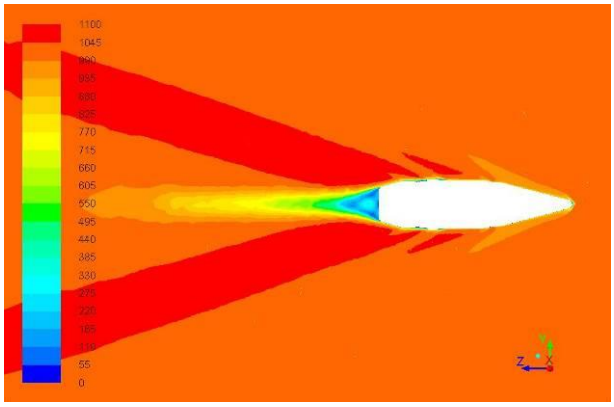

Fig. 5 *The flow over the original projectile, velocity[m.s^{-1}]*

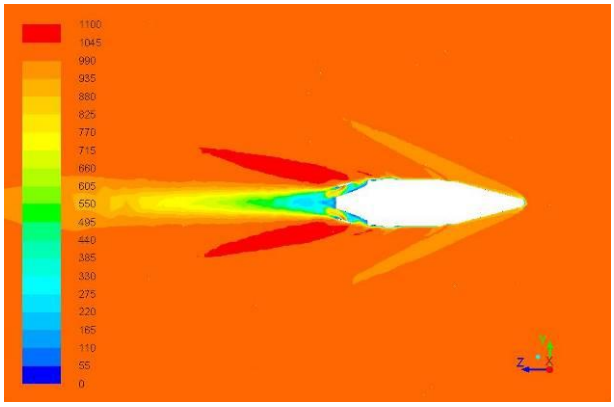

Fig. 6 *The flow over the projectile with internal channels, velocity[m.s^{-1}]*

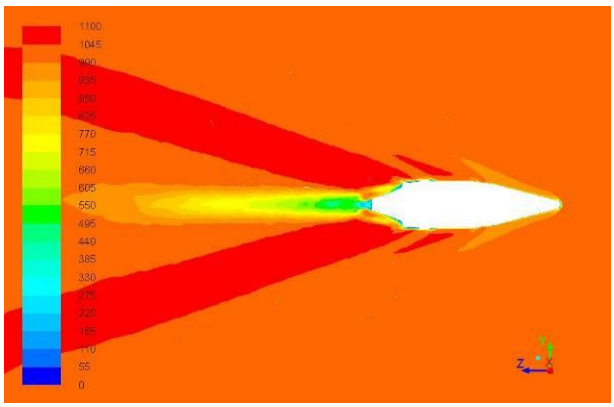

Fig. 7 *The flow over the projectile with outer grooves, velocity[m.s^{-1}]*

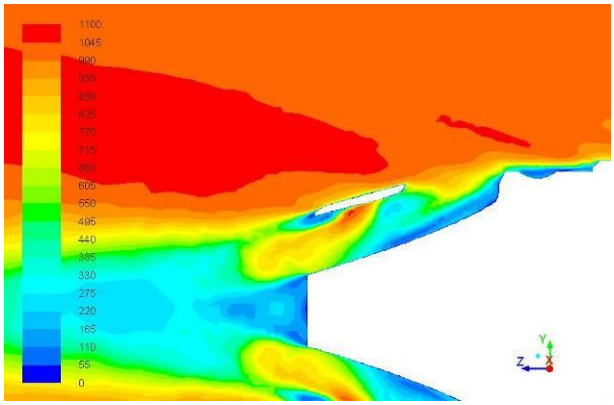

Fig. 8 *Detail of the velocity contour in internal channel[m.s^{-1}]*

Fig. 8 shows a detailed view of the contours of the velocity in a cross section of the projectile with internal channel modifications. As can be seen with a view of the velocity vectors (Fig. 9), whirling appears within the internal channel and behind the projectile; similarly, even with the outer grooves (Fig. 10 and 11).

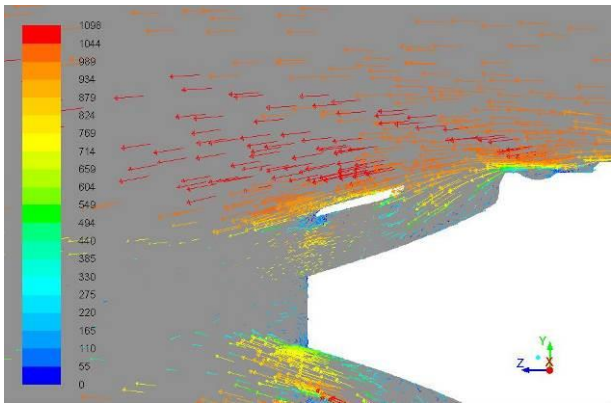

Fig. 9 *Detail of the velocity vectors in internal channel[m.s^{-1}]*

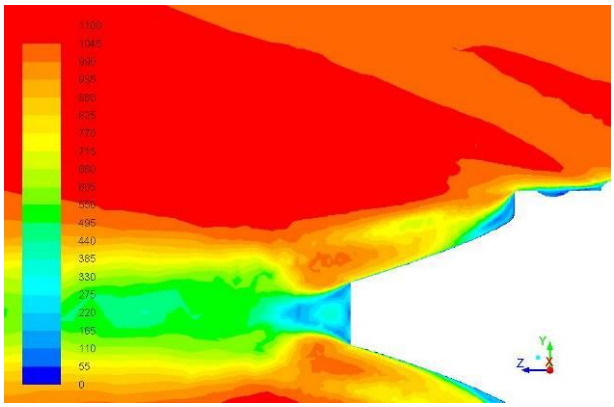

Fig. 10 *Detail of the velocity contour in outer grooves[m.s^{-1}]*

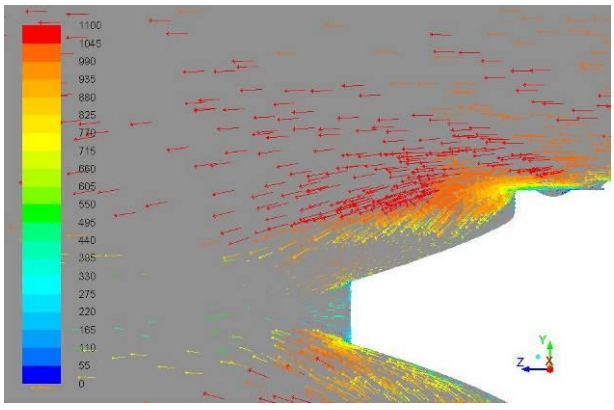

Fig. 11 *Detail of the velocity vectors in outer grooves[m.s^{-1}]*

Each simulation was then evaluated for drag coefficients (c_D) of the projectiles at selected flight Mach numbers (Tab. 1). The results are plotted in Graph 1. The results did not confirm the hypothesized the decline in projectile drag from the unmodified projectile to the internal channels. The projectile with internal channels and also the projectile with outer grooves in fact introduced slightly more drag. The drag coefficients don't increase rapidly. At the maximum velocity (M = 3) for the projectile with internal channels, the drag coefficient increases by 3 % and for the projectile with outer grooves, the drag coefficient increases by almost 7 %. It should however be noted that in the simulation, the projectiles were not rotating and thus were not permitted their ideal flow patterns in and around the modified regions of interest.

Tab. 1 *Projectile drag coefficient*

M	c_D [1]		
[1]	**Original Projectile**	**Projectile with channels**	**Projectile with grooves**
0.6	0.2265	0.3388	0.3163
1	0.6625	0.6841	0.6737
1.5	0.7765	0.7700	0.8185
2	0.6311	0.6544	0.6922
2.3	0.5708	0.5867	0.6207
2.6	0.5198	0.5359	0.5606
2.9	0.4767	0.4884	0.5091
3	0.4636	0.4770	0.4942

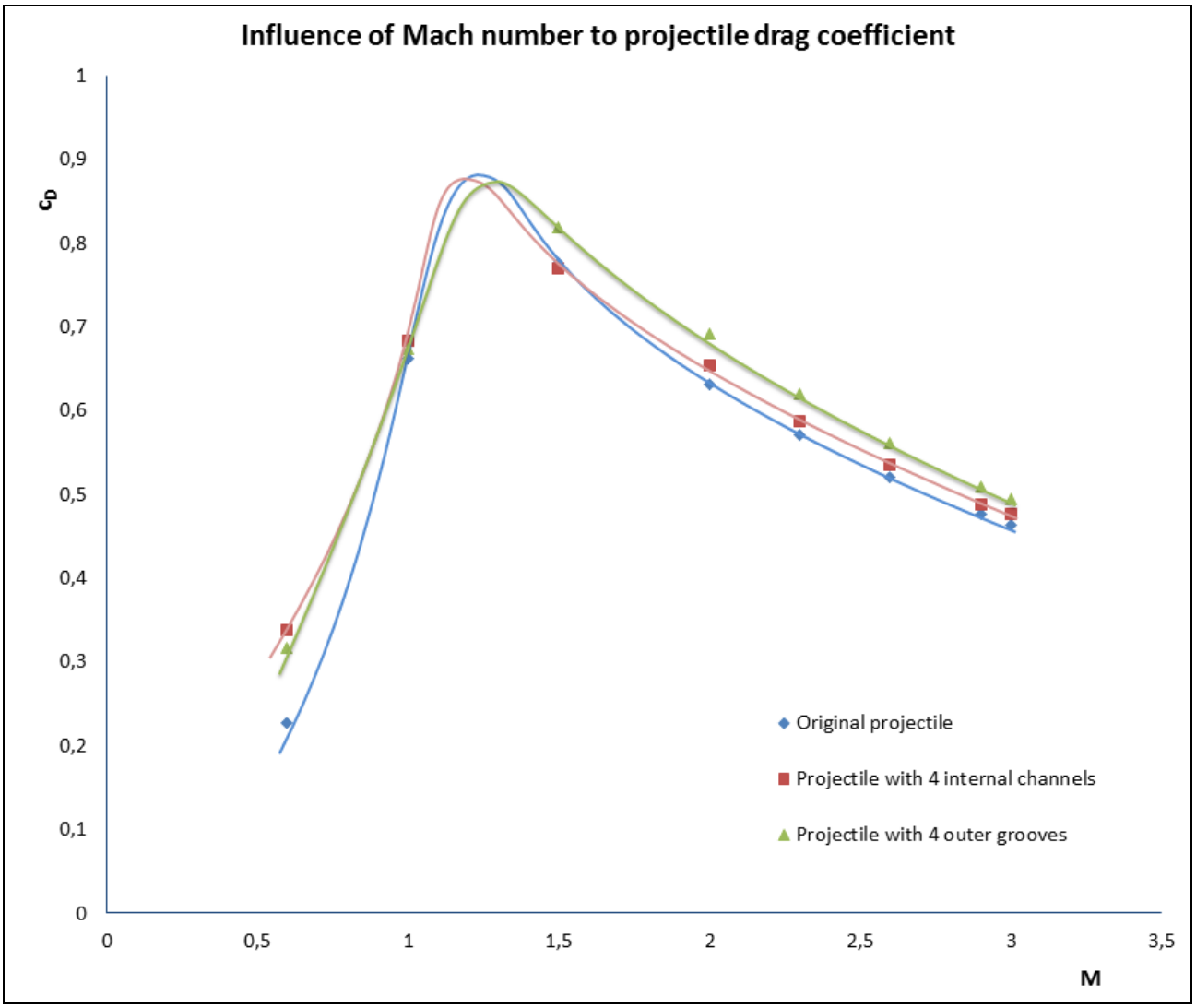

Graph 1 *Projectile drag coefficient*

4 Experiment

Due to time constraints, experimentation with projectiles built to the same specification as those presented in the CFD simulations were not able to be performed. However, shooting experimentation with a projectile with a similarly modified back part, does provide some important insight. Such a test was conducted in the last year by Sellier and Bellot a.s. [4]. Using a .308 Winchester shotgun, the experiment consisted of firing 50 pieces of modified and unmodified projectiles with the same amount of gunpowder at a target placed at different distances. The specific modification consisted of 6

grooves made on the projectile with sharp edges and with an axis parallel to the projectile (Fig. 12). The following measurements were performed during the testing:

Projectile velocity at a distance of 5 m from the mouth of the shotgun barrel (V5).

Projectile accuracy and velocity (V100) at a distance of 100 m from the mouth of the shotgun barrel.

Projectile accuracy at a distance of 550 m from the mouth of the shotgun barrel.

Fig. 12 *Modified projectiles with 6 grooves*

Experimental results showed that there was a greater decrease in average velocity (V5 - V100) between the unmodified projectiles and the projectiles with grooves over all 50 data points:

Original projectile: $V5 - V100 = 773.1 - 679.3 = 93.8\ m.s^{-1}$.

Modified projectile: $V5 - V100 = 776.2 - 674.1 = 102.1\ m.s^{-1}$.

Greater velocity decrease does not necessarily imply a greater drag coefficient. For example, the modified projectiles had less weight which likely explains the higher velocity V5 with modified projectiles. While not directly measured, some likely sources of drag from this modification are due to the fact that the grooves are parallel to the longitudinal axis of the projectile (not inclined) and have sharp edges.

The experiment also showed that the grooves on the back part of the projectile have a significant effect on accuracy at projectile impact. The largest distance from the center of the target of the unmodified projectiles at 100 m was 43.7 mm and at 550 m was 294 mm, while the projectile with grooves at 100 m was 22.0 mm and at 550 m was 242 mm.

5 Conclusion

The CFD simulations and shooting experiments disproved the hypothesis that adjusting the projectile's base will reduce the drag coefficient. While the drag coefficient was not reduced, the experiment did show that the grooving in the back part of the projectile strongly absorbs projectile swing and thus positively affects shooting accuracy. It may be assumed that the significant effect on accuracy will be the same for different calibers of artillery projectiles (including caliber 155 mm) [5]. It should also be remembered that for the shooting experiments, the center of gravity was shifted towards the tip of the projectile, the grooves are parallel to the longitudinal axis, the projectile weight dropped and the modifications were made with sharp edges. The next phase of research will include performing CFD simulations with rotations and carrying out shooting experiments with projectiles modified to the same specifications as the CFD simulations.

References

[1] KUSAK, J., PECHOUCEK, P., NOVAK, M. (2011). *Contribution to design of medium calibre projectiles.* In *ICMT´11 - International Conference on Military Technologies 2011*. Brno: University of Defence, ISBN 978-80-7231-787-5.

[2] KUSAK, J., LEHKY, L., PECHOUCEK, P., PRCHAL, P. (2012) *PV 2010-542, Střela s trubkovým penetrátorem*. Věstník ÚPV č.4/2012 CZ, EU Patent application No. 111 72 327.6.12.60.

[3] KOVARIK, J., KUSAK, J. (2013) *PV 2011-649, Střela*. Věstník ÚPV č. 17/2013 CZ, Patent No. 304 216.

[4] HRON, T. (2014). *Test of adjustment of projectile's base*. Sellier a Bellot a.s., Vlasim, Czech Republic.

[5] KUSAK, J. (2014). Study: *Možnosti zvýšení účinnosti střel ráže 12,7 až 155 mm.* Brno, Czech Republic.

Material analysis of damaged breech locking element of machine gun

David Kusmic[1], Zbynek Studeny[1], Emil Svoboda[1]
[1]Faculty of Military Technology, University of Defence in Brno. Kounicova 65, 662 10 Brno. Czech Republic.
E-mail:david.kusmic@unob.cz, zbynek.studeny@unob.cz, emil.svoboda@unob.cz

Weapons are special systems, which have high demand in terms of reliability, safety and durability especially in the case of automatic weapons. The most stressed parsts of weapons are barrels, breech, locking elements etc. This paper si focused on the failure of locking element, which is used for set the breech baffle and for locking of the breech. From the structural point of view the locking element is highly dynamically stressed component. During the shooting cycles are the shocks transferred into these components, therefore specified material requirements of the locking element are needed. The material of locking element must be modified to hard surface with tough core with thickness corresponding to the size and frequency of shocks to prevent the fatigue failure. The manufacturing documentation wasn´t available, therefore the chemical analysis was performed using the GDOES/Bulk method. The results were compared with material standards to determine the Czech steel equivalent. The damaged locking element was metallographically tested, the surface and microhardness testing was performed by Vickers method. The fracture surface morphology was using the light and electron microscopy (SEM) observed.

Keywords: Locking element, material analysis, failure

1 Introduction

This article describes the material and fractographic analysis of demaged breech locking element of machine gun. In this case is place and sampling method, as well the marking for easier orientation for measurements and analysis described. No drawings and no material informations used for the breech locking element manufacturing were not available. For this reason the GDOES/BULK chemical composition was measurement performed and subsequently it was determined the most progable Czech steel equivalent of the used steel for manufacturing of the breech locking element. The metallographic and fracture surfaces evaluation was performed using the light and electron microscopy. For the surface hardness measurement of the inner and outer surfaces and for microhardness testing was the Vickers method used and the obtained values were compared with the material standard and with undemaged breech locking element. From the structural point of view is the locking element highly dynamically stressed component. During the shooting cycles the shocks are transferred, therefore specified material requirements on the locking element are needed. The material of locking element must be modified to hard surface with tough core and with thickness corresponding to the size and frequency of shocks to prevent the fatigue failure.

2 Sampling and samples preparation

The nucleation cracks were found in the area of breech window radius and the propagation in the axial direction (see Fig. 1). Between the locking windows was the crack propagation in the axial direction found. The axial cracks between the breech windows split the breech locking element into two pieces.

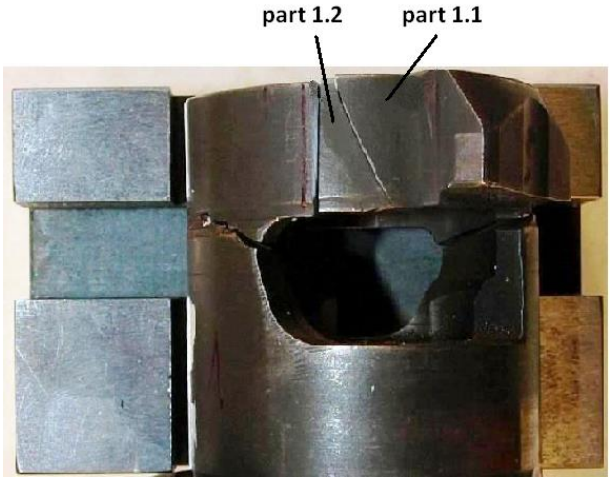

Fig. 1 *Demaged locking element of machine gun*

For the sampling and marking of samples marked as part 1.1 and part 1.2, near the fracture in radial direction, see Fig. 1. All samples were separated using the metallographic saw, due to elimination of the heat and mechanical affecting.

3 Chemical composition evaluation

The chemical composition of separated samples (fragments) was verified by GDOES/Bulk method using the LECO SA 2000 spectrometer. For the calibration procedure were the CKD 150A up to 189A standards used.
Mean values of three measurements of the chemical composition of the breech locking element are summarized in Tab. 1.

Tab. 1 *Chemical composition evalulation*

	Chemical composition [wt%]								
Elements	**C**	**Mn**	**Si**	**Cr**	**Ni**	**Mo**	**Cu**	**P**	**S**
GDOES/BULK	**0.14**	**0.34**	**0.20**	**0.99**	**3.21**	**0.23**	**0.20**	**0.008**	**0.006**
Normalized values of CSN 41 6420 steel	**0.10 – 0.17**	**0.30 – 0.60**	**0.17 – 0.37**	**0.60 – 0.90**	**3.20 – 3.70**	**-**	**-**	**max 0.035**	**max 0.035**

As mentioned above, the material used for designing of breech locking element was unknown. Each steel according to their standard contains a certain range of carbon and alloying elements. Therefore the determination of steel is based on the approximate chemical concentration measurement. The determination of steel was restricted by suitability for nitrocarburizing and by the Cr content, as carbide-like element, and by the Ni content, whose content has a significant effect on increasing of toughness of steel [1, 2]. Based on the chemical composition analysis was with most likely used the Czech 41 6420 steel established (DIN 14NiCr14). Chemical composition of the Czech steel CSN 41 6420 is shown in the Tab. 1, where is determined the chemical composition by the steel standard list (all values in wt%). Excellent accordance was found at the main elements of interest, like C, Mn and Ni. Only the Cr exceeded the specified range of 0.1 wt %. Lower concentration of Mo and Cu was found in the measured breech locking element.

4 Metalographical evaluation

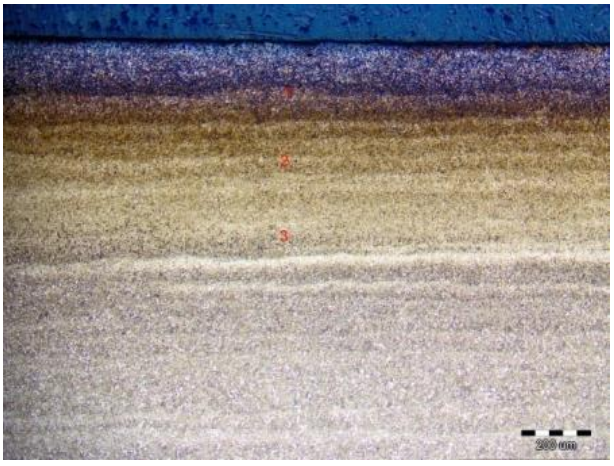

Fig. 2 *Microstructure from to surface to the core of steel, 100x*

Samples marked as part 1.1 and 1.2 were for metallographic evaluation separated by the metallographic saw from fragments of the damaged breech locking element (see Fig. 1) and then were prepared in the mass of DENTAKRYL. Prepared samples were gradually grinded by abrasive papers with decreasing grain size, polished by diamond paste and etched by NITAL etchant to make the microstructure visible. The metallographical documentation was performed using the metallographic light microscope Olympus GX 51.

Microstructure of nitrocarburized diffusion layer of the breech locking element fragment part 1.2 is seen on the Fig. 2 (magnification of 100x).
A detail of diffusion layer with a fine dispersion of carbides and nitrides from the surface to the core of the fragment part 1.2 using magnification of 500x is shown in the Fig. 3. The diffusion layer thickness is approximately about 0.5 mm. A more accurate thickness layer measurement is performed and explained in the Chapter 6.

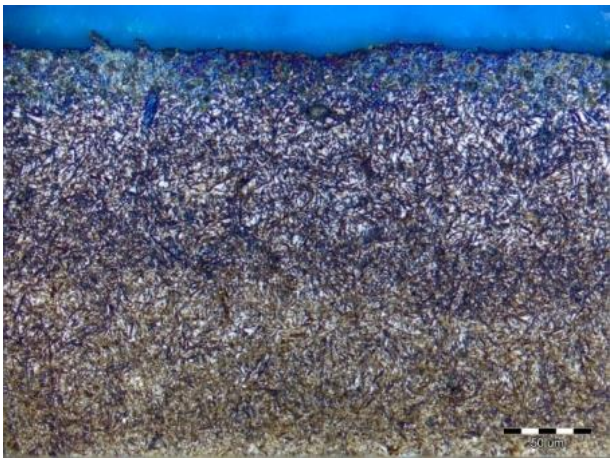

Fig. 3 *The diffusion layer of fragment – part 1.2, 500x*

The microstructure of the core of material is formed from low-carbon tempered martensite, typical for this type of steel. The found alloying elements have a positive influence to creation of nitrocarburized layer and completing the material characteristics. The proportion of Ni in the total volume of steel has a significant effect on growth of toughness values. The Ni dissolved in solid solution softens the crystallization (reduce the grain size) and moves the transition temperatures to the lower values, resulting to decreased susceptibility to brittle fracture; in combination with Cr (as carbide-like element which increases the surface hardness) has an effect on increasing the hardenability and toughness of the steel.

5 Fractography

The fracture surface morphology was macroscopically and microscopically analyzed. For the macroscopic evaluation was the light microscope Olympus SZXP used and for microscophic evaluation the electron microscope (SEM) Tescan Vega TS 5135.
The macroscopic documentation of crack propagation was analysed between the locking windows in the center part of arch of breech locking element see Fig. 4. There are some places that explain the mechanism of fracture on the fractured surface and give informations to form hypotheses about the crack initiation.

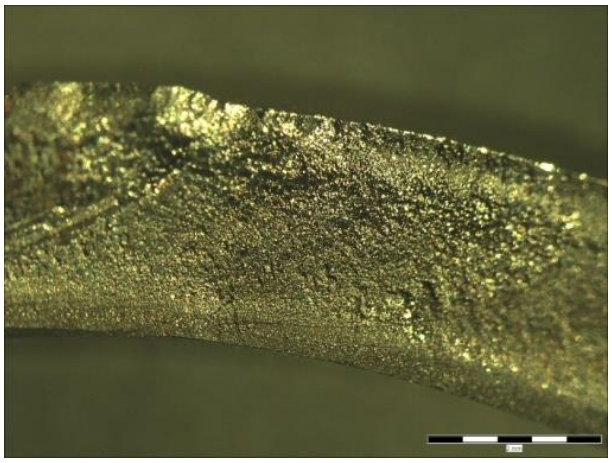

Fig. 4 *The center part of arch of breech locking element, 20x*

A nitrocarburized layer is markable at the periphery of damaged breech locking element in Fig. 4, thanks to the microstructure and its characteristics (high hardness) can be the fracture classified as low energy brittle fracture [3, 4]. This type of fracture is usually initiated from precarious metallurgical defects or technological origin, which is obviously not this case, or is initiated by structural or technological notches. In the case of analyzed damaged locking element of

machine gun can be the notch represented by the very small radius in the inner side of the locking window, which is impact tensile stress from the shooting cycles and can, under certain conditions, fill the conditions for crack initiation in the notch [5, 6]. Cracking lines perpendicular to the direction of tension are markable from the edge towards to the center of the fractured surface, as visible in Fig. 4. The fracture is characterised by high energy ductile fracture in this area, which rises towards in direction to the center of material to final rupture.
Observing the fracture surface leads to classification this rupture as a low cycle fatigue fracture. This conclusion is surpported by observation of cracking propagation during shooting. If the cracking propagation was classified as a graded type, which corresponds to the progress line of cracking in hundreds or thousands of units of shots (or cycles), then the argument supporting the low cycle fatigue cracking is correct.
The microscopical evaluation of ruptured surfaces in the core of material (ductile fracture) is documented in Fig. 5. A hole-structured fracture is markable in Fig. 5, which can be attributed to transcrystalic ductile cracking mechanism. Angles of facets, which were apparently created during the shear fracture process are visible in Fig. 5.

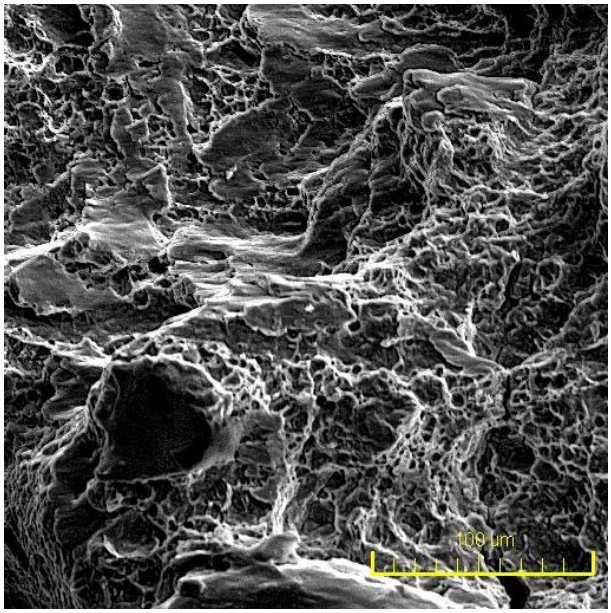

Fig. 5 *The center part of arch of breech locking element, 500x*

By microscopic observation of fracture surface was accumulation of holes found, forming a ductile separation. In combination of ductile separation and stress a ductile fracture in the core of the breech locking element material occurs.

6 Hardness and microhardness testing

The microhardness testing was realized on the cross-sectional fragment marked as part 1.1 in two direction, from the inner and from the outer surface to the core of material of the breech locking element and the surface hardness testing was also carried out. The surface hardness testing was realised under 1 kg (HV) and 10 kg (HV10) load using the LECO LV800 at surface hardness testing device. The surface hardness value was determined as average value of three measurements: 419±8 HV1 and 669±38 HV10. The microhardness profile testing was realised using the automatic microhardness tester LECO LM247at under loading of 50 g (HV0.05) by Vickers method [7].

Tab. 2 *Microhardness values and diffusion layer thickness (fragmentu part 1.1)*

	***Microhardnes* HV0.05**		***Diffusion layer thickness* [µm]**
	Surface	**Core of material**	
Inner surface	**762**	**500**	**452**
Outer surface	**767**	**490**	**440**

For the values of microhardness and diffusion layer depths measurement from inner and from outer surface of breech locking element fragment part 1.1, presented values are determined as average values of three measurements, see Tab. 2. A variance of microhardness values is evident in the microhardness profile plotted in Fig. 6. This variance is caused by

the heterogeneity of the microstructure and material properties under low loading during microhardness testing. Differences of microhardness values between the surface microhardness in the range of 762 ÷ 767 HV0.05 and of the values in the core in the range of 490 ÷ 500 HV0.05 are obvious (see Tab. 2).
The depth of nitrocarburized layer was set according to the DIN 50190 standard. According to the DIN 50190 standard is the diffusion layer border set as a total of microhardness value of the core in HV + 50 microhardness units [8].
The Tab. 2 shows, that the value of diffusion layer depth of breech locking element reached depth of approximately 0.45 mm (measured from both sides of fragment part 1.1). The microhardness profile measurement from surface to the core of material confirmed previous evaluation by light microscopy in Chapter 4.

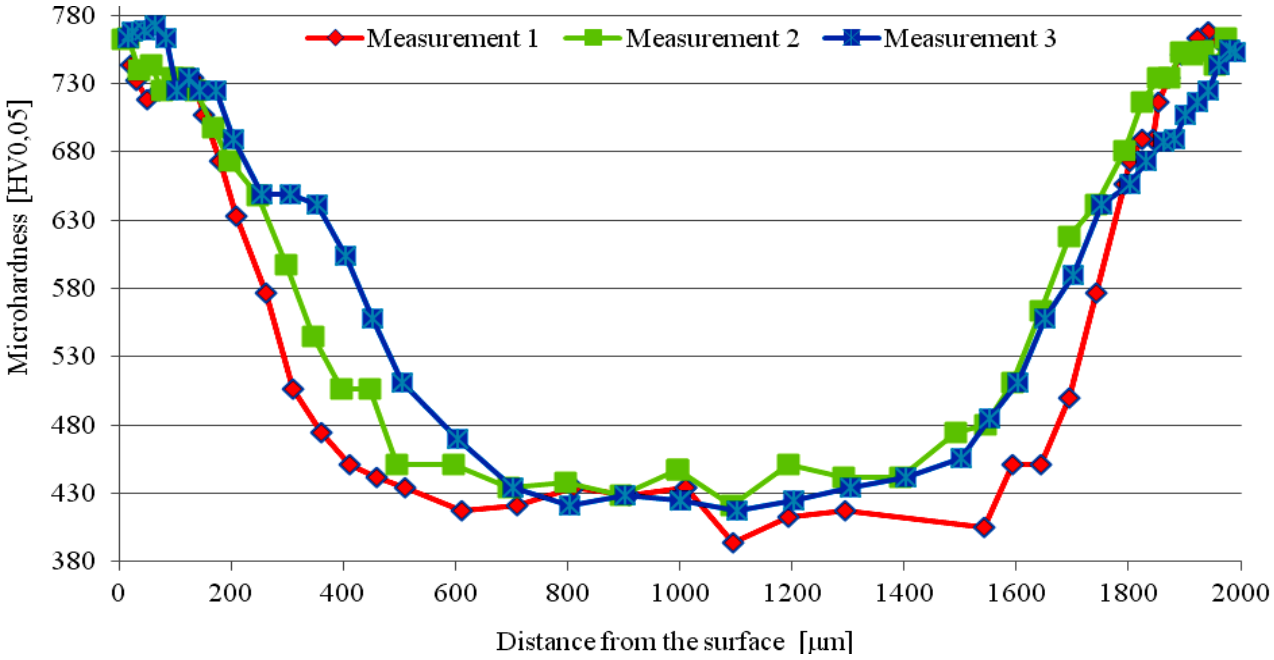

Obr. 6 *Microhardness profile measurementi HV0.05 through the part 1.1*

7 Conclusion

Based on the chemical composition analysis and alloying elements content comparison to the steel standard list was as most likely used steel, for the breech locking element manufacturing, the Czech 41 6420 steel established (DIN 14NiCr14).
The shape and structure of the fractured surface clearly leads to conclusion, that to the fracture of the breech locking element of machine gun by gradual propagation of low cycle fatigue fracture occured. The cracking initation was found in the small radius in the inner side of the locking window of the breech locking element. This small radius represents a stress concentrator from the constructional point of view [9]. In thus designed construction occurs gradually during the loading cycles to accumulation of stress up to reaching the critical value and to the crack nucleation, thanks to following cycles the fatigue fracture of the component occurs.
The diffusion layer depth measurement of nitrocarburized layer was realized using the microhardness testing, in direction from the inner and from the outer surface to the core of material of the breech locking element.
It was found that average depth of nitrocarburized layer reached value of 0.45 mm. Surface hardness values were set to average values of 419±8 HV1 and 669±38 HV10.
Using the metallographic analysis, hardness and microhardness measuring was concluded that on the surface of the breech locking element was created the nitrocarburized diffusion layer. Based on fracture surfaces evaluation was concluded that the ratio of breech locking element wall thickness and average depth of nitrocarburized layer is unsuitable. The breech locking element wall thickness is 2.5 mm and from the inner and from the outer surface to the core of material reached the nitrocarburized layer depth values of 0.45 mm, then the ductile core of material to transfer the gunshots is 1.5 mm thick. Thickness of 1.5 mm of ductile core of material is evidently not enough to absorbing the cyclical dynamic shocks from gunshots and to transfer this intensive loading.

Acknowledgement
The paper was prepared with the support of the Project for the Development of the Organization of the Department of Mechanical Engineering, UoD "Promoting Research, Science and Inovation in the Field of Engineering".

References

[1] HOLEMÁŘ, A., HRUBÝ, V. (1989): Iontová nitridace v praxi. SNTL, Praha 1989, pp. 178-180.

[2] PYE, D. (2003): Practical nitriding and ferritic nitrocarburizing. 2nd edition, Ohio: ASM International Materials Park 2003, pp. 127-129.

[3] SIRIN, S. Y., SIRIN, K., KALUC, E. (2008): Effect of the ion nitriding surface hardening proces on fatigue behaviour of AISI 4340 steel. In: *Materials Characterization*, vol. 59, 2008, pp. 351-358.

[4] STUDENÝ, Zbyněk; KUSMIČ, David. Influence Of Inclusions Size On The Nitrided Components Fatigue Life. In: *23rd International Conference on Metallurgy and Materials*. Brno: TANGER Ltd., Ostrava, 2014. ISBN 978-80-87294-52-9.

[5] KUSMIČ, D., DOAN, T., HRUBÝ, V., SVOBODA, E. (2013): Vliv plasmové nitridace na vrubovou houževnatost. In: *Transfer 2013*, pp. 55-60.

[6] DOBROCKÝ, D., DOAN, T., KUSMIČ, D., HRUBÝ, V. (2014): The Change Of Notch Toughness Parameters Of Steel After Plasma Nitriding. In: *ICMT´- 2014*, pp. 66-74

[7] ČSN EN ISO 6507-1 (420374): 2006 Kovové materiály - Zkouška tvrdosti podle Vickerse - Část 1: Zkušební metoda.

[8] DIN 50190-3 – Hardness depth of heat-treated parts; determination of the effective depth of hardening after nitriding. Deutsches Institut für Normung E. V., 1979.

[9] DOBROCKÝ, David; KUSMIČ, David. The Effect of Plasma Nitriding Process on the Change of Dynamic Parameters of Steel DIN 1654/4. *Manufacturing Technology*, 2015, vol. 15, no. 1, p. 14-20. ISSN 1213-2489.

Variability of application, special equipment operation using renewable sources of energy

Peter Lipták[1], Ivan Kopecký[1], Danka Rakúsová[1]
1Faculty of Special Technology, Trenčín University of A. Dubček in Trenčín, Pri parku 19, 911 06 Trenčín. Slovak Republic. [1]peter.liptak@tnuni.sk, ivan.kopecky@tnuni.sk, danka.rakusova@tnuni.sk

Abstract: Operation of special equipment largely depends on an early and operative delivery of needed input energy. By using semiconducting materials and other advanced material the delivery of input energy can be solved with modern renewable sources, especially in meeting tasks in areas located out of coverage by public electric power system. The same is valid for delivery of power in crisis situations. The authors of the paper summarize the results of research in range of „Application of renewable sources of energy in practice" project. A modeling system and computer simulation of renewable sources of energy was proposed in range of the project.
There is a presumption of application of a system for designing of power systems in logistic containers.
In the last paragraph there are lessons learned from logistic containers power balances that had been operated in SR Armed Forces mission abroad.

Key words: Renewable Sources of Energy, Photovoltaic Collectors, Logistic Container, Power Systems.

1 Introduction

Decreasing reserves of fossil fuels, growth of welt population as well as demands of individuals on energy all over the world, a deepening dependence of a nowadays civilization on a reliable power supply, threat to biosphere, caused in a large scale by power management generate environs in which the problem of a fast-pace application of alternative energy sources is a priority of the day.
The paper deals with a possibility how to use non-conventional energy sources in mobile logistic means. A need for energy of technological equipment in mobile means is different and therefore it is important to know to assign an optimum power source, which would be of a minimum dependence from a place of its operation. The most advantageous renewable sources of electric energy meeting the mobility terms include photovoltaic systems and wind-power installations.
Subsidies from European funds should promote a faster development of use of renewable energy sources in households for small devices. An installed power capacity of the devices is to be properly considered, as there will be supported installations of small photovoltaic systems and wind-power turbines with an installed power capacity up to 10 kW, solar power collectors for water heating, heat pumps and biomass boilers. [2]

2 Current power sources used for mobile logistic means in ISO 1C containers

Electric source aggregates (ESA) in ISO 1C containers, are designed for a production and distribution of electric power as a backup source to ensure an operation of electric devices in field conditions. They include a drive unit, an aggregate producing electric energy, a transformer and cable distribution network. A power block is installed in the ISO 1C container, it is heat and sound-proof, tempering and airing are provided by a built-in discharge fan and through orifices for airing with closing blinds. The container floor is designed in a form of a leak-proof tank to seize a contingent leakage of sealing liquids. The container includes a ready-to-use store for distribution cables and accessories of a power block. The ISO 1C container is equipped with large door with a visor and detachable panels for an easy a day-to-day servicing. [1]

2.1 Requirements for mobile repair means power sources

One of the most important requirement for power sources for mobile repair assets is their applicability in microclimate area with a climate in accordance with N 14 (STN 03 8206):

- Temperature ranging -35 °C up to +55 °C,
- Relative humidity of the air up to 30% at temperature of +25 °C,
- Speed of air flow up to 20 $m.s^{-1}$ from all directions,

Atmospheric precipitations in form of rains with intensity of 3 $mm.min^{-1}$ falling at an angle of 30° in all directions. [1]

They must be mounted so that they can be attached to several kinds of distribution systems:

- TN – C, 3 + PEN, 400/231 V – the most widely used four-conductor distribution system,
- TN – S, 3 + PE + N, 400/231 V – distribution system being used in the world,
- TT, 3 + PE + N, 400/231V – distribution system, scarcely used, however it occurs in power systems of special equipment,

- IT, 3 + PE + N, 400/231 V – isolated system being used mainly in special or medical equipment and in electric facilities for insular power equipment. [4]

A source or a set of electric power sources must be able to manage a load by supplying a stable frequencies and voltage. It is necessary to take into consideration an increased power take-off at inductive and capacity types of impedances upon commissioning, e.g. for series engines and a starting input power is from 1 to 1,5 fold of common input power, at inductive or asynchronous engines a starting input power used to be from 2,5 to 5 folds. Technical equipment of mobile repair assets may differ depending on assignment of a given repair asset.

3 Power balance of mobile logistic means

Technical equipment of mobile repair assets may differ depending on assignment of a particular repair asset.
To propose a set of sources of electric power in logistic assets, it is important to know an installed input that is a sum of all appliances in defined areas including supposed inputs of appliances that may be as:

- Permanently connected appliances,
- Appliances connected into plug circuits.

Table 1 shows an overview of most widely used logistic working places, their input, voltage system and a source of electric power.
An input includes a corrective coefficient, reducing a power required. The standard recommends the following coefficients:

Number of powered appliances / rooms	2	3	4	5	6	7	10	16	20
Coefficient	0,77	0,66	0,60	0,56	0,53	0,50	0,45	0,40	0,38

The designers can define respective coefficients based on their experience and knowledge. [1]

Tab. 1 *Electrical engineering parameters of some logistic container working places*

Designation and marking of a logistic container	**Voltage system**	**Maximum power input (kW)**	**Capacity of the source itself (kW)**
ISO 1C container – social one	TN.S 3+N+PE 400/230V AC 50Hz	18,2	0
ISO 1C container – water tank	TN.S 1+N+PE 1x 230V, 50Hz	1,25	0
ISO 1C container – accommodation 2 bed one	TN.S 3+N+PE 400/230V AC 50Hz	5,5	0
ISO 1C container – accommodation 4 bed one	TN.S 3+N+PE 400/230V AC 50Hz	5,5	0
ISO 1C container– briefing folding 3- wall	TN.S 3+N+PE 400/230V AC 50Hz	7,5	0
ISO 1C container- office	TN.S 3+N+PE 400/230V AC 50Hz	6	0
ISO 1C container – refrigerator for deceased	TN.S 3+N+PE 400/230V AC 50Hz	5,1	0
ISO 1C container – two chamber refrigerator	TN.S 3+N+PE 3x 400V, 50Hz	4,8	Combustion engine
ISO 1C container– surgery ambulance	TN.S 3+N+PE 400/230V AC 50Hz	9,5	
ISO 1C container – mobile workshop of „A", "B" and "C" types	TN.S 3+N+PE 400/230V AC 50Hz	15	5,1

For example:

The SR Armed Forces 1st Multifunctional Engineer unit, ISAF Afghanistan, camp 2 had installed in 2011 the appliances:

Containers -dwelling 15 pcs.....about 82, 5 kW
Containers social 2 pcs.....about 36,- kW
Containers water tanks 2 pcs.....about 2,5 kW

Containers three-wall 2 pcs.....about 12,- kW
Other appliances .....about 2,- kW
Total : **135,-** kW
Real electric input measured in June month 2011 at external temperature 42 °C was **34 kW.**
An electric input per 1 container was 1,62 **kW,** representing a value of **0,25** input power coefficient**.**

The SR Armed Forces 2nd Multifunctional Engineer unit ISAF Afghanistan camp 1 had in 2011 year the appliances installed:
Containers dwelling 23 pcs.....about 126,5 kW
Containers office 5 pcs .....about 30.- kW
Containers social 3 pcs .....about 58,5 kW
Containers as a briefing room 4 pcs..... about 30,- kW
Containers special 5 pcs.....about 31,- kW
Other appliances ..... about 4,- kW
Total: **280,- kW**
Real electric input power measured in June month 2011 at an external temperature 42 °C was **75 kW.**
An electric input per 1 container was **1,88 kW**, representing a value of **0,27** input power coefficient**.**

4 Renewable sources of electric power in currently used mobile logistic assets

One of the most ecological kinds of energy is an electric power gained directly through a transformation of solar radiation, which has been known since 19th century. It is not obvious to everybody that solar power engineering can contribute to production of electricity also in climate conditions with minor intensity of solar radiation. Solar energy falling on the Earth´s surface is of superabundance, however with a low density; in addition it is characterized by seasonal and daily variability affected also by weather. However majority of PV systems does not need a direct solar radiation.

4.1 Renewable sources – photovoltaic collectors

Photovoltaic is a set of technologies, transforming solar light (photons) into electricity using semiconductor materials. Process of a power transformation is a direct one (with no inter stages) and no emissions of greenhouse gases or particles are released in the process. Development of photovoltaic (PV) technologies was motivated 50 years ago by a need to ensure energy for satellites. Because of high prices their further application was limited only for some selected applications, e.g. in consumer electronics. Only reduction of prices in 90ss years was an impulse for development of systems for a distributed production of electricity. The largest barrier in using the photovoltaic is a higher investments comparing with standard power engineering technologies. [3]

Efficiency of electric power accumulation:

In case of electricity gained from photovoltaic, it is necessary to consider, whether the appliance will be supplied directly by photovoltaic panels, or by energy stored in accumulators.
Disadvantage with regard to photovoltaic collectors in power plants, supplying the energy directly into electricity supply system is a fact that a lower efficiency in mobile assets is caused by losses in energy accumulation.
Efficiency of a charging / discharging cycle itself depending on a type of accumulators ranges from 60 % up to 95 %. In terms of energy consumption for production and transport of accumulators, a total efficiency decreases to 50 % up to 60 %, only for lithium accumulator it can reach 70 %.
Crystal solar cells are integrated into so called solar modules, or panels and provide 100 - 130 W.m^{2}output. In our conditions a solar panel of 1m^2 surface produces 100 - 140 kWh of electric power per year. **[4]**

Fig. 1 *Examples of photovoltaic system application on mobile facilities. [7] [8]*

4.2 Renewable sources – wind turbines

Recently the wind power engineering has recorded an enormous development with an annual growth of output more than 30 %. Nowadays the wind power plants building with 1,5 - 2,5 MW output is a common occurrence. The wind turbines with a diameter from 0,4 m up to 80 m are applied producing from 0,25 kW up to MW in order. **[4]**

Fig. 2 *The most widely used constructions of wind turbines- with a vertical axle, with a horizontal axle* ***[4]***

5. Functional model of an insular system of energy renewable sources.

Energy need of a technological equipment in mobile container assets differs, and therefore it is necessary to know how to assign them an optimum power supply system. A draft of an optimum power supply set of renewable source of electric energy includes a developed functional model of an insular system of renewable source of energy.
Application of a functional model of an insular system of renewable power sources having been developed aiming to have at our disposal an experimental source of power supply out of coverage by power distribution system enables an analysis of operational parameters in particular conditions. A functional model in the Fig. 3 contains a photovoltaic panel and a wind turbine, as representatives of the most largely used renewable sources of energy (RSE), as well as energy accumulator, a microcomputer control and monitoring block and a stand-by power supply and optional appliances.

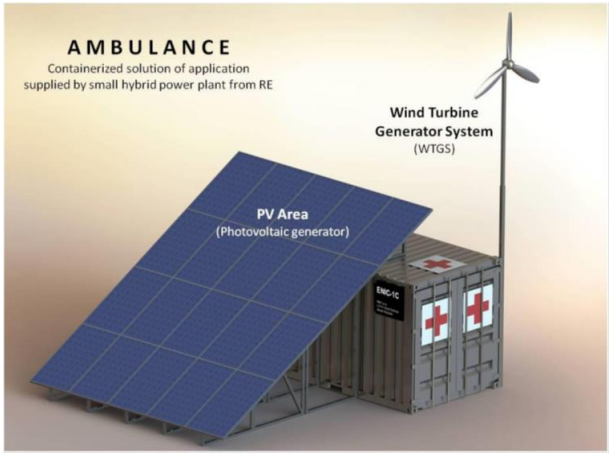

Fig. 3 *Examples of functional models of a Mobile power equipment*

This particular model configuration is aiming to serve as an object for a study of particular characteristics of power engineering units and their compatibility and in developing control software and to optimize a power complex arranged from selected power sources and electric power accumulators.

5.1 Structure of a mobile power equipment

A functional model of Mobile power equipment is in the Fig. 3 and a block arrangement of a whole RSE system is illustrated in the Fig.4. A RSE control panel serves as a central block for a control and management of attached appliances. The power sources and an accumulator operate on a direct current (DC); a power converter generates alternating current (AC) for standard appliances designed for mains 230V/50Hz voltage. Low voltage power DC buses as well as output AC buses are directed through a control panel, which can control them individually with power controllers.
The whole system is power autonomous; it needs no external power source. In case of a long-term inactivity of power sources a complete discharge of accumulator can be prevented if a control panel is completely disconnected. A system reset needs to be done manually. A control panel is equipped with real timekeeper, adjustable through a personal computer. A timekeeper has a back-up power supply, so it is active even in case when a control system is disconnected in emergency.
A control panel is equipped with alpha-numeric display and a row of keysets in order to monitor actual data on power sources, accumulator condition and actual power consumption.

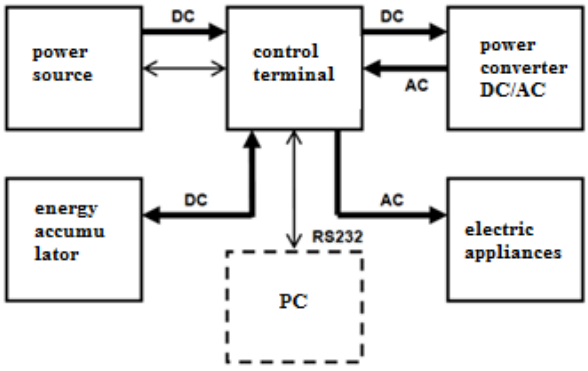

Fig. 4 *A block structure of a functional model of a Mobile power equipment from renewable power sources*

Experimental station functional blocks are divided in three parts in accordance with a transferred medium (electric energy, data, control signals):
A. Power distribution
B. Measuring network
C. Automatic control system.

Basic power units of an experimental station are the power sources:
a) Photovoltaic (PV) panel,
b) Thermo-electric generator (TEG),
c) Wind turbine (WT),

The electric energy accumulators are:
d) Battery accumulator of electric energy (BAE),
e) Balance accumulator of electric energy (BAE),
f) Supercapacitator (SC)

Stand-by power supplies are:
g) Motor-generator (MG),
h) Fuel cell (FC).

These power supply sources are connected to an internal distribution system of an experimental station. A measuring system is formed by a complex of readers from particular functional blocks and measuring devices.
A central functional block of an automated control system is a computer linked with output circuits of a measuring network, through which they transfer data on a condition of the power engineering part. **[5]**

5.2 OSE Expert system

An expert system is a computer software assets consisting of several functional modules enabling an optimum OSE for particular user requirements and for a particular allocation of the equipment.

It contains software means consisting of:

- library databases of equipment to obtain energy from renewable sources of energy,

- means to insert input and output parameters of the application,
- means for modification of local terms of the renewable sources of energy (RSE),
- a simulation instrument with an evaluation of the simulation results and
- a smart means for an optimization of a future application.

The expert system is divided into several modules:

- an interactive module to enter input parameters
- a module to choose functional blocks of the source from an option in library databases
- optimizing module
- simulation module
- module of an optimal system draft.

In the Fig. 5 there is a window with a bus power engineering structure.

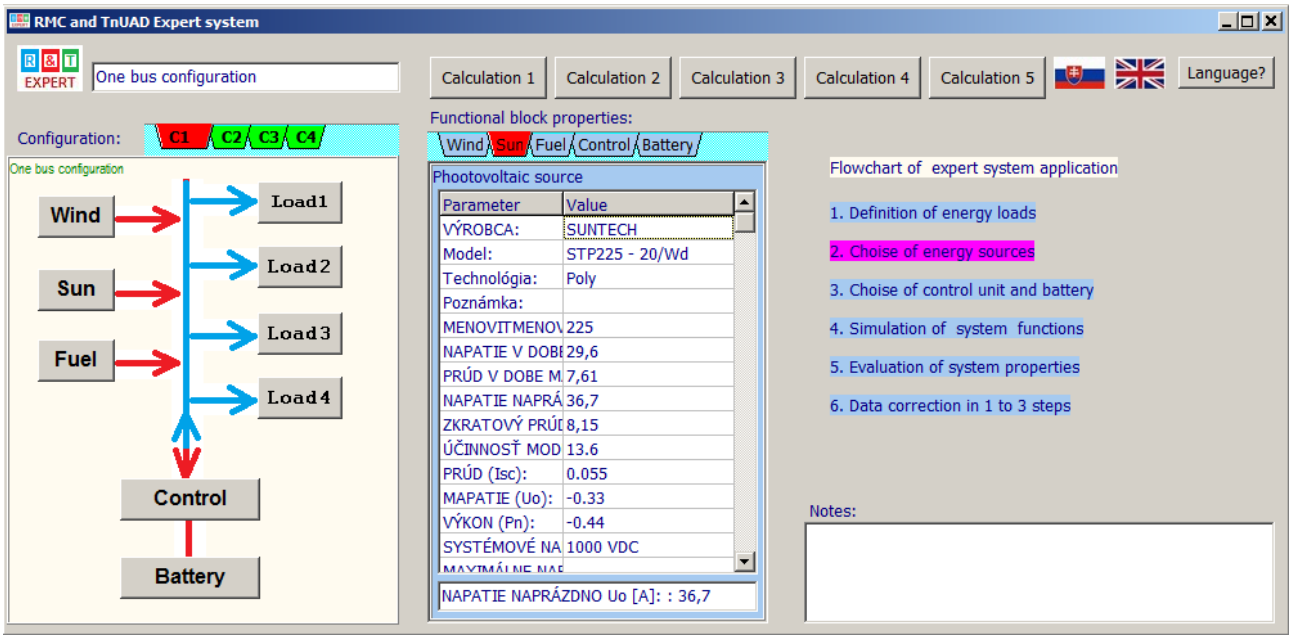

Fig. 5 *Main panel of an expert system; Slovak version one - bus arrangement.*

Input assets enabling an interactive setting of the following values:

- nominal output of power supplies and nominal inputs of appliances,
- parameters of an accumulation unit,
- criteria to control system activities,
- time and a time interval of a computing procedure.

The output parameters are displayed graphically as well as in a numerical form. The panel includes a graph on the operation of the refrigerator temperature regulator, moreover a graph illustrating condition of the accumulator electric charge and a graph displaying activity of the power sources.

A cumulative power balance of the process is one of the most important readout. It displays an energy supplied by particular sources and consumption divided into effective and redundant components. A course of a process can be influenced in an interactive way through changing input parameters and to reinitiate time countdown.

6 Conclusion

Functional model of an insular system of renewable source of energy was implemented aiming to have at disposal an experimental source of electric energy beyond reach of power distribution networks, that enables an analysis of operational parameters in particular conditions. Functional model contains a photovoltaic panel and a wind turbine, as representatives of the mostly used renewable sources of energy (RSE), as well as energy accumulator, microcomputer control and also monitoring block and a standby power supply and selected power appliances. A proposed functional model of an insular system of renewable sources of energy is applicable in a draft and solution of power needs of mobile logistic assets used in insular as well as in hybrid versions.

Acknowledgment

This publication was created in the frame of the project "Alexander Dubček University of Trenčín wants to offer high-quality and modern education", ITMS code 26110230099, based on the Operational Programme Education and funded from the European Social Fund.

References:

[1] LIPTÁK, P., KOPECKÝ, I., GALETA, A.,: Špeciálna technika, časť Stroje a zariadenia Trenčín, 2005, ISBN 80-8075-053-X,

[**2**] www.solarnenovinky.sk/…03/17/potvrdene-dotacie-v...

[3] ŠÚRI, M. : Solar Electricity and Prospects of its Generation in Slovakia. Život. Prostr., Vol. 40, No. 3, p. 127 – 132, 2006.

[4] KOPECKÝ, I., RAKÚSOVÁ, D.: *Hybridné fotovoltické zariadenia v urbanizovaných prostrediach* TRANSFER 2014 15. medzinárodná vedecká konferencia, Trenčín, 23. – 24. október 2014

[5] ÁČ, V., KOPECKÝ, I., JUS, M., TIMÁR, Š.: *VID Mobile power device from renewable resourses of electric energy ,* 2013 TnUAD Trenčín,

[6] ÁČ, V.,: *Modelovanie a počítačové simulácie systémov obnoviteľných zdrojov energie,* Čiastková správa z riešenia projektu ITMS č. 26220220083, TnUAD Trenčín 2015

[7] https://www.google.sk/search?q=solar+panels+on+shipping+container&biw

[8] http://solar.calfinder.com/blog/solar-contractors/solar-power-saves-lives-taxpayer-dollars-on-the-battleground

Application of modern technologies and materials in improving an ballistic protection

Peter Lipták[1], Ivan Kopecký[1]

[1] Faculty of special technology, Alexander Dubcek University of Trencin, , Pri Parku 19, 91106 Trencin, Slovakia,
E-mail: peter.liptak@tnuni.sk, ivan.kopecky@tnuni.sk

Abstract: In the paper there is given a characteristics of a term SPECIAL EQUIPMENT, a supposed classification of special equipment, possible heading of its development from a view of scientific and special activities. The starting points stem from orientation and heading of needs of Alliance groupings, assigned for defence needs, needs to solve non-standard situations, in range of which there is a supposition of development, operation and deployment of special equipment. The article presents also the results in scientific and special work achieved by the Special Technology Faculty of the Trenčín University called by Alexander Dubček in Trenčín. While increasing efficiency of ammunition, it is necessary to improve an individual ballistic protection, as well, keeping the weight on a present-day level. Metallic and non-metallic materials, being worked with advanced technologies allow that. The authors present conclusions from research of features of materials irradiated with electron beam. The paper concludes with presented possibilities for application of such materials aiming to reduce a lethal effect of a projectile from a view of person threat, material and premises.

Key words: Special equipment, Extreme Conditions, Crisis Situation, Classification of Special Equipment, Quality.

1 Introduction

Special technology faculty is assigned as specified by its designation to follow and to take part in research, development, production and operation of special equipment. Under a term of a „SPECIAL EQUIPMENT „in the past the mean was an equipment assigned for activities generally relating with military activities. The areas of assignment were preferably oriented into explosives, explosive objects and weapons. [11]. Special equipment is classified in such a way in bibliography coming from 70-80 ss of the last century,

- Explosives and pyrotechnical weapons.
- Blasting charges.
- Manufacturing technology and laborations.
- Weapons and sights.
- Ballistics.
- Explosive ordnance disposal.
- Ammunition and weapon testing.

Colleagues from University of Defence in Brno define special equipment as equipment that includes modern weapon systems, aviation, missile, land and air (naval) supporting, logistic, communication, intelligence and other equipment assigned for homeland protection, combat, security and non-military (humanitarian and others) operations and moreover equipment for combat against terrorism, organized crimes and other security activities, especially for ministry of defence, interior, authorities acting in crime proceeding, intelligence services and other agencies. It includes also equipment for forensic analysis of mobile phones, monitoring systems (for classified as well as public monitoring), anti-monitoring systems, communication equipment and systems for a legal wiretapping and others [6], [8].

A notion of a special equipment, defined by literature and within it by terminology e.g. [10], is in a current understanding characterized not only from a point of view of a user and an operator, e.g. SR Armed Forces, SR Ministry of Interior, etc., but also from a point of view of a construction uniqueness, its assignment, specificity, operation in special, non-traditional, e.g. extreme conditions, from a point of view of specificity of manufacturing systems and technologies. It exceeds far a term of weapons and explosives, carriers and weapon accessories, ballistic equipment and protection, sights, equipment and material gathered into so called material classes [10].

From a view of up-to-date characteristics of special equipment notion it is obvious that this issue will merit attention in the future. We suppose that the equipment will be specified within this notion:

- Equipment and material assigned to be used in so called crisis situations.
- Equipment and material for needs of a state protection. It is noteworthy that a term of so called material classes within the Slovak Republic Armed Forces is not topical.

- Products and services assigned by a united standardization and codification of the Alliance in terms of Act on the Defence standardization, codification and Government Product and Services Quality Assurance for defence needs. They are codifies in line with a special classifier „Classification of deliveries H2“, this one has been adjusted within NATO Alliance NATO [10].

- Equipment and material assigned to be applied in emergency situations and states.

- Equipment and material assigned for an application in non-standard conditions, e.g. in extreme conditions.

- Equipment and material assigned for specific, unique production and manufacturing systems.

- Equipment and material related with a presupposed research for a so called spatial industry.

2 Particularities of materials for special equipment

With regard to the fact that we have characterized special equipment as the equipment meeting particular conditions of construction for its assignment, uniqueness, operation in special, non-traditional, e.g. extreme conditions from a point of unique manufacturing systems and technologies we point out, that it far exceeded a definition for weapons, explosives and ammunition, carriers and weapon accessories, ballistic equipment and protection, sights, equipment and material summarized in so called material classes [11]. Production of special equipment falls within the area of the most demanding machine engineering production as from a technical point of view, as from a technological point of view, especially from a point of view of a failure-less function, reliability, climate and mechanical resistance to wear and lifetime in normal and extreme conditions [4].

As an example of uniqueness of materials for special equipment we point at their classification into:

- Materials for weapons and ammunition
- Aviation materials
- Material for missiles

In special equipment we can e.g. distinguish:

Materials for weapons and ammunition (small arms, antitank weapons, large calibre and artillery guns and small calibre rounds, ammunition of calibre 12,7 – 37 mm, ammunition for small antitank weapons, artillery ammunition, missiles, aerial bombs, hand grenades, engineer assets, signal and illuminating ammunition).

We differentiate:

- Steels of common quality,

- Steels for welded constructions and components,

- Steels for thermo-chemical processing,

- Heat treated steels,

- spring steels,

- highly alloyed steels,

- Armoured steels (ARMOX produced by a Swedish company SSAB Oxleösund a o.),

- Non-ferrous metals (Pb-Sb, Sn a o. compositions.), bronzes, brass aluminium alloys a.o.).

The most stressed:

- barrels,
- armoured protection (strength, ductility, preserving features also at height temperatures a.o.); heterogeneous structure, use of compound armours, armours with an air gap, ceramic material, light alloys, protection against radiation.

Features (as an example of material ARMOX 600T):

- yield point ≈ 1500 MPa,
- hardness ≈ 640 HBW,
- tensile strength ≈ 2000 MPa,
- tensibility ≈ 7 %,
- contractions 20 %,
- impact value as min. 20 $J.cm^{-2}$,
- through hardening capability,
- homeland provenance e.g. steel ≈ 16 642.

Tab. 1 *Chemical composition (the most important alloying components) of armours ARMOX (in wt%)*

C	Si	Mn	P	S	Cr	Ni	Mo	B
0,21 – 0,47	0,1 – 0,7	1,0 – 1,2	0,01 – 0,015	0,005 – 0,01	1,0 – 1,5	2,5 – 3,0	0,7	0,005

Management of special equipment, its control and regulation is provided by systems designed on the base of electro-technical, electric, optic-electronic and cybernetic devices. These devices consist and are designed from special equipment special materials for electrical engineering, optoelectronics [5]. Here, the semi conductive materials play significant role, in addition to conductive and non-conductive (insulators), magnetic materials.

Perspective and heading of these materials of these materials is oriented to the area of superconductive materials.

3 Achievements in application of high-strength materials on special equipment

TMS and low-temperature tempering is one of possibilities how to improve steel features. This technology is based on use of effect of a plastic deformation resulting in final mechanical-metallurgical parameters of steel. Nowadays an attention is focused primarily on VTMS technologies. A common rule applies that hardness increases with an increasing degree of deformation. In a great rate in a practical implementation of VTMS a limiting technological factor is a possibility of a momentary quenching of product after having finished its mechanical working, i.e. a possibility to prevent or in a certain extent to limit a static re-crystallization of austenite from quenching.

Tab. 2 *Mechanical features and scheduled chemical composition of some sheet plates made from armour ARMOX steels.*

Type	Characteristics									
Armox 440T	Scheduled chemical composition (significant alloying components) [wt%]									
	C	Si	Mn	P	S	Cr	Ni	Mo	B	
	0,21	0,-0,5	1,2	0,01	0,01	1,0	2,5	0,7	0,005	
	Mechanical features									
	Hardness [HBV]		KV-40^0 C [j]		Yield point [MPa]		Tensile strength [MPa]		Tensibility [%]	
									A5	A50
	420-480		min.30		min.1100		1250-1550		10	12
Type	Characteristics									
Armox 500T	Scheduled chemical composition (significant alloying components [wt%]									
	C	Si	Mn	P	S	Cr	Ni	Mo	B	
	0,32	0,1-0,4	1,2	0,015	0,010	1,0	1,8	0,7	0,005	
	Mechanical features									
	Hardness [HBV]		KV-40^0 C [j]		Yield point [MPa]		Tensile strength [MPa]		Tensibility [%]	
									A5	A50

	480-540		min.20		min.1250		1450-1750		8	10
Type	Characteristics									
Armox 600T	Scheduled chemical composition (significant alloying components) [wt%]									
	C	Si	Mn	P	S	Cr	Ni	Mo	B	
	0,47	0,1-0,7	1,0	0,01	0,005	1,5	3,0	0,7	0,005	
	Mechanical features									
	Hardness [HBV]		KV-40^0 C [j]		Yield point [MPa]		Tensile strength [MPa]		Tensibility [%]	
									A5	A50
	570-640		min.12		1500		2000		7	x

As a static re-crystallization progresses, hardness and tensibility of low-tempered martensite decrease. In case that a basic alloying steel base does not enable provision of sufficient restraining of development of re-crystallization process, it is possible to use a positive effect of micro-alloys, e.g. zircon additive, which prevents the re-crystallisation from development [1]. Next we provide an overview on source ARMOX materials. The higher content of alloying elements (Cr, Ni) in armour ARMOX type steel is needed to achieve requested features. Steel must have a low content of inclusions. Tab. 4.1.1 presents mechanical features and scheduled chemical composition of some armour sheet plates of ARMOX type.

On the above mentioned materials we applied cutting with water stream, cutting with plasma arc, cutting with plasma beam. Dimensions of testing samples are shown in Table 3.1.2. The tests were done on a general-purpose testing machine Instron 5500R .

The results after an experiment are in the Table 3.1.2, 3.1.3, 3.1.4.

Tab. 3 *Results of mechanical tests for a water stream*

Armox type	Thickness [mm]	Real Ø thickness [mm]	Yield point [MPa]	Strength limit Rm [MPa]	Ductility A5 [%]
440T	4	4,44	1226,76	1358,35	13,13
	5	5,45	1310,90	1413,10	11,25
	8	8,50	1277,25	1372,92	14,06
500T	4	4,38	1422,09	1614,32	14,38
	5	5,88	1414,98	1638,05	10,94
	8	8,49	1409,37	1620,13	13,44
600T	4	4,58	1562,12	2094,37	13,44
	5	5,48	1605,42	1967,90	10,63
	8	8,54	1630,44	2020,81	10,94

Tab. 4 *Results of mechanical test for a plasma arc*

Armox type	Thickness [mm]	Real thickness Ø [mm]	Yield point [MPa]	Strength limit Rm [MPa]	Ductility A5 [%]
440T	4	4,49	1163,19	1290,22	14,38
	5	5,43	1278,25	1340,51	11,88
	8	8,50	1054,80	1151,20	12,50
500T	4	4,42	1359,60	1539,89	9,38
	5	5,59	1389,70	1579,61	10,31
	8	8,48	1152,33	1288,00	12,50
600T	4	4,57	1529,79	1895,28	8,75
	5	5,79	1412,10	1710,13	9,06
	8	8,52	1251,12	1489,44	8,44

Tab. 5 *Results of mechanical test for a laser beam*

Armox type	Thickness [mm]	Real Thickness Ø [mm]	Yield point [MPa]	Strength limit Rm [MPa]	Ductility A5 [%]
440T	4	4,45	1227,64	1360,06	10,00
	5	5,45	1255,19	1383,54	13,75
	8	8,34	1134,35	1255,43	14,69
500T	4	4,43	1392,68	1579,15	9,69
	5	5,90	1391,13	1598,99	12,19
	8	8,45	1236,19	1404,65	12,19
600T	4	4,48	1556,29	1956,49	4,38
	5	5,32	1477,66	1811,13	4,69
	8	8,46	1342,35	1672,45	5,31

An example of a graph of values measured is shown in the Figure 1. An example of a tension chart is in the Figure 2.

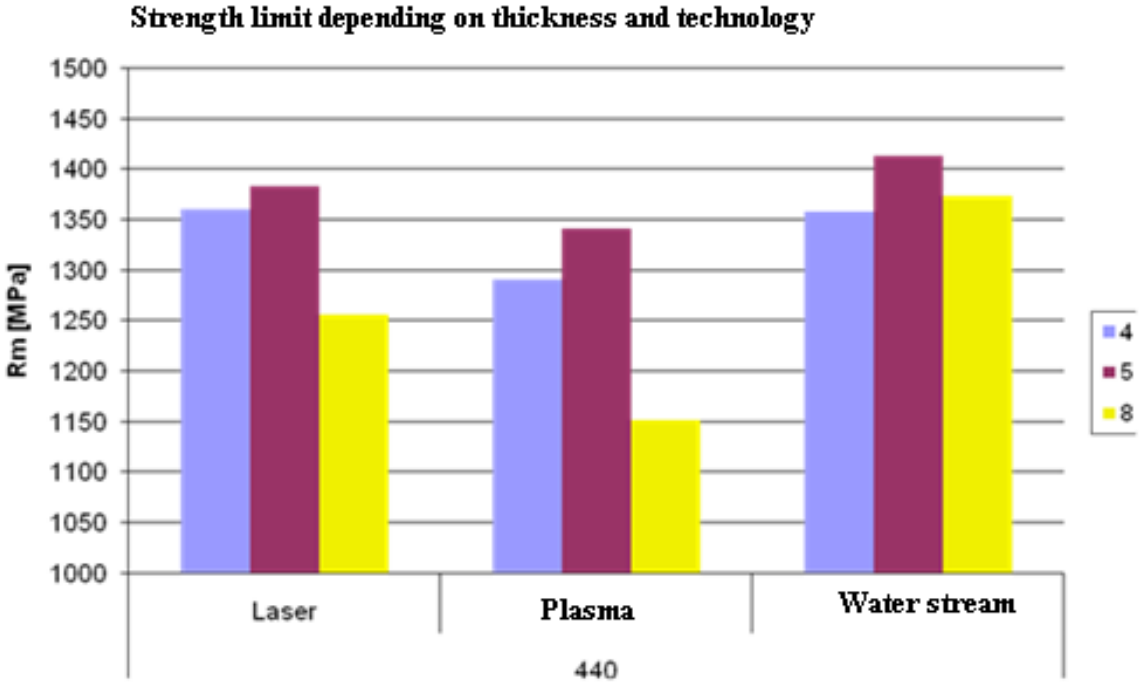

Fig. 1 *Strength limit depending on thickness and technology*

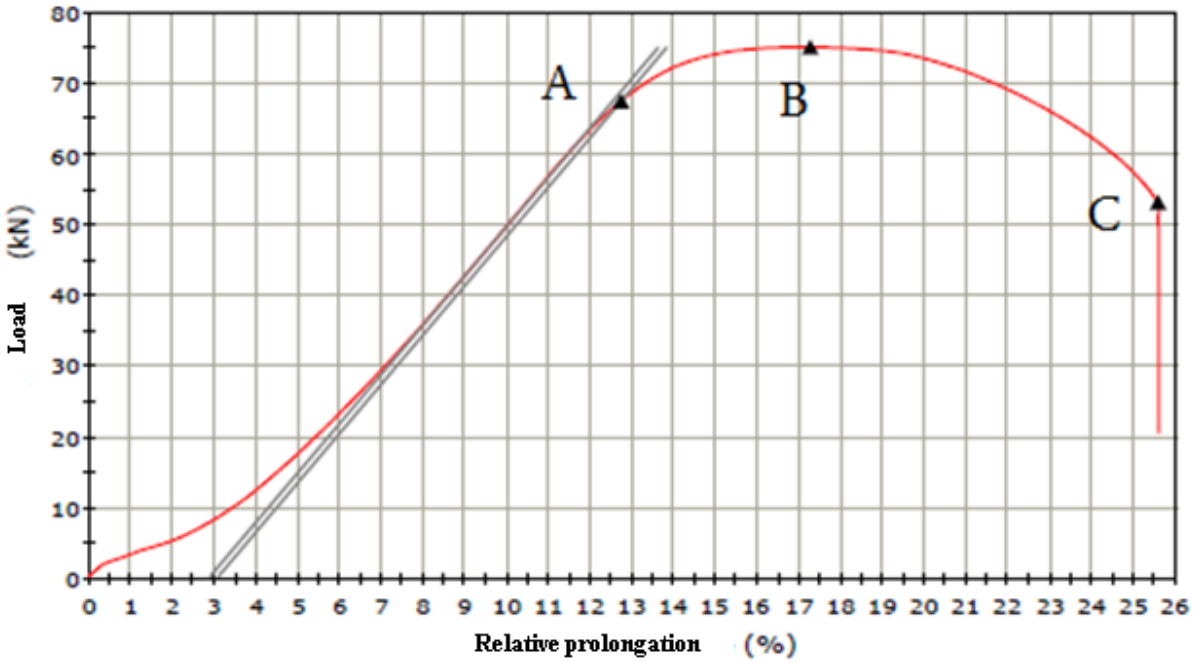

Fig. 2 *A tension graph for ARMOX 440T material with similarity for thicknesses 4 mm, 5 mm, 8 mm, VP, LL, PO division kind*

Based on above mentioned experiments there were recommended austenitic steels for production purposes for special equipment of a CONTAINER WITH A PROVIDED BALISTIC PROTECTION type having been treated by a technology of water stream division. The technology of water stream division has no effect on a change of mechanical features of the material purchased from a supplier. Rather great attention has been paid to a research of possibilities in welding from a point of view of micro hardness and effects of cutting technology on a change of a microstructure of ARMOX highly strong steels during their welding.

4 Conclusion and final summary

Need of science, research and education in area of special equipment is obvious. We can prevent the efforts from designing the special equipment and technology in other way through its complex definition meeting current needs of science, research and practice. Subsequently through publishing a proper encyclopaedic publication of a monograph type, where an issue of special equipment will be characterized in a complex way. Mutual cooperation of the Trenčín University called by Alexander Dubček in Trenčín with schools and institutions in Slovakia and abroad is a preposition for a development of special equipment in a complex notion. The Faculty of Special Technology of this university stands in front of an issue to organize a meeting of some selected schools, institutes and facilities of above mentioned parties on an international level aiming to solve an issue of an individual ballistic protection, material and equipment. We suppose that it will be possible still in 2015. An issue of materials and technologies for special equipment has historical roots abroad as well as in Slovakia and in the past also a successful history of cooperation. This is a base to start solving other, new projects being solved on an international level.

Reference

1. BALUŠEK, J., MATYÁŠ, M. *Technologické principy tepelně mechanického zpracování vysokopevných martenzitických ocelí.* Štúdia. Vítkovice, UMI.
2. GALETA, A., JOZEFEK, M., LIPTÁK, P. *Munícia a výbušniny.* Trenčianska univerzita Alexandra Dubčeka v Trenčíne, Fakulta špeciálnej techniky. Trenčín 2006. ISBN 80-8075-104-8.
3. GALETA, A., LIPTÁK, P. *Prístrojová technika zbraní.* Trenčianska univerzita Alexandra Dubčeka v Trenčíne, Fakulta špeciálnej techniky. Trenčín 2004. ISBN 80-8075-025-4.
4. JOZEFEK, M., LIPTÁK, P. *Meranie a skúšanie špeciálnej techniky.* Trenčianska univerzita Alexandra Dubčeka v Trenčíne, Fakulta špeciálnej techniky. Trenčín 2005. ISBN 80-8075-097-1.
5. HASSDENTEUFEL,J., DUBSKÝ,I., RAPOŠ,M., ŠANDERA, I. *Elektrotechnické materiály.* ALFA Bratislava, SNTL Praha. 1978. Č.63-555-78.

6. HRUBÝ, V., GREGER,M., NĚMEC,J., SILBERBAGEL, A. *Přehled materiálového inženýrství.* Kovosil Ostrava 2010, ISBN 978-80-903694-5-0 (obr. 125).
7. LIPTÁK, P. *Special Technique and response of special Technique Faculty of the Trenčin university called by Alexander Dubček Trenčin to its development.* In: 18. Medzinárodná vedecká konferencia Výzbroj a technika pozemných síl 2012, Liptovský Mikuláš Akadémia ozbrojených síl ge. M.R. Štefánika Liptovský Mikuláš, 7. – 8.11.2012. Elektronický zborník príspevkov, ISBN 978-80-8040-458-1. Str. 79-86.
8. MACKO, M. *Kinematic condition for revolver trigger release*. Sborník-B, Vojenská akademie, Brno. 2002, *ISSN 1211-1023*.
9. MANDELÍKOVÁ, L: *Analýza a interpretácia odborného textu.* (So zameraním na technický text). Trenčín: Trenčianska univerzita Alexandra Dubčeka v Trenčíne, Fakulta špeciálnej techniky 2012. 175 s. ISBN 978-80-8075-518-8
10. MERŇÁK, G. *Vyzbrojovanie v NATO*. In: Obrana, október 2007. Ministerstvo obrany SR r.č. 758/93, str. 18 -19.
11. URBAN L a kolektív. *SPECIÁLNÍ TECHNIKA I. a II*. FMVS a GŘE ZOS Brno. Praha 1976. Č. 730.2/199/72. DT 623.

Reviewers: Prof. Ing. Vladimír Bella, CSc., prof. Ing. Vojtěch Hrubý, CSc.

Reliability of Special Technique Materials

Peter Lipták[1], Jiří Stodola[2]
[1]Faculty of Special Technology, *Alexander Dubcek University of Trencin, Slovakia, Pri parku 19, Trenčín, Slovak Republic*, *E-mail: peter.liptak@tnuni.sk*
[2] Faculty of Military Technology, University of Defence, Czech Republic, Kounicova 65, Brno, Czech Republic, *E-mail: jiri.stodola@unob.cz*

Abstract. The typical features of advanced economics of industrial countries include robust scientific and technological development in branch of materials and other are characterized by effort to achieve the most effective production and utilization. Effectiveness and public productiveness can be achieved through quality projects, designs, manufacturing machines and equipment and of course through high-class designers, constructors, technicians and workers.

Keywords: Reliability, Special Equipment, Materials, Quality, Safety

1 Introduction

In former times the price was decisive in sales; today mostly the quality determinates the price. The term of quality in EU countries is based on a supposition that a product is of high quality, providing that it meets requirements set by standards. The quality of a product is a set of features stating the capability of the product to fulfill functions it has been assigned for. The term of quality includes technical aspects (functional, utility features), economic features (purchase price and running costs), environmental features etc. Modern concept of quality is based on the fact, that an evaluation of utility features is left for effects by market mechanisms; however they are relatively strictly evaluated by authorized laboratories through a certification of security, hygienic and environmental properties of products. Extremely important are e.g. environmental features, protecting interests of a whole society. They include namely

- A possibility of a product disposal, its recycling and its return into a lifecycle,
- Contents of expended energy and material – economy,
- Environmental characteristics in proper sense (emission, waste, noise, vibrations, radiation burdens on environment etc.),
- Toxicological characteristics – e.g. a level of a possible threat in accident environs etc.
- Reliability, namely a long term failure less operation and a good sustainability without increased requirements for spare parts or without a need to replace a product and for additional consumption of raw material, materials, energy, human labor etc.

From the above mentioned it results explicitly that a quality product must be reliable. However from a range of quality parameters it is obvious, that an issue of quality is not only a matter of production, but it relates an activity which should be ensured in all phases of the product´s lifecycle, i.e. in pre-manufacturing, manufacturing phases, in a phase of its use until its shutdown from operation, its ecological disposal and return to next lifecycle. A whole range of interconnected activities with numerous feedbacks links take part in each such phase aiming to ensure a quality. From a general term is not therefore an essential to define a separate level of reliability, but an optimization of a whole system. The rate of optimization can be expressed using a simple model, which in some way expresses an operational effectiveness of the system in a following form [1]

$$U_p = N(t) \cdot R(t) \cdot P_p(t) \quad , \tag{1}$$

where
U_p … an operational effectiveness of the system, $N(t)$ …level of performing the function, $R(t)$ …failure less operation, $P_p(t)$ … system availability.

In this simplified model we can understand an operational effectiveness as an ability of a given technical system to fulfill fictions at a certain time and in given conditions. Such understood operational effectiveness is a certain criteria of quality and utility of the system and it is understood with its technical an economic parameters, in conditions in which such system was created, in which it has been operated and maintained. Such model describes an operational effectiveness as a connection of the level of performing the function of availability, failure-less operation and sustainability. Such model describes an operational effectiveness with a probability, that a level of performing the function will meet the requirements, for which it has been created, designed and manufactured; that a system will be working in a defined time frame with no failures and also, that in a given time period it will be available for operation. It results from model (1) that the same operational effectiveness can be achieved at a relatively low level of failure-less operation (so with a defective construction and a resulting low level with an inherent reliability) and a high level of availability or vice-versa.

2 Effects Having Impact on Reliability

In analysis the reasons and major consequences of failures we always have to consider whether the consequences of failures are acceptable from a point of threat to a life, health or whether the failures do not result in large economic losses. The failures resulting in life menace fall under a significant component of reliability, which is called security. In some areas, nuclear power engineering a.o. is a minimum level of security defined by legislation, it is internationally unified and it is proved by state supervision authorities usually through a certificate proving that the requirements defining the minimum level of failure are met. From these points it is obvious, that a maximum level of failures, it means reliability is limited through requirements defining the minimum level of security and it cannot be exceeded, even at the price that the economic optimum will not be achieved. In stating the requirements on reliability of special equipment it is necessary to start from a system of operation, which is usually formed by three basic subsystems, namely: a man, an engine and environment. If we should express a philosophy of requirements on reliability and its legislative definition, we could note:

1. The catastrophic and critical failures must not exceed a defined level, or its socially accepted level is defined in such a way that a menace of catastrophic or critical failure is not higher or lower than in other areas (society, transport, industry a.o);
2. It means. e.g. that a rate of catastrophes or critical failures e.g. in air transportation must be lower than in areas of other kind of transportation;
3. It is desirable, that a trend in a rise of catastrophic failure is of decreasing trend in a time period, or in certain low stabilized rates of catastrophes or critical failures the constant levels can be admissible;
4. Probability of a rise of a catastrophic or a critical failure considered per an operational unit (km, motohour, standard hour, flying hour, a.o.) related to a total lifetime of a technical system $F_k(t) \leq 10^{-7} - 10^{-9}$.

The requirement expressed in point 4 is based on a general term of reliability applied for a risk of failures. We suppose a probability $P(x)$, expressing a fact, that a resistance to failure is equal or lesser than a certain value x. Likewise a probability, that an operational load causing failures is equal or greater than a certain value x, is $Z(x)$; the probability, that an operational load is ranging from x up to $x + \Delta x$, is then $Z'(x)$. For a certain value x the probability of a failure is equal to a probability, that an operational load is ranging from x up to $x + \Delta x$, multiplied by a probability, that a resistance to failures is lesser than x. A total probability of a failure is given by a relation [2]

$$F_X = \int_0^x P(x).Z'(x)dx \quad . \tag{2}$$

An acceptable (limit) value of such understood probability is derived from a time development of a failure rate for particular areas (military, engineering, transport, a.o.). It results from a relatively similar statistic information (namely in aviation, rail and road transport a.o.) related to an operational unit that a rate of catastrophic and critical failures decreases over time. This fact is then used in practice to define socially accessible catastrophic and critical failures, casualties, intensities of subsystem failures etc. For an objective understanding of a catastrophic or critical failure is needed to distinguish the reasons resulting from a failure of a technical equipment, machine and reasons resulting from a failure by a human actor. From a relatively long-term statistics of reasons of catastrophes, critical failures and accidents (from aviation, traffic accidents a.o.) is known, that a decisive reason of such failure used to be a human actor. A man as a reason of failure is inherent not only in failures by an operator, maintenance faults, failing in management, but also in reasons which have not been explained. It seems that a human actor participates in up to 40 – 50% of reasons of failures, whereby the reasons caused by environment (traffic density, black ice, haze a.o.) are represented in about 10 – 20 % and proper technical failure, including servicing and unknown reasons form only 30 – 40% [3]. A human actor as a reason of unreliability, from practical reasons used to relate to a man as a subsystem of a given technical system (a vehicle, an aircraft, a nuclear power plant a.o.). However such definition is not fully correct and with a technical development, roboting and automation has been still specified. It seems that also the failures of a given inherent unreliability can be caused by a deficiency of a human actor in a whole lifecycle from assignment, designing, manufacture, installation until an operation itself, figure 8. From a point of view of influence of a human actor on reliability it is needed to note, that a human psychic, its physical abilities result from a long-term evolution. He significantly differs in relation to modern equipment, equipment and devices, whose features and capabilities change and improve with each new type. Theoretical papers and practical experience show, that a fairly significant factor from a point of reliability is an interaction between a man – machine, and more over in a stress situation. From these facts four basic areas can be created [2], [4], which are in mutual interaction, they are interlinked and have a reciprocal influence and namely:

- A selective choice of qualified operators; it seems, that an additional influencing on a human actor is a complex process, which can be facilitated in a qualified selective choice from a set of candidates, whereby we start from inherent and gained capabilities of the applicants.
- Qualification training of operators; it is a long-term, systematic process, being held not only in period of a preparation for a profession, but during a whole period when performing a particular profession; such process includes not only a comprehensive theoretical training, achieving of practical capabilities skill, but mainly proper practical skills, including experience from nonstandard situations.
- Concept of machines and systems of their support; it relates solutions, leading to a situation when an operator is transferred from a position of a manual operating staff to a position taking-decision in non-computed

situation of course having sufficient classified information and first of all into a control position; in controlling the machine, the threat of faults and failures must be minimized in a system way (the machines are to be designed using a so called "fool-proof" method, or "a machine resistant to faults").

- Legislative – normative barriers; each system has its own restrictions, parameter limitations with a certain restrictions and limits; "a human actor" subsystem must observe such restrictions defined as binding regulations, instructions, acts, measures, prohibitions, recommendations and other administrative restrictions; they should be documents, which do not "tie-up the hands" to an operator, but on the contrary, they form a set of important information necessary for meeting the mission and of a needed level of reliability.

Complexity and heterogeneity of a human factor meanwhile does not allow simulating theoretically nor in an experimental way all non-standard stress situations. Therefore up to now a decisive criterion is a real operation. The incentives then for corrective measures then stem from it and background papers to achieve a higher level of reliability in new generation systems. A need of obtaining objective information about a real operation stands out from these views. A logical modification of a term of responsibility can be found based on a preliminary monitoring of information from operation. [1], [2]: „A product is reliable if during its lifetime it follows a supposed rule of its behavior. In case of deviation, it is unreliable". The issue of reliability from these viewpoints can be expressed by an interaction of free or more precisely four agents, namely: manufacturer, human factor as an operator and an important role of a state as a state supervisor, which is a guaranty of all-society interests. A state supervision makes an influence on safety and reliability, namely through binding legislative papers in area of design, construction, production, testing, certification, operation, maintenance, including preparation and testing of manufacturing operators. For example in the field of aviation, nuclear plants, important industrial areas, transportation and others the state supervision must pursue a permanent monitoring of a level of responsibility of systems and to draw consequences from found deficiencies as against a manufacturer as against an operator. There are the consequences in maintenance resulting from these facts (RCM a.o.) [2], which have to be dynamic and they must systematically respond to a found level of reliability as well as to financial costs. Objective systematic monitoring of the reliability state however leads to a detection of failures and in its consequences it decreases an ability to meet an operational task – a mission [2]. For these reasons they are looking for such methods, which can decrease the negative consequence of an objective detection and such failures, which can not affect a safety or a reliability of the task. Opinions on the admissibility of certain disorders are contained, for example used in standard design philosophy, as safe after a failure, as well, so called "fail - safe". Today, several methods are elaborated on the admissibility of certain failures for meeting a task, but opinions on them are not yet clear, and they vary considerably in different regions. If a fully objective assessment, of the likelihood of danger to the operation is possible with a with a broken part and if such assessment is made with relatively simple criteria and an acceptable confidence, then it will contribute significantly to the operative decision making in the operation and also to significant financial savings. It stems from those considerations that in complex systems, a complex fault as such is irrelevant but its consequences are decisive.

3 Conclusion

The submitted text outlines a possible systemic approach to reliability and durability of special equipment and their structures, which can be, in various specific applications differently modified, which always depends on the consequences of any critical or catastrophic failures. Everyone is aware of the fundamental differences in the consequences of failure for special equipment, aircraft equipment, nuclear facilities or conventional machinery. The reason is that in some applications in special equipment, as well as air transport, etc. is the probability of catastrophic failure actually the probability of death of people. Development of technology, however, needs the quantification of critical and catastrophic failures, and in the sense that it uses such probability, which corresponds to less than one disaster in the life of the entire file structure under consideration as e.g. for transport airplanes means $F(t) = 10^{-7}$. We note, however, that it is a probability of occurrence in a highly complex mechatronic complex system, from any, usually in the present state of knowledge, exactly unobservable causes. It follows that the probability of catastrophic failure of the subsystem should be in order of $F(t)=10^{-8}$ respectively $F(t) = 10^{-9}$ or even smaller. Probability of catastrophic failure $F(t) = 10^{-9}$ is so small that its experimental demonstration represents an extremely extensive tests which are currently unfeasible and that are not yet implemented only in exceptional cases (shuttles, especially important weapons systems, etc.).

References

[1] BARLOW, R.E., PROSCHAN, F. Mathematical Theory of Reliability. Golub, G.H., Stanford University, 1996.

[2] LIPTÁK, P., STODOLA, J. Dependability Engineering for Special Purpose Machines Equipment. Monograph. 1st Edition. A. Dubcek University of Trencin, 2011. ISBN 987-80-8075-481-5. (102 p).

[3] BARÉNYI, I., HÍREŠ, O. Mechanical Properties of Forgigs depending on the Changes in Shape and chemical Composition of Inclusions. In: *Metalurgia*. ISSN 0543-5846. Vol. 49, No. 4, 2010, p. 313-316.

[4] BARÉNYI, I., HÍREŠ, O.,LIPTÁK, P.,HLÁDEK, M. Changes in Microstructure and Microhardness after Application of unconventional Cutting Technologies on Armoured Steels In: *Journal of international scientific publications. Material, Methods & Technologies*. ISSN 1313-2539. Vol. 5, Part 1, 2011, p. 249-255.

Compressive creep testing of $MoSi_2$-SiC nanocomposites

Natália Luptáková[1,2], Beáta Ballógová[3], Petr Dymáček[1,2]
[1]CEITEC-IPM, Žižkova 22, 616 62 Brno, Czech Republic. E-mail: luptakova@ipm.cz
[2]Institute of Physics of Materials, Academy of Sciences of the Czech Republic, Žižkova 22, 616 62 Brno, Czech Republic. E-mail: pdymacek@ipm.cz
[3]Institute of Materials Research of Slovak Academy of Sciences, Watsonova 47, 040 01 Košice, Slovak Republic, E-mail: bballokova@imr.saske.sk

The aim of this study is to investigate the creep resistance of molybdenum disilicide ($MoSi_2$-SiC) based composites with different types of embedded particles. The materials were prepared via powder metallurgy using high temperature controlled reaction sintering (CRS). The creep experiments were performed in uniaxial compression at constant stress in the temperature range from 1273 K (1000 °C) to 1473 K (1200 °C) for applied stress from 50 to 100 MPa. Creep was tested by stepwise loading: in each step, the load was changed to a new value after steady state creep rate had been established. The applied stress dependences of the creep rate at different temperatures were analyzed in terms of stress exponent (*n*) and activation energy (*Q*). Possible rate-controlling mechanisms were suggested.

Keywords: $MoSi_2$-SiC, creep test, compressive creep, stress exponent, activation energy

Introduction

Material such as Mo, which has several excellent electro-mechano-thermal properties, is used for many applications, but suffers from severe oxidation problems. $MoSi_2$ is a substitute material for such applications, due to its excellent resistance to oxidation at high temperature. $MoSi_2$ single crystals exhibit macroscopic compressive ductility at temperatures below room temperature in some orientations. Polycrystalline $MoSi_2$ possesses elevated temperature creep behavior which is highly sensitive to grain size. $MoSi_2$-SiC composites show an important combination of oxidation resistance, creep resistance, and low temperature fracture toughness [1]. The silicide $MoSi_2$ can best be described as a borderline ceramic-intermetallic compound. A generic definition of a ceramic is that a ceramic is a solid, ionocovalent, inorganic compound. Applying this definition to $MoSi_2$ indicates its borderline nature, since it differs from a ceramic only because its atomic bonding is a mixture of covalent and metallic. $MoSi_2$ possesses ceramic-like high-temperature oxidation resistance, and metal-like electrical conductivity [2].

Industrial applications include furnace elements and components, power generation components, high-temperature heat exchangers, gas burners, lances for liquid metals and glasses, igniters, and high-temperature filters. Aerospace applications include turbine aircraft engine hot-section components such as blades, vanes, combustors, nozzles, and seals. Automotive applications involve components such as turbocharger rotors, valves, glow plugs, and advanced turbine engine parts [1].

This material exhibits ceramic-like brittleness at room temperature, and hence fracture toughness is a major issue. It also shows metal-like plasticity at elevated temperatures, with the result that creep resistance is a major issue. Moreover, the high temperature strength of this material is a problem, and incorporation of SiC into the $MoSi_2$ matrix provides a compromise. [1-3].

A number of factors have been observed to improve the elevated temperature creep resistance of these materials. The introduction of SiC nanocomposites significantly improves high-temperature creep resistance. Creep rates of material containing 20 vol. % SiC have been reported to be approximately two orders of magnitude lower than those of polycrytalline $MoSi_2$. Alloying with WSi_2 has also been observed to improve creep rates, but to a lesser extent than SiC additions. Effects of nanocomposites additions and alloying have been seen to be additive. SiC nanocomposites have generally been observed to be more effective than SiC particles in terms of improving creep resistance, indicating an importance of reinforcement shape morphology on creep behavior of these composites. An important observation which has been made is related to the competing effects of SiC reinforcing addition volume fraction and associated gram size of the $MoSi_2$ matrix on the creep resistance of $MoSi_2$-SiC composites. As SiC is added, the grain size of the $MoSi_2$ is reduced. This leads to a maximum in the composite creep rate with volume fraction of SiC addition. Creep rates for 5, 10 and 20 vol. % SiC particle reinforced composites are higher than those of unreinforced $MoSi_2$ while creep rates of a 40 vol. % SiC particle composite are substantially lower. This behavior is related to the fact that, with increasing SiC addition, the grain size of the $MoSi_2$ matrix is reduced. The reduced matrix grain size then promotes the operation of grain boundary

sliding creep mechanisms [2].

Experimental materials and methods

The starting material was prepared according to patent [4]. The method is based on high-energy milling (HEM) of high purity coarse-grained powders of Mo and Si with mean grain size 100 to 500 μm. After several hours of milling in a planetary mill Pulverisette 5 (made by Fritsch) in argon atmosphere highly dispersed powder mixtures were obtained. In order to prepare the composites, nano-sized SiC dispersoid ceramic particles were also introduced into the matrix during the milling process. Milled mixtures were compacted by cold pressing to high densities (above 95% of theoretical density) and subsequently by pressureless reaction sintering at 1773 K (1500 °C) in vacuum. Compression creep tests were performed on shaped specimens - small prisms (2 x 2 x 4 mm^3) for compressive creep tests were cut by electric discharge technique. Typical microstructure of $MoSi_2$-nanoSiC composites in polarised light is shown in Fig. 1 [5].

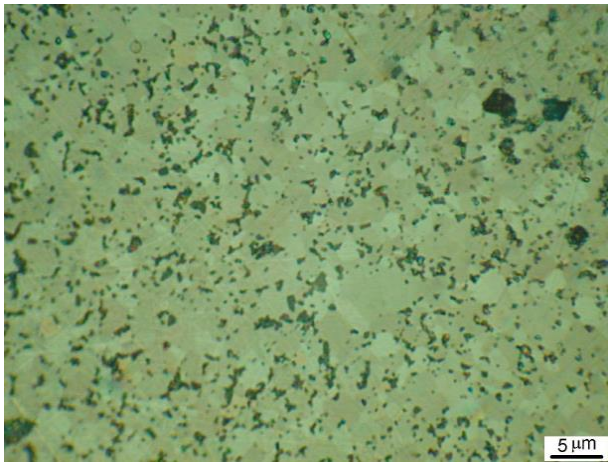

Fig. 1 *LOM micrograph of $MoSi_2$ + 10 % nanoSiC [5]*

Results and Discusion

Figure 2 shows typical creep curves in terms of deformation vs. time plots, measured in compression at 1273 and 1473 K (1000 and 1200 °C) and constant loading of 100 MPa. The highest creep rate, increasing with temperature, has been observed for the monolithic material.

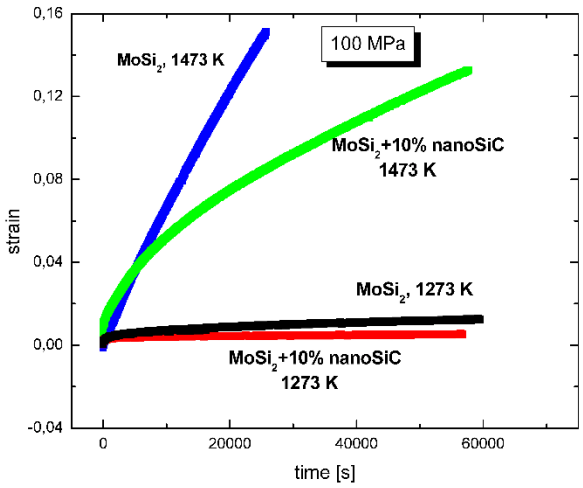

Fig. 2 *Creep curves for studied materials (stress 100 MPa, temperatures 1273 and 1473 K)[3]*

Figure 3 shows the creep strain rate as function of the applied stress (50, 80, 100 MPa) at temperatures 1273 K and 1473 K (1000-1200 °C). In the case of the composite, the stress exponent is equal to 1.23 at 1273 K (1000 °C) but at 1473 K (1200 °C) it increases up to 3. These values indicate that the dislocation climb, which is controlled by the atomic

diffusion, determines the final creep rate. For cases when the stress exponent "*n*" is lower than 3 it is usually assumed, that the creep rate is connected to the transitional mechanisms, which include both dislocation climb and dislocation glide. The temperature dependence of the steady-state creep rates is shown in Figure 4. The apparent values of activation energies are basically independent of load in the measured stress range (50-100 MPa).

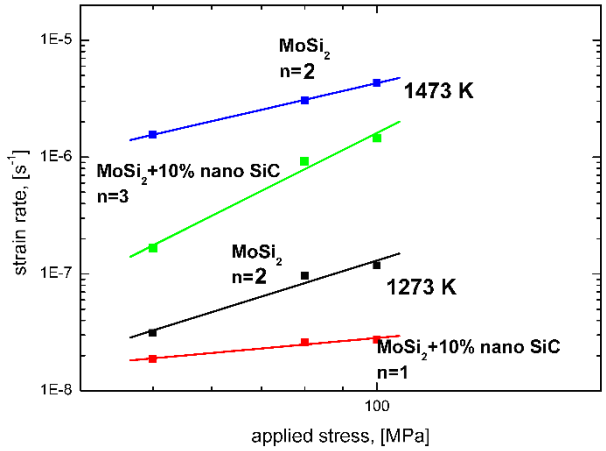

Fig. 3 *Creep rate as a function of applied stress, temperatures 1273 K and 1473 K [3]*

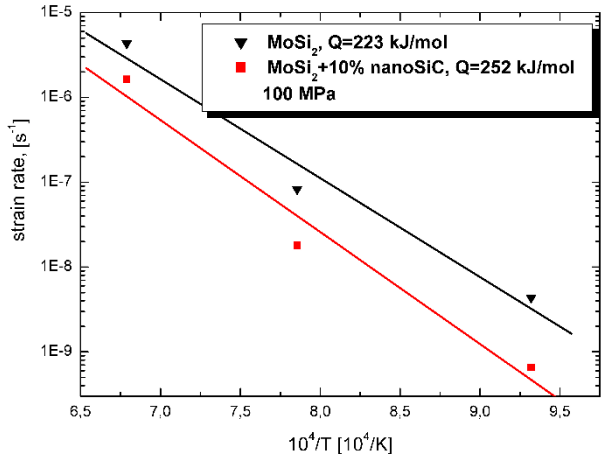

Fig. 4 *Temperature dependence of the steady-state creep rates [3]*

Sadananda et al. [6] showed that creep resistance of polycrystalline $MoSi_2$ is very sensitive to grain size and is controlled mainly by dislocation glide and climb as well as by grain boundary sliding. For composite materials they that have found for 5 % to 20 % of SiC particles the creep rates were higher than for monolithic $MoSi_2$. This is because higher volume fraction of SiC particles diminishes the mean matrix grain size which facilitates grain boundary sliding. According to results published in [7], which give the stress exponent in $MoSi_2$ based materials between 1 and 2, it is suggested that the dominant mechanism of creep deformation is atomic diffusion (probably Coble or Nabarro-Herring model).

Diffusion creep occures $\sigma/G \leq 10^{-4}$ (where σ is stress and G is shear modulus). Two mechanisms are considered important in this region. The first one takes place at high temperature by diffusion of vacancies via lattice (Nabarro-Herring creep) producting an increase in the length of grain along the direction of the applied (tensile) stress. Creep occurring by boundary diffusion is known as Coble creep. It occurs at lower temperature than Nabarro-Herring creep and result in sliding of the grain boundaries. Generally, both Nabarro-Herring and Coble mechanisms, operating in a parallel way, contribute to the diffusional creep [8]. The agreement between apparent activation energies for different types of $MoSi_2$-based materials suggests that diffusion takes place mostly inside the $MoSi_2$ grain, which corresponds to the Nabarro-Herring mechanism. According to Kofstad [9], the activation energy of diffusion of silicon atoms within $MoSi_2$ crystals is 250 $kJ.mol^{-1}$, which corresponds to the results obtained at low stresses (< 20 MPa). In literature there are no reliable accurate values of Mo diffusion within $MoSi_2$ but according to Sadananda they fall within interval 350-450

$kJ.mol^{-1}$.

Conclusion

Conclusions can by summarized in the following point:

1. Creep characteristics of experimental materials confirmed improved creep resistance of composite when compared to monolithic $MoSi_2$. However, with increasing temperature the creep resistance of the composite significantly declines, particularly at temperatures above 1473 K.
2. The values of stress exponents and activation energies measured for compressive creep suggest that the dominant mechanism of creep deformation is diffusion of atoms (Coble or Nabarro-Herring model). Based on apparent activation energies it is probable that the diffusion takes place mostly inside the $MoSi_2$ grains, i.e. Nabarro-Herring mechanism is prevalent. The higher Q_A value measured in $MoSi_2$-10% nano SiC (429 kJ/mol) suggests presence of additional mechanisms, most probably grain boundary sliding at higher temperatures, which is enabled by present amorphous phase along boundaries. This means that at higher temperatures the creep resistance of the composites sharply decreases because of their finer grains.

Acknowledgement

This work was realized in CEITEC - Central European Institute of Technology with research infrastructure supported by the project CZ.1.05/1.1.00/02.0068 financed from European Regional Development Fund.

Refereces

[1] AJAYAN, P. M., SCHADLER, L. S., BRAUN, P. V. (2003). *Nanocomposite Science and Technology*, pp. 68 – 69. Wiley-VCH, Weinheim.

[2] PETROVIC, J. J. (1995). Mechanical behavior of $MoSi_2$ and $MoSi_2$ composites. In: *Materials Science and Engineering A*, Vol. 192-193, No. 1, pp. 31 – 37.

[3] BALLÓKOVÁ, B., BESTERCI, M., HVIZDOŠ, P. (2009). High temperature properties of the $MoSi_2$ and $MoSi_2$-SiC nanocomposites. In: *High temperature materials and progress*. Vol. 28, No. 5, pp. 271 – 276.

[4] SCHOLL, R., KIEBACK, B. *Patent DE 44 18 598 A1*.

[5] BALLÓKOVÁ, B. (2008). *Štruktúra a mechanické vlastnosti kompozitov na báze $MoSi_2$*. PhD Thesis. [In Slovak], p. 98. ÚMV SAV, Košice.

[6] SADANANDA, K., FENG, J., JONES, H., PETROVIC, J.J. (1992). Creep of molybdenum disilicide composites. In: *Mater. Science and Eng.* A. Vol. 155, pp. 227 – 239.

[7] SADANANDA, K., JONES, H., J FENG, J., PETROVIC, J.J., VASUDEVAN, A.K. (1991). Creep of monolithic and SiC whisker-reinforced $MoSi_2$, In: *Ceram. Eng. Sci. Proc.* Vol. 12, No. 9 – 10, pp. 1671 – 1678.

[8] ČADEK, J. (1988). *Creep in metallic materials*, pp. 205 – 209. Academia Prague, Prague

[9] KOFSTAD, P. (1966). *High Temperature Oxidation of Metals*, John Wiley & Sons, New York.

Statistical monitoring of decrease of surface eccentricity and hole of barrel tubes from high strength steels under the production conditions

Jozef Majerík[1], Jozef Šandora[1], Jaroslav Jambor[2]
[2]Faculty of Special Technology, Alexander Dubcek University of Trencin. Pri Parku 19, 911 05 Trencin. Slovakia. E-mail: jozef.majerik@tnuni.sk
[3]Alexander Dubcek University of Trencin. Studentska 2, 911 50, Trencin. E-mail: jaroslav.jambor@tnuni.sk. Slovakia

This work investigates issues of BTA drilling of deep holes with slenderness ratio L:D = 45÷60 of high strength steels with a tensile strength of *Rm* = 1350÷1600 MPa. Methodology for testing of surface when turning and boring deep holes after drilling accordingly, heat treatment, straightening annealing and stress relief, was based on the statistical monitoring of eccentricity surface deviation from the theoretical axis of the bore axis for instruments with changeable carbide cutting inserts with CVD/PVD coatings under operating conditions with the number of 30 pieces. Measurement results of eccentricity of surfaces for locating strips before and after machining (as in turning and drilling for more cuts) are statistically processed in tables and graphs, as well as the obtained and acquired results. Article presents the optimized parameters of BTA drilling. Originally used tools for drilling were upgraded by using carbide inserts of type 14.171.55-00/0400 or /0250 by Krupp WIDIA. Influences of factors are discussed, and the monitoring of factors that produce holes of desired eccentricity are present.

Keywords: Barrel Tube, BTA System, Deep Hole Drilling, Surface Eccentricity, Statistical Monitoring

Introduction

BTA (Boring and Trepanning Association) deep hole drilling is applied for machining bore holes with a high length to diameter ratio. The slender tools involved make BTA processes highly susceptible to chatter vibration [1–4]. For the production of these parts an adaptation of the manufacturing process used as well as development of new technologies becomes necessary [2]. The quality of machining in deep-hole drilling has been studied under various machining conditions [1–5]. These studies employed the one-variable-at-a-time technique, which is time consuming and incapable of yielding conclusions that are associated with a statistical level of confidence [6]. It is desirable to select a combination of optimum machining conditions to produce holes of good quality. [17]. Investigating chatter vibration in deep drilling, including process damping and the gyroscopic effect were developed by Mehrabadi et al [19]. Deep holes drilling is a complex process in which the metal is removed by the cutting action and the surface quality is largely determined by the burnishing action of pads set behind the cutting edge. There are three main techniques available for deep drilling, i.e. gun, BTA and ejector drillings. The basic principles of each process are the same, relying on cutting edges and pads [7]. Deep holes drilling methods are used for producing holes with a high length-to-diameter ratio, good surface finish and straightness. The process is subject to dynamic disturbances that are classified as either chatter vibration or spiralling. In work of authors Messaoud and Weihs [20], nonlinear time series modeling is used to setup an on-line modeling approach of the time varying dynamics of the process. Then the proposed on-line monitoring strategy can detect the start of the transition from stable drilling to chatter vibration and some alarm signals are related to changing physical conditions of the process. Vasilko and Simkulet [21] studied a phenomenon of twist drill. During drilling it behaves like a helical spring, it turns as a result of cutting resistance after first turn and it tries to screw off and screw in, which leads to the occurence of torsional vibration. Lattner and Holesovsky [23] presented a list of hypotheses that are based on the assumption that the higher the roughness, the lower the durability in machining. Vasilko [22] also presented new experimental dependence in machining. In scientific study of authors Gao, Cheng and Kirkwood [15] is presented the investigation of machining mechanisms in boring and trepanning association (BTA) deep hole drilling processes. The cutting mechanisms investigated are focused on the chip deformation and associated drilling forces in deep holes situation in particular. Their investigation also describes the measurement and analysis of the forces including the axial force in BTA deep hole machining. Early research on deep hole drilling focused mainly on the hole qualities with respect to drilling conditions [12, 16] or specific phenomenon like chip congestion [9]. Later studies established the force system [14]. Biermann, Sacharow and Wohlgemuth [3] have reported simulation system for the idealized BTA (Boring and Trepanning Association) deep hole drilling process. Methods of computer graphics allow the realistic modeling of the cutting edge and the workpiece. The simulation is able to calculate the sweep volume, cutting forces, and regenerative tool vibrations. It is also possible to generate the resulting geometry of the workpiece depending on the eigenfrequencies of the boring bar and on the process parameters.

Ramakrishna Rao and Shunmugam [5, 6, 18] analyzed the axial and transverse profiles of holes obtained from BTA drilling, and Katsuki et al. [8,11] studied the influence of workpiece geometry on the axial hole deviation in deep-hole drilling. Katsuki et al. [8, 11] investigated the role of single- and multi-edge tools in hole deviation. Their experimental data and theoretical analyses suggested that tool geometry imbalanced the cutting forces and caused hole deviations [10]. Katsuki et al. also investigated how an inclined workpiece front face and pre-drilled pilot holes affected the hole deviation. Authors Chin et al. [13] investigates the shaft behavior of BTA deep hole drilling tool. Comparisons between theoretical and experimental results confirmed the validity of the constructed equations. Their studies disclosed build the knowledge

about the tool shaft and pave the way for future research concerning the correlation between the tool shaft and cutting process taking place on the cutting head.

Methodology of experiments and chosen methods of processing results

Experimental tests of turning, boring of deep holes and reaming on holes of Ø 125H8mm from high strength steels with tensile strength R_m = l440 to 1500 MPa were realized in specific manufacturing conditions na on the special types of lathe machines ŠKODA SUA 100P x 8000mm and SUR 350 x 8000mm. Boring of holes (the last cut - bore) were realized on machine tool SIG B31/8 NC. In the process of turning, bohring and reaming were used cutting tools with coated carbide inserts of types P25 and P30CN, what led us to analyze of literature sources and own realized experiments (see in Fig. 1). When boring deep holes had to be original tool holders adjusted with using special carbide insert WIDIA KRUPP of type 14.171.55-00/0400 TN and for the last cut of type 14.171.55-00/0250 TN (ISO-P25). After drilling of BTA system with tool head of type T-MAX COROMANT from the both sides and from one side before heat treatment were the machined parts refined to required strength. Then the parts were straightened after the heat treatment when the eccentricity were checked on the surface of strips used before during drilling.
The parts were annealed of internal stresses removal after straightening at temperatures of 50 to 100 ºC lower than was annealing temperature. It was the first checked the circumferential run-out of barrel tubes surface in the middle strip before rough turning. Machined part are then clamped and centered in the hole on both sides. Then was turned a in the middle of the flat diameter and then was roughing surface. After roughing the surface and release of stationary support was surface eccentricity on the same strip measured again and recorded graphically.

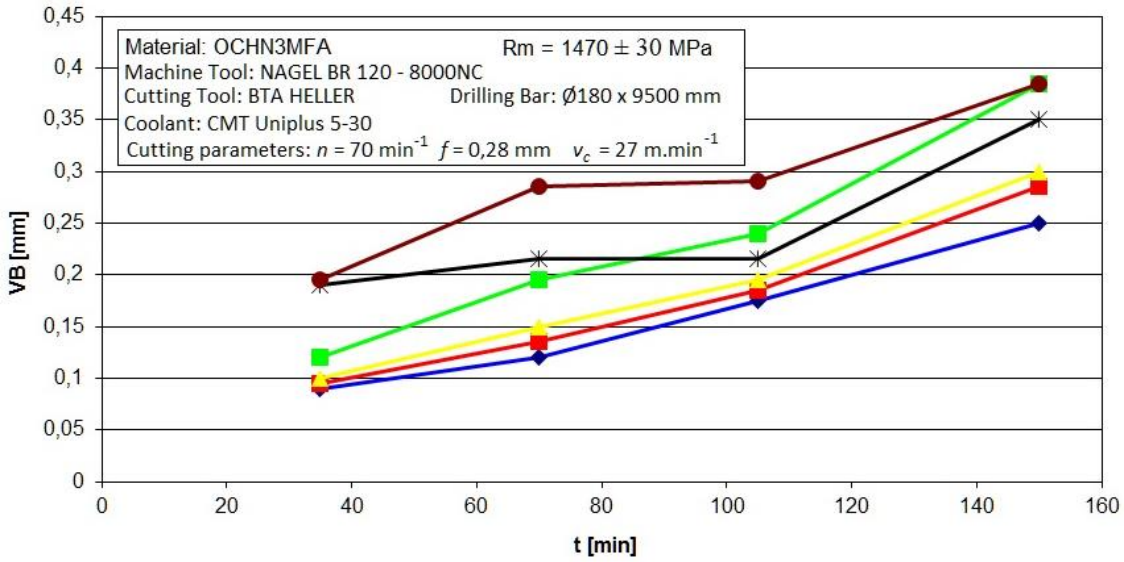

Fig. 1 *Graphical dependence of wear VB [mm] versus time t [min] when bohring a hole ±Ø123,5 x 6020mm with non coated cutting carbide insert TTX and with coated cutting insert WIDIA KRUPP type TN (ISO- P25)*

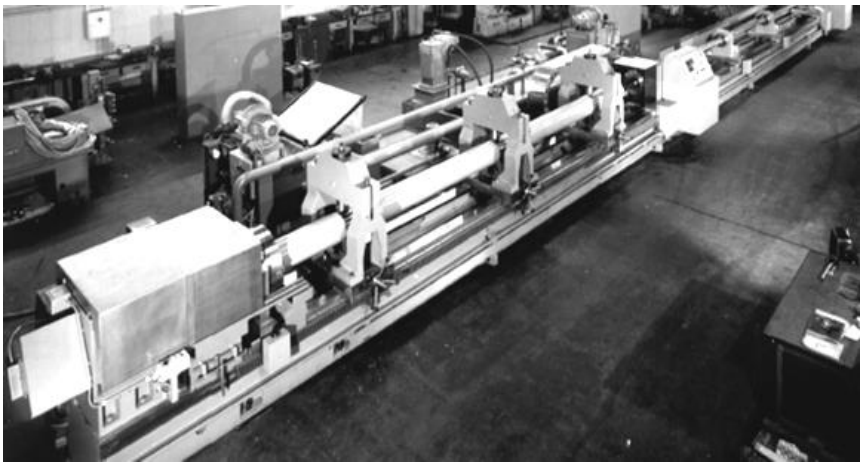

Fig. 2 *An overview of horizontal deep hole NC machine tool for drilling and bohring of deep holes*

The obtained results correspond to the measurement of 30 pieces of parts produced on the same machine and the same cutting conditions (v_c, f) before turning, as a result of deformation and residual stresses and inaccuracy of straightening after roughing of eccentric surface. The statistical results are in Tables 1 and 2 for turning of outer surfaces. The circumferential run-out of strips were checked also before bohring of eccentric holes. The strips were turned before boring with run-out up to h = 0,02 mm, with roughness Ra = 1,6 to 3,2 μm. Maximal eccentricity of hole were checked on the opposite side by measuring of surface. In bohring on deep drillong machine tool (Fig. 2) with a constant allowance were monitored values of axial force (F_o), cutting performance (P_c) and after drilling of overal length also wear of cutting insert and these values were processed into the tables.

Statistical methods of surface eccentricity measurement, results and discussion

Experimental tests of rough turning (1st cut), was realized with negative coated cutting inserts SNUN 190412 P30CN, but also with positive geomerty of type SPUN 190612, respectively in other cuts with type SPUN 150412 P30CN with TiCN coating. The choice of cutting conditions resulted from chcemical composition and strength of the workpiece material and for class of machinability TO = 9b to 8b is then k_v = 0,32 to 0,25. Then from normative of cutting conditions for a_p = 5mm, f = 0,5mm, T = 130min, for cemented carbide P30CN PRAMET and by the criteria of tool wear VB_k = 0,8mm, is optimal cutting speed v_c = 25 to 35m.min^{-1}, using coolant with emulsion E5%. The statistical results of surface eccentricity measurement before and after rough turning on lathe machine ŠKODA SUA 100P x 8000, using a cutting inserts with negative geometry as can be seen in Fig. 3a, b and in Table 1.

		a	b
Selective average	x (h)	3,77	1,57
Selective scatter	s^2	0,2849	0,1584
Experimental standard deviation	s	0,5337	0,3980
Interval estimates of parameters of the normal distribution	μ	3,6507÷3,8893	1,384÷1,756

Table. 1 *Statistical evaluation of results values from figures 3a,3b*

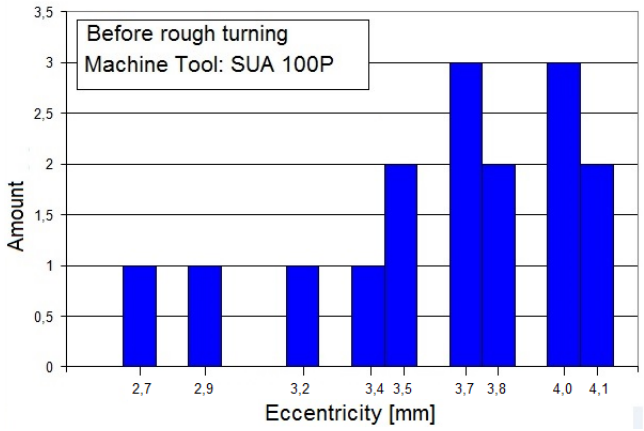

Fig. 3a *Graphical dependence of overall amount of pieces versus eccentricity of machined surfaces before roughing*

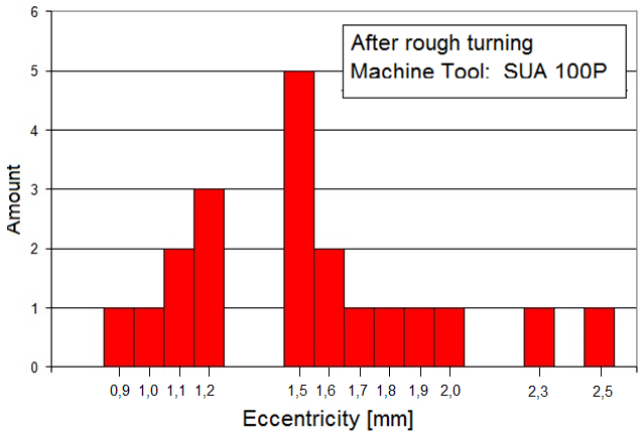

Fig. 3b *Graphical dependence of overall amount of pieces versus eccentricity of machined surfaces after roughing*

The statistical results of eccentricity measurement before and after rough turning realized in lathe machine type SUR 350x8000, using cutting tool with carbide insert with positive geometry can be seen in (Fig. 4a, b) and numerical values in Table 2.

		a	b
Selective average	x (h)	3,793	1,303
Selective scatter	s^2	0,1517	0,1658
Experimental standard deviation	s	0,3895	0,4072
Interval estimates of parameters of the normal distribution	μ	3,648÷3,938	1,151÷1,455

Table.2 *Statistical evaluation of results values from figures 4a,b*

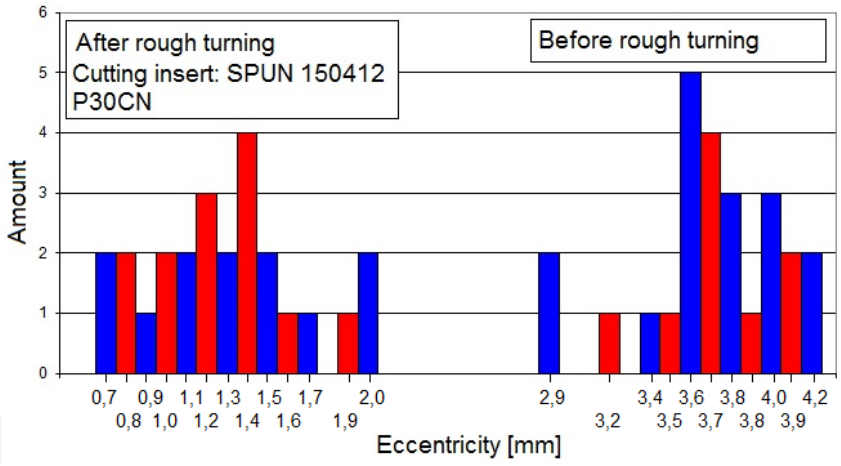

Fig. 4a, b *Graphical dependence of overall amount of pieces versus eccentricity of machined surfaces before and after roughing on SUR 350 machine and carbide insert type SPUN 150412 P30CN with positive geometry*

Statistical results can be seen also in Fig..3a,b respectively in .Fig.. 4a,b, and in Table 1 and 2. They show, that the residual stresses and surface eccentricity after turning (1st cut), which are measured in the center strip, particularly affects the stiffnes of technological system, but also the geometry of coated cutting insert. The average values of surface eccentricity on the same strips, are lower after rough turning in lathe machine tool with lower stiffnes of technological and using coated carbide insert of the comparable qualitybut with positive geometry.

		a	b
Selective average	y_k	2,015	1,035
Selective scatter	s^2	0,33882	0,1422
Experimental standard deviation	s	0,582	0,377
Interval estimates of parameters of the normal distribution	μ	1,743÷2,287	0,859÷1,211

Table 3 *Statistical evaluation of results values from figures 5a,5b*

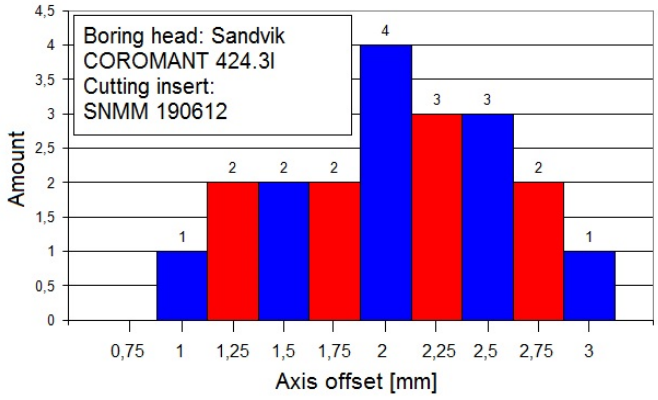

Fig. 5a *Graph of hole axis deviation from the theoretical axis(misalignment hole)in the middle of the strip after bohring with BTA tool with negative geometry of used carbide insert type SNMM 190612 P25*

Eccentrical cut in boring of deep holes on the firt cut after measured on strips using ultrasound device, that strips were before boring just turned, as is presented in the chart in Fig.5a, 5b, Fig. 6a, 6b and Table. 3. The importance of gradual allowance cutting in turning and then surface hole borhing to more cuts reflected even more in the production of components of strength R_m = 1500 to1600 MPa. Finishing of hole components after reaming and after completion of the outer surface is made by honing in the horinzontal honing machine with *Ra* = 0,4 to 0,8μm.

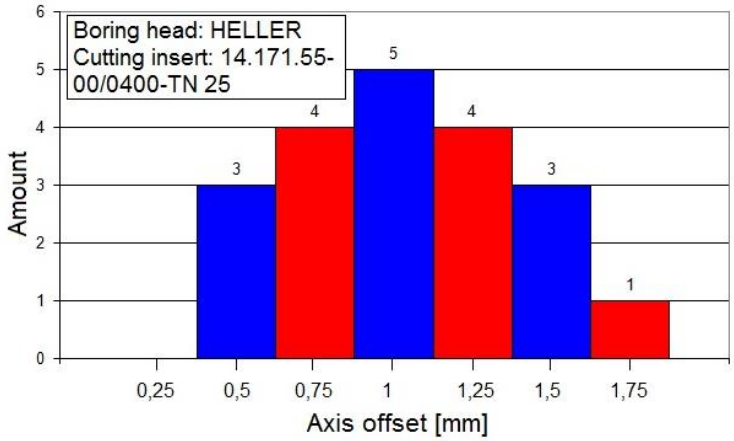

ȝ. 5b *Graph of hole axis deviation from the theoretical axis(misalignment hole)in the middle of the strip after bohring with BTA tool with positive geometry of used carbide insert type SPUN 190612 P30*

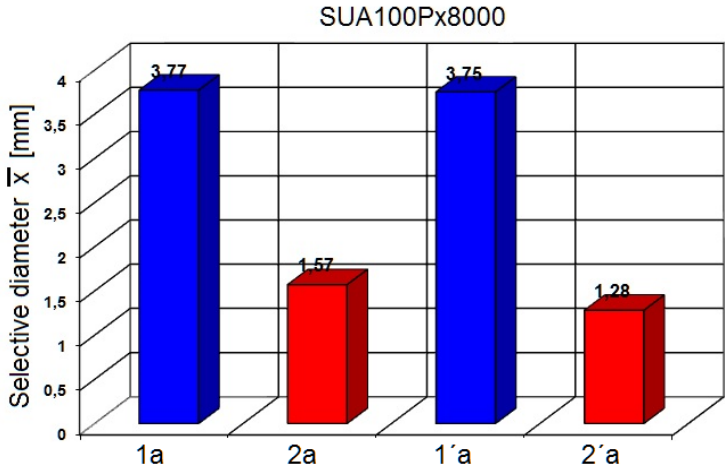

Fig. 6a *The decrease in eccentricity of the average surface sample with gradual machining of allowanceto more cuts realized on lathe machine of type SUA 100P with higher stiffness*

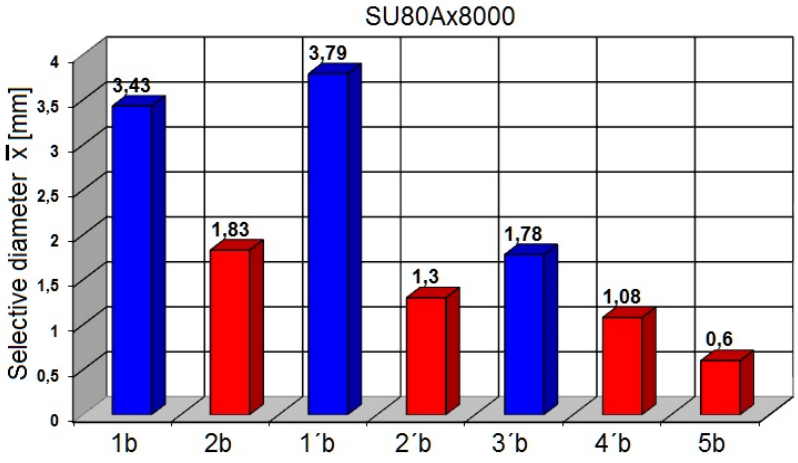

Fig. 6b *The decrease in eccentricity of the average surface sample with gradual machining of allowanceto more cuts realized on lathe machine of type SU 80A with lower stiffness*

Fig. 7 *An overall view for parts of types propeller shaft and high pressure cyllinders after drilling, bohring andsurface machining for more cuts*

Conclusion

When turning surfaces or during boring and reaming technology of deep holes of material with strength R_m = l440 to 1600 MPa is required to use cutting tools only with coated carbide insert, because hard and wear resistant CVD/PVD coatings reduces adhesion to a minimum and prevent to diffusion wear. In this way can reach tool durability of T = 90 to 150 min, which is necessary in term of boring and reaming and have to be equal T_L = (0,5 to 1).L (m). The permissible tool wear despite of lower cutting speeds v_c = 25 to 35m.min^{-1}, is only half, than that of mild steels with equal length and decises in range of VB_k = 0,3 to 0,4mm. Coated carbide inserts reached at the same cutting parameters the increase of durability from 28 to 32%. When boring deep holes there is regularity that the tool life and durability of used cutting insert have to reach at least half the time of boring the hole length. It is much better if the durability of carbide insert is equal to the entire length of time of boring the workpiece. Size of axis deviation from the theoretical axis of the hole is conditional on the size of the used feed growth which increases the number of the cuts and the quality of the carbide insert i s γ_o = 0^o. By increasing the strength of parts after heat treatment and clearance is increased residual stresses in the surface and the eccentricity (roundness) of the surface to be straightening reduce the value of eccentricity h = 3 to 4mm, ie. Eccentricity is e = 1,5 to 2mm, rather than in the original production of R_m = 1000 to1200mm, when were h = 6 to 8 mm and e = 3 to 4mm. Since the direction of the additional deformation due to residual stresses after turning and boring is spatially oriented stochastic and should be used more cuts (2 to 3), because only gradually remove material by turning and drilling of bore hole by the outer surface reduces the values. It is necessary to chcek the surface eccentricity on the turned strips with the ultrasound device before start the hole boring. As a reslut of changeable cutting forces and torques influence in turning and boring due to change of depth of cut a_p, may be formed vibration and in boring technology a stress of boring bar for buckling and torsion. It would be desirable also in the production of tubes (Fig. 7) of high strength steels (with the strength of 1860 MPa) to use the technology of deep holes boring not by the pressure but by the tension, as in boring of hydraulic cylinders of length 11m customary. Since this is a technology implemented at expensive machines and expensive part number then is chosen a methodology of experimentation statistical monitoring in production conditions, which is verified by introducing the production of new types of products. In conclusion, it is important to pay attention to the accuracy of the drill's components listed in the soft state.

Acknowledgement

Author would like to acknowledge the experimental facility provided by the Faculty of Special Technology (A. D. University of Trencin) in cooperation with the ZTS production engineering company in Dubnica nad Vahom to carry out this experimental work and research.

References

[1] DUBOVSKA R., ŠANDORA, J., MAJERIK, J. (2014). *Vŕtanie a výroba hlbokých otvorov*, 261 p., Tisk J+K, Hradec Králové.

[2] ZABEL, A., HEILMANN, M. (2012). Deep hole drilling using tools with small diameters - Process analysis and process design. In: *CIRP Annals – Manufacturing Technology*, Vol. 61, pp. 111-114. Elsevier USA

[3] BIERMANN, D., SACHAROW, A., WOHLGEMUTH, K.. (2009). Simulation of the BTA deep-hole drilling process. In: *Production Engineering.*, Vol. 3, pp. 339-346. Springer Verlag.

[4] WEINERT, K., WEBBER, O, PETERS, C. (2005). On the influence of drilling depth dependent modal damping on chatter vibration in BTA deep hole drilling. In: *CIRP Annals – Manufacturing Technology*, Vol. 54, pp. 363-366. Elsevier USA.

[5] RAMAKRISHNA RAO, P. K., SHUNMUGAM, M. S. (1987). Analysis of axial and transverse profiles of holes obtained in B.T.A. machining. In: *International Journal of Machine Tools and Manufacture*, Vol. 27, pp. 505-515. Elsevier Limited.

[6] RAMAKRISHNA RAO, P. K., SHUNMUGAM, M. S. (1988). Wear studies in boring trepanning association drilling. In: *Wear*, Vol. 124, pp. 33-43. Elsevier BV.

[7] EL KHABEERY, M. M., SALEH, S. M., RAMADAN, M. R. (1991). Some observations of surface integrity of deep drilling holes. In: *Wear*, Vol. 142, pp. 331-349. Elsevier BV.

[8] SAKUMA K., TAGUCHI, K., KATSUKI, A. (1980). Study of deep hole drilling with solid boring tool. In: *Bulletin of the JSME*, Vol. 23, pp. 1921-1928.

[9] CHIN, J. H., WU, J. S. (1993). Mathematical models and experiments for chip signals of single-edge deep hole drilling. In: *International Journal of Machine Tools and Manufacture*, Vol. 33, pp. 507-519. Elsevier Limited.

[10] DENG, C. S., HUANG, J. C., CHIN, J. H. (2001). Effects of support misalignments in deep-hole drill shafts on hole straightness. In: *International Journal of Machine Tools and Manufacture*, Vol. 41, pp. 1165-1188. Elsevier Limited.

[11] KATSUKI, A., SAKUMA, K., TAGUCHI, K., ONIKURA, H., AKIYOSHI, H., NAKAMUTA, Y. (1987). Influence of tool geometry on axial hole deviation in deep drilling: comparison of single and multi-edge tools. In: *JSME International Journal*, Vol. 30, pp. 1167-1174.

[12] CHIN, J. H., LEE, L. W. (1995). A study on the tool eigenproperties of a BTA deep hole drill-theory and experiments. In: *International Journal of Machine Tools and Manufacture*, Vol. 35, pp. 29-49. Elsevier Limited.

[13] CHIN, J. H., HSIEH, C. T., LEE, L. W. (1996). The shaft behavior of BTA deep hole drilling tool. In: *International Journal of Mechanical Sciences*, Vol. 38, pp. 461-482. Elsevier Limited.

[14] PERNG, Y. L., CHIN, J. H. (1999). Theoretical and experimental investigations on the spinning BTA deep-hole drill shafts containing fluids and subject to axial forces. In: *International Journal of Mechanical Sciences*, Vol. 41, pp. 1301-1322. Elsevier Limited..

[15] GAO, C. H., CHENG, K., KIRKWOOD, D. (2000). Investigation on the machining process of BTA deep hole drilling. In: *Journal of Materials Processing technology*, Vol. 107, pp. 222-227. Elsevier BV.

[16] CHIN, J. H., SHEU, S. D. (2007). Strengths and weaknesses of finite element modeling deep hole drilling as compared with beam and column equations. In: *International Journal of Advanced Manufacturing Technology*, Vol. 32, pp. 229-237. Springer London.

[17] DENG, C. S., CHIN, J. H. (2005). Hole roundness in deep-hole drilling as analysed by Taguchi methods. In: *International Journal of Advanced Manufacturing Technology*, Vol. 25, pp. 420-426. Springer London.

[18] RAMAKRISHNA RAO, P. K., SHUNMUGAM, M. S. (1987). Investigations into surface topography, microhardness and residual stress in Boring Trepanning Association machining. In: *Wear*, Vol. 119, pp. 89-100. Elsevier BV.

[19] MEHRABADI, I. M., NOURI, M., MADOLIAT, R. (2009). Investigating chatter vibration in deep drilling, including process damping and the gyroscopic effect. In: *International Journal of Machine Tools and Manufacture*, Vol. 49, pp. 939-946. Elsevier Limited.

[20] MESSAHOUD, A., WEIHS, C. (2009). Monitoring a deep hole drilling process by nonlinear time series modeling. In: *Journal of Sound and Vibration*, Vol. 321, pp. 620-630. Academic Press Inc.

[21] VASILKO, K., SIMKULET, V. (2012). Phenomenon of twist drill. In: *Manufacturing Technology*, Vol. 12, pp. 281-285.

[22] VASILKO, K. (2014). New experimental dependence of machining. In: *Manufacturing Technology*, Vol. 14, pp. 111-116.

[23] LATTNER, M., HOLESOVSKY, F. (2014). Effect of machining the load capacity notched components. In: *Manufacturing Technology*, Vol. 14, pp. 47-50.

The Effect of Plasma Nitriding Parameters on the Thickness of Nitrided Layers

Ondrej Pilch, Frantisek Snahnican, Vojtech Hruby, Zbynek Studeny
Department of Mechanical Engineering, Faculty of Military Technology, University of Defence. Kounicova 65, 662 10 Brno. Czech Republic. E-mail: ondrej.pilch@unob.cz, frantisek.snahnican@unob.cz, vojtech.hruby@unob.cz, zbynek.studeny@unob.cz

This paper is aimed at chemical-heat treatment of a selected material. The plasma nitriding layers were applied on the 41CrAlMo7-10 steel. The influence of plasma nitriding parameters on the thickness and microhardness of nitrided layers were investigated. Plasma nitriding was performed at 500°C with a mixture atmosphere of H_2 and N_2 in the plasma nitriding equipment. The pressure of plasma nitriding process was determined to be 280 Pa. The period of the plasma nitriding process was changeable from 5 to 30 hours. The microstructure and mechanical properties of the nitrided layers were studied by using GDOES spectrometry, optical microscopy, and hardness testing. The depths of the plasma nitriding layers were also estimated using cross-sectional microhardness profiles. Microhardness and surface hardness of mentioned samples were significantly increased. The measurements have shown that the period of plasma nitriding process has a significant influence on the depth of nitriding.

Keywords: Plasma Nitriding, Microhardnes, Nitriding Period, Nitrided Layer,

1 Introduction

Currently, considerable effort is devoted to innovation in the area of research and development of materials and technologies. An appropriate combination of materials and surface treatment technologies can be achieved as a significant improvement of material properties [1]. Suitably selected surface treatment can significantly change the properties of material and improve its residual and fatigue life [2]. The plasma nitriding process depends on the suitable selection of material. It is important to verify suitability of selected material for chemical-heat and heat treatment [3]. From an ecological point of view, the nitriding process is more preferable than chrome plating [4].

The aim of this study is to comprehensively assess the effect of the nitriding period on the thickness of nitrided layers for selected material. The evaluation of time influence as parameter of nitriding process requires knowledge of material surface treatment technology. It is important to study the suitability of selected steels, to suggest the appropriate time for the nitriding process of selected materials and to study the process of experimental methods used to measure and assess the created nitrided layer [5].

2 Experimental part

Steel 41CrAlMo7-10 was selected for the experiment. For the experiments, round bars were collected. The diameter of the bar was 50 mm. The bar was 250 mm long and subsequently cut into discs of 10 pieces of 8 mm thickness. These samples of circular shape were identified (marked) and subsequently heat treated, tempered (hardened and tempered) to medium strength values (table 1).

Tab. 4 Heat treatment of selected steel

Material	***Hardening***		***Tempering***	
	Temperature [°C]	***Method of cooling***	***Temperature [°C]***	***Method of cooling***
41CrAlMo7-10	*940*	*oil*	*650*	*oil*

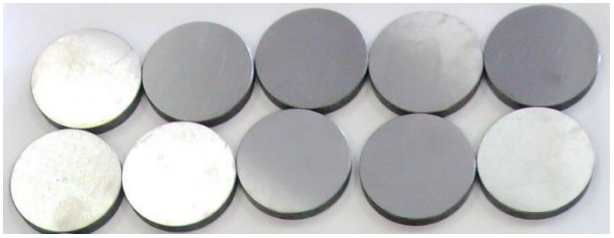

Fig. 8 After grinding on the horizontal grinding machine with magnetic clamping plate

After heat treatment operations the hardness of the samples were measured by using Vickers microhardness method [6]. The Vickers microhardness method consists of 5 measurements [7]. From this measurement was calculated the average value, which was 308 HV5. The chemical composition of samples was verified by GDOES method on GDOES LECO analyzer SA 2000 on the BULK mode, which is designed for the volumetric analysis of materials [8]. The results

of the measurement method GDOES BULK mode are displayed in Table 2.

Tab. 5 Chemical composition of steel

C	***Mn***	***Si***	***Cr***	***Al***	***Mo***	***P***	***S***
GDOES/BULK							
0,42	*0,38*	*0,31*	*1,51*	*0,85*	*0,17*	*0,010*	*-*
Standard STN							
0,35-0,42	*0,30-0,60*	*0,17-0,37*	*1,35-1,65*	*0,70-1,10*	*0,15-0,25*	*max 0,035*	*max 0,035*

Method: GDOES / Bulk; Device: SA 2000 Leco; Calibration Standards CKD 180A to 189A; Reported are the average of 10 measurements.

After the heat treatment, the technology of plasma nitriding was used for creation of plasma nitride layers [9]. The parameters of the plasma nitriding process were designed according to find the effect of process duration to the creation of required nitrided layers. The nitridation period was altered during the plasma nitriding process (table 3). Plasma nitriding was performed on equipment from RÜBIG PN 70/120.

Tab. 6 Parameters of plasma nitridation

Temperature [°C]	***Nitriding period [h]***	***Gas flow H_2/N_2 [l.min^{-1}]***	***Voltage [V]***	***Pressure [Pa]***	***Pulse length [µs]***
500	*5/ 10/ 20/ 30*	*24/8*	*520*	*280*	*100*

At the experimental analyzer GDOES Leco SA 2000, mode QDP (Quantitative Depth Profiling) was evaluated concentration profile of the nitriding layer [10]. The depth of one measurement was set at to 20 µm. The results of the measurement are shown as the concentration dependence of C and N, by percentage weight with depth below the surface of Fig. 2. Calibration of nitrogen: JK41-1N and NSC4A standards.

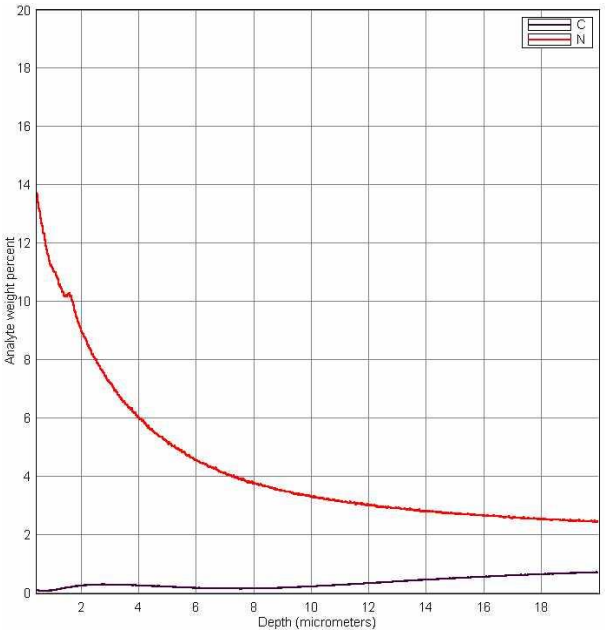

Fig. 9 The concentration profile of the nitriding layer steel 41CrAlMo7-10 (PN 5hours)

After plasma nitriding process the microstructure and the thickness of plasma nitride layer was documented on the optical microscope Olympus GX51. The results are displayed in Fig. 3. The observation was carried out using 500× magnification.

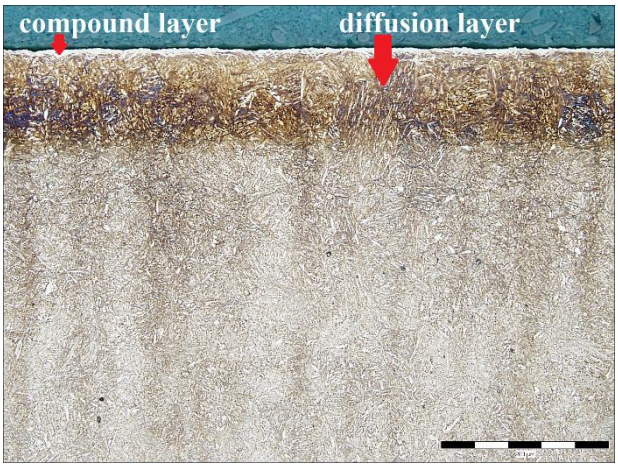

Fig. 10 Microstructure of sample by the optical microscope; magnification 500×

Microhardness and nitrided layer thickness was evaluated using automatic microhardness tester LM 247 AT LECO equipped by AMH43 software. The load for the test was set at 50 g and 10s dwell time [11]. The calculation of Nht thickness was determined FROM following equation in accordance with DIN 50190 standard:

$$X = [(Y * 0.1) * 10] + 50 \quad (1)$$

where X is Nht thickness in mm, Y is the average microhardness value from five indentation patterns in HV 0.05. Individual microhardness depth profiles are presented in figure 4. The trends from Fig. 4 represent microhardness of the diffusion layer. All measurements were performed under the same conditions. Microhardness was measured on each of samples. The outputs of all microhardness measurements are shown in Tab. 4, Tab. 5.

Tab. 7 Nitrided layer thickness

Thickness of compound zone [µm]	***Nht thickness [µm]***	***Period of process [h]***
3.3	*173*	*5*
4.9	*263*	*10*
4.9	*292*	*20*
3.5	*423*	*30*

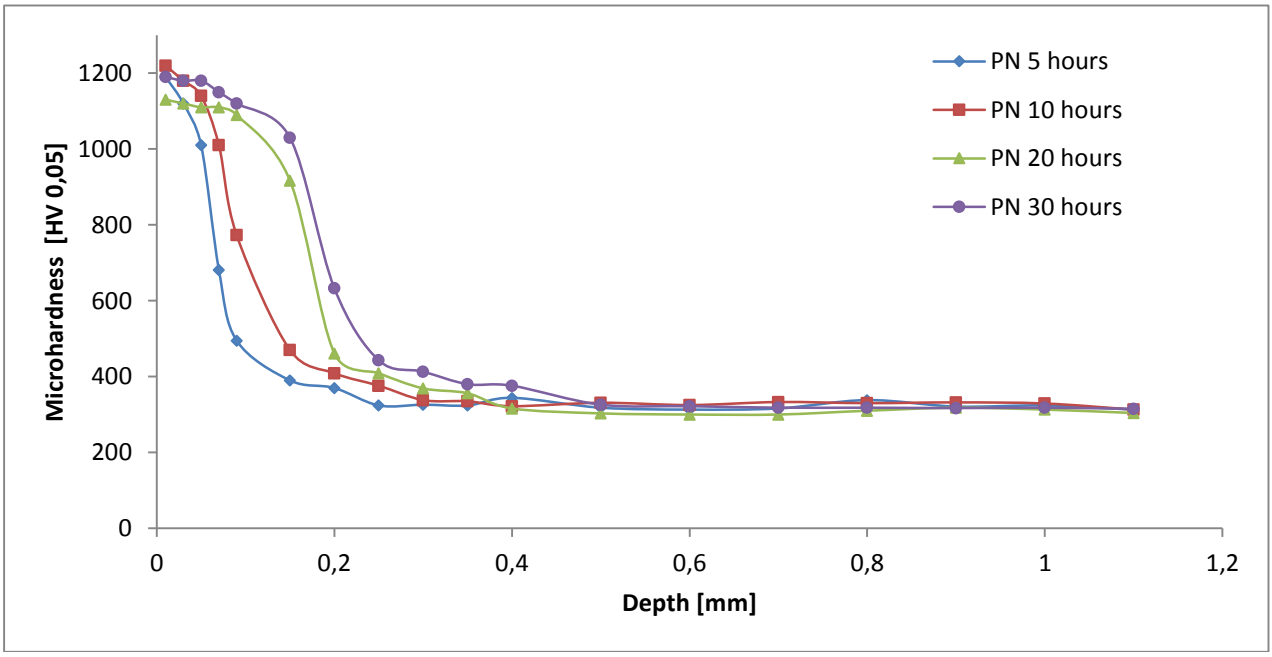

Fig. 11 Microhardness depth profiles

Tab. 8 Results of microhardness depth profiles

Depth [mm]	***Microhardness [HV 0.05]***			
	5 hours	***10 hours***	***20 hours***	***30 hours***
0,01	*1190*	*1220*	*1130*	*1190*
0,03	*1120*	*1180*	*1120*	*1180*
0,05	*1010*	*1140*	*1110*	*1180*
0,07	*681*	*1010*	*1110*	*1150*
0,09	*495*	*773*	*1090*	*1120*
0,15	*390*	*470*	*917*	*1030*
0,20	*370*	*409*	*461*	*633*
0,25	*324*	*376*	*409*	*443*
0,30	*326*	*338*	*369*	*413*
0,35	*324*	*335*	*356*	*380*
0,40	*344*	*322*	*316*	*376*
0,50	*318*	*331*	*303*	*326*
0,60	*313*	*325*	*300*	*322*
0,70	*316*	*333*	*300*	*318*
0,80	*338*	*330*	*310*	*318*
0,90	*321*	*332*	*318*	*317*
1,00	*324*	*329*	*313*	*318*
1,10	*313*	*313*	*304*	*315*

3 Results

The assumption that the influence of nitriding time increases the thickness of the nitriding layer was confirmed experimentally on the 41CrAlMo7-10 steel. The surface hardness of plasma nitriding layer increased from 300 to 1250 HV 0.05, values are displayed in Fig. 4. Microhardness and Nht thickness of nitrided layers were measured in accordance with DIN 50190 standard [11]. Measurements of microhardness have shown that the period of plasma nitriding process had significant influence on the thickness of the nitriding layer. By analyzing the results of the experiment was found that Nht thickness was after five hours of plasma nitriding 173 µm. The thickness of the nitriding layer was changed by altering time. The nitrided layer thickness 263 µm was created after ten hours of process. After twenty hours of plasma nitriding process the thickness of nitriding layer was increased to 292 µm. The Nht thickness 423 µm was reached by thirty hours of plasma nitriding. It is obvious that increasing of plasma nitriding duration increase the thickness of the nitriding layer, which is shown in Fig. 5.

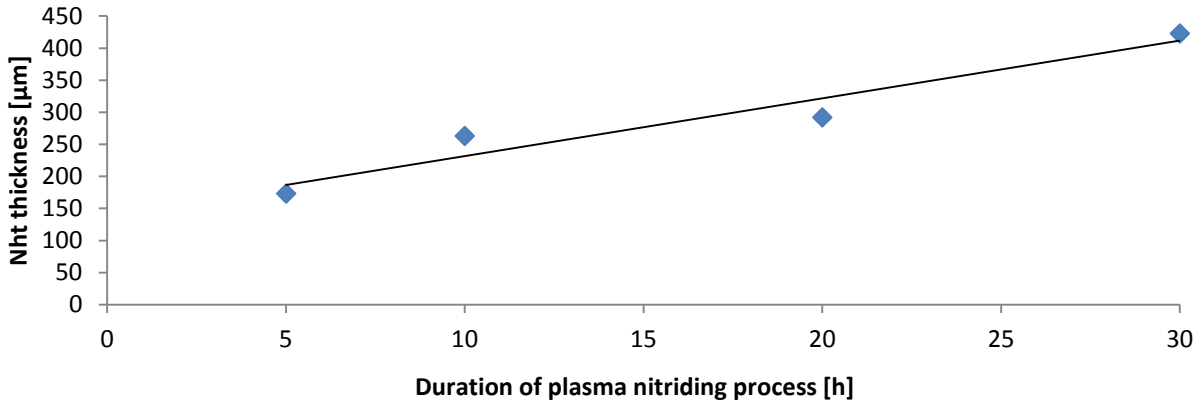

Fig. 12 The thickness of nitriding layers

4 Conclusion

The experiment showed that the plasma nitriding of nitriding steel 41CrAlMo7-10 formed a layer which comprises of a white (compound layer) and the diffusion layer. The parameters of the nitriding layer are shown in Tab. 4. After plasma nitriding, the mechanical properties of steels were improved. After plasma nitriding the surface hardness was significantly increased. Hardness and microhardness of created nitrided layers were examined and compared. The results are shown in Fig 4. The experiment results showed that the duration of nitriding process changed the thickness of the nitriding layer (figure 5).

Acknowledgements

The paper was prepared with the support of the Project "Promoting Research, Science and Innovation in the Field of Engineering" of the Department of Mechanical Engineering, University of Defence.

References

[1] HRUBÝ, Vojtěch; POKORNÝ, Zdeněk; LIPTÁK, Peter. *Plasma nitriding of cavities.* Rzeszów, Poland: RSdruk, Podgórska 4, 35-082 Rzeszów, 2013, 162 p. ISBN 978-83-63666-93-4.

[2] STUDENÝ, Zbyněk. Analysis of the influence of initiating inclusions on fatigue life in plasma nitrided steels. Manufacturing Technology, 2015, vol. 15, no. 1, p. 99-105. ISSN 1213-2489.

[3] HRUBÝ, V.: Povrchové vrstvy ocelí a jejich příprava iontovou nitridací, Brno 1991,

[4] RIE, K.T.: Recent advances in plasma diffusion processes. ISSN, 1999

[5] POKORNÝ, Zdeněk; KADLEC, Jaromír; HRUBÝ, Vojtěch; et all. HARDNESS OF PLASMA NITRIDED LAYERS CREATED AT DIFFERENT CONDITIONS. *Chemické listy*, 2011, vol. 2011, no. 105, p. 717-720. ISSN 1213-7103.

[6] EN ISO 6507-1 Metallic materials – Vickers hardness test – Part 1: Test method. 1998

[7] STN EN ISO 14577-1: *Metallic materials Instrumented indentation test for hardness and materials parameters* - Part 1: Test method

[8] PAYLING, R.; JONES, D.; BENGTSON, A. Glow Discharge Optical Emission Sepctometry. England: John Wiley & Sons Ltd. 1997. ISBN 0-471-96683-5

[9] HRUBÝ, Vojtěch; POKORNÝ, Zdeněk; BARBORÁK, Oto. Characteristics of plasma nitrided layers in deep holes. *KOVOVE MATERIALY-METALLIC MATERIALS*, 2012, vol. 3, no. 50, p. 209-212. ISSN 0023-432X.

[10] Kadlec, J.: *Metodika hodnocení chemickeho složení a vlastností povlaků* $FeFe_2O_4$, 2008, 18s. Univerzita obrany, Brno ISBN: 978-7231-474-4

[11] DIN 50190-4:1999, *Hardness depth of heat-treated parts - Part 4: Determination of the diffusion hardening depth and the diffusion depth*

Characteristics of plasma nitrided layers

Zdenek Pokorny, Zbyněk Studeny, Miroslav Pospichal, Zdenek Joska, Vojtech Hruby
[1]Faculty of Military Technology, University of Defence, Kounicova 156/65, 662 10 Brno, Czech Republic. E-mail: zbynek.studeny@unob.cz

This article deals with mechanical and chemical properties of nitrided layers which were created by plasma nitriding technology. The aim is to achieve an enhanced surface hardness, better wear resistance, reduced friction coefficient, increase fatigue limit or corrosion resistance. Experiments are focused on using of plasma nitriding process for surface treatment of cavities with diameter of 6 mm. Nitrided layers were applied to steel PO 209 which were subsequently evaluated by metallographic, GDOES, XRD microanalysis and microhardness methods. The results of measurement showed trends of chemical composition of alloying elements after chemical-heat treated process through the length of cavity. Plasma nitriding process is applied for increasing of surface hardness of material in deep cavities. Mechanical properties of tested material were significantly increased. Surface hardness and microhardness is depended on content of nitride formed alloying elements in material.

Keywords: nitriding; microhardness; nitrided layer; Nht thickness.

1 Introduction

The plasma nitriding is usually applied to already heat-treated material, i.e. after heat-treatment process [1]. The aim is to achieve an enhanced surface hardness, better wear resistance, reduced friction coefficient, increase fatigue limit or corrosion resistance. The nitriding process developed nitrides of iron in the diffusion layer which caused low increase of microhardness. The main elements that caused increasing of properties are alloying elements as molybdenum, vanadium, aluminum or chrome. During plasma nitriding process, two layers are created. On the surface of material established the compound layer consisted of ε-Fe2-3N and γ-Fe4N phase [2, 3]. This type of layer has been very hard and brittle with good friction and anticorrosion properties [2]. This layer is very good evaluated by metallographic methods. The thickness and hardness of γ´-Fe4N depends on quantity and quality of alloying elements [3]. The composition of diffusion nitrided layers can be effectively influenced by chemical composition of nitriding atmosphere [5]. This article describes the chemical and mechanical properties of nitrided layers which were created inside the cavities. Nht thickness [4] of mentioned sample is subsequently compared with content of alloying elements and nitrogen. This study deals with chemical and mechanical properties of nitriding layers were created by pressure of 400 and 500 Pa. Chemical composition of steel was verified for selected chemical elements by GDOES/Bulk method on LECO SA 2000 spectrometer and local measurement of composition was carried out on SEM microscope with micro analyzer Philips Edax 9900. Microstructure was evaluated by laser confocal microscopy Olympus OLS 3000. Thickness and microhardness of plasma nitrided layers were measured by microhardness method in accordance with DIN 50190 standard on automatic microhardness tester LECO LM 247 AT. The thickness of compound layer was measured by optical microscope OLYMPUS GX 51 equiped software ANALYSIS.

2 Sample preparation

Bars of PO 209 steel in untreated state were cylinder bored with diameter of 6 mm. Samples of length 500 mm were heat treated in accordance with Tab. 1.

Table 1. *Temperatures of heat-treated steels*

Procedure	Temperature (°C)
Oil quenching	940
Salt tempering	650

A microhardness of untreated material of samples was 550 HV0,05. Plasma nitriding was carried out in PN 60/60 RÜBIG furnace according to Tab. 2. The charge was consisted of 2 cylindrical samples (cavities) which were plasma nitrided at the pressure of 400 and 500 Pa for 6 hours.

Table 2 *Parameters of plasma nitriding process*

Temperature [°C]	**500**
Duration [h]	**6**
Gas flow H_2/N_2 [l.min^{-1}]	**24/8**
Bias [V]	**530**
Pressure [Pa]	**400 500**
Pulse length [µs]	**100**

After plasma nitriding process, the samples with the diameters of 6 mm were cut off. The length of the first sample was 30 mm, each other was 12 mm. The lengths of next samples were following: 30, 42, 54, 66, 78, 90, 102, 114, 126, 138, 150, 162, 174, 186, 198, 210, 222, 234, 246, 258 mm.
All samples were wet grounded using silicon carbide paper with grit from 80 down to 2000 and subsequently polished. Confocal laser microscope LEXT OLS 3000 with outstanding resolution of 0.12 µm and magnification range from 120x to 12400x was used for observation, cross-structure documentation and compound layer evaluation (Fig. 1). Chemical composition of material was measured by GDOES/Bulk method (Tab. 3).

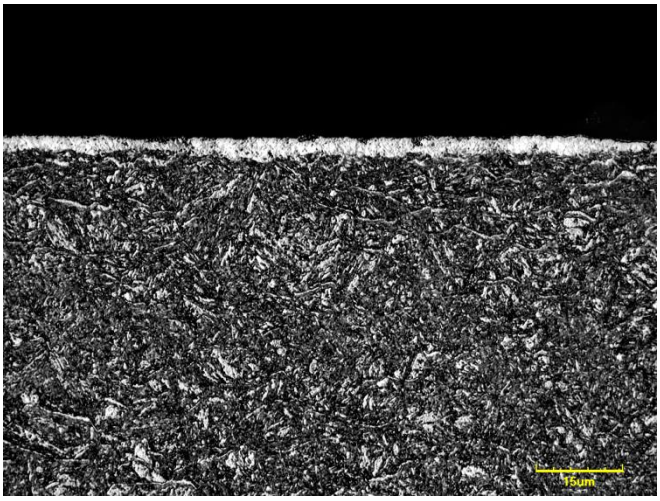

Fig. 1 *The chemically etched confocal cross-sectional structure of tempered steel, compound layer (top of surface) and diffusion layer below, magnification 500x*

Tab. 3 *Chemical composition of PO 209 steel*

C	**Mn**	**Si**	**Cr**	**Mo**	**V**	**P**	**S**
GDOES/Bulk							
0,30	0,47	0,25	2,95	0,89	0,28	0,002	0,001
DIN standard							
0,30 – 0,35	< 0,60	< 0,35	2,80 – 3,20	0,80 – 1,20	0,25 – 0,35	< 0,025	< 0,010

Glow discharge optical spectroscopy (GDOES) measurements were performed in LECO SA-2000, with argon glow discharge plasma excitation source, calibration of nitrogen: JK41-1N and NSC4A standards.
The microhardness was measured in accordance with Fig. 2 by Vickers microhardness method on the automatic microhardness tester LM 247 AT LECO at 50 g load and 10 s dwell time. The major Vickers microhardness numbers were derived from five measurements as an average value according to Fig. 3 and the results are displayed in Fig. 4.

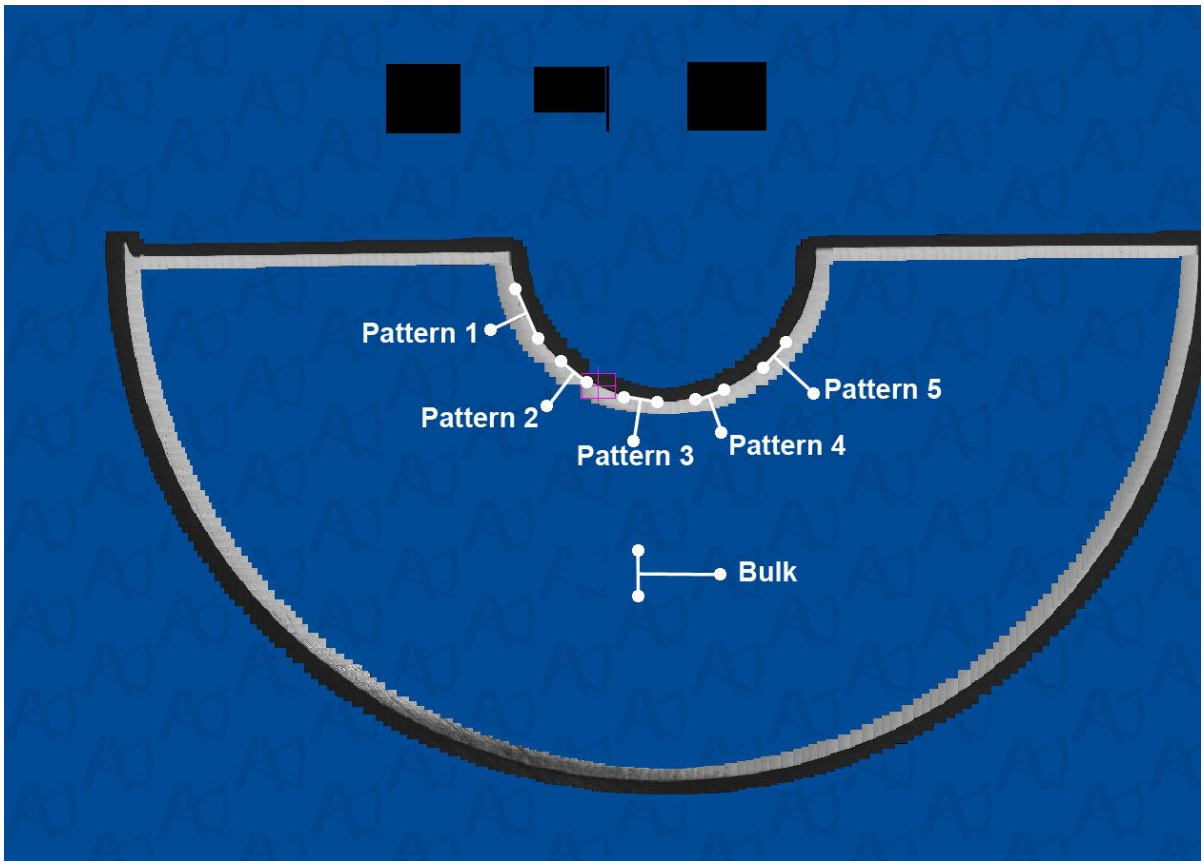

Fig. 2 *Real image of measured sample from LM 247*

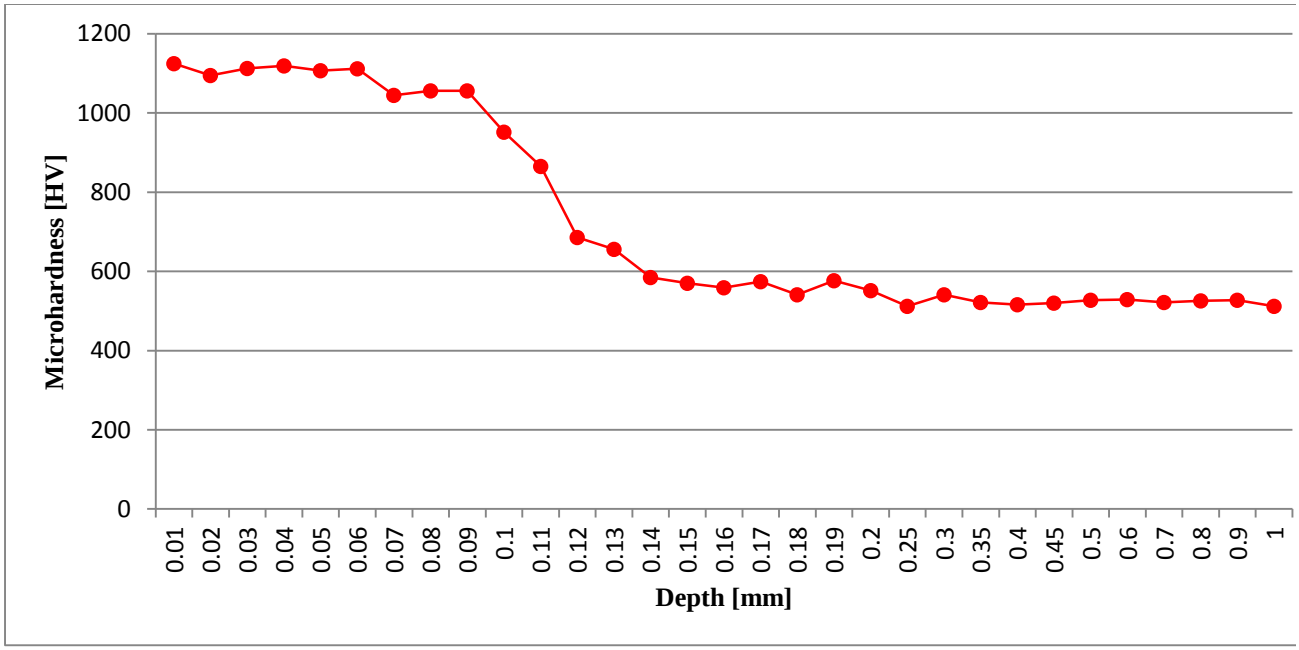

Fig. 3 *Microhardness depth profile; measured in length 30 mm from forepart; plasma nitriding process 500°C/6h/500Pa*

Following equation was used for calculation of Nht thickness X (1) in accordance with DIN 50190 standard:

$$X = [[Y * 0.1] * 10] + 50. \quad (1)$$

Where, X is Nht thickness in mm, Y is the average microhardness number from five indentation´s patterns in HV 0.05 [kg].

The local chemical compositions of plasma nitrided layers in length of cavity were observed by SEM method in combination with energy dispersive micro analyser PHILIPS EDAX 9900. Measurement of nitrogen content and alloying elements was performed from two local spaces by 25x magnification. The results from analysis are shown in Tab. 4.

Tab. 4 *Trends of microhardness thickness and nitrogen concentration after plasma nitriding process 500°C/6h/400 – 500Pa*

Length [mm]	Nht thickness [mm]		Cr [wt. %]		Fe [wt. %]		N [wt. %]	
	400 Pa	500 Pa	400 Pa	500 Pa	400 Pa	500 Pa	400 Pa	500 Pa
30	0.12	0.14	3.55	4.00	80.37	86.35	7.22	5.66
52	0.12	0.14	3.53	4.84	81.56	84.28	6.15	7.36
64	0.11	0.12	3.37	3.63	84.03	87.04	6.05	6.25
76	0.11	0.12	3.24	3.83	81.94	86.51	7.26	6.34
88	0.09	0.11	3.09	4.03	84.69	86.15	5.99	6.39
100	0.09	0.11	3.23	3.5	84.74	87.7	5.82	6.10
112	0.09	0.10	3.24	3.71	83.90	86.88	6.28	6.10
124	0.06	0.09	3.25	3.85	84.30	86.58	6.24	6.35
136	0.00	0.09	3.47	3.96	87.23	85.34	2.12	6.34
148	0.00	0.07	3.47	3.94	85.93	89.56	1.86	6.22
160	0.00	0.00	3.41	3.71	88.41	90.76	1.45	2.99

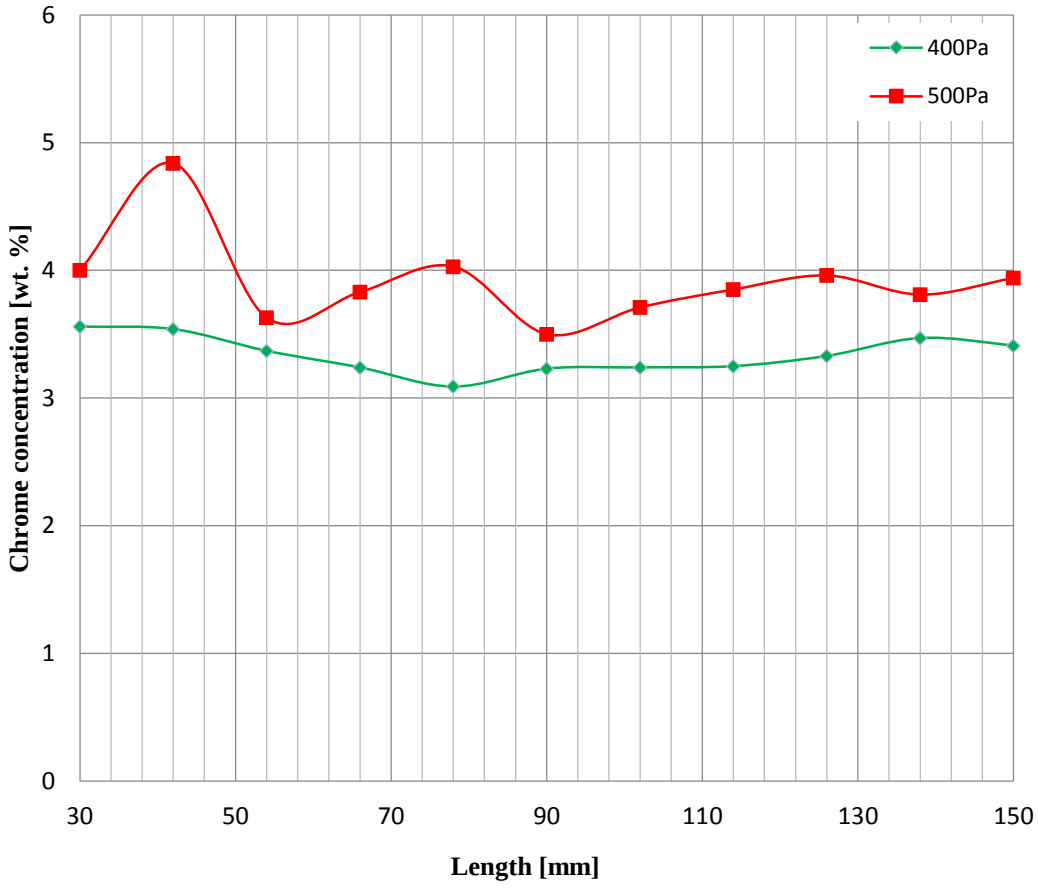

Fig. 4 *Chrome concentration changes caused by plasma nitriding process; plasma nitriding process 500°C/6h/400 and 500Pa*

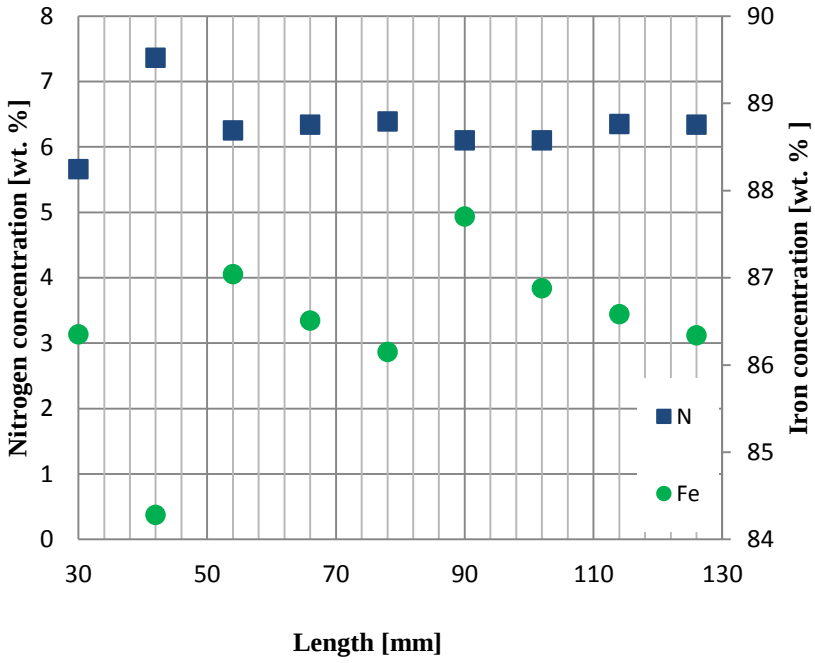

Fig. 5 *Dependence of Fe-N alloys; plasma nitriding process 400°C/6h/500Pa*

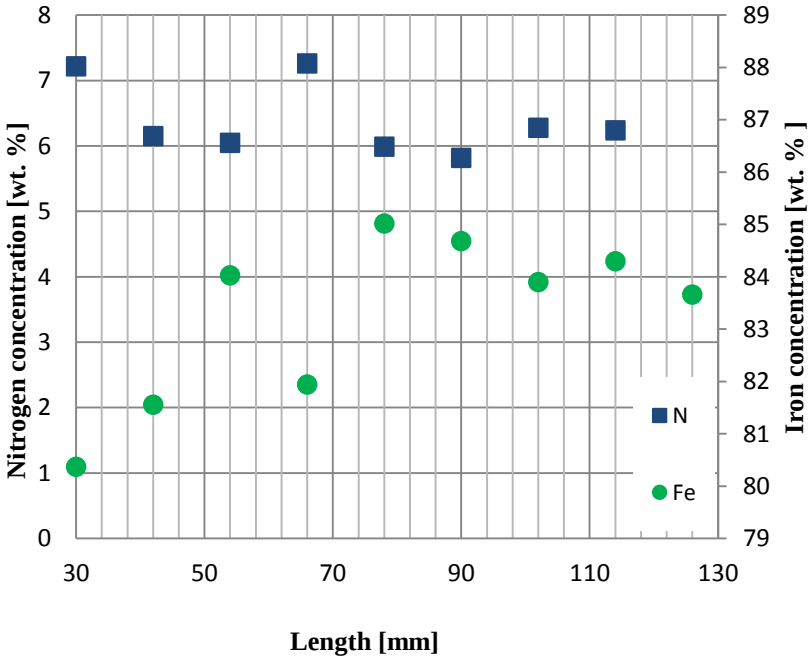

Fig. 6 *Dependence of Fe-N alloys; plasma nitriding process 500°C/6h/500Pa*

4 Results and discussion

Heat-treated samples with diameters of 6 mm which were plasma nitrided at pressure of 400 and 500 Pa were investigated and subsequently compared. Microhardness of depth profiles of plasma nitrided layers confirmed enhancement of microhardness about 550 HV0.05 which is shown in Fig. 3. Nht thickness of plasma nitrided layer was measured in accordance with DIN 50190 standard (1) [4].

The cavity attained Nht thickness 0.14 mm in length 30 mm in case of nitriding pressure 500 Pa and 0.12 mm in case of pressure of nitriding 400 Pa. Measurement shows increasing of surface hardness by increasing of pressure of plasma

nitriding process from 400 to 500 Pa. The value of microhardness in depth 30 mm corresponds to the value of surface hardness. By increasing length in cavity, the nitriding gradient is going down what is shown in Fig. 7. The last value of measured microhardness (1) was found in length 138 mm (400 Pa) and 150 mm in case of 500 Pa (Tab. 4, Fig. 7) The thickness of diffusion layer was in both cases equidistant. Some similarity is visible in Fig. 4 from expression of chromium concentration. On the base of evaluated measurement it has been expected that other increasing of pressure of process should increased Nht thickness in length of cavity what is shown in Fig. 7 for pressure 400-500 Pa. In length 30 mm from forepart of cavity was Nht thickness increased from 0.12 mm (pressure 400 Pa) to 0.14 mm (pressure 500 Pa). However, on the surface of steel the Nht thicknesses were in all cases really identical.
The results data from measurement of chemical analysis were graphically arranged, according to the position of plasma nitrided sample surface from the cavity side. The courses provided basic information about the length in cavity to which was the plasma nitriding process effective (Fig. 4-6).

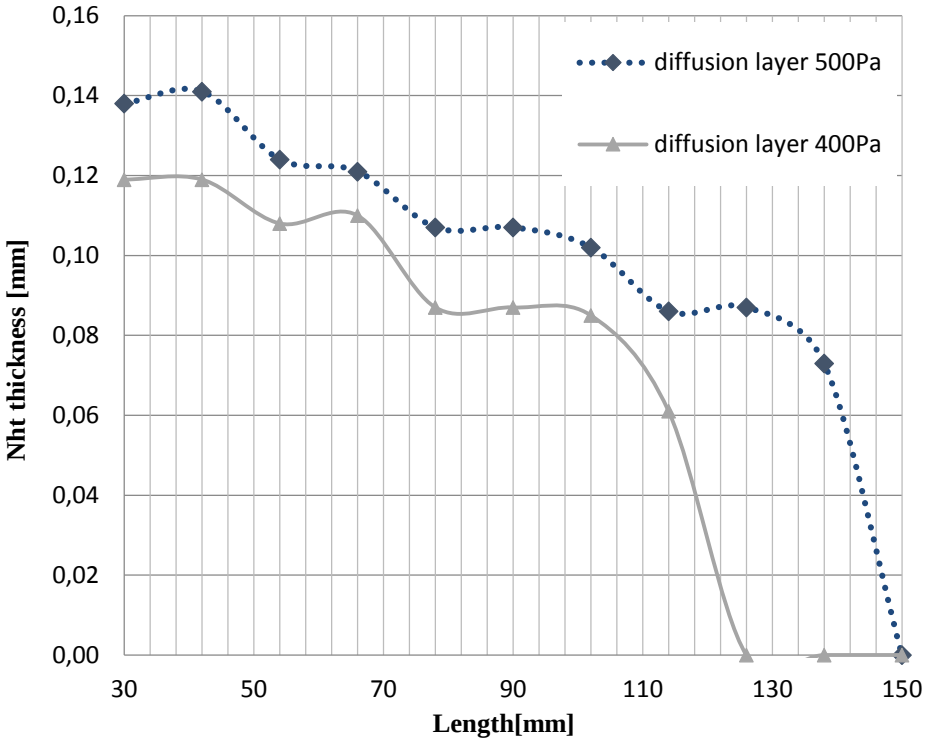

Fig. 7 *Comparison of microhardness in cavities with diameter of 6 mm*

5 Conclusions

Experiment showed that plasma nitriding process is applicable not only for flat surfaces but for deep narrow cavities. These created nitrided layers improve corrosion resistance and mechanical properties of steel. Created nitrided layers can be used in automotive and weapon industry. It was proven that used pressure has remarkable influence on the plasma nitriding in length of cavity and to the formation of nitrides in diffusion layer, what is displayed in Fig. 7. Results show very close relation between pressure, Nht thickness and length in cavity. Equidistant trend of both mathematical expressions of Nht thickness of diffusion layers shows dependence of pressure of process to Nht thickness. By other increasing of pressure it has been probably increased the length and Nht thickness more in this case increasing about 100 Pa. Peculiarities of experiment seem to be a deviation of chromium. Results of deviation are displayed in Fig. 4. Fig. 5, 6 has been show concentration of nitrogen and their significant influence on the thickness of nitrided layers.

Acknowledgement

The paper was prepared with the support of the Project for the Development of the Organization of the Dep. of Mechanical Engineering, UoD "Promoting Research, Science and Inovation in the Field of Engineering".

References

[1] HORAK, V., KULISH, V., HRUBY, V., MRAZKOVA, T. Model of the Hardness Prediction for the Diffusion Nitriding. In. 9th International Conference on Mathematical Problems in Engineering, Aerospace and Sciences "ICNPAA 2012". New York: American Institute of Physics, Conf. Proc. 1493, 2012, s. 486-491, ISBN 978-0-7354-1105-0, ISSN 0094-243X.

[2] JONSTA, P., MARSALEK, P., HAVLIK, J., JONSTA, Z., VALICEK, J. Influence of Spur Gears Hardened Method to Allowable Stress Numbers for Bending. Key engineering materials, Vol. 607 (2014), pp 11-14, (2014) Trans Tech Publications, Switzerland, doi:10.4028/www.scientific.net/ KEM.607.11

[3] POKORNY, Z., HRUBY, V., BARBORÁK, O. Characteristics of plasma nitrided layers in deep holes. KOVOVE MATERIALY-METALLIC MATERIALS, 2012, vol. 3, no. 50, p. 209-212. ISSN 0023-432X.

[4] ČSN ISO 14577-1 METALIC MATERIALS – Instrumected indentation test for hardness and materials parameters – Part 1: Test method.

[5] POKORNY, Z, KADLEC, J., HRUBY, V. Mechanical Properties of Steels after Plasma nitriding Process. Journal of Materials Science and Engineering A 1, 2011, vol. 2011, no. 6/2011, p. 42-45. ISSN 1934-8959.

Influence of initial carbon concentration on nitride layers

Miroslav Pospíchal, Renata Dvořáková, Zbyněk Studený, Zdeněk Pokorný
Faculty of Military Technology, University of Defence, Kounicova 156/65, 662 10 Brno, Czech Republic. E-mail: miroslav.pospichal@unob.cz, zdenek.pokorny@unob.cz

The properties of plasma nitride layer are determined except technological parameters by chemical compositon and structure of steel. Experiments were carried out on ARMOX 500T steel. Firstly, the samples of steel were carburized and isothermal hardened. After quenching the course of microhardness was measured from surface to the core of material. Samples were cutted off on metallographic saw and subsequently grinded from the surface to the core of material. All depths of grinded surface from surface to the core were exactly defined. The chemical composition was verified in each prepared samples. Samples with changeable content of carbon were nitrided by plasma nitriding technology. All properties of plasma nitriding layers were evaluated.

Keywords: Diffusion, Plasma nitriding, Armor steel

1. Introduction

The difusion process during plasma nitriding process is influenced by technological conditions of nitriding process (temperature, time, voltage, pressure, concentration of nitriding atmosphere, pulse length), by chemical composition and structure of nitrided material. The properties of diffusion layer are influenced by alloying elements and type of microstructure of steel. The effect of alloying by substitution elements on process of nitrogen diffusion is significantly demonstrated in high alloyed steels. The aim of present work is to study carbon redistribution in plasma nitrided steel and their effect of carbon content to thickness of coumpound layer and diffusion layer created after plasma nitriding process. The chemical-heat treatment process was applied to specimens which were taken from one piece of armoured steel. The evaluation and validation of chemical composition of ARMOX were perfomed as a first part of experimental work. The basic structures of determined specimens were identical. The changes of carbon content in measured depth were reached by grinding of carburized sample layer to accurately specified areas from surface part to the core of sample.

2. Experiment

Steel ARMOX 500T was used for all performed experiments. Steel for specimens is distributed to market as a steel plate 500x500 mm and the thickness 4.4mm [4]. Steel plate is consist of 2 plates 4.4 mm thick which are bolted. Steel plates were carburized from one side only in CODERE 251-70/60 C 11/3 applience for 10 hours with carbon potential of the furnace atmosphere 1.1 wt.% C. After carburizing the plate steel were quenched from carburizing temperature to 830°C. After temperature stabilizing the plate were sealed in salth bath AS 140 and austempered for 1 hour. The specimens were prepared from carburized plates from distace min. 100 mm far from the edge. The specimens of size 140x40 mm were produced. The evaluation of carbon effect on properties of plasma nitrided layers was carried out on specimens which were cooled during grinding. The specimens were used for experiments concerning analysis of chemical composition after heat treatment. The chemical composition of steel before and after treatment is shown in tab. 1.

Tab. 1** Chemical composition **of experimental steel

Element	Armox 500T [wt%] basic material		Armox 500T [wt%] Cemented
	Measured by GDOES (BULK)	Normalized values	Measured by GDOES (BULK)
C	0.30	max. 0.32	0.96
Mn	0.76	max. 1.2	0.78
Si	0.25	max. 0.4	0.23
Cr	0.47	max 1.00	0.45
Ni	0.84	max 1.80	0,86
Mo	0.31	max.0.7	0.32

The specimens were successively grinded to determined depths and subsequently measured. The chemical composition of prepared specimens was performed by using GDOES/BULK method on spectrometer SA-2000 LECO. The depth of grinding and relevant measurement of carbon concentration is displayed in tab. 2.

Tab. 2 Nitrogen concentration in depth (measured under surface)

Specimen no.	Depth under surface (mm)	Concentration of C (wt.%)	Specimen no.	Depth under surface (mm)	Concentration of C (wt.%)
1	**-0.15**	**0.89**	**5**	**-1.29**	**0.56**
2	**-0.18**	**0.87**	6	-2.31	0.43
3	-0.52	0.81	7	-3.50	0.43
4	**-0.77**	**0.75**	8	-4.44	0.42

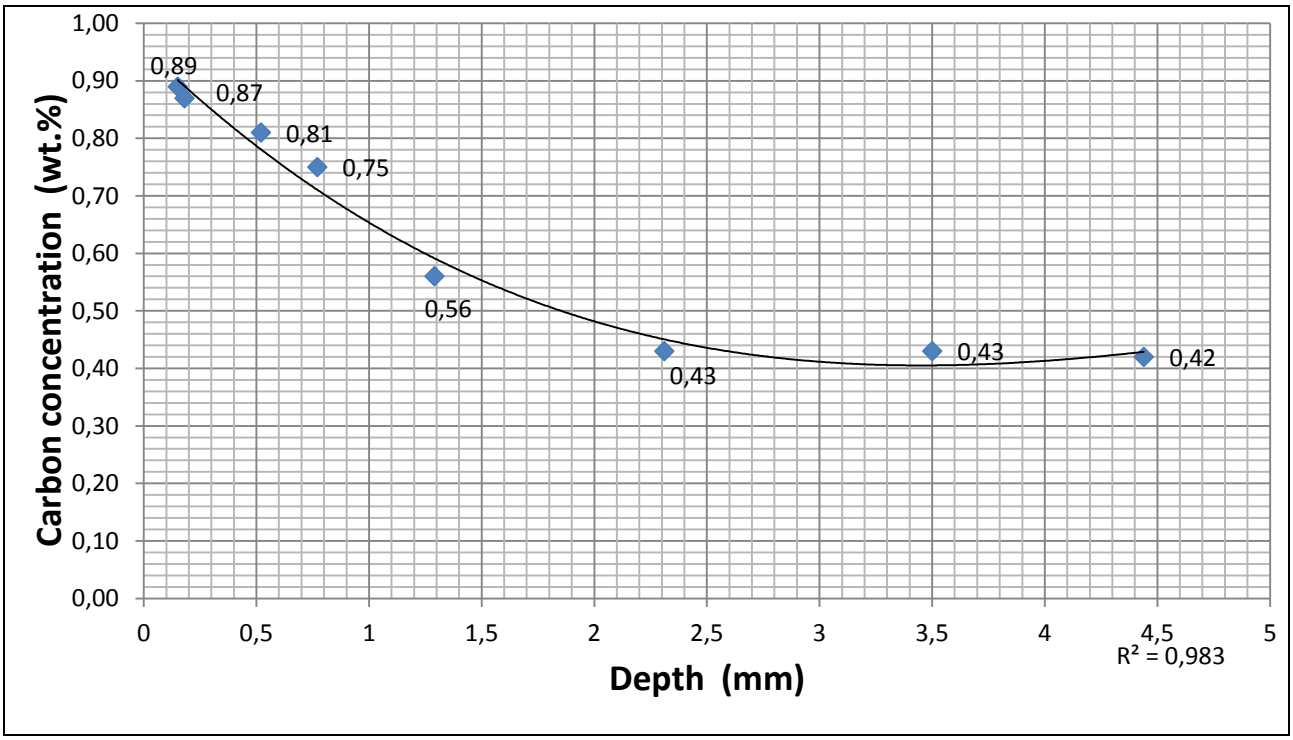

Fig. 1 Carbon concentration in depth of cemented surface

Increased content of carbon on specimens 6-8 is caused by performation of carburizing atmosphere between screw connection. For other explanation will be omitted. The dependence of carbon content on depth is given in fig. 1.

The carburized specimens were plasma nitrided in RUBIG PN60/60. The conditions of proces are displayed in tab. 3.

***Tab. 3** Plasma nitriding process parameters*

Technology	Temperature	Time	Atmosphere $H_2 : N_2$	Voltage	Pressure	Pulse length
Plasma nitriding	500°C	12 h	24 : 8	530 V	280 Pa	100/200 µs

For plasma nitriding process the specimens 1, 2, 4 and 5 were selected (tab. 2). GDOES/QDP method was used for verification of carbon and nitrogen concentration in depth 15µm. The nitrided layer was evaluated by metallographic method on optical microscope Olympus GX 51.

3. Results of the experiments

In plasma nitriding process the nitrided layer were created on all selected samples. The diffusion layer was consisted of lower bainite with changeable content of nitrogen and carbon ionts. The chemical composition of compound zone and the transition to diffusion layer was evaluated to depth 15 µm under intial surface. The curves of nitrogen and carbon concentration are given in fig. 2 and fig.3.

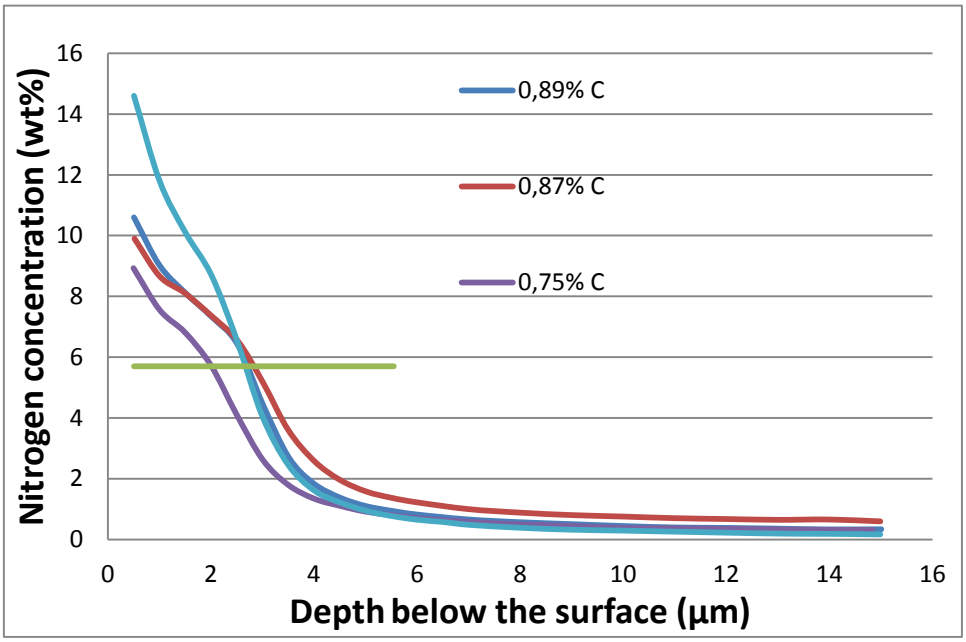

Fig. 2 The change of concentration of nitrogen

The distribution of nitrogen ionts in coumpound zone established after plasma nitriding process is explained by existens of nitrogen potential of used technologie and the conditions of diffusion in nitrided material. The use of nitriding atmosphere in ratio 75%H_2 + 25%N_2 can be expected the creation of Fe_4N in diffusion and compound layer [5]. From concentration curves given in fig. 2 is evident the heterogeneity of compound layer. This layer occurs as gamma phase Fe_4N and epsilon phase $Fe_{2-3}N$ and theta phase Fe_2N of specimen no. 5. The types of nitrides are of course-influenced by carbon concentrations which were detected from depth 0.1 µm under surface. The presense of carbon ionts can contribute to transformation of Fe_4N to $Fe_{2-3}N$ (ε) because the concentration of nitrogen can be lower than stated in equilibrium state of the system Fe-N.

The distribution of nitrogen ionts in coumpound layer and diffusion layer is given nitrogen potential. Next important parameter is definitely connected by condition of diffusion of nitride material. Usage of nitriding atmosphere 75%H_2 + 25%N_2 is possible to expect the creation of nitrided layer which will be created by diffusion layer and compound zone Fe_4N [5]. The trend of nitrogen concentration in compound zone (fig. 2) shows heterogenenous composition contented nitrides Fe_4N, $Fe_{2-3}N$ (ε) and of course minimum proportion of Fe_2N in case of sample 5. The proportion of mentioned nitrides is mostly influenced by carbon content. Carbon was detected to depth 0.1 mm under grinded surface. The presence of ionts of carbon can lead to transformation of Fe_4N to $Fe_{2-3}N$ (ε). The content of nitrogen should have lower level than equilibrium state Fe-N. Fig. 2 shows nitride layer created till 2.0 to 2.8 µm by compound zone. The change of carbon concentration in surface part of samples is in dependence on depth under surface displayed in fig. 3.

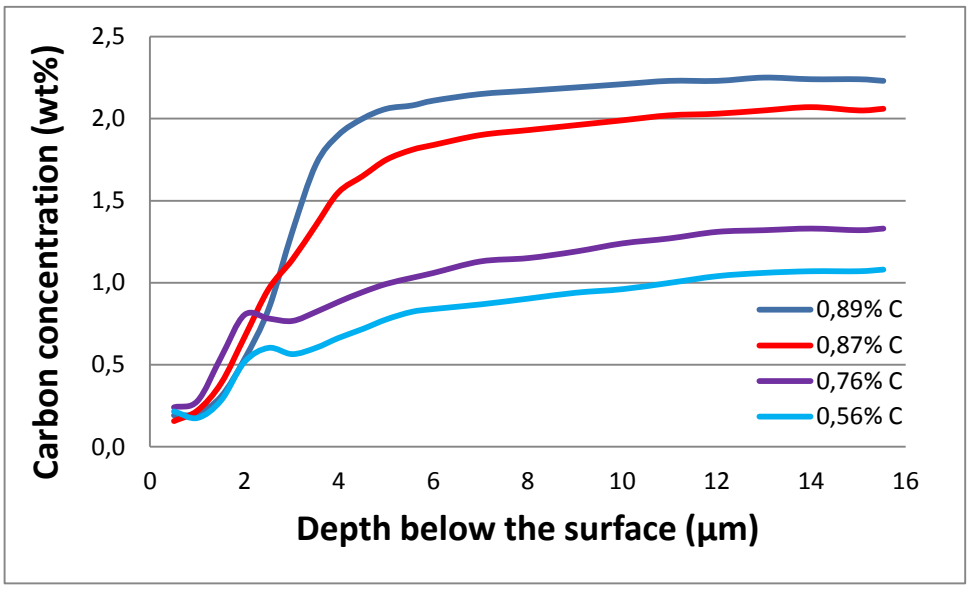

Fig. 3 The change of concentration of carbon

Fig. 3 shows the mechanism of nitrogen diffusion. During nitrogen saturation of surface the carbon diffusion occurs from compound zone area. This mechanism caused increasing of carbon in diffusion layer. The maximum of carbon concentration of measured area was reached in depth 15 µm for all default concentrations. The trend shows other increasing of carbon concentration.

The thicknesses of compound zone were metallographic evaluated (fig. 4.7 – 6.2). The measured results show incoherence between thickness of compound zone evaluated from chemical composition and thickness evaluated by optical method. Thicknesses evaluated by using optical microscopy method reached higher values than in case of chemical analysis evaluation by GDOES method which was determined from eqiulibrium state Fe-N.

Tab. 4 *Comparing of thicknesses of compound layer*

No.	Thickness GDOES method (µm)	Thickness metalography method (µm)
1	2.7	6.2
2	2.8	5.6
4	2.0	4.7
5	2.7	4.7

Metalographic check is more suitable principe for evaluation of thickness of compound zone than mentioned method GDOES:

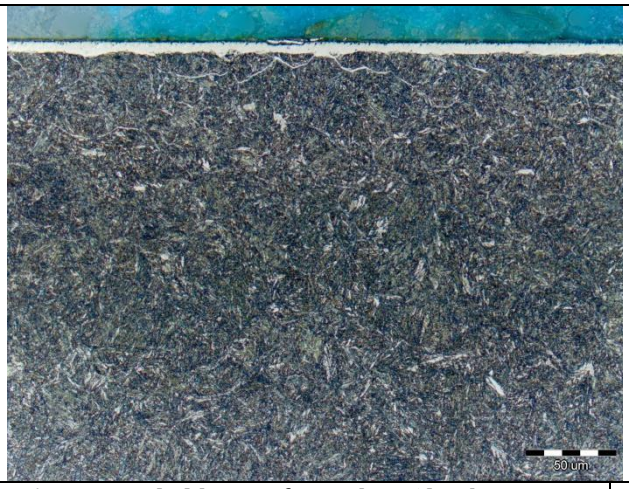

Fig. 4 *Nitrided layer of sample 1 (depth 0.15 mm / carbon content 0.89 %)*

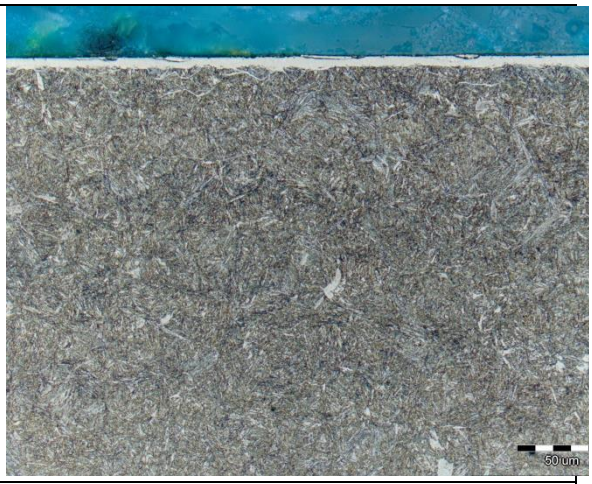

Fig. 5 *Nitrided layer of sample 3 (depth 0.18 mm / carbon content 0.87 %)*

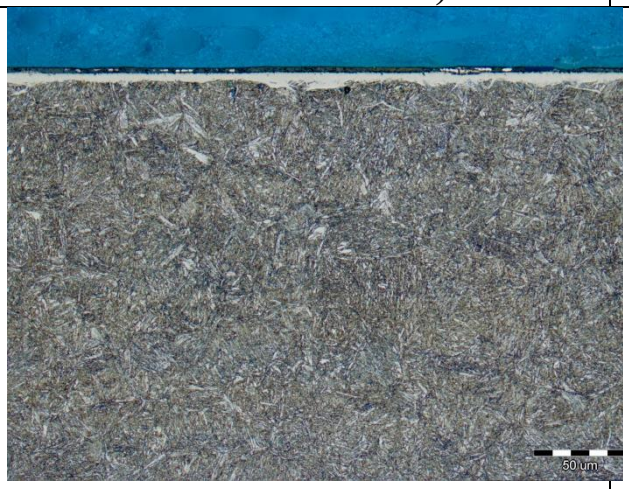

Fig. 6 *Nitrided layer of sample 4 (depth 0.15 mm / carbon content 0.77 %)*

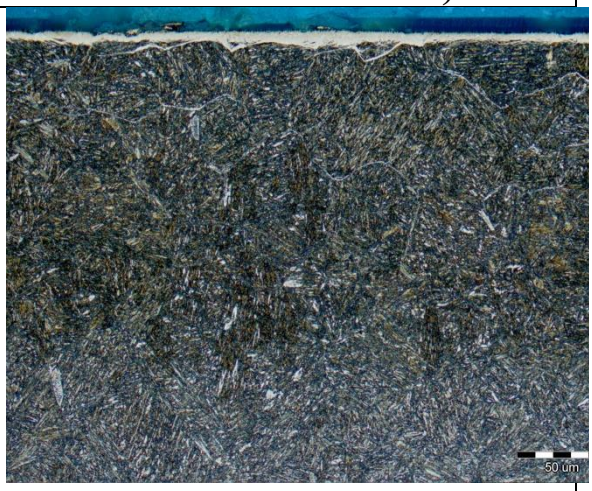

Fig. 7 *Nitrided layer of sample 5 (depth 1.29 mm / carbon content 0.56 %)*

5. Conclusion

Experiments were performed on samples with difference carbon content in surface layer. All samples were cut from one plate where all other elements were constant except carbon. The microstructure was identical in all cases.After plasma nitriding process selected samples were checked due to verification of nitrogen and carbon concentration to depth 15µm. The analysis of changes in carbon concentration caused by the plasma nitridation process shows that carbon peak were created in all samples The maximal concentration of carbon in carbon peak was in checked interval 0.89 až 0.56 wt% caused by default content of carbon in surface layer. Maximal value of concentration in carbon peak 1.08 wt% was reached in case of default carbon concentration 0.56%wt. By increasing of default carbon concetration 0.89 wt% increased carbon concentration to 2.24 wt%.

In area of compound zone the influence of carbon concentration was not confirmed. Some differences in carbon concentration were observed in some areas of this layer but direct link of nitrogen concentration on carbon concentration has not been confirmed.

It was proven that the increasing of compound zone thickness is connected with increasing of default carbon content in material and increasing of carbon content in carbon peak.

The comparison of thickness of compound zone determined from chemical composition by GDOES method and by metallographic method how that the thicknesses of compound zone determined by metallographic method reached high values of thickness than in case of GDOES method. The reason should be in deviation of chemical composition estimated from equilibrium state Fe-N in transition part of compound zone and diffusion layer. The deviations from equilibrium occur due to technology of plasma nitriding.

Initial concentration of carbon minimally affects the chemical composition (nitride types) of compound zone but the thickness of compound zone is significantly influenced. The decisive factor for nitriding layer parameters will be probably high content of substitutional alloying elements that significantly affect the diffusion near the surface of a part.

Acknowledgement

The paper was prepared with the support of the Project for the Development of the Organization and by the Specific research project 2014 of the Department of Mechanical Engineering, UoD "Promoting Research, Science and Inovation in the Field of Engineering".

References

[1] NIKOLUSSI, M., LEINWEBER, A., et al. Examination of phase transformations in the system Fe-N-C by means of nitrocarburising reactions and secondary annealing experiments, the α+ε two-phase equilibrium. In: *Material Research*, 98 (2007) 11, p. 1086-1092, ISSN 1862-5282.

[2] PYE, D. *Practical nitriding and ferritic nitrocarburizing*, USA 2003, ISBN 0-87170-791-8.

[3] HOLEMÁŘ, A., HRUBÝ, V. *Plazmová nitridace v praxi*, SNTL, Prague 1989, ISBN 80-03-00001-7.

[4] DATA SHEET, Armox 500T, SSAB Oxelösund, Version 2007-10-01,2p.

[5] Davis, J.R., *Surface Hardening of Steel,* ASM International Materials Park, 2002, ISBN: 0-87170-764-0

Experimental Detection of the Characteristics Magnetorheological Dampers Applied into Military Vehicles Operated in Multinational Missions

Vladimír Sedlák[1], Mariana Kuffová[2]
[1]Armed Forces Academy of General Milan Rastislav Štefánik, Department of Mechanical Engineering, Demänová 393 Liptovský Mikuláš, Slovak Republic, e-mail: vladimir.sedlak@mil.sk
[2]Armed Forces Academy of General Milan Rastislav Štefánik, Department of Mechanical Engineering, Demänová 393 Liptovský Mikuláš, Slovak Republic, e-mail: mariana.kuffova@aos.sk

This article discusses the research of magnetorheological (MR) dampers based suspension system and applies it to military vehicle for vibration control with a focus on measuring it is the characteristics and practical testing. MR dampers are compact and suitable for industrial suspension applications. Continuously variable damping is controlled by the increase in yield strength of the MR fluid in response to magnetic field strength. The MR damper is under different test conditions alternating expansion and contraction. The load cell senses the reaction force shock from which it is evaluated damping force. The program allows on-line monitoring of measured data, direct view depending on the force vs. piston velocity F-v force vs. piston stroke F-z and characteristics to verify the speed limits regulation and global characteristics of the damper. Especially most of vehicles for military purpose have bad inertial condition and severe operating condition such as the rough road driving, and need a high mobility in the emergency status. It is necessary to apply the controlled suspension system in order to improve the vehicle mobile stability and ride comfort ability of crews.

Keywords: Magnetorheological, Military Vehicle, Characteristics of the Damper

1 Introduction

Military vehicles are subject to large vibrations which can have severe affects on drivers, crew and load. Ride quality is influenced by vehicle vibrations, which may be induced by a variety of sources including roadway roughness or off road terrain, or thay may be internaly generated forces produced by vehicle subsystems, such as the engine, or the suspension mechanisms of weapons. Both short but high vibration peaks as well as long duraction, high frequency vibrations can pose either disorientation and safety problems or a healt threat to passengers of a vehicle. Most ground vehicles are equipped with passive spring and damping devices which have reached a high level of sophistication. However, they can usualy only be tuned to a good performance in a relatively small operational range (weight, speed, excitation level) or they perform only moderately well over a wide operational range. Semi-active suspension based on dampers, a concept also known as active damping, has reached production stage for vehicles, and has been proposed for military vehicles sucha s light armoured vehicles. It has proven to be an effective way to cope with a number of conflicting requirements, especially comfort, ride handling, ground contact of the tire, road friendliness, and it works well for a wide range of applications and over a large operational range.
Some smart materials have the ability to change from a liquid to a solid almost instantly when placed near a magnet. These materials have multiple properties, e.g., electrical, magnetic, mechanical and thermal and can transform energy that can be altered using some external fields. The Magneto-Rheological (MR) fluids are field responsive rheology where their fluid and other properties are controlled by varying the external magnetic field.
As up-to-date devices dramatically improve their dynamic properties, a need arises to effectively control vibrations in them. By limiting vibrations greater precision of the devices is achieved thereby allowing for a larger variety of applications. The devices also become more user-friendly as they do not emit harmful vibrations or high intensity noise. The use of dampers with magnetorheological fluids (MR dampers) enables more effective vibration control in mechanical devices as is the case in conventional damping systems. One of the advantages of MR dampers is easy adjustment of the damping force in a wide range which is achieved by a change of the magnetic field. The structure of a linear MR damper is shown in Fig.1.

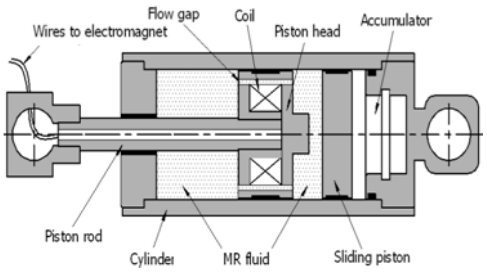

***Fig. 1** MR damper*

Magnetorheological fluid is a colloidal suspension of magnetically polarised particles with diameters of 0.5 to 10 μm in a carrier fluid, mostly synthetic oil with a low evaporation rate or water [1]. A typical MRF contains from 20 to 80% of ferromagnetic particles, by weight. The main feature of the fluid is dramatic change of viscosity and, consequently, of shear stress upon the application of a magnetic field. The stress changes during the increase and decrease of magnetic flux density occur in microseconds. The fluids retain their properties in the temperature range from −40°C to 150°C. Relative magnetic permeability of the fluid is small, $\mu_r < 10$ [2, 3].

2 Mathematical Model of a Vibrating System with an MR Damper

A car suspension includes an MR-damper is modeled as shown in Figure 2, the figure shows a two degree of freedom system represents a quarter car model. The mass of the vehicle is represented by the sprung mass $\mathbf{M_B}$ and the mass of the wheel and associated components is represented by the unsprung mass $\mathbf{M_W}$. The two masses vertical motions are described by the displacements $\mathbf{x_B}$ and $\mathbf{x_W}$ for sprung and unsprung mass respectively. The road excitation disturbance is represented by $\mathbf{x_r}$ and the passive spring and tyre stiffness are $\mathbf{k_s}$ and $\mathbf{k_t}$ respectively neglecting the tyre damping compared to the system damping. By applying Newton second law to the quarter car model, the equations of motion for the masses $\mathbf{M_B}$ and $\mathbf{M_W}$ are:

$$\mathrm{M_B}\ddot{x}_B + k_s(x_B - x_W) + f_d = 0, \tag{1}$$

$$\mathrm{M_W}\,\ddot{\mathrm{x}}_\mathrm{W} - \mathrm{k_s}\ (\mathrm{x_B} - \mathrm{x_W}) - \mathrm{k_t}\ (\mathrm{x_r} - \mathrm{x_W}) - \mathrm{f_d} = 0, \tag{2}$$

where $\mathbf{f_d}$ is the MR damper force;

$$f_d = C_1\ (\dot{y} - \dot{x}_W) + k_1\{(x_B - x_W) - x_0\}, \tag{3}$$

where $\mathbf{C_1}$ is viscous damping coefficient which produce the system roll-off at low velocities and $\mathbf{x_0}$ is initial deflection for the damper accumulator which is represented by the stiffness $\mathbf{k_1}$;

$$\dot{y} = \frac{1}{C_1 + C_0}\ \{\alpha Z + C_0\,\dot{x}_B + C_1\,\dot{x}_W + k_0\,(x_B - y)\}, \tag{4}$$

where **Z** is Bouc-Wen variable governed by

$$\dot{\mathrm{Z}} = -\gamma\,|\dot{x}_B - \dot{y}|Z\,|Z|^{n-1} - \beta\,(\dot{x}_B - \dot{y})|Z|^n + \delta\,(\dot{x}_B - \dot{y}), \tag{5}$$

where **α** and **δ** are functions of the applied magnetic field and related to the height, width and slope of the pre-yield hysteresis loop.
β, **γ** and **n** give the basic configuration of the hysteresis loop.
In order to consider the damper force $\mathbf{f_d}$ is dependent on the input voltage, the following linear relations can be used [4,5]:

$$\boldsymbol{\alpha} = \boldsymbol{\alpha_a} + \boldsymbol{\alpha_b}\,\boldsymbol{V}, \tag{6}$$

$$\boldsymbol{C_1} = \boldsymbol{C_{1a}} + \boldsymbol{C_{1b}}\,\boldsymbol{V}, \tag{7}$$

$$\boldsymbol{C_0} = \boldsymbol{C_{0a}} + \boldsymbol{C_{0b}}\,\boldsymbol{V}, \tag{8}$$

where **V** is given by the following differential equation:

$$\dot{V} = -\sigma\,(V - v), \tag{9}$$

where **v** is the voltage applied to the damper and **σ** is a constant governing the rate of change of magnetic field to reach the equilibrium of the MR fluid.

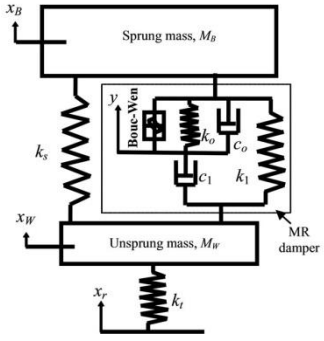

Fig. 2 *Quarter car model with MR damper*

3 MR Shock Absorber and Experimentation

A MR shock absorber as shown in Figure 3 has been bought from the LORD Corporation USA, i.e., RD-8041-1(long stroke).

Fig. 3 *Figure of MR damper RD-8041-1(long stroke)*

In this MR shock absorber, MR fluid flows from a high pressure chamber to a low pressure chamber through an orifice in the piston head (www.lord.com). The MR shock absorber is compact and is suitable for industrial suspension applications. Continuously variable damping is achieved by developing a variable magnetic field strength. The technical specifications of the shock absorber is as under [6]:

Stroke	74 mm
Extended Length	248 mm
Body Diameter	42.1 mm max
Shaft Diameter	10 mm
Tensile Strength	8896 N max
Damper Forces (Peak to Peak)	5 cm/sec @ 1A >2447 N 20 cm/sec @ 0A <667 N
Operating Temperature	71 °C max
Weight	0,919 kg

Tab. 1 *Typical Properties**

**Data is typical and not to be used for specification purposes.*

The shock absorber is tested to check its performance. The setup of the lab as shown in Figure 4 is used for this purpse. The Hydraulic pulsator simulates kinematic and force requirements to 200Hz frequency and force of 40kN. The MR damper is under different test conditions alternating expansion and contraction. The load cell senses the reaction force shock from which it is evaluated damping force. The shaker has a maximum displacement (peak to peak) of 20 mm. The program allows on-line monitoring of measured data, direct view depending on the force vs. piston velocity F-v force vs. piston stroke F-z and characteristics to verify the speed limits regulation and global characteristics of the damper. The Shaker can be used for both horizontal and vertical vibrational analysis. The test device includes a computer that uses the A / D convertor controls the movement of the hydraulic servo valve. The shaker is controlled by PC Based Digital Vibration Controller cum analyzer with built-in signal conditioner unit. The controller unit of the shaker is a close loop control system. The set-up has a compatible data acquisition and instrumentation system which gives the data in the form of force, velocity, displacement and acceleration with respect to time. On the shaker system, the MR shock absorber is mounted. Subsequently, the computer records the measurement variable measured as the damping force, displacement piston, from which subsequently may determine the time derivative of the piston velocity. The force experienced by the piston rod, which was prevented from motion, was sensed by a load cell fixed at the top of the MR shock absorber while the displacement is recorded through displacement sensor [7].

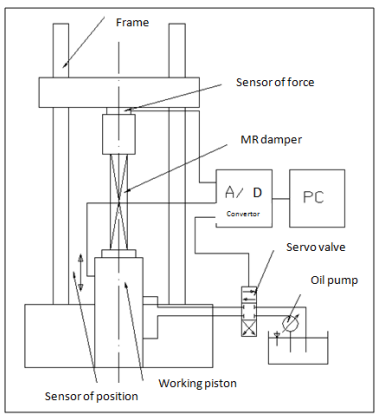

Fig. 4 *Schematic layout of test stand*

4 Results

- **Experiment with variable input electrical current**

Figure 5 shows the variation of damping force v/s displacement of the shock absorber for one cycle. The Figure shows that as the value of current increases the damping force increases and the displacement of the piston is decreased. The damping force is low for zero current and it increases gradually as the current is increased. Evaluation of the impact of input electrical current to the test damper is undertake a series of sinusoidal movements. Measurement is carried out for four constant electric currents, which have a value of 0 A, 0.5 A, 1 A, 1,5 A a 2 A. For illustration Figures 5 and 6 of the possible characteristics of dampers, force vs. stroke F-x and force vs. velocity F-v. Transferred of MR damper RD-8041-1 for 74 mm stroke at a frequency of 1.6 Hz. Curve of F-v characteristics increases along with the increase of the input electric current [8].

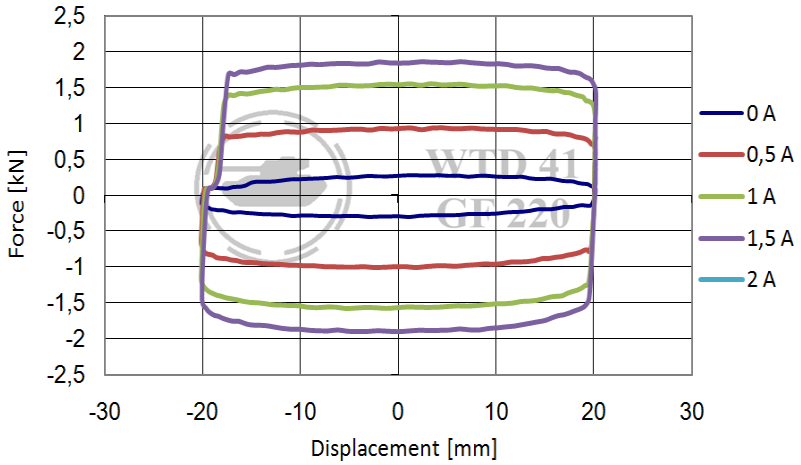

Fig. 5 *Force vs. Displacement Curves with Different Levels of Current*

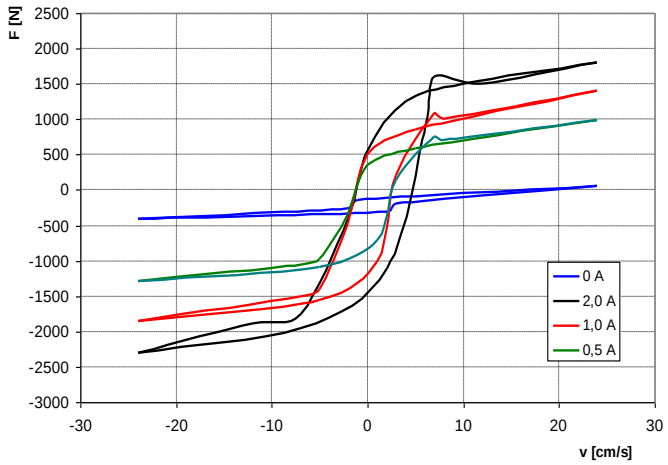

Fig. 6 *Measurement of force vs. velocity F-v*

- **Experiment with variable frequency**

Experimental measurement points to changes in the characteristics of damper at different frequencies. Damper is driven by a sinusoidal excitation with four different frequencies of 0.25 Hz, 0.5 Hz, 1 Hz, 2 Hz. For illustration experimental measurements are shown in Figures 7 and 8 in which the measured characteristics of the damper stroke at 4.1 cm, and input electric current 1 A. The results indicate an increase in damper absorbing power according to the increase of the excitation frequency [7].

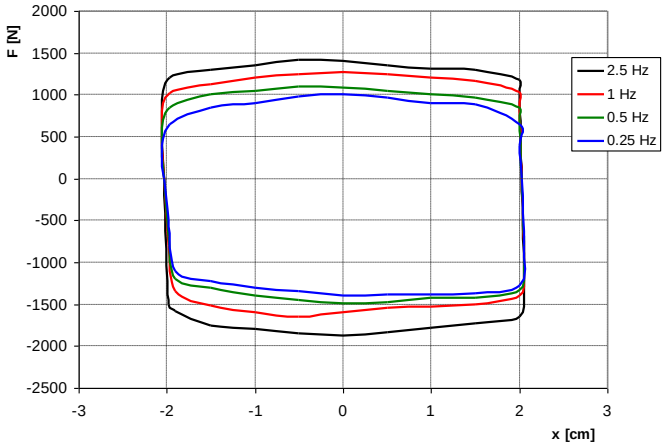

Fig. 7 *Measurement of force vs. stroke F-x*

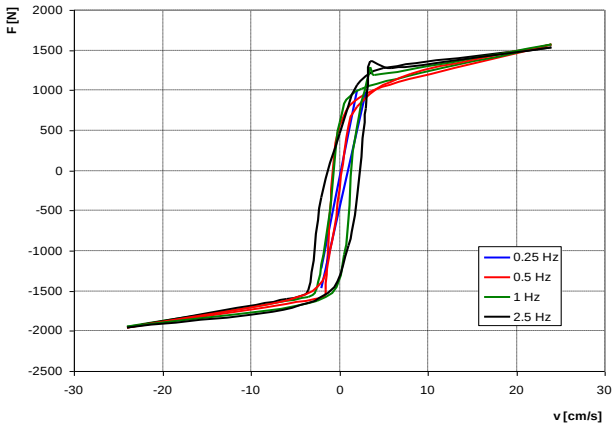

Fig. 8 *Measurement of force vs. velocity F-v*

5 Application into Military Vehicles

Dampers with controllable fluids have long been a topic for military vehicles. Since military vehicles are by nature often operating at rough terrain, the question of vibration reduction is of great importance. The following example is a description of an investigations made with the help of dynamic driving simulations to improve the ride comfort of cross-country vehicles through controlled chassis [9].

The high mobility requirements for the investigated vihicles in heavy terrain resulted in a relatively rigid tuning of the spring/suspension system. When looking at the tipical operational profile of these vehicles it becomes clear that more than 90% of the rides take place on roads, tracks and rough tracks. A controlled chassis would ensure the same mobility in heavy terrain and improve the ride comfort both on bad road stretches and in easy terrain. By this means the average speed can be increased while reducing the stress for the crew at the same time. A high ride comfort is especially necessary for fatigue-free driving over long distances and will essentially contribute to the operational security for the crew.

6 Conclusion

In this paper, the basic theory behind the MR Shock absorbers, its testing and evaluation is carried out. A MR shock absorber from Lord Corp. USA is bought and tested in the laboratory. The results presented in this paper show the good efficiency of vibration damping. The above results show that the user can have a very good control over the damping force of the MR shock absorber by varying the input current which is supplied to the magnetic coil of the absorber. This is a necessity for a semi-active vibration control system. The result further showed that the damping force is not zero at zero input current, i.e., at off-state. It is because of the fact that fluid viscosity alone is responsible for the damping effect in the off-state. It is equivalent to failure/mal-function of the electro-magnetic coil or fail-safe condition.

Acknowledgement

The authors gratefully acknowledge WTD 41 GF 220 for making this project possible under the SVK-DEU-AVT-14 P/1 Support Project.

References

[1] BUTZ, T., von STRYK, O.: Modelling and Simulation of Rheological Fluid Devices; Sonderforschungsbereich 438: Technische Universität München, Universität Augsburg: Preprint SFB-438-9911 (99), s. 1-35.

[2] MILECKI, A., SĘDZIAK, D.: Modelling and control of magnetorheological fluid damper, Computer Applications in Electrical Engineering, Poznań University of Technology, Poznań 2004, pp. 566-575.

[3] SZELĄG, W., Finite element analysis of coupled phenomena in magnetorheological fluid devices, COMPEL – The International Journal for Computation and Mathematics in Electrical and Electronic EngineeringJames and James Science Publ., No.2, Vol. 23, No. 3, 2004, pp. 813-824.

[4] SPENCER, B. F., DYKE, S. J., SAIN M. K. and CARLSON, J. D., "Phenomenological Model for Magnetorheological Dampers," Journal of Engineering Mechanics, Vol. 123, No. 3, 1997, pp. 230-238. doi:10.1061/(ASCE)0733-9399(1997)123:3(230).

[5] LAM, A. H.-F. and LIO, W.-H., "Semi-Active Control of Automotive Suspension Systems with Magnetorheological Dampers," International Journal of Vehicle Design, Vol. 33, No. 1-3, 2002, pp. 50-75.

[6] www.lord.com

[7] DANKO, J., "The influence of semi-active system on twin-axle automobile suspension," Disertation thesis, Faculty of Mechanical Engineering, The Slovak University of Technology, Bratislava 2006, pp. 111-117.

[8] SVK-DEU-AVT-14 P/1 Support Project in Bundeswehr Technical Center for Automotive and Armored Vehicles (WTD 41) in Trier (Germany)

[9] HÖNLINGER, M., GLAUCH, U., „Mobility Analysis of a Heavy Off-Road Vehicles Using a Controlled Suspension," RTO/AVT Specialists Meeting on „Structural Aspects of Flexible Aircraft Control", Ottawa, Canada, October 1999, published in RTO MP-36.

Deposition of aluminium oxide (Al_2O_3) coatings on aluminium substrate using anodizing processes

Frantisek Snahnican
Faculty of Military Technology, University of Denefce, Brno, Kounicova 65, Czech Republic, frantisek.snahnican@unob.cz

The aim of this paper is to describe anodizing technology for deposition of Al_2O_3 coatings on Al substrates. Various methods of layer deposition were used for the experiments. Deposition was carried out in acidic environments, using sulphuric acid (H_2SO_4) and chromic acid (H_2CrO_4). Several samples were heat treated (annealed). Chemical composition of the substrate and the coating was tested by GDOS method using SA2000 and GDS 500A devices. Surface morphology and structure were evaluated by SEM, using VEGA5135 electron microscope. Selected mechanical properties as thickness, microhardness and adhesion were also determined.

Keywords: coatings, aluminium oxide, microhardness, surface morphology

1 Methods of anodizing

Commonly used processes of anodizing differ in the composition of the used bath and the type of electrical current used. Mainly used is the direct current, less often alternating current and sporadically alternating current superposed by direct current can be used. Recently pulsating current is gaining prominence in practice. Created oxide layer permits only one way flow of electricity, therefore alternating current can be used for anodizing.

1.1 Baths with sulphuric acid

Chemical reactions during anodizing of aluminium in sulphuric acid

Overall equation:

$$2Al + 3H_2O \xrightarrow{H_2SO_4} Al_2O_3 + 3H_2 \quad (1)$$

Reaction on cathode:

$$6H_3O^+ + 6e^- \rightarrow 3H_2 + 6H_2O \quad (2)$$

Reaction on anode:

$$3SO_4^{2-} + 3Al + 3H_2O - 6e^- \rightarrow Al_2O_3 + 3H_2SO_4 \quad (4)$$

Final process:

$$3H_2SO_4 + 6H_2O \rightarrow 6H_3O^+ + 3SO_4^{2-} \quad (5)$$

In the bath, close to the anode aluminium ions react with water and sulphate ions SO_4^{2-}, creating aluminium oxide, which is the desired protective coating. Meanwhile the dissolution of already created aluminium oxide by sulphuric acid occurs, producing aluminium sulphate, which stays in the bath. The last reaction is undesirable, since it removes aluminium oxide from the deposited coating and consumes free sulphuric acid. Decreasing the amount of sulphuric acid present in the bath decreases the conductivity of the electrolyte. The rate of decomposition of the coating is increased with temperature of the bath and with higher concentration of sulphuric acid. Effective cooling and stirring of the electrolyte suppresses the undesired decomposition of the coating. Generally used anodizing process in sulphuric acid with direct current uses current density of 1-1,5 $A.dm^{-2}$.

Coatings created by anodizing provide excellent corrosion resistance. If the thickness of the coating is sufficient and its pores are closed, then the coating is durable even in high temperatures, and has good ability to withstand mechanical wear, and therefore can be used as electrical insulation. Coatings have a very solid look, which can be further improved by painting. Thick and hard coatings can crack under stress, but even the damaged coating has good adhesion to the substrate. Coatings increase adhesion of organic coatings and overlays. Anodizing is commonly used on industrial products, e.g. kitchen aids, tools. Anodizing is being used on parts exposed to corrosive environments, e.g. airplane construction, ships or building construction.

Electrolytes work with various concentrations of sulphuric acid. Most commonly used concentrations are 15-27%, with voltages of 12 to 18 V and current densities of 1-2 $A.dm^{-2}$. These electrolytes are relatively cheap and under correct circumstances are very reliable. They require adequate cooling and stirring. Highest operating temperature should never exceed 20°C. The remains of sulphuric acid on the surface and inside the coating have to be removed after anodizing process under water current. Anodizing is not suitable for parts that were riveted or have capillary openings, cracks, pores,

etc., since it is problematic to remove acidic remains from these imperfections. The duration of anodizing depends mainly on the desired thickness of the coating. Commonly used durations are 20-30 minutes, for thicker layers (max. 25µm) 120 minutes. Obtained coatings are transparent and brittle.

Objects with low necessary corrosion resistance can be anodized in sulphuric acid by alternating current. This anodizing process is slower; coatings have a smaller thickness (5µm) and are porous. With alternating current higher efficiency of electrolyte can be achieved and further forming is possible.

1.2 Chromic acid baths

Anodizing in chromic acid is used on parts for very corrosive environments. The acidic remains of anodizing in sulphuric acid are removed with high difficulty. Failure to completely remove the acid results in deep corrosion of material. These problems are not present after anodizing in chromic acid. Baths contain approximately 100g.l^{-1} of chromium trioxide. Working temperature of this process is 35°C and therefore does not require intensive cooling. Voltages used are 30 – 40 V and current densities are 0,3 – 0,5 A.dm^{-2}. This method can be used for anodizing riveted assemblies and porous materials because the remains do not cause corrosion. Obtained coatings are milky in colour. This process is commonly used in aerospace applications.

2 Aluminium oxide Al_2O_3 coatings on aluminium substrate

Coatings of aluminium oxides were anodized in two different electrolytes on aluminium or aluminium alloy substrates. Chemical compositions of substrate materials were determined by GDOES/Bulk machine, SA 2000, manufactured by Leco. Results are presented in table 1. Samples had dimensions of 60 by 45 by 3 mm. Anodizing was carried out in aqueous solution of H_2SO_4 on samples 31 and 32, and in solution of chromium trioxide CrO_3 for samples 33 and 34. Before beginning of anodizing process samples made of aluminium alloy were etched in a solution of sodium hydroxide (NaOH) as described in table 2.

Table 1 Chemical composition of aluminium alloy for Al_2O_3 coating

Sample	**Chemical composition (%)**									
	Al	Mn	Si	Cr	Ni	Mo	W	Ti	Sn	Fe
Al alloy	98,6	-	0,180	0,017	-	-	-	-	0,084	0,241
Analysis parameters: U = 800 V, I = 25,0 mA, p_{Ar} = 273,3 Pa										

Table 2 Parameters of aluminium alloy substrate etching

Sample no.	**NaOH concentration (g.l^{-1})**	**Temperature (°C)**	**Etching time (min)**
31	50	30 – 50	5
32	100	30 – 50	2
33	50	30 – 50	10
34	100	30 – 50	10

2.1 Aluminium oxide Al_2O_3 coating in sulphuric acid bath

Before anodizing, all samples were degreased in ethanol and etched in sodium hydroxide solution. Two types of coating deposition were used

Simple anodizing in sulphuric acid was carried out on sample no. 31. Etched and cleaned sample was fixed in a stand and submerged into a bath of sulphuric acid, cooled to 14°C. Into the same bath an aluminium cathode was also submerged. Electrodes were connected to a stabilized direct current source. Using a potentiometer, the values of current were slowly adjusted to the desired value of 2 A. Given the surface of the cathode we produced current density of 1,5 A.dm^{-2}. Duration of process was 20 minutes. After removal of the anodized sample, the acidic bath was cooled back to 14°C, since its temperature was increased during the anodizing process.

The anodizing process for the sample no. 32 had a modified electrolyte, consisting of H_2SO_4 with added $CuSO_4$ of concentration of 3 g.l^{-1}. Duration of the process was 2 minutes. After the initial 2 minute period, the direction of the current was reversed and deposition of copper was carried out for 20 seconds. This process was repeated six times.

Subsequently, six processes were carried out by anodizing the samples for 2 minutes with following 10 second period of reversed current and joint copper deposition. The processes were repeated 12 times. The resulting coating consists of 12 layers of Al_2O_3 interlaced by 11 layers of copper (CuO_x). The goal of this method of material deposition was modification of electrical conductivity of the coating and change in optical properties of this coating.

Anodizing period and temperature of the bath were chosen according to the available equipment of the laboratories. Limiting factor was the temperature of the bath, which must not exceed 25°C after 20 minutes of coating deposition. No equipment was available to cool or stir the bath. Each anodized sample was cleaned under a stream of water and further neutralized in a 1% solution of NH_4OH (neutralization of sulphuric acid) and finally washed in cold water for 2 minutes. On both samples the pores on coatings were closed by cooking them in distilled water for 15 minutes. Afterwards the samples were cleaned under a stream of cold water, washed in ethanol and dried in hot air.

Sample no. 32 was annealed for 2 and 6 hours at 500 °C in a muffle furnace. Annealing was carried out in air atmosphere. After annealing the sample was quickly cooled by a stream of cold water, dried and used for analysis. Tested parameters were mainly chemical composition, adhesion (tested by indentation method), hardness and surface morphology.

2.2 Morphology of aluminium oxide Al_2O_3 coating – anodized in a sulphuric acid bath (sample no. 31)

Coatings created by anodizing in sulphuric acid after sealing pores in boiling distilled water have a specific surface morphology. Its structure is shown on Fig. 1. To evaluate the coating structure, its thickness and adhesion, the substrate with the coating were broken along one axis and bent by 90 degrees along an axis perpendicular to the breakage.

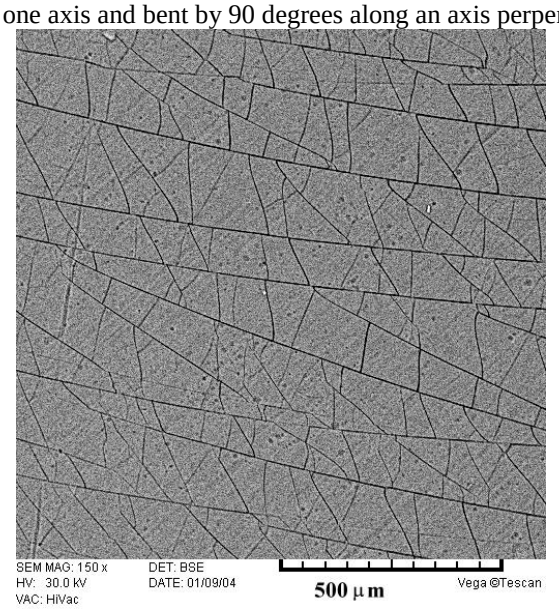

Fig. 1 Surface morphology of sample no. 31, magnification 150×

After preparations the sample was studied under an electron microscope under small angles (several degrees). Fig. 2 illustrates the resulting cracks in the coating which correspond to the lines visible on Fig. 1.

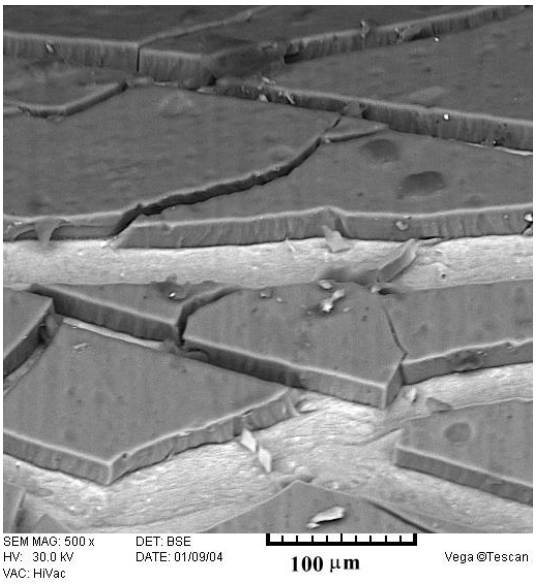

Fig. 2. Cracked coating on sample no. 31, magnification 500×

Fig. 3 shows a detail view of one segment of the coating, which was used to measure the thickness (again under a small angle).Both Fig. 2 and Fig. 3 show very good adhesion of the coating to the substrate material.

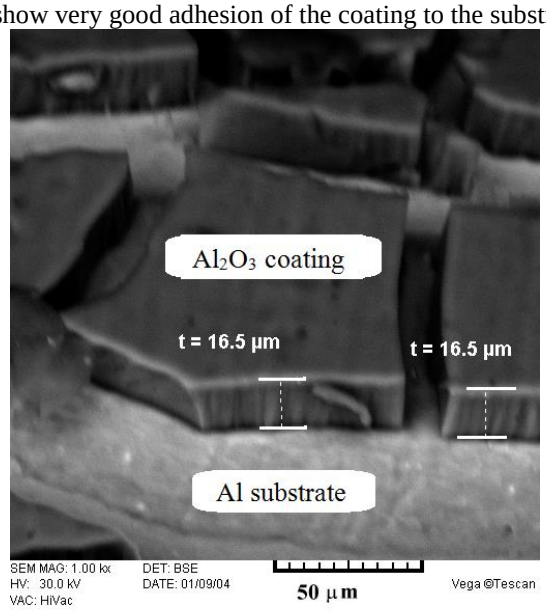

Fig. 3. Thickness of the coating on sample no. 31, magnification 1000×

Surface morphology of an aluminium oxide coating (Al_2O_3) after annealing, chemical composition of the coating on sample no. 32.

Coatings created by anodizing in sulphuric acid and subsequently annealed for 6 hours (BSE) is shown on Fig. 4. Both figures show sharply bordered polyhedral grains. These grains vary in size from tens to hundreds of micrometers. Even after the annealing process, the coating was

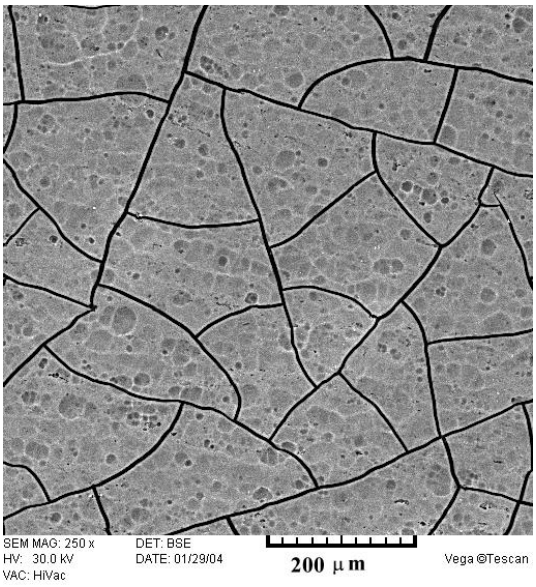

Fig. 4. Surface after 6 hour annealing at 500°C, BSE, magnification 250×

Even after the annealing process, the coating had a relatively low conductivity. Nevertheless using the QDP method a spectrum was obtained, Fig. 5. The spectrum was highly diffusive due to the oscillation of parameters. In spite of this, the layered structure of the coating is apparent. We can clearly see repeating bands of high concentrations of oxygen and aluminium (as aluminium oxide, Al_2O_3) and layers consisting of deposed copper (Cu). The copper is present either in pure form or as a chemical compound.

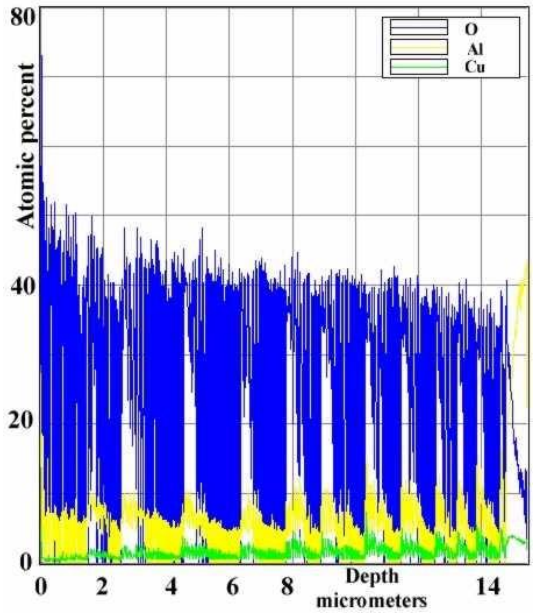

Fig. 5. Depth profile of sample no. 32

3 Anodized coatings of aluminium oxide (Al_2O_3) created in chromium trioxide (CrO_3)

The equipment necessary for anodizing in chromic acid (H_2CrO_4) is largely similar to those used for anodizing in sulphuric acid. The sample no. 33 was placed into an aqueous solution of chromic trioxide (CrO_3) with concentration of 150 $g.l^{-1}$. Subsequently anodizing process was effected. An aluminium plate with thickness of 1 mm and total surface area of 1,45 dm^2 was used as a cathode.

Parameters of anodizing process were set as: temperature of the bath 45°C, duration of coating deposition 30 minutes, current 0,3A, voltage 32 V and current density 1,5 $A.dm^{-2}$.

The sample was removed from the bath and rinsed under a stream of cold water for 2 minutes. Afterwards the sample

was placed into boiling distilled water for 15 minutes. Then the sample was washed in cold water and ethanol. Finally the sample was air dried. The sample no. 34 was treated similarly as sample no. 32, except the number or repetitions of the process was set as 10.

Since the vapours created by baths containing chromium trioxide (or Cr^{6+}) are considered a health risk, all the following experiments were executed in a sealed fume hood with appropriate filtration devices. For the same reasons, waste waters from all processes were collected into a special polypropylene (PP) vessel and disposed accordingly to safety regulations.

3.1 Adhesion and thickness of aluminium oxide coating – anodized in chromium trioxide

The following experiments were carried out on sample no. 33. Coating created during the anodizing process in CrO_3 was tested for adhesion using the indentation method. Adhesion was evaluated after indentation with force F_1 = 1 471 N (Fig.6) and F_2 = 2 452 N (Fig. 7).

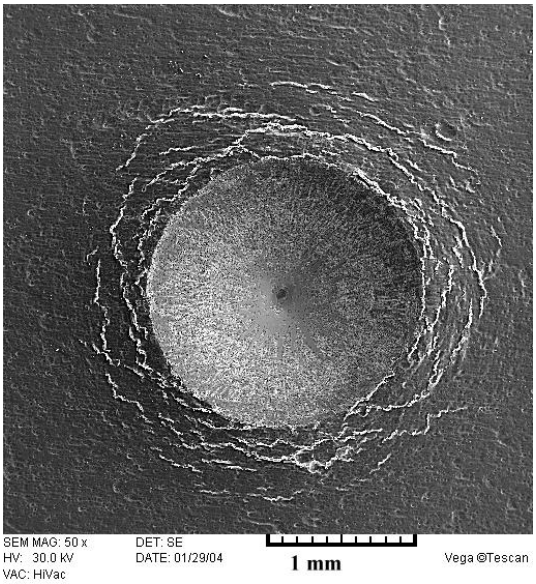

Fig. 6. Indentation test, F_1 = 1 471 N, magnification 50×

Both pictures show webs of concentrically arranged cracks, which have in both cases almost the same diameter. In addition to the cracks on the surface, the coatings is also deformed around the area of indentation and on the internal surface of the imprint a visible adhesion is still detectable.

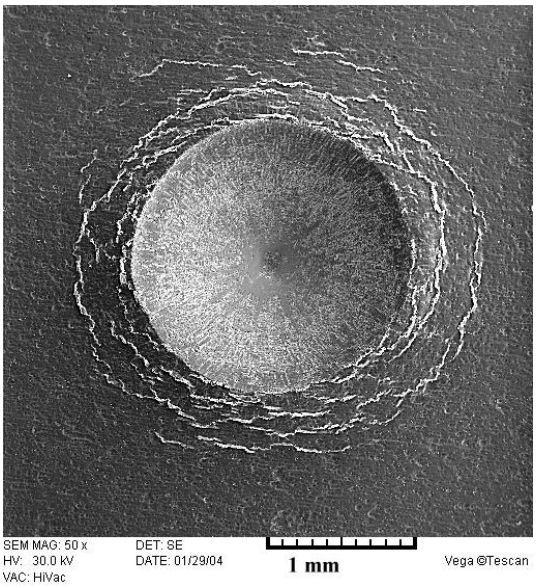

Fig. 7. Indentation test, F_2 = 2 452 N (no.33), magnification 50×

4 Measurement of hardness of the aluminium oxide coating using the Vickers microhardness method

Microhardness using the Vickers method was measured on the Leco M 400 hardness tester. Loading force was F = 0,490 N (HV 0,05). Arithmetic means of five measurements are presented in Table 3. The hardness of sample no. 32 is significantly higher than that of all other samples.

Table 3. Microhardness testing of Al_2O_3 coatings

Sample	Hardness HV 0,05	Load (N)	Note
31	42,7	0,490	
32	246,4	0,490	Annealed 500 °C, 6 hours, air
33	52,2	0,490	
34	31,6	0,490	Annealed 500 °C, 6 hours, air

4.1 Evaluation of the possibility of initiation of a glow discharge on the surface of an Al_2O_3 coating

Al_2O_3 coatings were considered as oxygen metrology standard for optical emission spectroscopy with direct current glow discharge. These coatings are essentially nonconductive, simple experiments were carried out, trying to increase their conductivity.

According to the methodology used on the samples no. 32 and 34, copper was not deposited as a continuous layer, but as a series of formations (Fig. 8) growing out of pores in the aluminium oxide coating (Fig. 9). The size of the copper dendrites depends on the duration of the deposition process and their shape on the current density during galvanic deposition of copper. These coatings were further heat treated.

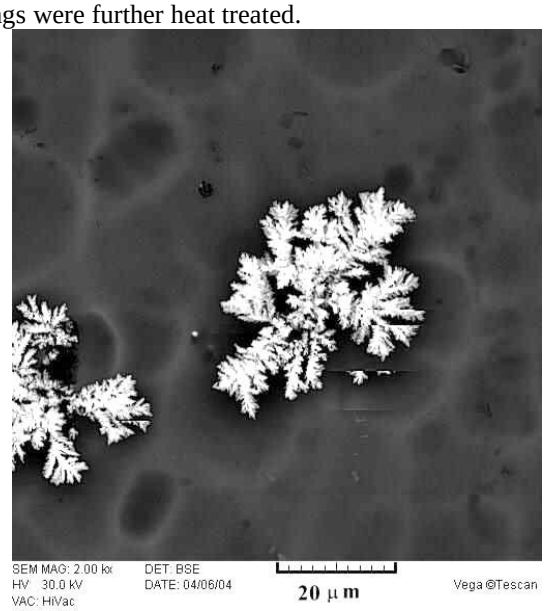

Fig. 8 Deposited copper dendrites, magnification 2000×

Unsealed coatings of aluminium oxide (Al_2O_3) always have pores. The deposition of copper on these pores is a variant of porosity test by copper (II) sulphate ($CuSO_4$). The number of pores in the Al_2O_3 coating directly influences the amount of segregated copper.

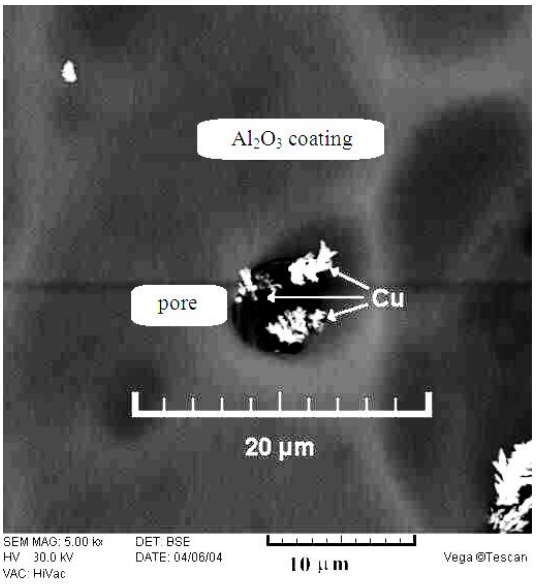

Fig. 9 Initial phase of copper deposition (no.32), magnification 5000×

Ability to ignite a glow discharge on the surface of these coatings was tested under conditions necessary for analysis of chemical composition in the SA 2000 spectrometer. Therefore the testing conditions consisted of voltages between 700 and 1000 V, current of 35 mA and argon pressures from 250 to 400 Pa. On the coating of the sample no. 32, the glow discharge was successfully ignited in 80 percent of experiments. Complete analysis was completed in 20 percent of experiments. The discharge was usually unstable during the whole measurement and took place between sealed pores. On the coating of the sample no. 34, the glow discharge was ignited every time, but in 100% of experiments this discharge died after several seconds.

5 Conclusions

The technology of deposition of Al_2O_3 coatings was evaluated. By using various environments for deposition, different surface morphologies of the coating were obtained. Their morphology was studied under electron microscopes. GDOS method was used, to better understand the chemical composition of the created surface layers. After experimenting with glow discharge ignition, we can conclude, that aluminium oxide coatings are not yet ready to be used as a metrology standard of oxygen for direct current method of glow discharge optical emission spectroscopy (GDOES), since the ability to ignite the discharge or its sustainability are very unpredictable and unreliable.

Acknowledgements

The paper was prepared with the support of the Project "Promoting Research, Science and Innovation in the Field of Engineering" of the Department of Mechanical Engineering, UoD.

References

[1] R. Payling, D. Jones, A. Bengtson, Glow Discharge Optical Emission Spectrometry, John Wiley Sons, New York 1997, ISBN 0-471-96683 5, 846 s.

[2] K. Kocman, P. Němeček, J. Kadlec a kol., Aktuální příručka pro technický úsek, Kapitola 6/8 Moderní povrchové technologie, Praha, Verlag Dashőfer 1998/ 1999/2000, ISBN 80-902247-2-5,180 s.

[3] J. A. Wingrave, Oxide Surfaces, Marcel Dekker, Inc., New York 2001, ISBN 0-8247-0000-7, 524 s.

[4] I. Vrublevsky, V. Parkoun, J. Schreckenbach, G. Marx, Study of porous oxide film growth on aluminum in oxalic acid using a re-anodizing technique, Applied Surface Science, Article in Press.

[5] C. Le Paven-Thivet, S. Fusil, P. Aubert, C. Malibert, A. Ozime, Ph. Houdy, On the existence of a nanometric multilayered structure in Al2O3/Al thin films, Thin Solid Films 446 (2004), pp. 147-154.

[6] S. Haq, A. Carew, R. Raval, Nitric oxide reduction by Cu nanoclusters supported on thin Al2O3 films, Journal of Catalysis 221 (2004), pp. 204-212.

Material Analysis of 120 mm Mortar Projectile Stabilizer

Zbyněk Studeny, Zdenek Pokorny, David Kusmič, Emil Svoboda
Faculty of Military Technology, University of Defence, Kounicova 156/65, 662 10 Brno, Czech Republic. E-mail: zbynek.studeny@unob.cz,

The article deals with the evaluation the state of 120 mm mortar projectile stabilizer. It assesses a crashed projectile, whose stabilizer got stuck in the barrel during the shot. The evaluation includes the analysis of the mechanical properties, especially hardness, besides the evaluation of cracks, structure and chemical composition of the materials used. Cracks are documented with Olympus GX 51 optical microscope and Tescan Vega TS 5135 electron microscope. The chemical composition was assessed by EDS method on the Noran System Six/300 device. The hardness values of the stabilizers were obtained by LECO LV800AT hardness tester, the microhardness measurement used LECO LM247AT equipment. Material properties and microstructure evaluation was compared with the documents available in the metallurgical laboratory of the Department of Mechanical Engineering.

Keywords: 120 mm mortar projectile stabilizer, woody crack.

1 Introduction

The article deals with the material state of 120 mm mortar projectile, especially its stabilizer part that got stuck in the barrel after firing. As indicated by accessible sources the stabilizer was made of aluminium alloy AlZn6Mg2Cu according to CSN 42 4222 [1]. Material analysis was performed using the facilities of the Department of Mechanical Engineering. The analysis order was done as sampling, sample preparation, microstructure control, plus the checking of the chemical composition of components of interest arising from the control of the microstructure, followed by the evaluation of fracture surfaces. An equivalent material used to produce samples to test the tensile strength and decide the notch toughness was not available. The course of micro-hardness for the stabilizer part was measured from the surface to the material core as well as the material surface hardness.

2 Assignment Specification for Material Analysis

A damaged stabilizer part of 120 mm mortar projectile was delivered for the analysis. Year of manufacture of the stabilizer was 1988. The projectile crashed during the shot, as the projectile body was expelled from the mortar barrel and the stabilizer got stuck in the barrel. The separation of the body from the projectile stabilizer occurred within the union thread at the end of the stabilizer, see Fig. 1. The separation of the projectile body from the stabilizer is evident in Fig. 1 left part (crack 4). There took place also a subsequent delaminating of the stabilizer, its longitudinal splitting (crack 2) and the separation of a peripheral relatively regular equidistant crack of woody character (crack 5).

Fig. 1 *Radial view of the stabilizer with the defined points of displayed cracks*

3 Sampling and Sample Preparation

Samples were taken from the stabilizer union thread part uniting it with the projectile body according to the metallographic sample preparation rules. Etching was applied to create microstructure by use of a metallographic etchant of 10 ml of 48% HF + 90 ml H2O. Samples were intensively rubbed for 15s to create the structure.

Fig. 1 shows spots of cracks in the stabilizer observed. In the upper part is seen the whole course of the crack with the separated stabilizer part at the bottom of Fig. 1. Axial view in Fig. 2 allows observe the crack 5 on the left, and especially an equidistant crack at the right side end that extends practically over the entire stabilizer through holes for passing the flame up to the stabilizing fins.

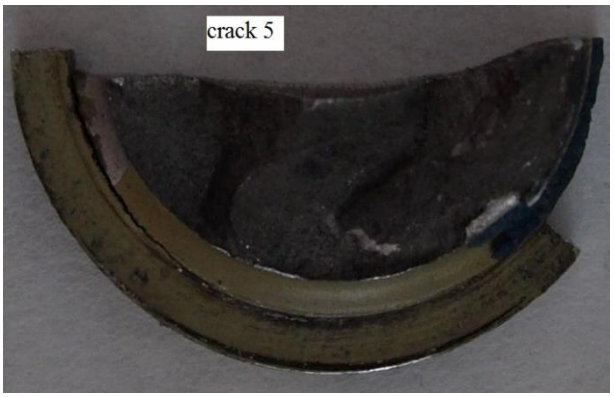

Fig. 2 *Axial view of the stabilizer crack 5*

4 Checking the Microstructure

After etching by the above etchant, the revealed microstructure was documented on the microscope Olympus GX 51. Fig. 3 shows a lined longitudinal structure with high proportion of impurities. The foreign inclusions seen in longitudinal planes have high content of Fe and Mn. A lined pattern is evident in the radial direction parallel to the longitudinal axis of the mortar projectile stabilizer. The lined microstructure is clear until the final crack of the whole stabilizer whose woody nature arranged in mutually parallel planes runs from the lined structure.

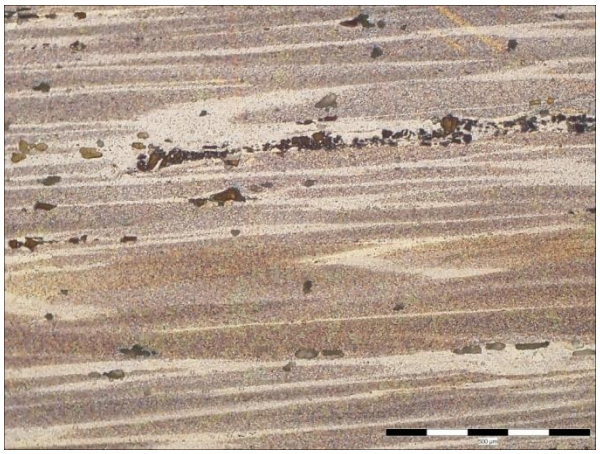

Fig. 3 *Stabilizer, radial sectional view, 800x*

Fig. 4 shows a visible crack that goes through the area with a low proportion of the precipitates as a result of the chemical composition heterogeneity (dendrites segregation). It is the crack on the right part of Fig. 2, which goes along the curvature of the equidistant surface stabilizer in the thread zone serving as union with the projectile body. From the macroscopic point of view, the stabilizer design looked as if it were a combination of several pipes together, e.g. by pressing. Comparison of the structure morphology on both sides of the crack inevitably leads to a conclusion that the corresponding shapes of dendrites suggest the same material. This, therefore, refutes the idea of the projectile part composition of several separate tubes. The idea also supports the crack tip found in Fig. 4 where there is again the crack clearly running along grain boundaries due to the segregation.

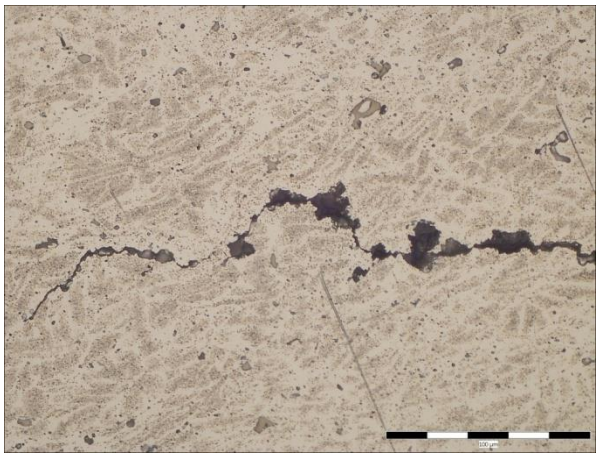

Fig. 4 *The crack tip – axial view, 500x*

Samples of all the three or four projectiles clearly show the lined structure with a significant proportion of foreign inclusions and impurities. In the cross section of each sample, i.e. in axial view, is always evident the form of dendrites with randomly distributed iron-based impurities. This indicates significant heterogeneity in material of the stabilizer.

5 Checking the Chemical Composition

Analysis of chemical composition of foreign inclusions was done by Noran EDS device Systemsix/300. Table 1 shows the values of the content elements recommended by the CSN 42 4222 [1]. The image of the measured area is obtained by an electron microscope and then processed by Noran system for specific chemical analysis.

Table 1. *The chemical composition of the stabilizer aluminium alloy according to CSN 42 4222*

Designation (Standard)	**Alloyed**						**Foreign inclusions**		
Elements [%]	**Mg**	**Zn**	**Cu**	**Mn**	**Cr**	**Al**	**Fe**	**Si**	Total
CSN 42 4222	1.8 to 2.8	5.0 to 7.0	1.4 to 2.0	0.2 to 0.6	0.1 to 0.25	Rest	0.5	0.5	1.2

Table 2. *The chemical composition of three measured inclusions in the stabilizer aluminium alloy*

Element	**Weight %**		
Inclusion	1	2	3
O*	31.29	27.23	30.68
Mg	3.65	10.84	2.48
Si	8.43	1.79	7,38
Cr	5.35	---	3.67
Mn	12.62	4.55	13.42
Fe	24.10	23.29	29.12
Cu	6.55	9.93	6.07
Zn	8.00	22.38	7.19

* The calculated amount of oxygen fixed in the oxide form to the respective elements

Measurements of the chemical composition of three selected inclusions in the stabilizer were done at spots at a magnification of 2000x. The resulting values for each element spot measurement are listed in Table 2. The measurements showed a high proportion of Fe, Mn and Zn in the three inclusions indicated. Also the share of Si is not negligible, causes brittleness of inclusions and has considerable influence for the crack spreading.

6 Evaluation of Crack Surfaces

The scanning electron microscope Tescan Vega TS 5135 was utilized to evaluate the crashed stabilizer cracked surfaces. Cracks were identified and documented in line with their distribution in Fig. 1. Cracks 1, 2, 3 and 5 had the same characteristics of woody cracking. Spacing of cracks ran along the stabilizer longitudinal axis. Crack 4 is documented in

the place where the mortar projectile body was detached from the stabilizer; its morphology was then different from the previous cracks.

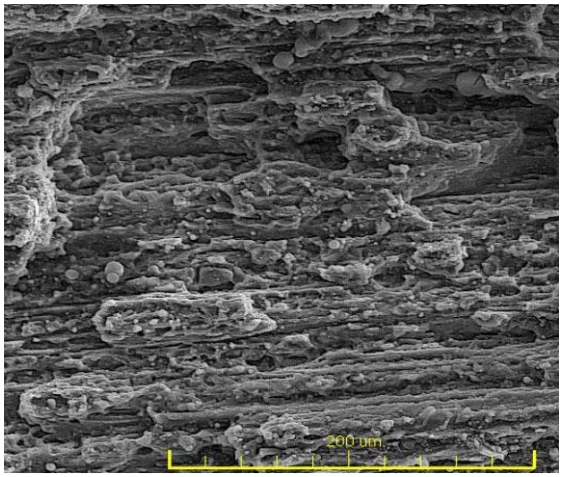

Fig. 5 *Crack 1, 500x SE*

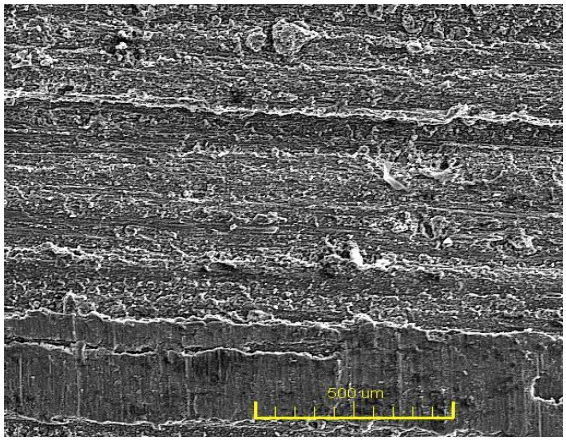

Fig. 6 *Crack 3, 100x SE*

Fig. 5 documents a crack on the stabilizer edge at a magnification of 500x. Apparently, there is significant fracture spacing with larger formations and areas that show signs of displacement or rather stripping off, probably the fracture itself in the radial direction. There are small spherical particles, admixtures, added to the crack. Crack 3 in Fig. 6 is scanned from the crack inner side and has a drastically axial shift in its line-like structure. Such a shift was apparently gained at concurrent actions of the longitudinal crack and crack 4 in Fig. 7, which separated the projectile body from the stabilizer. The morphology of crack 4 corresponds to a torsional rupture due to angle of inclination of the crack surfaces at approximately 45° to the longitudinal axis of the projectile stabilizer.

Fig. 8 shows crack 5 at a magnification of 1000x. This crack was gained from a separated part of the stabilizer equidistant crack. Its character follows up the previous cracks 1 and 3. Again, it is evidently of woody structure and globular admixtures with distinct shear surfaces.

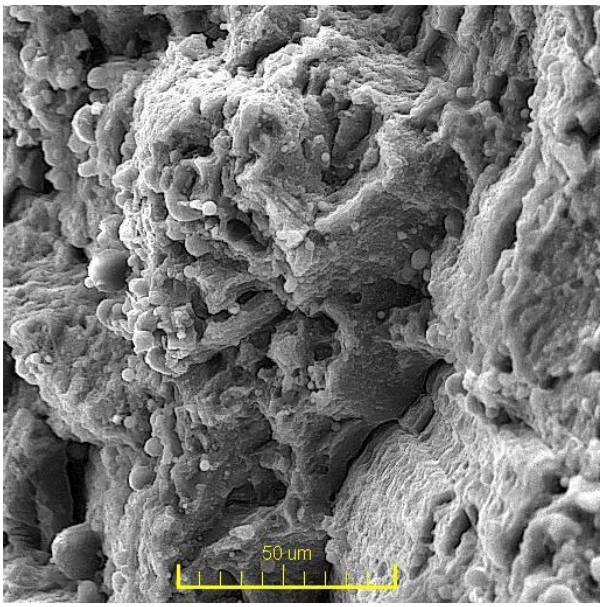

Fig. 7 *Crack 4, 1000x SE*

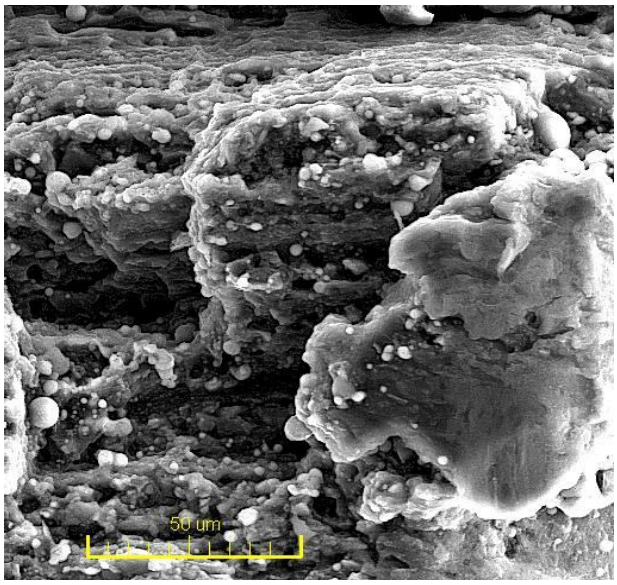

Fig. 8 *Crack 5, 1000x SE*

7 Checking the Mechanical Properties

The hardness tester LECO LV800AT and microhardness LECO LM247AT were used to test hardness. The hardness and microhardness tests were conducted according to Vickers hardness method [2].
Since the standard [1] contains only the Brinell hardness values [3], it was necessary to use a conversion according to [4] for the comparison of measured values. The hardness test was performed at a load HV10 and microhardness load HV0.05. The results are shown in Table 3, together with the size of the measured diagonals of individual indentations. The standard [1] indicates the lowest level of hardness after hardening heat HB 130, which, by the conversion according to DIN EN ISO 18265 [4], corresponds to the numerical value of the Vickers hardness (HV). It is evident that the hardness value is approximately by 54 units higher than those mentioned in the standard, what may lead to lower toughness of the material and thus the tendency to crack.
The increased hardness may be associated with conditions and storage time if the stabilizer was not stored at a constant temperature. A major influence to change the properties of the aluminium alloy used can have time and storage conditions (currently with the present sample period is 27 years from production).
The course of microhardness obtained by way of the above microhardness tester is shown in FIG. 9. The stabilizer showed apparent downward tendency of microhardness values from the surface to material core.

Table 3 *Results of Vickers hardness tests*

Mortar Projectile 1		
d1	d2	HV10
337,6	303,7	180,4
314,3	342,8	171,8
295,5	323,1	193,8
Σ		182

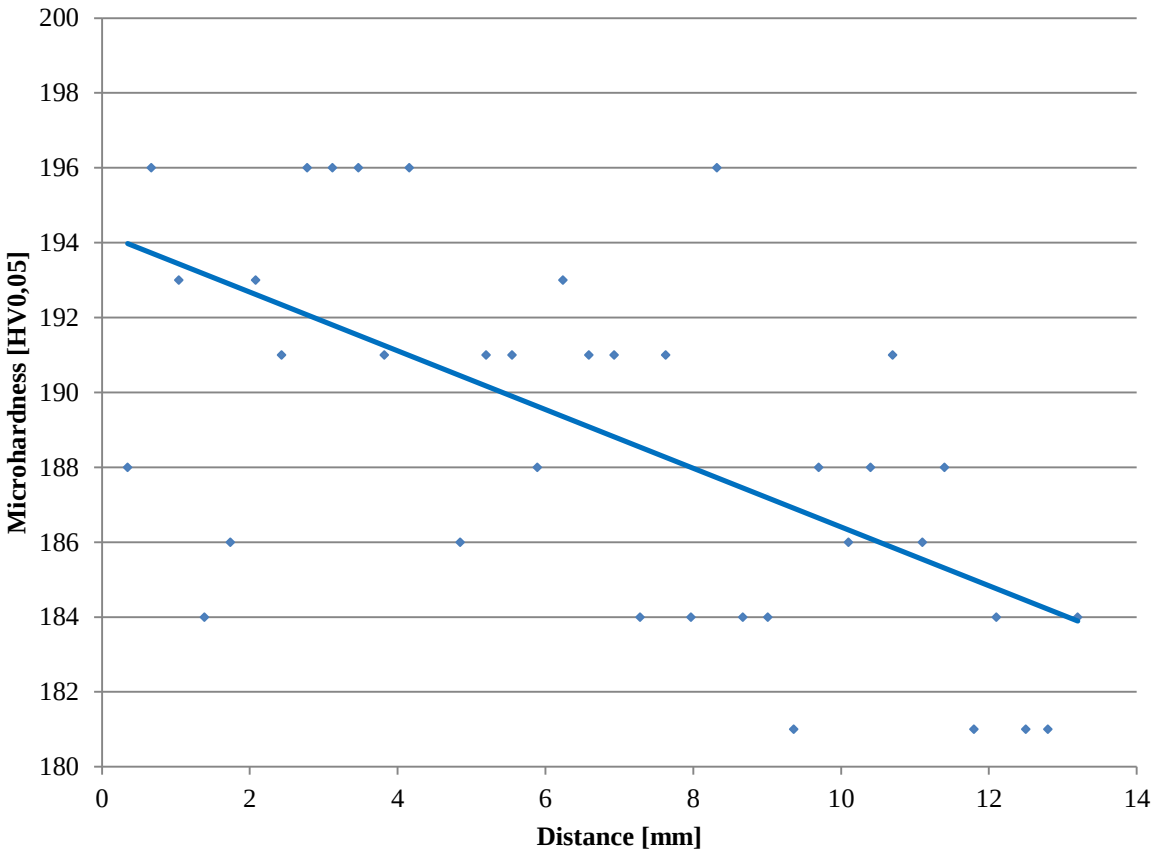

Fig. 9 The course of the stabilizer microhardness

8 Conclusions

The material analysis shows that the stabilizer was made of one piece of material that experienced a woody crack equidistantly with the stabilizer surface. The crack spreads to follow the grain boundary of precipitate areas. The structure of the material exhibits a marked lined feature.

Following the evaluation of the stabilizer fracture surfaces, it is possible to state that the crack running through nearly the entire cross section of the material has a refractive woody nature. The projectile body was separated from the stabilizer as a consequence of the ductile crack in torsion, which is illustrated by the slope of crack surfaces.

Tests of the hardness and microhardness by Vickers method revealed that the material had a significantly higher hardness than that mentioned in the standard. The hardness was higher on average by 42%, resulting in lower toughness and therefore a higher brittleness of the material. Such an increase in hardness was probably due to natural age hardening during storage.

Acknowledgement

The article was composed with the financial support of "Project Development Organization" at the Department of Mechanical Engineering, FVT, UO Brno.

References:

[1] ČSN 42 4222: Slitina hliníku tvářená – Formed aluminium alloy – 42 4222 AlZn6Mg2Cu. 1978

[2] ČSN EN ISO 6507-1 (420374): Kovové materiály - Zkouška tvrdosti podle Vickerse - Část 1: Zkušební metoda. 2006 – Metallic materials - Vickers hardness test - Part 1: Test method 2006

[3] ČSN EN ISO 6506-1(420359): Kovové materiály - Zkouška tvrdosti podle Brinella - Část 1: Zkušební metoda. 2006 Metallic materials - Brinell hardness test - Part 1: Test method. 2006

[4] ČSN EN ISO 18265 (420379): Kovové materiály - Převod hodnot tvrdosti. 2006 – Metallic materials – Conversion of hardness values. 2006

Problematika střel typu frangible

Autoři : Ing.Václav Svachouček,CSc v.svachoucek@tiscali.cz
Ing.Ivo Adam adam@prototypa.cz

Anotace

The author deals with characters of cartridges with bullets of the type FRANGIBLE, an assessment of these cartridges in relation to the user and at the same time experience from own production of these bullets in the Czech Republic.

V příspěvku se autoři zabývají vlastnostmi nábojů se střelami typu FRANGIBLE, hodnocením nábojů s těmito střelami ve vztahu k uživatelům a dále zkušenostmi z vlastní výroby těchto střel v České republice.

1. Úvod

Frangible střely jsou novým fenoménem v oblasti sportovního, loveckého a specielního určení nábojů. Frangible střely jsou již známy cca 80 let.
Historie těchto střel, jejichž základní podstatou je, že po nárazu na pevnou, odolnou překážku se rozpadnou na menší fragmenty nebo až prášek, se začíná psát začátkem 50.tých let minulého století. První pokusy a řešení střel spočívaly v uložení malých kuliček (kovové, plastové, keramické) do pláště nebo obalu, nebo zalité v pryskyřici a byly to především střely (resp. revolverové náboje) na ochranu proti zvířatům, hadům apod.
Následovalo řada řešení, které byla chráněna patenty, pro zajímavost uvádíme jedno řešení, také chráněno US patentem - Pb kuličky malého průměru jsou umístěny do textilního obalu- jako polštář, polštář vložen do plastové kukly - plášť střely a střely byly laborovány do revolverových nábojnic r.38 Special. Tyto náboje dlouhou dobu byly používány specielními složkami a to především službou ochrany letadel. Náboje uvedené konstrukce byly vyráběny také v ČSFR pod označením Short Stop a to ve dvou provedeních, lišících se rychlostí střely, nebo také dopadovou energií.
Veliký rozvoj FRG střel byl iniciován americkou námořní pěchotou a to především možnost využití střel pro vojenské účely, především při operacích vyloďování nebo výsadku námořní pěchoty na pevninu. Cílem bylo, aby se střely při střelbě od výsadkových lodí neodrážely, ale o boky lodi se jen roztříštily a tak aby nedocházelo k zraněním vojáků vlastních výsadkových jednotek.
V 80. tých letech se FRG střely začínají prosazovat při výcviku střelbou u policejních jednotek a následuje rozšíření FRG střel do civilní sféry.
V současné době (viz katalogy, presentace firem na výstavách, patentové spisy) nabízí střely resp. náboje s těmito střelami řada firem a vývoj v oblasti FRG střel je velice intenzivní- viz patentové spisy.
V 80-tých letech začaly tyto střely být intenzivně studovány i v ČSFR a to jak z pohledu volby materiálů, technologie výroby, požadavků uživatele, toxicity povýstřelových zplodin, fragmentace střely, ranivé balistiky a především funkční zkoušky získaných střel a nábojů.

2 Vlastnosti střel typu FRG

Výhody FRG střel

FRG střely se obecně sestávají z práškového nebo jemného zrna kovu nebo oxidu kovu, případně keramických materiálů a solí, pojiva a pomocných látek (barviva, kluzné materiály a pod). Vzhledem k této základní konstrukci FRG střel následně vyplývá obrovské spektrum použitelných látek a materiálů pro jejich výrobu.

Obecné výhody FRG střel :

- technické řešení a použité materiály pro výrobu FRG střel umožňují i netradiční řešení střel – střely typu FRG, střely typu FMJ s FRG jádrem, střely FRG galvanicky pokovené, střely SP, střely semi průbojné, střely FRG průbojné s kovovým nebo keramickým jádrem a pod,
- výroba je technologicky schůdnější, principielně jednodušší oproti klasickým střelám,
- při použití střel typu FRG je omezený ohrožený prostor,
- menší technický rozptyl střel (vliv použité technologie a nářadí na výrobu),
- použitelnost v stávajících, zavedených nábojnicích a to bez jejich úprav,
- náboje s střelami FRG jsou použitelné v zbraních (dané ráže) bez úprav zbraně,
- možnost netradičního řešení střel, vhodné řešení ve vztahu k použití a ve vztahu k zákazníkovi,
- použité materiály jsou s výhodou netoxické (jak ve výrobě střel, tak i při použití),
- střely při výrobě je možno značit, pro pozdější identifikaci,
- použité materiály jsou recyklovatelné,
- jedná se o nový směr v oblasti konstrukce komponent pro výrobu střeliva,

Některé nevýhody :

- v některých případech omezená doba použití,
- vyšší nároky na skladování,
- vyšší možnost poškození střely při manipulaci s nábojem (vybíjení a opětovné nabíjení a pod)
- při použití některých práškových materiálů (Cu,W) výrazně vyšší cena oproti klasické střele FMJ s Pb jádrem,
- při použití některých kovových prášků a některého tvaru zrna, může docházet k vyššímu opotřebení hlavně,

3. Základní problém střel typu frangible

Základní problém užití frangible střel nábojů je především v oblasti legislativy. Není jasná nebo specifikovaná hranice na rozdělení střel z pohledu rozkladu střely a tedy jejím učinku v cíli. Střely (náboje) jsou použitelné v civilní sféře při výcviku, sportovní střelbě a nebo při použití specielními složkami, nebo také střely resp. náboje s těmito střelami na povolené a zakázané.
Na základě zkušeností autorů s těmito střelami, dále řady konzultací s odborníky a pod, vyplynula potřeba se tímto problémem kvalifikovaně zabývat a byl podán projekt v rámci programu TIP na MPO. Projekt pod číslem TI 4-015 byl schválen a řešení zahájeno.
Jedním z cílů projektu bylo vypracování postupu pro hodnocení střel typu frangible z pohledu jejich užití a tedy vlastního rozkladu střely.
S ohledem na zadání – základní rozdělení střel (nábojů s těmito střelami) na povolené a zakázané z hlediska užití, bylo nutno se v rámci řešení projektu také zabývat vlastní výrobou vzorků střel a řešit střely, které budou plnit požadované parametry střel (nábojů) zakázaných a povolených.

4. Výroba vzorků střel a nábojů

Frangible střely zatím nikdo v ČR nevyrábí, obtížný je i dovoz samotných střel, ale ani dovoz nějakého typu střely typu FRG požadovanou problematiku řešení projektu by neřešil.
Jednalo by se o jeden vzorek, nějakých parametrů, který by asi pokryl jen nějakou část řešení.
Bylo tedy nutno, souběžně s rešerší problematiky ve vztahu k testování, řešit i prototypovou výrobu střel s vlastnostmi, které budou odpovídat požadavkům předpokládaného výstupu řešení a vlastní požadovaný výstup řešení.
Ing. Svachouček se problematikou konstrukce, vhodných materiálů a poloprovozní výroby střel typu FRG zabývá delší dobu a tak bylo možno po přípravných a studijních pracech začít již v prvním roce řešení projektu s experimentálními zkouškami v rámci řešení projektu.

Výroba vzorků FRG střel byla prováděna v následujících krocích :

- základní konstrukční návrh FRG střely,
- základní projekce výroby vzorku střely (materiály, optimální poměry komponent, způsob a kvalita promísení, setřesná hustota směsi, výsledný výlisek a jeho kvalita prolisování, lisovací tlaky a pod),
- návrh a výroba výrobního přípravku pro výrobu střel- matrice, lisovací trny, manipulační desky,

4..1 Vlastní výroba střel typu frangible:

Při výrobě vzorků střel byl ověřen a používán následující sled operací:

- sítování materiálů na požadované frakce, vážení jednotlivých materiálů, přesušení,
- míchání směsi pro výrobu FRG střel,
- volumetrické dávkování směsi do lisovacích matric,
- výroba střel lisováním v matricích,
- vypichování střel z matric,
- rozměrová a hmotnostní kontrola vyrobených střel,
- tepelná úprava některých variant vzorků FRG střel,
- rozměrová, hmotnostní a vzhledová kontrola po tepelných úpravách střel,

V průběhu řešení byla ověřována řada kovových prášků (W, Fe, Sn, Cu, Bi, Zn) a solí ($BaSO_4$, $CaCO_3$) a řada organických pojiv a o různé zrnitosti – PE, PP, PTFE, PVC s cílem vyrobit vzorky střel a následně nábojů , které bude možno definovat jako FRG - srovnávací (referenční) a které budou splňovat základní podmínky zadání pro hodnocení střel typu FRG :

- střely budou typu frangible,
- definovaný rozklad těchto střel s ohledem na hustotu materiálu střely , dopadovou energii střely a materiál cíle,
- ověření střel střelbou na definované překážky a komparace výsledků střeleb s střelbou na biologický materiál,
- střely umožní následně vzájemně posoudit-hodnotit zkoušené střely typu FRG, z pohledu střely povolené a střely zakázané pro civilní použití,

4.2 Použité technologie výroby vzorků střel

Pro výrobu vzorků střel byly použity následující technologie :

- výroba střel lisováním směsi prášků za studena,
- ověřeno dále následné zpracování – tepelná úprava vyrobené střely v peci, teplota temperance byla volena s ohledem na typ plastového pojiva,
- výroba střel plastikárenskou technologií- pomocí střikolisu – viz obr.8,

4.3 Výroba nábojů

Vzorky pro testování a řešení metody zkoušení byly vyráběny v následujících rážích 9 mm Luger a 357 Magnum .

Výroba vzorků nábojů r. 9 mm Luger a 357 Magnum byla prováděna na laboračním zařízení pro přebíjení nábojů od f-mi Hornady.

V průběhu laborace FRG vzorků střel bylo nutno upravit laborační nástroje (matrice a trny) pro vlastní laboraci nábojů..

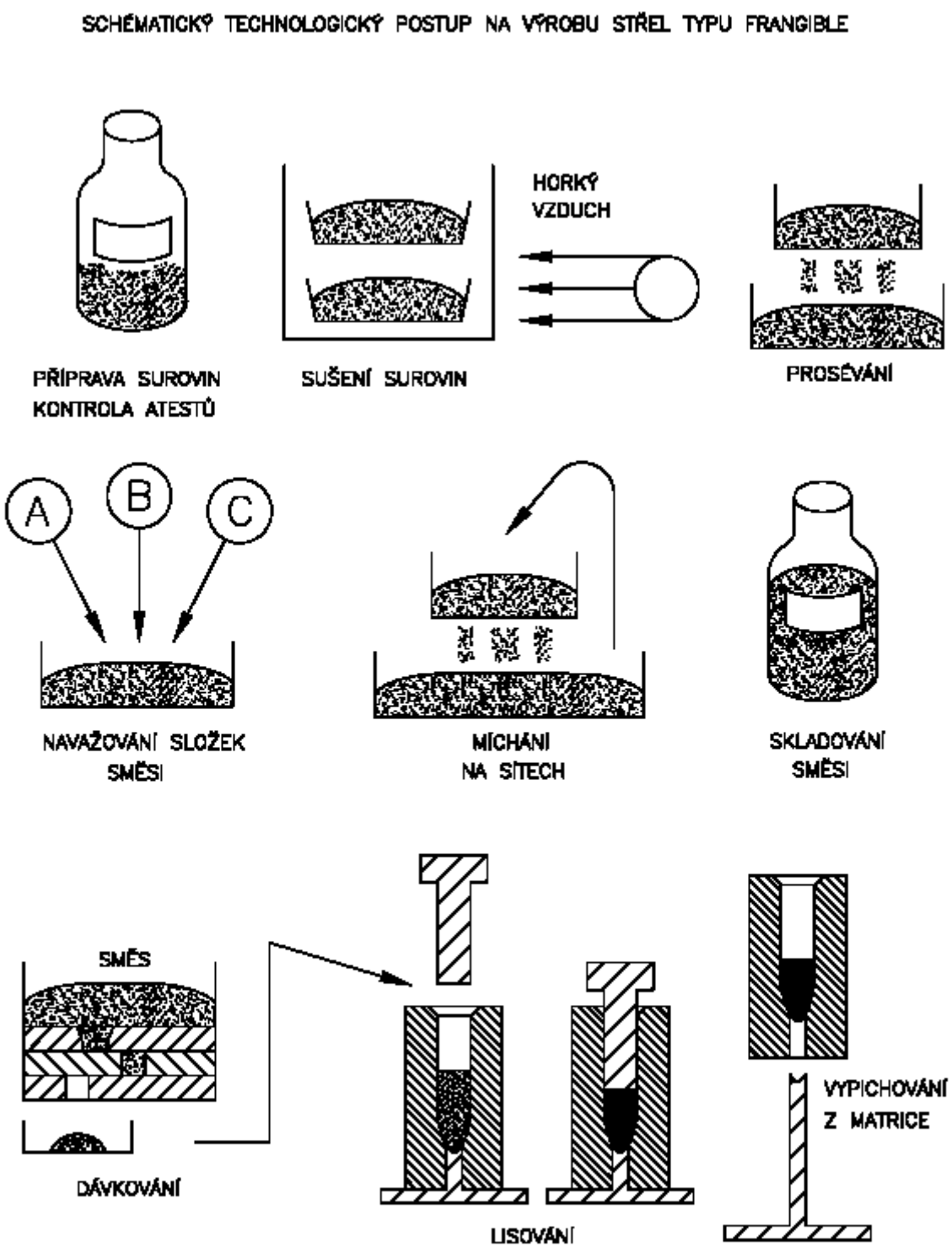

Schéma výroby FRG střel- lisování

Obr. 1 Nástroj na výrobu FRG střel - sestavený

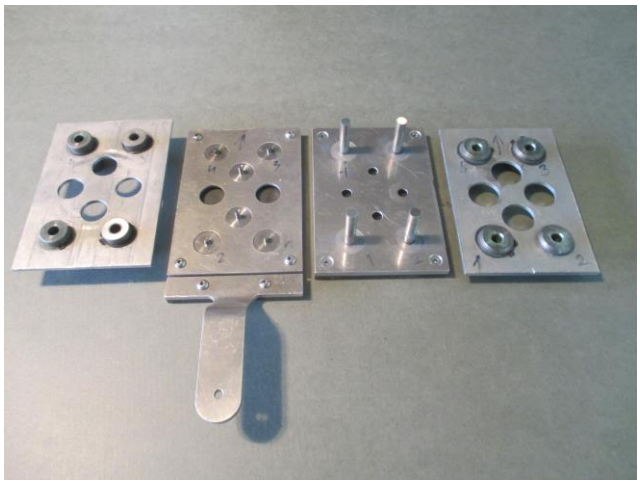

Obr.2 Nástroj na výrobu FRG střel- rozložený (osazeny 4 matrice, nástroj projektovaný na 8 matric)

Obr.3 Vzorky střel FRG a náboje r. 9 mm Luger

Obr.4 Vzorky střel FRG (materiál zleva Sn, Bi, 2 x Fe – barvené)

Obr.5 Vzorky střel r. 9 mm Luger + FRG střela z Fe pro ráži 12

Obr. 6 Vzorky střel r. 12 z Fe a Bi

Obr.7 Vzorky střel (klasické + FRG) po zkoušce střelbou do bloku plynosilikátu (zleva – Sinterfire, Remington-Desintegrator, MEN-QD-1, FRG-Fe, FRG-Bi, FRG-Fe

Obr. 8 Střely FRG z materiálu PE/Cu (hnědé) a PE/BaSO4 (zelené)

Obr.9 Náboje r. 9 mm Luger s střelami FRG z materiálu Sn a Fe

Obr.10 Náboje r. 9 mm Luger s střelami FRG z materiálu Sn a Fe

Obr.11 Náboj r. 9 mm Luger s střelou FRG-Fe a vstřel do plynosilikátové tvárnice

Obr. 12 Náboje r. 357 Magnum po laboraci, střela FRG-Fe

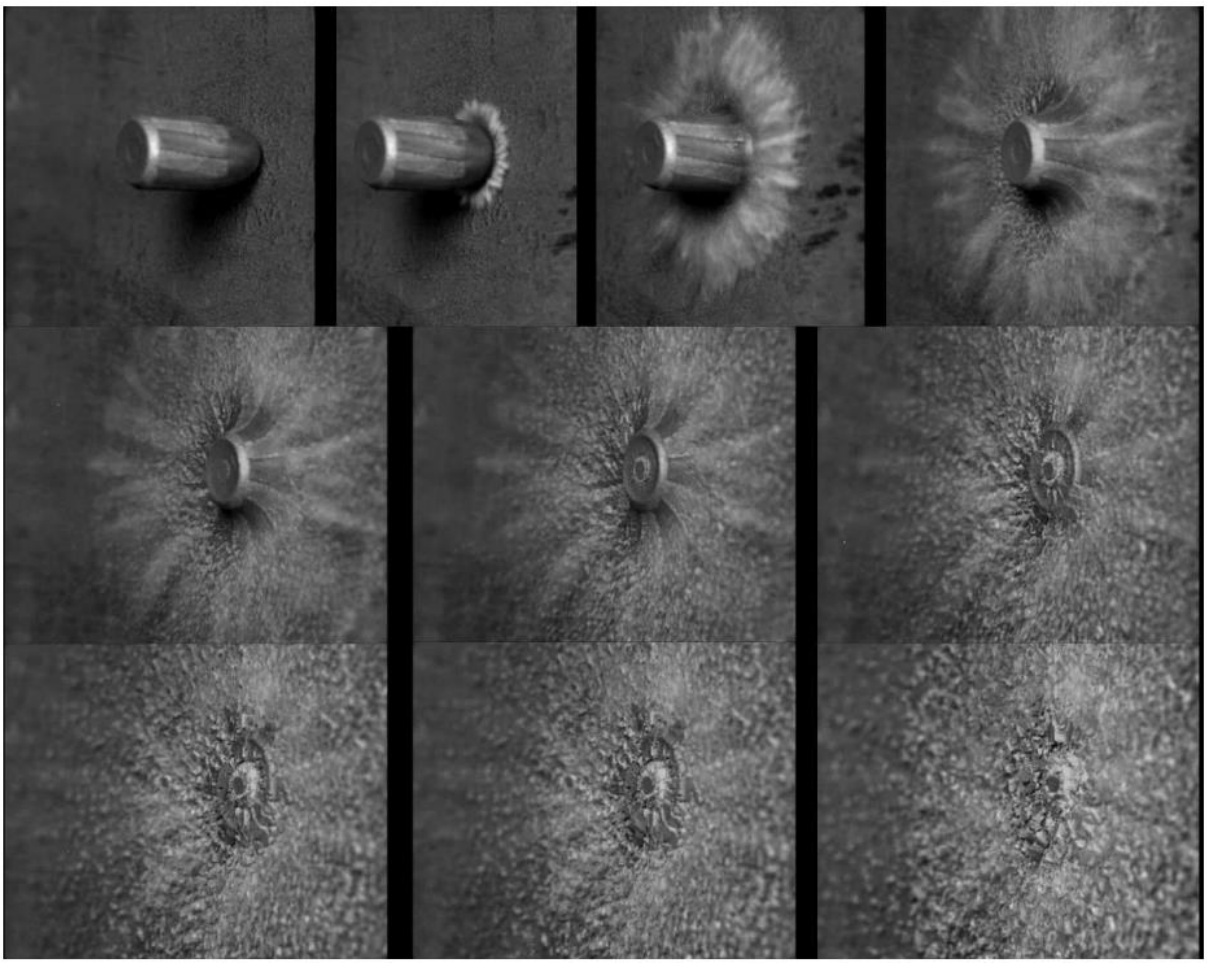

Obr.13 Rozklad frangible střely (složení Fe + PTFE) v ráži 9 mm Luger při nárazu na Fe plech síly 3 mm

4.4 Dílčí závěr

V průběhu řešení projektu byly získány obrovské zkušenosti v oblasti vhodných materiálů, technologií výroby střel a technologií laborace nábojů. Dále se povedlo vyřešit vhodnou sestavu střely typu FRG v ráži 9 mm L a 357 Magnum a následně vyrobit náboje v danných rážích, které splňují požadavky zadání projektu – tzn. referenční náboje pro posouzení, zda-li je zkoušený náboj vhodný pro použití v civilní sféře, tak i specielní užití, nebo také zda-li se jedná o náboj s střelou FRG , který je pro civilní použití z pohledu účinků a ranivé balistiky zakázaný.

5. Vývoj zkušebních metod

V rámci řešení projektu bylo rozpracováno a částečně ověřeno několik postupů a metod pro hodnocení střely nábojů s střelami typu frangible jako např.:

a) hodnocení samotných střel:

- stlačení střely lisem, definovaným tlakem, hodnotí se stupeň rozkladu nebo deformace střely při dosažení určitého tlaku,
- mechanické namáhání střely na kladivu Masseta – hodnotí se, při jakém přirychlení dojde k rozkladu střely,
- rozklady střely, který je způsoben pádem závaží z určité výšky,

- dynamické namáhání střely vzrůstajícím tlakem, do určité zbytkové výšky střely, snímá se průběh tlaku v závislosti na čase,

b) hodnocení střel cestou náboje :

- střelba na definované překážky (plechy – Al, Fe, Cu, kombinace plechů, dřevo, tvárnice Ytong, balistický gel, blok z želatiny),

Při hodnocení možných metod pro zkoušení se zvažovala kriteria :

- reprodukovatelnost výsledků,
- plnění požadavku na hodnocení „frangibility“ střely,
- proveditelnost testů,
- vzájemná závislost výsledků zvolené metody s výsledky testů na náhradní materiál (balistický gel, a pod)

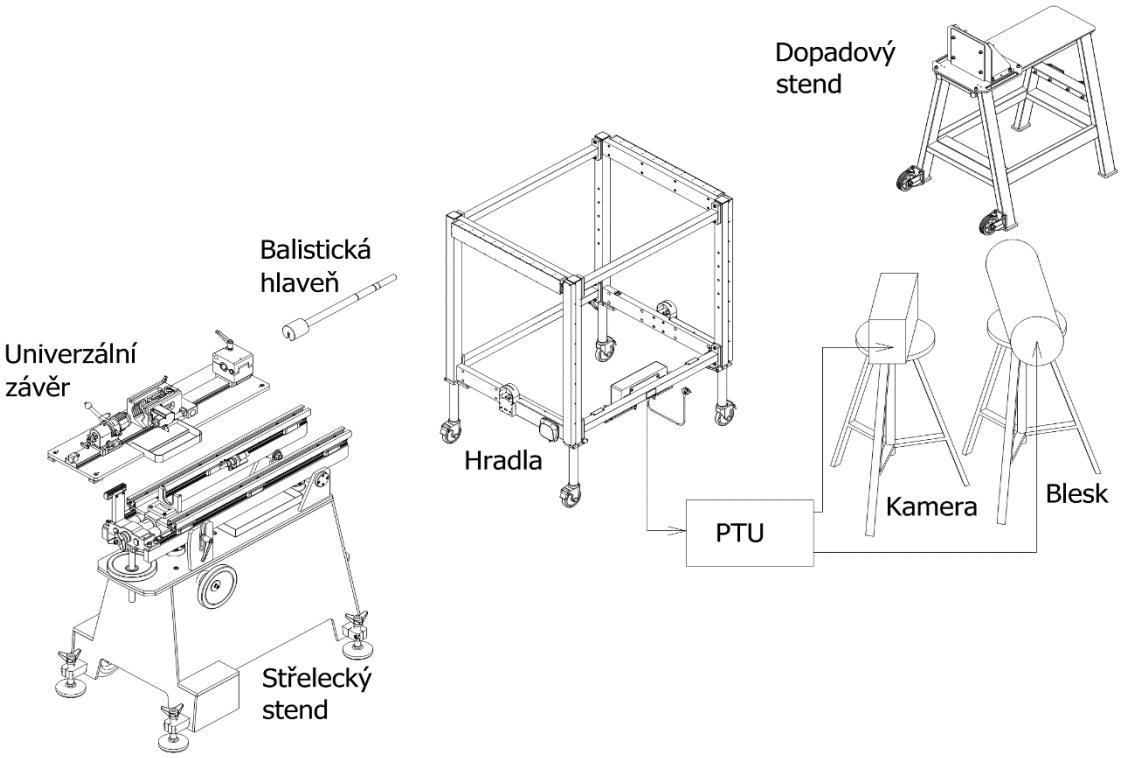

Obr. 14 Schematické uspořádání pracoviště

Obr.15 Foto uspořádání pracoviště (bez stendu s hlavní)

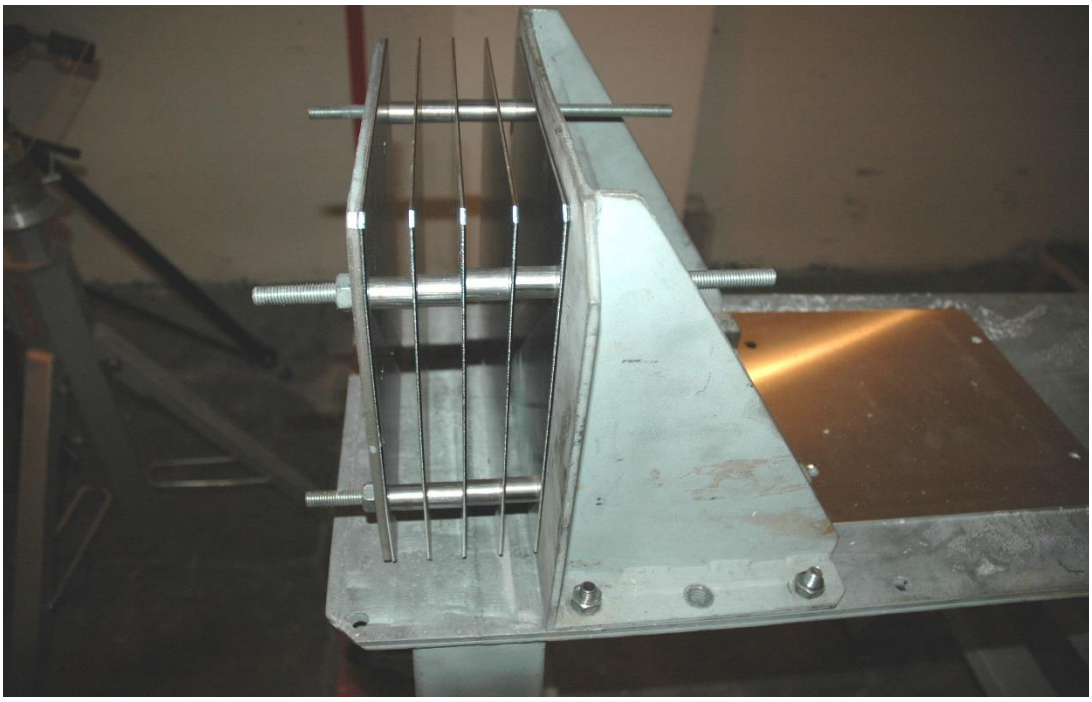

Obr.16 Foto uložení zkušebních plechů

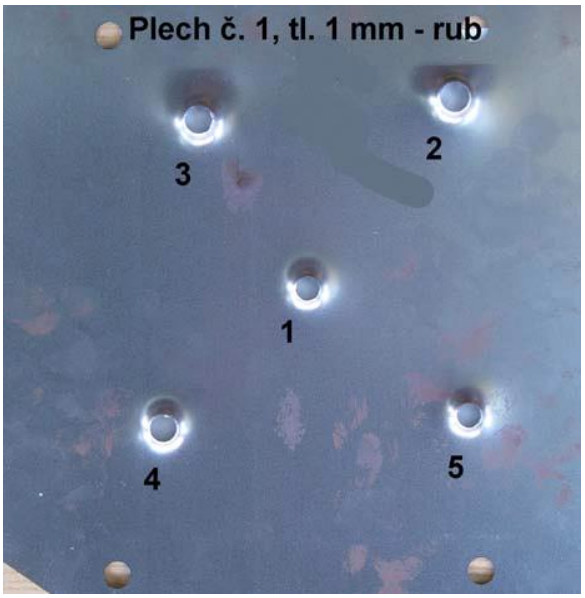

Obr.17 Pohled na 1. zkušební plech

V průběhu řešení projektu byla vypracována a řadou střeleckých zkoušek ověřena metoda pro hodnocení střel typu frangible. Tato metoda, kdy se střílí náboj z balistické hlavně a střela dopadá na definovanou sestavu Al a Fe plechů umožňuje rozdělit zkoušené vzorky střel typu frangible. Dělení střel / nábojů s těmito střelami/ je z pohledu rozkladu střely , tedy i z pohledu ranivé balistiky a střely /náboje/ je tak možno dělit na dvě základní skupiny a to:

- povolené pro civilní použití,
- zakázané pro civilní použití,

6.. Závěr

V průběhu řešení danného projektu byla ověřena řada práškových směsí kovů (Fe, Cu, W, Sn, Zn, Bi), oxidů kovů (Cu2O, CuO, Fe2O3, SnO2), solí (BaSO4,CaCO3) a vhodných pojidel (PE, PVC, PA, teflon, šelak), technologie výroby lisováním prášků a výroby pomocí plastikárenských lisů.. Vyrobené vzorky střel byly ověřeny praktickou střelbou . Následně byly vytipované vzorky ověřeny, spolu s zahraničními vzorky frangible střel/nábojů/ navrženou metodou pro hodnocení střel typu frangible s cílem definovat střely typu frangible, resp. hranici rozkladu střely za definovaných podmínek a tak definovat technickou hranici střely /náboje/ , které bude možno použít v civilní sféře – tedy povolené a na náboje, které budou pro použití v civilní sféře zakázané.

Application of duplex layer on piston rings

Milan Vnouček, Antonín Kříž, Karel Radl

University of West Bohemia, Faculty of Mechanical Engineering. Univerzitní 8, 306 14 Pilsen. Czech Republic. E-mail: vnoucek@kmm.zcu.cz

Recently, a progress in the development of gasoline internal combustion engines has resulted in increased demands on piston rings. Piston rings are loaded with higher temperature and pressure. These requirements are particularly significant at TSi, TCe or T-GDI engines. Piston rings are treated with various surface finishes. The most commonly used finishing is by nitriding or chrome plating. The combination of these treatments influences behaviour and resistance of piston rings. This paper deals with the nitriding of chrome plated piston ring. Nitriding was performed using plasma nitriding or gas nitriding. Duplex layer produced in this way has different properties than either of the layers used individually.

Keywords: Duplex layer, piston ring, plasma nitriding, gas nitriding, chrome plating

V současnosti je kladen stale větší důraz na efektivnost a ekologický provoz a výkon spalovacích motorů s ohledem na co možná nejmenší náklady na výrobu. Tyto požadavky vytváří v oblasti konstrukce a použitých materiál spalovacího motoru do mezní hodnoty použitelnosti. Tento fakt se však nepříznivě odráží ve spolehlivosti motoru. Následné opravy nelze provádět bez specializovaných přípravků. Mezi komponenty nejvíce namáhané v motoru patří tzv. pístová skupina, která se skládá z pístu, ojnice, ojničního čepu a sady pístních kroužků. Tato konstrukční skupina je také zodpovědná za převod tepelné energie na energii mechanickou. Jelikož se jedná o pohyblivé součásti s velkým tepelným zatížením, hrají významnou roli ve ztrátách spalovacího motoru. V literatuře[1,2,3] se nejčastěji vyskytuje údaj, že tato skupina způsobuje až 30% vnitřních ztrát motoru. V současné době je proto velkou snahou automobilového průmyslu tyto ztráty minimalizovat a zvýšit tak výkon motoru. Toho lze dosáhnout jednak konstrukčními změnami, jednak změnou použitých materiálů nebo jejich modifikací. V dnešní době moderních vysoce namáhaných motorů, kdy se stále více přistupuje k zvyšování kompresního poměru, se z tohoto důvodu také zvyšují tlaky plynů uvnitř spalovacího prostoru[1,2]. Dokonale utěsnit tento prostor je nejdůležitější funkcí pístního kroužku. Dále slouží k udržení vyhovující tloušťky olejového filmu, který je potřeba při styku PK a pístu s válcem. Neméně důležitou úlohou je odvod tepla z těla pístu na plochu válce. Je vidět, že PK pracují za velmi obtížných podmínek, přesto je na ně kladeno mnoho požadavků. Při výběru materiálu k výrobě pístních kroužků platí omezení několika základními požadavky, které by měl materiál splňovat. Mezi tyto požadavky patří dobrá odolnost proti opotřebení, malý sklon k zadírání, schopnost nouzově vydržet i při nedostatečném mazání bez „přidírání“ tzn. jistou samomaznou schopnost, korozní odolnost, tvárnost materiálu. Materiál musí vydržet vysoké namáhání na ohyb, snést vysoké rázy od vratného pohybu pístu a mít dobrou tepelnou stálost. Hmotnost pístního kroužku by měla být co nejnižší s ohledem na velikost setrvačných sil pístové skupiny[2,3]. Z ekonomického hlediska jsou žádoucí co nejnižší náklady na výrobu a nízkou nákupní cenu materiálu. Pístní kroužky se dělí na dva základní typy: těsnící a stírací Pro experiment byly použity stírací pístní kroužky s různou povrchovou úpravou. Byla porovnávána tvrdost pístního kroužku bez povrchové úpravy, nitridovaného pístního kroužku, kroužku chromovaného a duplexně zpracovaného.

Obr. 1 Ukázka pístu s pístními kroužky motoru škoda EA 111 1,6 l pístní kroužky jsou uspořádány od shora jako 2x těsnící a 1x stírací

Pro experiment byl jako základní materiál použit BS-17, což je nerezová chromová ocel splňující požadavky dle ISO 6621-3, třídy 60 a podtřídy 66. Ocel je dodávána jako polotovar v podobě pásky, ze které se vyrábějí ocelové těsnící pístní kroužky, které se dále připravují na nitridaci.

Struktura materiálu je zušlechtěná s rovnoměrně rozloženými karbidy.

Chemické složení v %:

C	Cr	Si	Mo	Mn	V	P	S
0,65-0,95	17-19	max. 1	0,9-1,5	max. 1	0,07-0,15	≤0.040	≤0.040

Tab. 1 Chemické složení oceli BS-17

Mechanické hodnoty základního materiálu:

Tvrdost	300 – 450 HV 5 58 – 65 HR30N
Modul pružnosti	210 000 N/mm^2
Specifická hmotnost	7,7 g/cm^3

Tab. 2 Mechanické hodnoty dodávaného materiálu

Pracovní plocha pístního kroužku je lapovaná. Tvrdost základního materiálu se pohybuje v rozmezí stanovenou normou jak je možno odečíst z grafů. Tvrdost HV0,1 základního materiálu se zkoušela na několika místech pístního kroužku. Vtisky byly vytvořeny na pracovní ploše pístního kroužku a dále pak na bočních plochách a ve středu. Byly vytvářeny ve vzdálenostech přibližně 50 µm, aby nedocházelo k jejich vzájemnému ovlivňování.

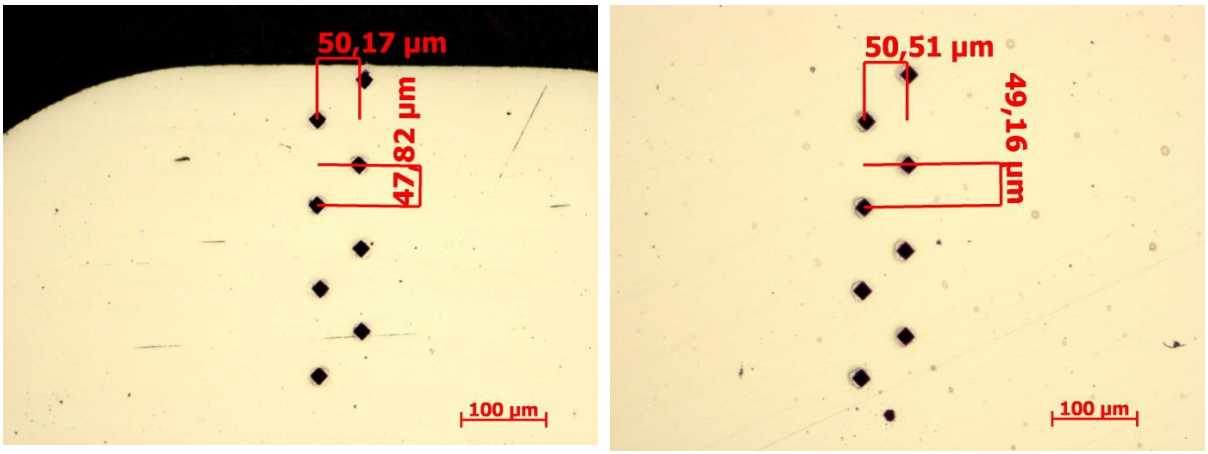

Obr. 2 Ukázka linie na pracovní ploše a ve středu vzorku

Vtisky v těchto polohách PK se hodnotou tvrdosti od sebe lišily jen minimálně a spadaly do rozmezí daného normou pro daný materiál. Průměrná dosahovaná tvrdost byla 390 HV0,1

Jelikož hloubka nitridace byla předpokládána cca 100 µm a mikrotvrdost cca 800-600 HV0,1 je velikost úhlopříček cca 16 µm. Dle normy ČSN EN ISO 6507-1 lze nejbližší vedlejší vtisk položit min. ve vzdálenosti 2x velikost úhlopříčky, proto byly vtisky kladeny dle obr. 2; 3. Stejným způsobem bylo postupováno u všech vzorků. Měření tvrdosti HV0,1 bylo provedeno na bočních a horních plochách metalografického výbrusu v příčném stavu. Měřená plocha byla před měřením upravena broušením.

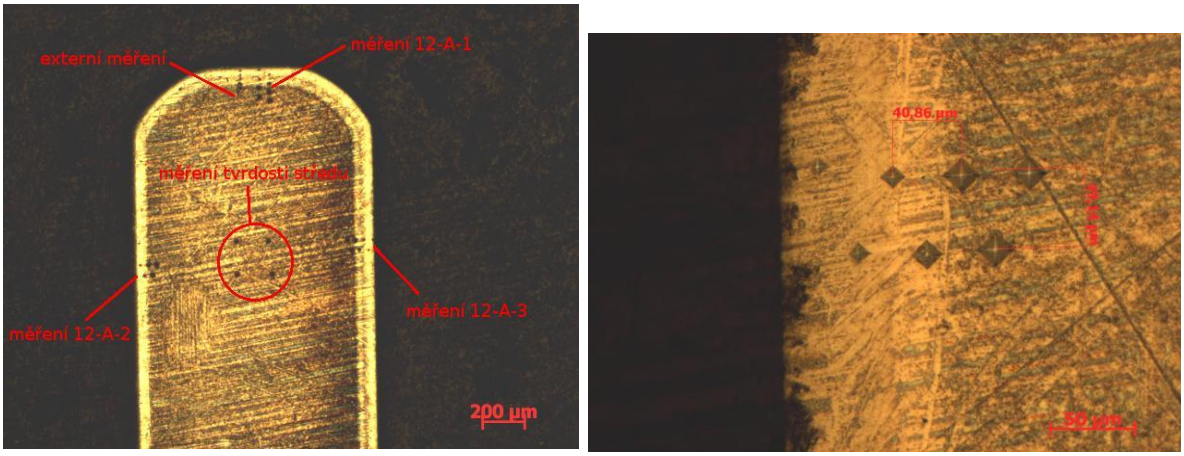

Obr. 3 Rozmístění vtisků mikrotvrdosti HV0,1 na povrchu a ve středu vzorku pístního kroužku

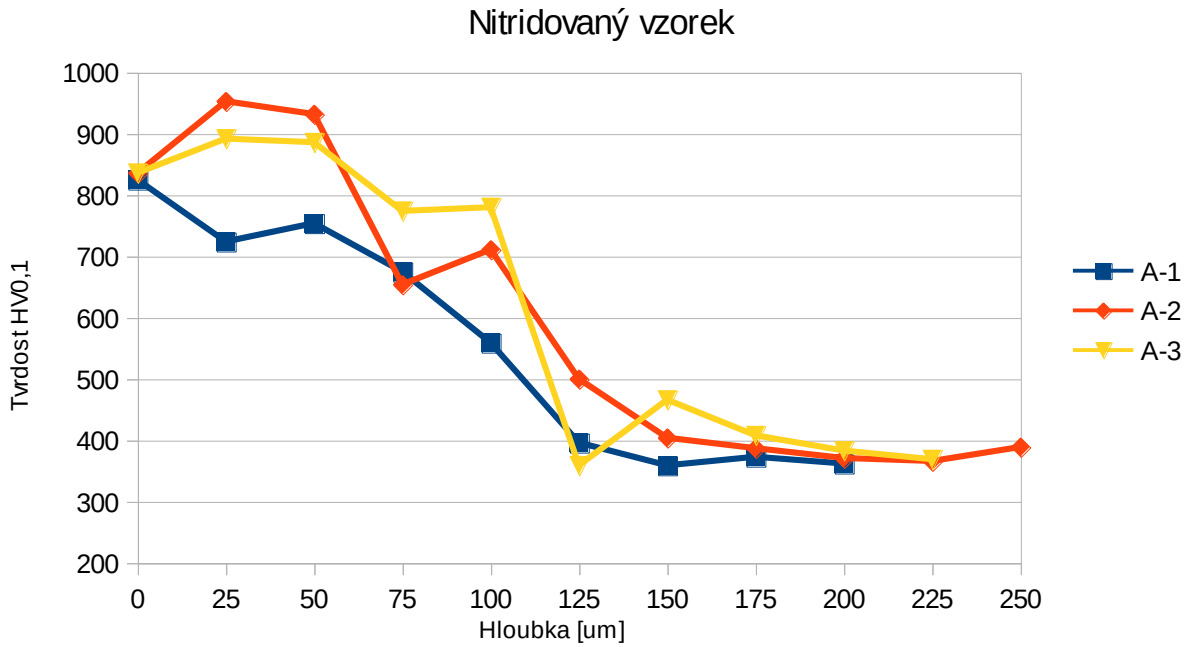

Graf 1 Hloubkový profil tvrdosti nitridované ho pístního kroužku

hloubka µm	A-1	A-2	A-3	A-střed
0	825	836	836	362
25	724	953	892	380
50	754	932	886	378
75	675	654	774	**průměr**
100	559	711	780	**373,3 ±7,6**
125	396	500	359	
150	359	404	466	
175	373	387	408	
200	362	371	383	
225		366	369	
250		389		

Tab. 3 Naměřené hodnoty nitridovaného pístního kroužku

Velmi podobných hodnot dosahují pochromované pístní kroužky, kdy pracovní plocha je opatřena vrstvou tvrdého chromu. Základní materiál je stejný.

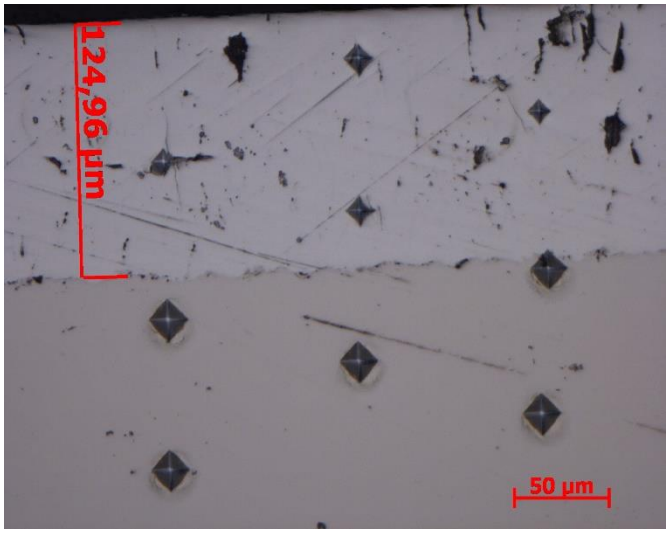

Hloubka (um)	HV0,1	Střed
0	593	412
25	1014	416
50	925	417
75	634	434
100	457	425
125	398	**Průměr**
150	417	
175	410	**421±7**
200	425	

Obr. 4 a Tab. 4 Chromovaný pístní kroužek s vtisky mikrotvrdosti HV0,1

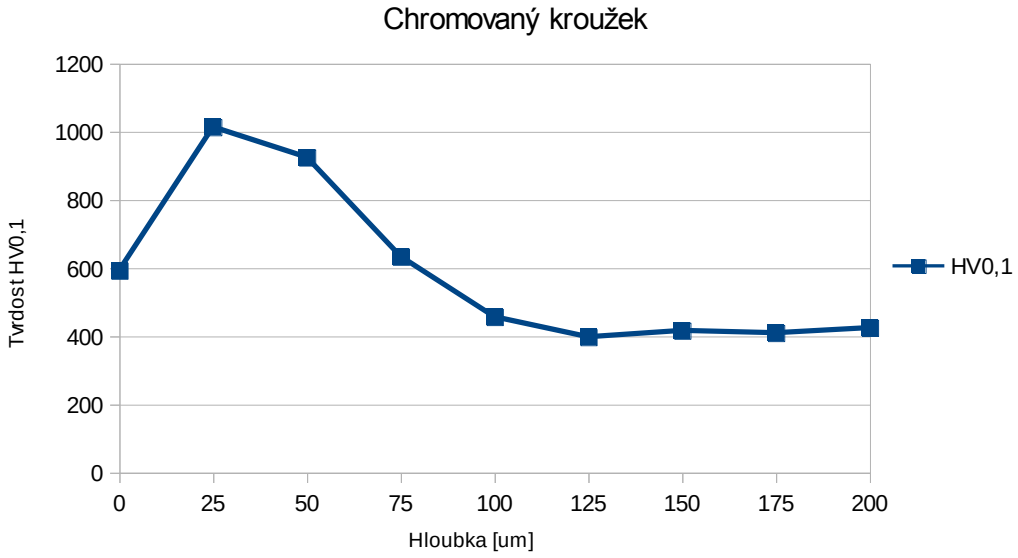

Graf 2 Hloubkový profil chromovaného pístního kroužku

Chromované pístní kroužky byly dále podrobeny nitridaci v peci. Očekávané vlastnosti byly následující. Vysoká tvrdost CrN spolu s nízkou křehkostí umožní vytvořit větší tloušťku chromového povlaku s velmi dobrou přilnavostí. Dále má CrN dobré třecí vlastnosti při sníženém mazání. Očekávaná tvrdost cca 2000 HV0,1 a koeficient tření proti oceli 0,3-0,4[3].

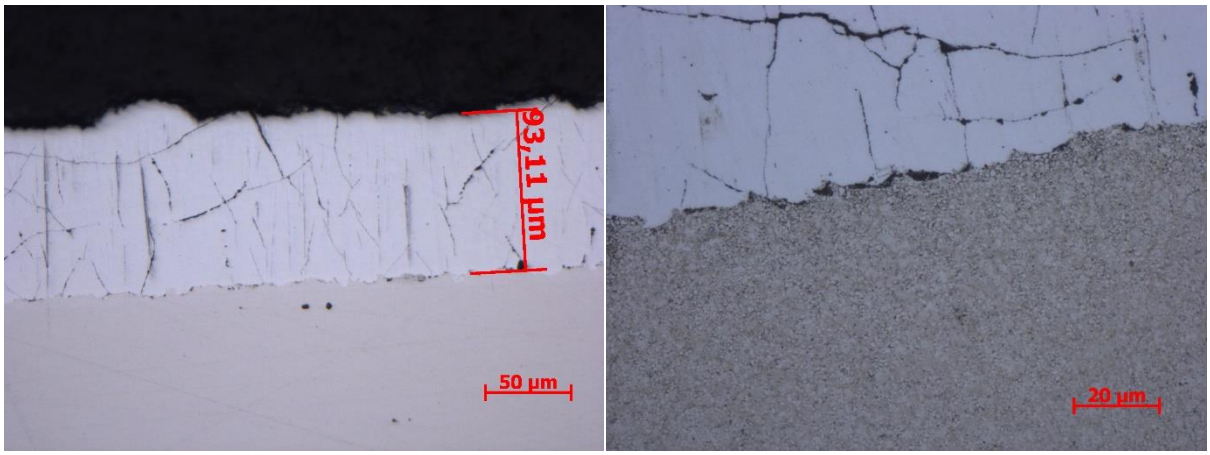

Obr. 5 Stav nitridované chromové vrstvy

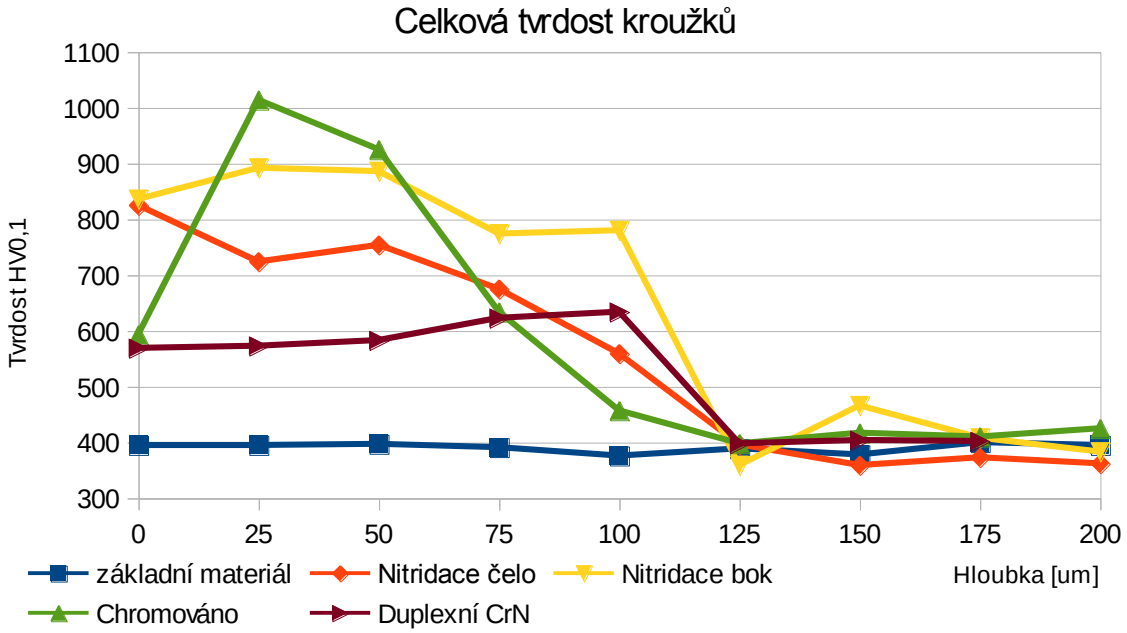

Graf 3 Celkový hloubkový profil tvrdosti různě zpracovaných pístních kroužků

Ve vrstvě Cr po nitridaci se objevila síť trhlin kolmých na rozhraní a dále trhliny cca pod úhlem 45°. Tyto neočekávané trhliny způsobily pokles tvrdosti Cr vrstvy. Koheze s podkladovým materiálem není narušena a síť trhlin se vyskytuje pouze v chromové vrstvě. I když se zdá, že tento stav nebude pro použití v oblasti pístních kroužků zcela ideální, bylo by možné ho využít na boční straně pístního kroužku z důvodu vytváření olejového rezervoáru. Využitelnost tohoto stavu na čelní pracovní ploše je podmíněna zajištěním třecích vlastností. Vývoj nových modifikací pístních kroužků jde slibným směrem vedoucím ke snižování třecích ztrát spalovacích motorů. Kromě modifikace vlastností samotných pístních kroužků je potřeba se věnovat komplexně modifikaci třecí dvojice pístní kroužek-válec při různých podmínkách zatížení spalovacích motorů.

Poděkování:
Tento příspěvek vznikl na základě řešení projektu SGS-2015-016 „Analýza povrchů konstrukčních celků a nástrojů metodou integrity povrchu a dopady na užitné vlastnosti“.

Použitá literatura:

[1] http://www.cesomot.cz/doc_cz/GOETZE-pistni-krouzky.pdf
[2] FEDERAL-MOGUL BURSCHEID GMBH. Piston Ring Handbook [online]. 2008 [cit.2013-10-21]. Dostupné z WWW: http://korihandbook.federalmogul.com/en/index.htm
[3]ANDERSSON, Peter, Jaana TAMMINEN a Carl-Erik SANDSTRÖM. Piston ring tribology: A literature survey. Espoo: Technical Research Centre of Finland, 2002. ISBN 951–38–6107–4.

PROGRAM SEMINÁŘE/FRAMEWORK PROGRAM

XIII. Odborný seminář "Materiály a technologie ve výrobě speciální techniky 2015"

13th Seminar „Materials and Technologies in Special Technics Production 2015"

20. 5. 2015

	Registrace účastníků/Registration Kasárna na ul. Šumavská 4, učebna 5B Barracks, Šumavská str. 4, Lecture hall 5b	**8.00 – 9.00**
	Zahájení semináře/Opening Vojtěch Hrubý, Univerzita obrany, Brno	**9.00 – 9.05**
1.	**Vystoupení ředitele Úřadu pro obrannou standardizaci, katalogizaci a státní ověřování jakosti a předsedy semináře** Martin Dvořák, Úř OSK SOJ, Praha, ČR	**9.05 - 9.20**
2.	**Prezentace firmy/Commercial presentation - OLYMPUS** Karel Dám, Martin Hlaváč	**9.20 - 9.35**
3.	**Material Analysis of Nickel Superalloy for Military Technology** Petr Jonšta, Irena Vlčková, Zdeněk Jonšta	**9.35 - 9.50**
4.	**Experimental Detection of the Characteristics Magnetorheological Dampers Applied into Military Vehicles Operated in Multinational Missions** Vladimír Sedlák, Mariana Kuffová	**9.50 - 10.05**
5.	**Prezentace firmy/Commercial presentation - ZWICK/Roell** Michal Reinisch	**10.05 - 10.20**
6.	**Safety of lithium – ion batteries** Jiří Vondrák, Marie Sedlaříková	**10.20 - 10.35**
7.	**Compressive creep testing of MoSi2-SiC nanocomposites - Vyžádaná přednáška** Natália Luptáková	**10.35 - 10.50**

	Přestávka /Coffee break	**10.50 - 11.15**
8.	**Material analysis of projectile hard core** Ján Bezecný, Ján Štrba, Andrej Dubec	**11.15 - 11.30**
9.	**Influence of admixtures on mechanical features of artillery barrels** Ondrej Híreš, Peter Lipták, Danka Rakúsová	**11.30 - 11.45**
10.	**Analysis of surface integrity in hardened steel Vanadis (1.2379)** Viliam Cibulka, Mária Šurláková	**11.45 - 12.00**
11.	**Statistical Monitoring of Decrease of Surface Eccentricity and Hole of Barrel Tubes from High Strength Steels under the Production Conditions** Jozef Majerík	**12.00 – 12.15**
12.	**Problematika střel typu frangible** Václav Svachouček, Ivo Adam	**12.15 - 12.30**
	Závěr semináře/Closing the seminar	**12.30**
	Oběd/Lunch	**12.30 - 13.30**
	Návštěva veletrhu IDET 2015/Visit the IDET 2015 fairs	**od 14.00**
	Náhradní přednášky/Spare lectures	
13.	**Influence of Projectile Base Modifications** Adolf Jílek, Jan Kusák	
14.	**Application of duplex layer on piston rings** Milan Vnouček, Antonín Kříž, Karel Radl	

OLYMPUS

Your Vision, Our Future

DSX510

DSX510i

DSX110

Prvotřídní optika.
Špičková digitální technologie.
Perfektní kombinace.

Optodigitální mikroskopy řady DSX.

Pro více informací o DSX mikroskopech navštivte naše internetové stránky www.olympus-ims.com/opto-digital

Olympus Czech Group, s.r.o., člen koncernu,
Evropská 176/16, 160 41 Praha 6, tel.: +420 221 985 267, +420 221 985 111
e-mail: mikroskopy@olympus.cz

www.olympus.cz